Sites NGHP-01-17

By T. Collett, M. Riedel, J. Cochran, R. Boswell, J. Presley, P. Kumar, A. Sathe,
A. Sethi, M. Lall, and the National Gas Hydrate Program Expedition 01 Scientists

Scientific Investigations Report 2012–5054

U.S. Department of the Interior
U.S. Geological Survey

Contents

Background and Objectives....899
Operations....899
Hole NGHP-01-17A....899
Hole NGHP-01-17B....905
Lithostratigraphy....905
Lithostratigraphic Units....906
Lithostratigraphic Unit I....906
Subunit Ia....906
Subunit Ib....907
Subunit Ic....942
Sedimentary Environment....942
Gas-Hydrate Occurrence....943
Inorganic Geochemistry....944
Interstitial Water Chloride and Salinity....944
Gas-Hydrate Distribution....956
Sulfate and Alkalinity Concentrations: Characterization of the SMI....957
Bromide Concentrations....957
Organic Geochemistry....957
Microbiology....964
Hole NGHP-01-17A....964
Physical Properties....965
Infrared Imaging....965
Environmental Conditions....965
Infrared Images....965
Core-End Temperature Readings....978
Index Properties....978
Strength....981
Electrical Resistivity....981
P-Wave Velocity....983
Magnetic Susceptibility....993
Thermal Conductivity....993
Downhole Temperature Measurements....993
Pressure Coring....993
Pressure Core Operations and Measurements....993
Gas-Hydrate Concentration, Nature, and Distribution from Pressure Coring....1026
Downhole Logging....1027
Operations....1027
Logging Data Quality....1040
Logging Units....1045
Gas-Hydrate and Free Gas Occurrence....1045
References Cited....1047

Figures

1. Bathymetric map showing Site NGHP-01-17 in the Andaman area 900
2. Detailed map of the area in the Andaman Islands showing Site NGHP-01-17 and location of key seismic lines 901
3. Seismic line AN-01-34 crossing Site NGHP-01-17 902
4. Seismic line AN-01-27 crossing north of Site NGHP-01-17 903
5. Seismic line AN-01-29 crossing south of Site NGHP-01-17 904
6. Map showing all holes occupied at Site NGHP-01-17 905
7. A, Lithostratigraphic summary of Hole NGHP-01-17A. B and C show an expanded scale of A 907
8. A, Summary plot of coarse fraction showing the relative abundances of foraminifera, total calcareous and total biosiliceous materials, and pyrite at Site NGHP-01-17 910
9. A, Ash beds, B, bioturbated occurrences of ash, and C, disseminated occurrences of ash observed throughout Lithostratigraphic Unit I 924
10. A, Summary of the ash types, thickness, and occurrences with depth and the colors of ash versus depth. B, Ash colors plotted individually by thickness versus depth in Lithostratigraphic Unit I. C, Ash occurrences plotted individually by thickness versus depth in Unit I 927
11. Core temperature and catwalk infrared camera imagery compared to the occurrences of ashes and several downhole logging data sets 944
12. Concentration-depth profiles of A, chloride and B, salinity at Hole NGHP-01-17A. C, Cross plot between dissolved chloride concentration and salinity, showing a good correspondence for samples deeper than 180 mbsf, where both parameters are primarily influenced by dilution of the fluids by hydrate dissociation 954
13. A and B, Visual and infrared images of core samples with ash-bearing hydrate layers. C, Visual and images of a core with no apparent lithologic control of the IR signal 955
14. Concentration-depth profiles of A, alkalinity; B, sulfate; and C, sulfate, methane, and alkalinity 958
15. A, Concentration-depth profile of dissolved bromide, and B, depth profile of Br^-/Cl^- ratios at Hole NGHP-01-17A 959
16. Plot of headspace methane gas concentration with depth for Hole NGHP-01-17A 966
17. Plot of headspace carbon dioxide gas concentration with depth for Hole NGHP-01-17A 967
18. Plot of headspace and free/void gas methane to carbon dioxide gas ratio with depth for Hole NGHP-01-17A 970
19. Plot of free gas and PCS gas methane to ethane ratio with temperature at increasing depths for Hole NGHP-01-17A 972
20. Catwalk temperature and humidity measurements as a function of time during drilling operations at Site NGHP-01-17. 979
21. Infrared track imaging and the derived downhole temperature profile for Hole NGHP-01-17A in three sections 984
22. Comparison of core end infrared images from adjacent to an IR anomaly and away from an IR anomaly 987

23. Detailed example of infrared (IR) anomaly (Section NGHP-01-17A-53X-6, 47–62) 988
24. Sequence of infrared images and Delta T's during processing of an interstitial water sample containing an IR anomaly for IW sample NGHP-01-17A-53X-6, 47–62 cm after splitting. 989
25. A, Digital image of interstitial water (IW) sample NGHP-01-17A-53X-6, 47–62 cm after splitting; B, IR image of IW sample NGHP-01-17A-53X-6, 47–62 cm after splitting; C, Merged visible and IR images of IW sample NGHP-01 17A-53X-6, 47–62 cm after splitting, showing location of cold anomaly on the split sample and in relationship to sample lithology 990
26. Digital visible image of interstitial water sample NGHP-01-17A-53X-6, 47–62 after splitting, showing lithology, cold anomaly, and resulting chlorinity values 991
27. Profiles of core recovery, index, and strength properties for Hole NGHP-01-17A 994
28. Profiles of infrared images, core recovery, electrical resistivity, acoustic *P*-wave velocity, magnetic susceptibility, and thermal conductivity for Hole NGHP-01-17A 995
29. Shear strengths normalized to the effective vertical stress versus sub-bottom depth for Hole NGHP-01-17A 1008
30. Peak and remolded vane shear strengths and sensitivity for Hole NGHP-01-17A 1008
31. Apparent formation factor versus sub-bottom depth for Hole NGHP-01-17A 1024
32. Geothermal gradient and estimated depth to the BSR from *in situ* temperature measurements for Hole NGHP-01-17A 1026
33. Temperature and pressure versus elapsed time for each pressure-corer deployment as recorded by the corer's internal data logger 1028
34. Temperature versus pressure for each successful pressure corer deployment, showing trajectories relative to gas-hydrate stability at 30 ppt and 35 ppt salinity 1030
35. Data collected at near in situ pressure and 7 °C for Cores NGHP-1-17A-38Y, -49E, and -81E, including X-ray images, gamma density, and *P*-wave velocity 1031
36. Summary of data taken from successful pressure cores before, during, and after depressurization, including gamma-density profiles collected before and after depressurization, X-ray images collected before and after depressurization, and line-scan images collected after depressurization 1034
37. Pressure versus volume for successful pressure cores, also showing placement of gas samples 1038
38. Pressure versus time for the depressurization of successful pressure cores 1039
39. Methane phase diagram for Site NGHP-01-17, with total methane concentration measured from the three successful pressure cores at Site NGHP-01-17 1041
40. Summary of the wireline logs recorded during the two triple-combo runs in Hole NGHP-01-17B 1042
41. Sonic waveform amplitude and coherence data and velocity logs measured by the DSI in Hole NGHP-01-17B 1043
42. Preliminary stacks derived from the waveforms recorded during the VSP survey in Hole NGHP-01-17B 1044
43. Water saturations from Archie's equation and wireline porosity and resistivity logs in Hole NGHP–01–17B 1046

Tables

1. Smear slide data for Hole NGHP-01-17A 912
2. Coarse fraction (>63 mm) sieve data for Hole NGHP-01-17A 918
3. Volcanic ash occurrences at Hole NGHP-01-17A 930
4. Interstitial-water data for Hole NGHP-01-17A 946
5. Interstitial-water data corrected for drill-water contamination based on sulfate concentration, for Hole NGHP-01-17A 951
6. Headspace gas composition for Site NGHP-01-17 960
7. Void gas composition for Site NGHP-01-17 968
8. Pressure Core Sampler gas composition for Site NGHP-01-17 971
9. List of microbiological samples taken for Site NGHP-01-07 973
10. List of infrared images collected from Hole NGHP-01-17A 980
11. List of infrared image files collected on section ends from Hole NGHP-01-17A 982
12. List of temperature-probe data collected at bottom of cores from Hole NGHP-01-17A 992
13. Moisture and density (MAD) physical properties for Hole NGHP-01-17A 996
14. Vane shear strength results for Hole NGHP-01-17A 1004
15. Torvane strength results for Hole NGHP-01-17A 1005
16. Pocket Penetrometer strength results for Hole NGHP-01-17A 1006
17. Wenner array electrical resistivity and formation factor results for Hole NGHP-01-17A 1009
18. Contact *P*-wave velocity results determined on split cores sections from Hole NGHP-01-17A 1024
19. Thermal conductivity results for Hole NGHP-01-17A 1025
20. *In situ* temperature measurements for Hole NGHP-01-17A 1026
21. Summary of pressure-coring operations at Site NGHP-01-17 1027
22. Methane-hydrate volume and concentration in pore space for successful pressure cores at Site NGHP-01-17 1040

Site NGHP-01-17

By T. Collett, M. Riedel, J. Cochran, R. Boswell, J. Presley, P. Kumar, A. Sathe, A. Sethi, M. Lall, and the National Gas Hydrate Program Expedition 01 Scientists

Background and Objectives

Site NGHP-01-17 (Prospectus Site ANGH01) is located at 10° 45.1912'N, 93° 6.7365'E in the Andaman Sea along the eastern coast of the Andaman Islands (figs. 1 and 2). The water depth is ~1,344 m. There has been no record of drilling/coring in this area and the preliminary investigation of the seismic data showed a seismic reflection that could be interpreted as a BSR. However, this reflection occurs at an unusually great depth of ~600 mbsf. The seismic data provided were also not entirely conclusive if this horizon had a reflection polarity that is opposite to that of the seafloor.

The objectives of the work carried out at this site follow the general objectives of the India NGHP Expedition 01:

- Determine if gas hydrate is present at this site and if the BSR-like seismic event is related to gas hydrate;
- Study the occurrence of gas hydrate and establish the background geochemical, geological, geophysical and microbiological baselines for gas-hydrate proxy studies;
- Define the relationship between the sedimentology and structure of the sediments and the occurrence and concentration of gas hydrate;
- Calibrate remote sensing data such as seismic data by acquiring wire-line log data;
- Verify the depositional environment at Site NGHP-01-17.

Two seismic lines are used to describe the seismic-stratigraphy of this site (figs. 3 and 4). Line AN-01-34 (oriented N-S) crosses the site at shot point 1866. The strata appear to generally parallel the seafloor. To the S of the drill site, however, a buried ridge can be seen (shot point 1770) with syndepositional deformation features. Several onlaps are observed below a depth of 2.1 sec TWT; above this depth sediments are mostly seafloor-parallel. This can be interpreted that the ridge may have been uplifted while sedimentation was going on. However, rate of uplift may have slowed (or completely stopped) and sediment draped completely over the ridge. In the perpendicular direction along seismic line AN-01-29, two ridges can be identified with Site NGHP-01-17 in the saddle between the ridges (fig. 5).

A prominent BSR is present in most of the data in this region. However, the depth is estimated at ~600 mbsf, which is unusually deep. Given a water depth of ~1,344 m and assuming a methane/sea-water system as well as similar geothermal gradients as seen off the East and West coast of India, the BSR should be only around 250–300 mbsf. Possible explanations include (a) very low geothermal gradient, (b) the presence of higher hydrocarbons other than just pure methane (that is, Structure-II or Structure-H gas-hydrate formers), and (c) no gas hydrate but a possible opal-CT phase boundary.

Operations

This operations summary covers the Leg 4 transit from Site NGHP-01-16 (step out from Site NGHP-01-07) to Site NGHP-01-17 (ANGH01) and drilling/coring operations for Holes NGHP-01-17A and HNGHP-01-17B (fig. 6). Schedule details and statistics for this site can be found as Appendixes:

- Appendix 1: NGHP Expedition 01 Operations Schedules
- Appendix 2: NGHP Expedition 01 Operations Statistics

Included in the "Methods" chapter and the glossary is a list of standard or commonly used operations terms and acronyms.

Hole NGHP-01-17A

Hole NGHP-01-17A was first occupied on Leg 4 of NGHP Expedition 01. This was the first site to be drilled on the Andaman convergent margin. The 746 NMI move from Site NGHP-01-16 was completed in 71 hr at an average speed of 10.5 knots. The vessel was switched from cruise mode to DP mode at 1526 hr on July 20, 2006, and a positioning beacon was deployed at 1600 hr. The same BHA as was used on previous sites was used for this hole however the drill collars had to be picked up after having been laid out to the storage rack for the long transit to the Andaman operating area.

Hole NGHP-01-17A was planned as a continuous APC/XCB cored hole to 700.0 mbsf with several pressure coring packages targeting the gas-hydrate stability zone (GHSZ). Temperature measurements were also to be taken using the APCT-3, APCT, and DVTP systems to define a thermal gradient from seafloor to TD. Wire-line logging was also planned using the triple combo, FMS-sonic, and VSP tool strings.

The drill string was tripped to bottom. The bit was positioned at a depth of 1,348.0 mbrf for the first spud attempt. Because recovery with the first barrel was less than 1 m the decision was made to re-spud the hole. The bit was lowered 3.0 m to a depth of 1,351.0 mbrf and Hole NGHP-01-17A was

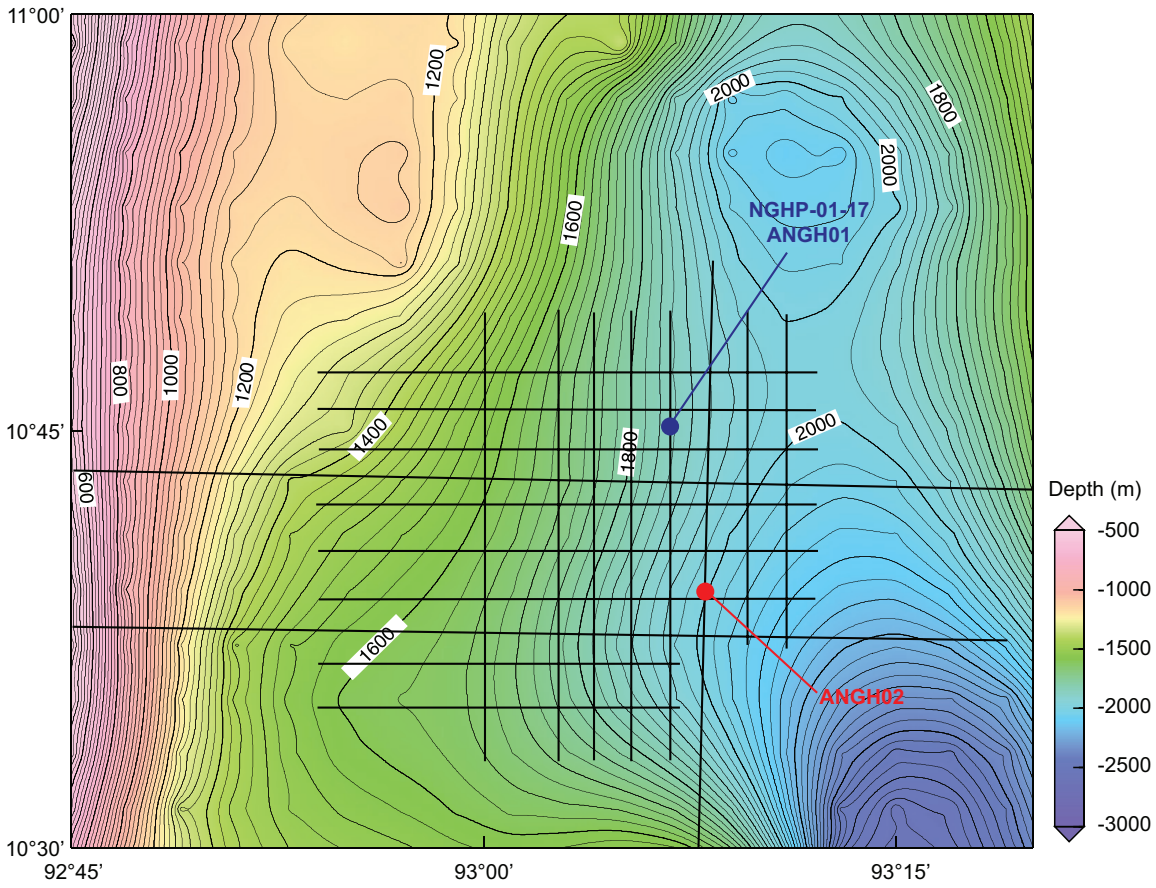


Figure 1. Bathymetric map showing Site NGHP-01-17 in the Andaman area (Prospectus Site ANGH01). Key seismic lines are also shown.

spudded at 2100 hr on July 20, 2006 establishing a seafloor depth of 1,356.0 mbrf. The PDR depth for this site, corrected to the rig floor DES, was 1,358.4 mbrf. APC Core NGHP-01-17A-01H was on-deck at 2110 hr and APC coring continued through Core NGHP-01-17A-13H to a depth of 118.5 mbsf. APC coring was halted after Core NGHP-01-17A-13H when over pulls of 25,000 to 30,000 lbs were reached. However, the primary reason for stopping APC coring was related to core receiving platform safety and core material preservation. Core liners were beginning to swell in the areas of gas pockets and these areas could not be drilled quickly enough to safely relieve the pressure. In addition, core material was rapidly being extruded and lost from the ends of the liners. Historically, the XCB coring process alleviates much of the phenomenon experienced with APC coring.

Three temperature measurements were taken using the APCT-3 shoe on Cores NGHP-01-17A-03H, NGHP-01-17A-05H, and NGHP-01-17A-07H (23.5 mbsf, 42.5 mbsf, and 61.5 mbsf, respectively).

Coring continued using the XCB coring system for Cores NGHP-01-17A-14X through NGHP-01-17A-19X to a depth of 175.5 mbsf. The first pressure core taken using the FPC system (Core NGHP-01-17A-20Y) was cut to a depth of 176.5 mbsf. This was followed by three more XCB cores (NGHP-01-17A-21X through NGHP-01-17A-23X) to a depth of 203.9 mbsf setting up the first DVTP temperature measurement. Thirteen more XCB cores (NGHP-01-17A-24X through NGHP-01-17A-36X) were then cut to a depth of 328.0 mbsf. A series of pressure cores were then taken beginning with the first PCS core (NGHP-01-17A-37P) cut to 329.0 mbsf and the second FPC core (NGHP-01-17A-38Y) cut to 330.0 mbsf. The second DVTP temperature measurement was then taken followed by another four XCB cores (NGHP-01-17A-39X through NGHP-01-17A-42X) to a depth of 366.8 mbsf. A third DVTP temperature measurement was taken before cutting five more XCB Cores NGHP-01-17A-43X through NGHP-01-17A-47X to 412.7 mbsf. This set up the second series of pressure cores beginning with the second PCS Core NGHP-01-17A-48P to 413.7 mbsf followed by the first HRC Core NGHP-01-17A-49E to 414.7 mbsf. The fourth DVTP temperature measurement was then taken followed by another nine XCB Cores NGHP-01-17A-50X through NGHP-01-17A-58X to a depth of 499.6 mbsf. The third series of pressure cores included the third PCS Core NGHP-01-17A-59P cut to a depth of 500.6 mbsf followed by the third FPC Core NGHP-01-17A-60Y cut to a depth of 501.6 mbsf. A fifth DVTP temperature measurement was taken before cutting nine more XCB Cores NGHP-01-17A-61X through NGHP-01-17A-69X to 586.3 mbsf. The fourth series of pressure cores included the fourth PCS Core NGHP-01-17A-70P cut to a depth of 586.8 mbsf. This core was stopped after only 0.5 m of advance due to lack of measurable forward progress for a 15 minute period. The PCS

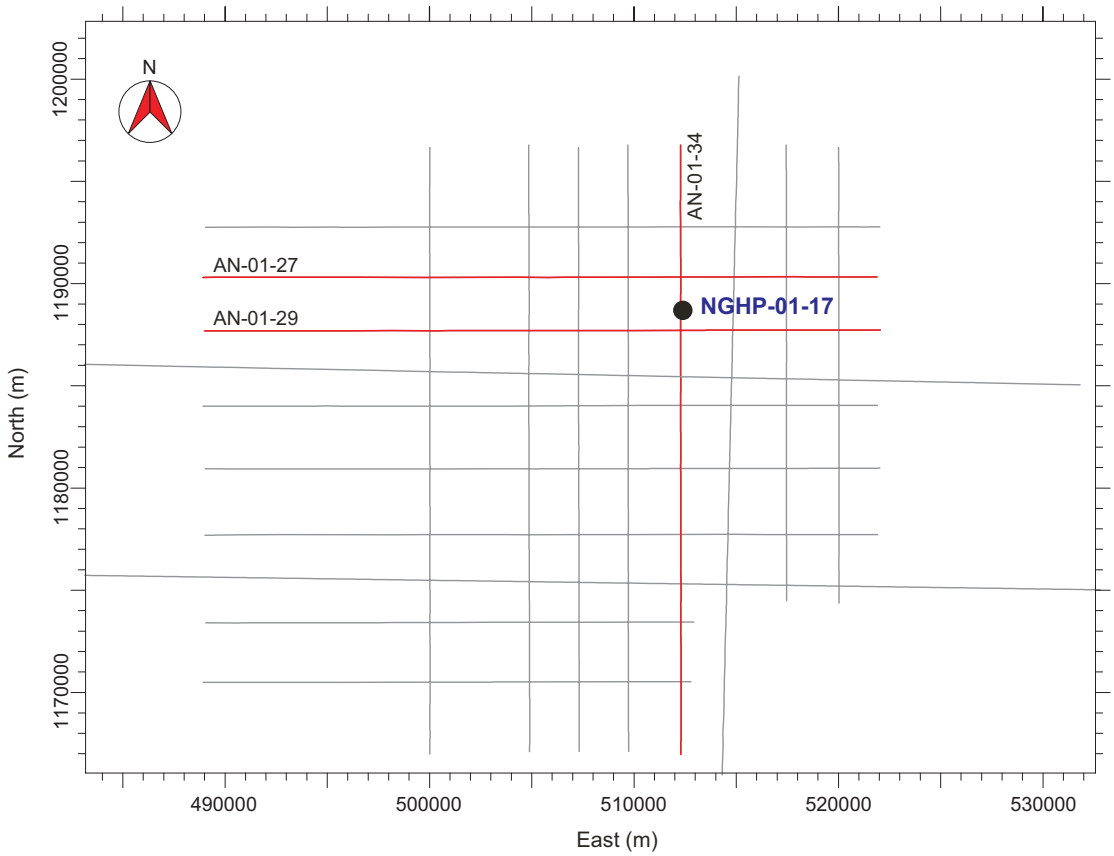


Figure 2. Detailed map of the area in the Andaman Islands showing Site NGHP-01-17 and location of key seismic lines.

core was followed by the second HRC Core NGHP-01-17A-71E cut to a depth of 587.8 mbsf and a sixth DVTP temperature measurement. Four XCB cores (NGHP-01-17A-72X through NGHP-01-17A-75X) were then cut to 625.0 mbsf. A seventh DVTP temperature measurement was taken at this depth before cutting an additional four XCB cores (NGHP-01-17A-76X through NGHP-01-17A-79X) to 662.7 mbsf. Here the eighth and final DVTP measurement was taken. This was followed by a single XCB core (NGHP-01-17A-80X) to 672.3 mbsf and the third HRC pressure Core NGHP-01-17A-81E was cut to 673.3 mbrf. Coring concluded in this hole with the final two XCB cores (NGHP-01-17A-82X and NGHP-01-17A-83X) to a total depth of 691.6 mbsf. The original target depth for this hole was 700.0 mbsf, however core had fallen out of the preceding barrel resulting in an inability to properly land and seat the next core barrel. This core barrel was recovered with hard pieces of remnant core material and the problem was corrected when the following barrel landed correctly. At that point, however, it was decided to minimize risk of hole loss and further coring was terminated.

A total of eight DVTP temperature measurements were taken in this hole; however, two of the last four did not provide good data due to formation cracking. Fortunately, the last measurement, taken at 662.7 mbsf was very good. That measurement, along with another fairly successful measurement at 587.8 mbsf, provided enough data to define an accurate temperature gradient for the hole.

For all HYACINTH pressure coring systems (FPC and HRC), a 15–20 min wait period was employed at the mudline on the way in the hole and again during retrieval. This was to cool the core barrels down thus aiding in keeping any entrained gas hydrate within the stability field. At the rig floor all pressure core barrels (PCS, FPC, and HRC) showing signs of proper actuation were placed in the moon pool ice bath prior to processing.

The hole was swept with 50 bbl of Sepiolite; the top drive was set back after pulling two-stands of drill pipe, and a wiper trip to logging depth and back was made. Seventeen meters of fill on bottom was circulated out of the hole with another 50-barrel Sepiolite mud sweep. The LFV go-devil was deployed and the hole was displaced with 260 barrels of 10.5 ppg Sepiolite mud. The drill pipe was then pulled back positioning the EOP at a logging depth of 62.2 mbsf.

Rig-up for wire-line logging began at 0900 hr on July 26, 2006. The first logging run was made with the triple combo tool suite. This tool string had no trouble exiting the drill pipe; however, a bridge was contacted at 144.0 mbsf. This point also corresponded closely to a core with only 7 percent recovery. After it became evident that the bridge could not be passed, the hole above that point was logged, and the tools were recovered. After tying back the logging sheaves, the EOP was lowered by four-stands to 175.0 mbsf. The triple combo tool suite was then re-deployed. This time the tools were only able to be lowered to 191.0 mbsf, a mere 16.0 m below the bit.

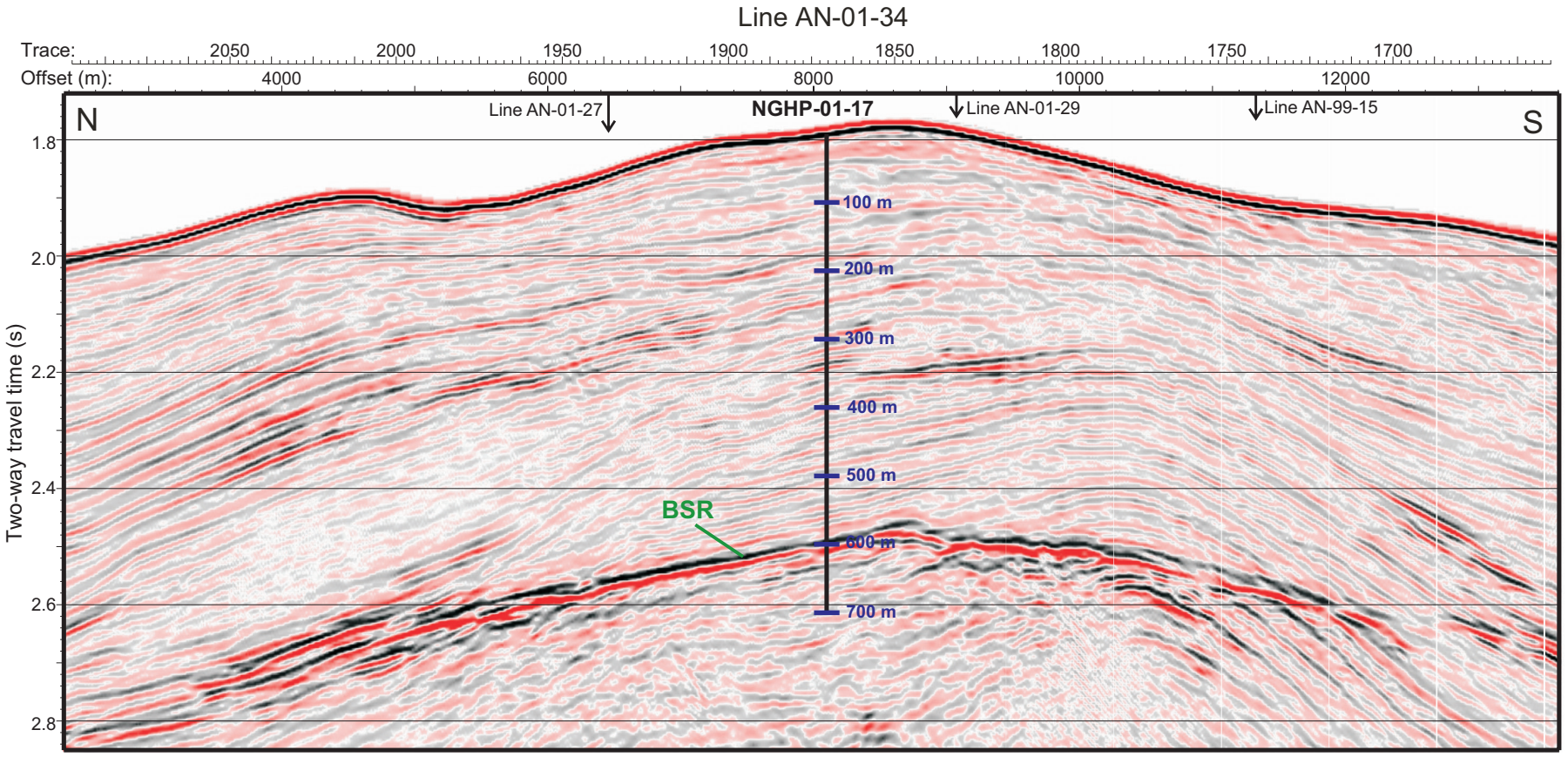


Figure 3. Seismic line AN-01-34 crossing Site NGHP-01-17. Most of the sediments appear to be seafloor parallel with some small inclination. Depths of BSR and formation tops were estimated using a uniform velocity of 1,600 m/s. [BSR, bottom-simulating reflector; m/s, meters per second]

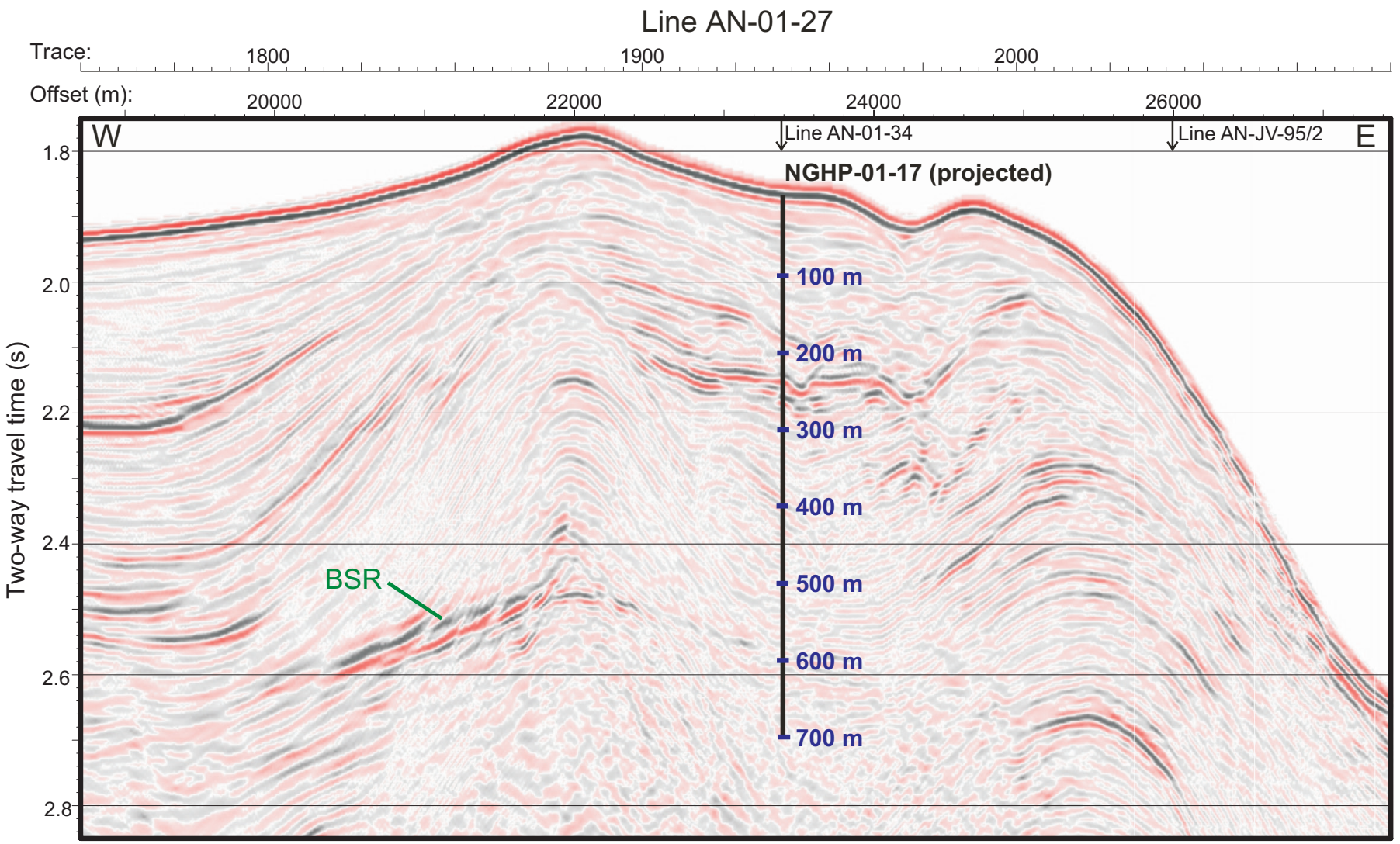


Figure 4. Seismic line AN-01-27 crossing north of Site NGHP-01-17. This line shows prominent ridges with Site NGHP-01-17 located within the saddle between the two ridges.

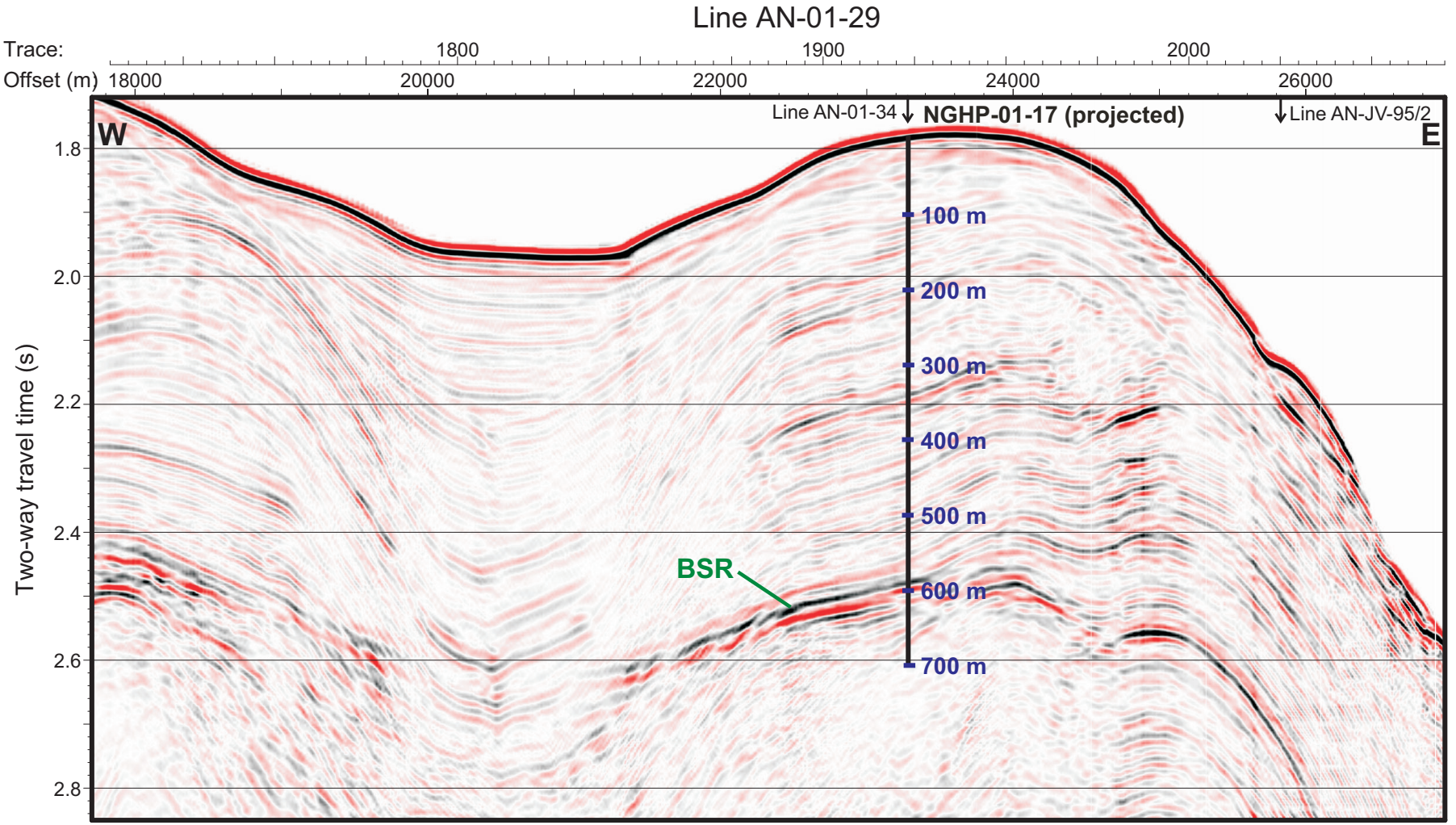


Figure 5. Seismic line AN-01-29 crossing south of Site NGHP-01-17.

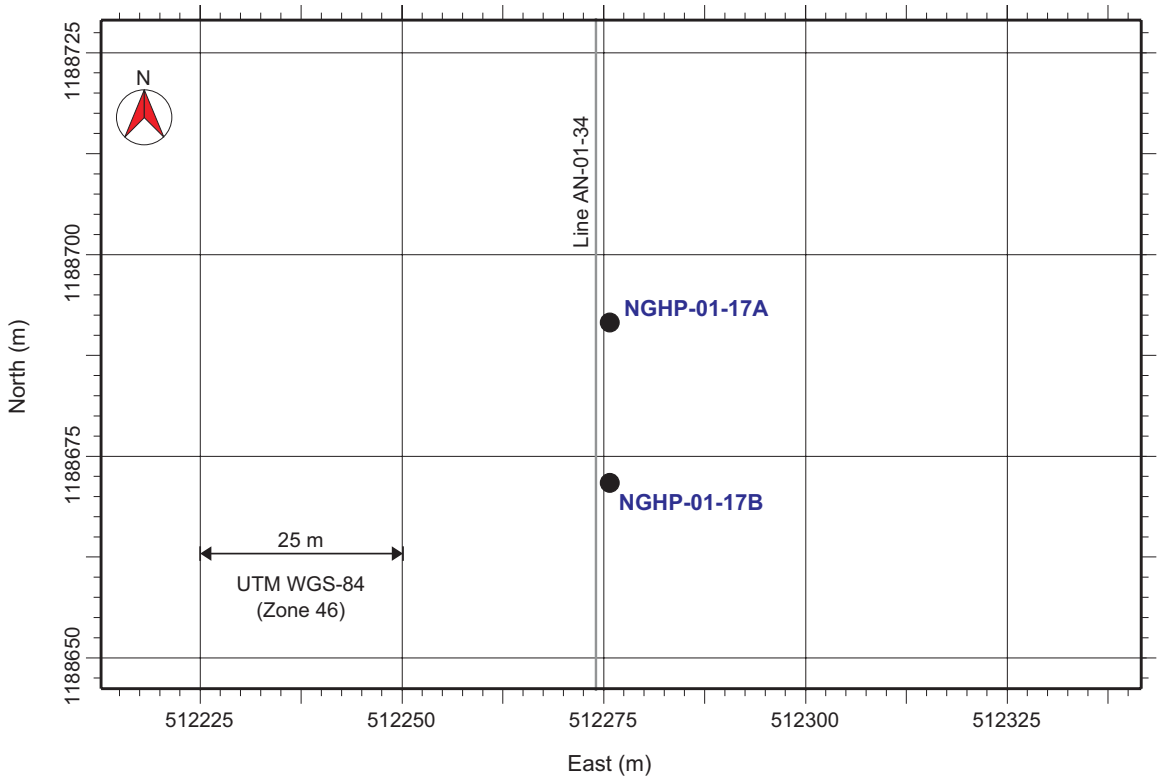


Figure 6. Map showing all holes occupied at Site NGHP-01-17 (ANGH01).

The logging tools were pulled out and laid down by 1815 hr. After rigging down the logging sheaves, the drill string was pulled clear of the seafloor at 2010 hr on July 26th, ending Hole NGHP-01-17A and beginning Hole NGHP-01-17B.

Hole NGHP-01-17B

The vessel was offset 20 m due S of Hole NGHP-01-17A and Hole NGHP-01-17B was spudded at 2100 hr. The same seafloor depth as at Hole NGHP-01-17B was assumed for the new hole. Nine hours were spent drilling to a depth of 270.0 mbsf (at an average net ROP of 30.0 m/h) and another 8.5 hours were spent drilling to a depth of 485.0 mbsf (at an average net ROP of 25.3 m/h). At this point the center bit was recovered, inspected, and re-deployed. Drilling continued for another 7.0 hours (at an average net ROP of 30.7 m/h) to the original target depth of 700.0 mbsf. At this point the decision was made to extend the hole approximately 20.0 meters to ensure that logs could be recovered across the BSR. Due to a significantly slowed ROP, drilling was ultimately halted at 0400 hr at a total depth of 718.0 mbsf. The hole was swept with fifty barrels of Sepiolite, the LFV go-devil was deployed, and the hole was displaced with 260 barrels of 10.5 ppg Sepiolite mud. The drill pipe was then pulled back positioning the EOP at a logging depth of 127.6 mbsf.

Rig-up for wire-line logging began at 0830 hr on 28 July. The first logging run was made with the triple combo tool suite. The tools were unable to pass 237.0 mbsf and were subsequently recovered after logging up from that point. One-half hour was spent securing the logging line and lowering the drill pipe four-stands to a depth of 270.0 mbsf. The triple combo tools were made up a second time and this time reached the total hole depth of 718.0 mbsf. Tools were out and laid down by 2000 hr. The second tool suite consisted of the FMS-sonic. This tool string also reached TD and the tools were out and laid down by 0430 hr on July 29, 2006. The VSP logging tools were deployed third in the sequence. This tool reached 629.0 mbsf and logs were recovered above that point. Once VSP operations were completed, the tools were recovered, and the wire-line sheaves were rigged down by 1630 hr. As on earlier sites, all VSP operations were conducted while adhering to the IODP policies and mammal protection guidelines. The drill string was pulled clear of the seafloor at 1645 hr. The pipe trip continued back to the surface and the BHA/drill collars were laid down in anticipation of the pending 727 NMI (2.9 day) transit to the Mahanadi (MNGH) drill sites. The beacon was recovered at 1733 hr. Thrusters were raised and the rig was secured for transit. The vessel got underway for Site NGHP-01-18 (MNGH-Reliance 5) at 2030 hr on July 29, 2006. This officially completed operations at Site NGHP-01-017 and the Andaman operating area.

Lithostratigraphy

Site NGHP-01-17 was the first and only site located offshore of the Andaman Islands. Hole NGHP-01-17A was drilled, and cored to a total depth of 691.6 mbsf. An offset well (NGHP-01-17B) was subsequently drilled to 718 mbsf and wire-line logged (see “Operations”).

We divide the sedimentary sequence recovered at Hole NGHP-01-17A into one main lithostratigraphic unit (Unit I, with three Subunits: Ia, Ib, and Ic; figs. 7A, 7B, and 7C, and Site NGHP-01-17 Visual Core Descriptions) based on sedimentological criteria (that is, variations in lithology and grain size), physical properties (for example, magnetic susceptibility and density) and wire-line logging data (for example, wire-line density). We also integrate the core data with the available seismic data to help define and interpret the stratigraphic section cored at Site NGHP-01-17. Although the vast majority of the stratigraphic sequence cored at Site NGHP-01-17 consists of nannofossil oozes, there are distinct changes in the abundance of foraminifera and siliceous microfossils that help to distinguish the Subunits at this site (figs. 7A, 7B, and 7C, and Site NGHP-01-17 Visual Core Descriptions). Preliminary biostratigraphic work suggests that the age at the bottom of the hole is ~12.3 Ma (see below).

Lithostratigraphic Units

Lithostratigraphic Unit I

Intervals: Hole NGHP-01-17A, Sections NGHP-01-17A-01H-1 to NGHP-01-17A-23X-CC

Depth: Hole NGHP-01-17A, 0–691.6 mbsf

Age: ~Late Miocene to Recent

In Lithostratigraphic Unit I, core recovery was good for the upper ~145 mbsf, including APC Cores NGHP-01-17A-01H to NGHP-01-17A-13H and the first three XCB Cores, NGHP-01-17A-14X to NGHP-01-17A-16X. From ~145 mbsf to the base of Unit I, recovery was slightly poorer (fig. 7 and Site NGHP-01-17 Visual Core Descriptions), possibly due in part to gas-hydrate occurrence (see "Gas-Hydrate Occurrence"). Based on changes observed in the carbonate and biogenic silica content of the sediments, Unit I was subdivided into three Subunits (Ia, Ib, and Ic) that are described below.

Subunit Ia

Intervals: Hole NGHP-01-17A, Sections NGHP-01-17A-01H-1 to NGHP-01-17A-15X-CC

Depth: Hole NGHP-01-17A, 0–136.8 mbsf

Age: Late Pliocene to Recent

Lithostratigraphic Subunit Ia (figs. A and 7B) is composed of foraminifera-rich and foraminifera-bearing nannofossil ooze that ranges in color from greenish grey (10GY 5/1) to dark greenish grey (10Y 4/1 and 5GY 5/1; fig. 7 and Site NGHP-01-17 Visual Core Descriptions). Two biostratigraphic datums were used to estimate a preliminary chronology for this Subunit. The first occurrence (FO) of the planktonic foraminifera *Globigerinoides ruber*, pink var. (at ~23 mbsf at Site NGHP-01-17) is at 0.4 Ma (Thompson and others, 1979). Using this first datum, we calculate a mean sedimentation rate of 5.75 cm/kyr for the upper 23 mbsf (fig. 8). The second datum used is the last occurrence of the calcareous nannofossil group *Discoaster* spp. at 108 mbsf, which approximately marks the Pliocene-Pleistocene boundary (~2 Ma). The sedimentation rate calculated for the upper of 108 mbsf using this second datum is 5.4 cm/kyr, which is similar to the sedimentation rate for the upper 23 mbsf. The extrapolation to the bottom of Subunit Ia of an average 5.6 cm/kyr suggests a Late Pliocene to Recent age for Subunit Ia. Additional post-cruise nannofossil biostratigraphy, however, may help refine this initial estimate.

Visible foraminifera tests and calcareous shell fragments occur throughout Subunit Ia (figs. 7A, 7B and Site NGHP-01-17 Visual Core Descriptions); they are also abundant in smear slides (table 1) and, particularly, in the coarse fraction (table 2). Rare occurrences of woody debris are also observed in four locations throughout the Subunit (fig. 7B and Site NGHP-01-17 Visual Core Descriptions). Authigenic carbonates (likely calcite crystals) are observed in significant abundance in the clay size fraction in smear slides from Core NGHP-01-17A-15X (figs. 7A, 7B, Site NGHP-01-17 Visual Core Descriptions and table 1). These precipitates appear to have significantly cemented the surrounding sediments, producing more lithified sediments that were more difficult to drill (see "Operations"). Bioturbation is abundant and iron sulfide and pyrite precipitates are common throughout the entire Subunit (figs. 7A and 7B, and Site NGHP-01-17 Visual Core Descriptions). Down-core magnetic susceptibility values (figs. 7A and 7B) remain low throughout Subunit Ia and show very little variability, consistent with the homogeneous nature of the sediments throughout the Subunit. A subtle high in magnetic susceptibility near the top of the Subunit may be due to the presence of ferrimagnetic, metastable iron monosulfides (gregite or pyrrhotite).

The major lithologies of Lithostratigraphic Subunit Ia, determined from smear slides, consist primarily of clay-sized (70–100 percent) grains with minor amounts of silt-sized grains (up to 30 percent; table 1). Minor lithologies described in smear slide include volcanic ashes, iron sulfide-rich zones, and organic-rich intervals. The volcanic ash beds vary in color (including light gray, white, and pink) and are present either as beds, bioturbated beds, burrow fills, or disseminated in sediments sporadically throughout Subunit Ia (figs. 9 and 10 and table 3).

Non-biogenic components identified in smear slides are only present in low amounts (trace to 5 percent) in the major lithologies, but increase in the ashes (table 1). The only major exception to this is the presence of pyrite, which increases in abundance near the bottom of the Subunit. The total biogenic component of the sediment is dominated by calcareous nannofossils, which comprise 52 percent to 97 percent of the total (biogenic and non-biogenic) sediment grains (table 1). Foraminifera occur (trace to 60 percent) in smear slides; however, they are more abundant (30 percent to 87 percent) in the coarse fractions of the sediments (table 2) throughout the Subunit. As noted above, authigenic carbonate precipitates were observed in smear slides near the bottom of the Subunit in Core NGHP-01-17A-15X (table 1).

Subunit Ib

Intervals: Hole NGHP-01-17A,
Sections NGHP-01-17A -16X-1
to NGHP-01-17A-38X-3

Depth: Hole NGHP-01-17A, 136.8–334.5 mbsf

Age: ~Late Miocene to Late Pliocene

Lithostratigraphic Subunit Ib (figs. 7A and 7B, and Site NGHP-01-17 Visual Core Descriptions) is composed primarily of nannofossil ooze; however, in places, authigenic carbonate-rich and carbonate-bearing nannofossil ooze (Cores NGHP-01-17A-17X and NGHP-01-17A-23X) and foraminifera-bearing nannofossil ooze (Core NGHP-01-17A-20Y) are observed. Sediments range in color from greenish grey (10GY 5/1) to dark greenish grey (10Y 4/1; 10GY 4/1; and 5GY 4/1). Visible foraminifera tests and calcareous shell fragments occur discontinuously throughout the upper part of Subunit Ib (figs. 7A and 7B, and Site NGHP-01-17 Visual Core Descriptions) and are also identified in smear slides (table 1) and coarse fraction descriptions (table 2). However, in the coarse fraction, unbroken foraminifera tests decrease in abundance compared to the overlying Subunit Ia (fig. 8 and table 2). There is also a small increase in the amount of total biosiliceous components present in both smear slides and coarse fraction descriptions (tables 1 and 2). Authigenic carbonates (likely calcite or dolomite crystals) are observed in significant abundance in the clay size fraction in smear slides from Core NGHP-01-17A-17X, Core NGHP-01-17A-18X, and Cores NGHP-01-17A-22X through NGHP-01-17A-27X (figs. 7A and 7B, Site NGHP-01-17 Visual Core Descriptions, and table 1). Again, drilling was difficult through sediments rich in authigenic carbonates, which suggests cementation and lithification of these zones (see "Operations" and "Downhole Logging"). Bioturbation is common throughout most of the Subunit. Pyrite and other iron sulfide minerals are common throughout Subunit Ib and visible on the split core surfaces and in smear slides (figs. 7A and 7B, Site NGHP-01-17 Visual Core Descriptions, and table 1) and increase substantially in the coarse fraction relative to the overlying Subunit (table 2). Magnetic susceptibility (figs. 7A and 7B) remained low and showed little variation throughout Subunit Ib. Volcanic ash was a far less common occurrence in Subunit Ib than in Subunit Ia (fig. 10 and table 3). Volcanic ashes, light gray or white colored, are present either as discontinuous beds, bioturbated beds, burrow fills, or disseminated through sediments intermittently throughout Subunit Ib (figs. 9 and 10, and table 3).

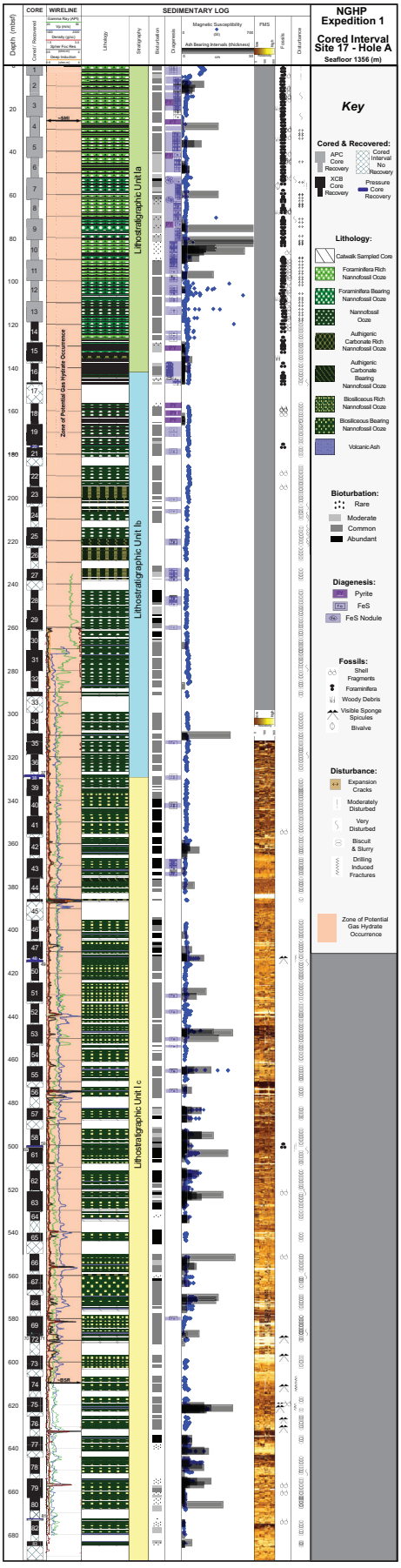
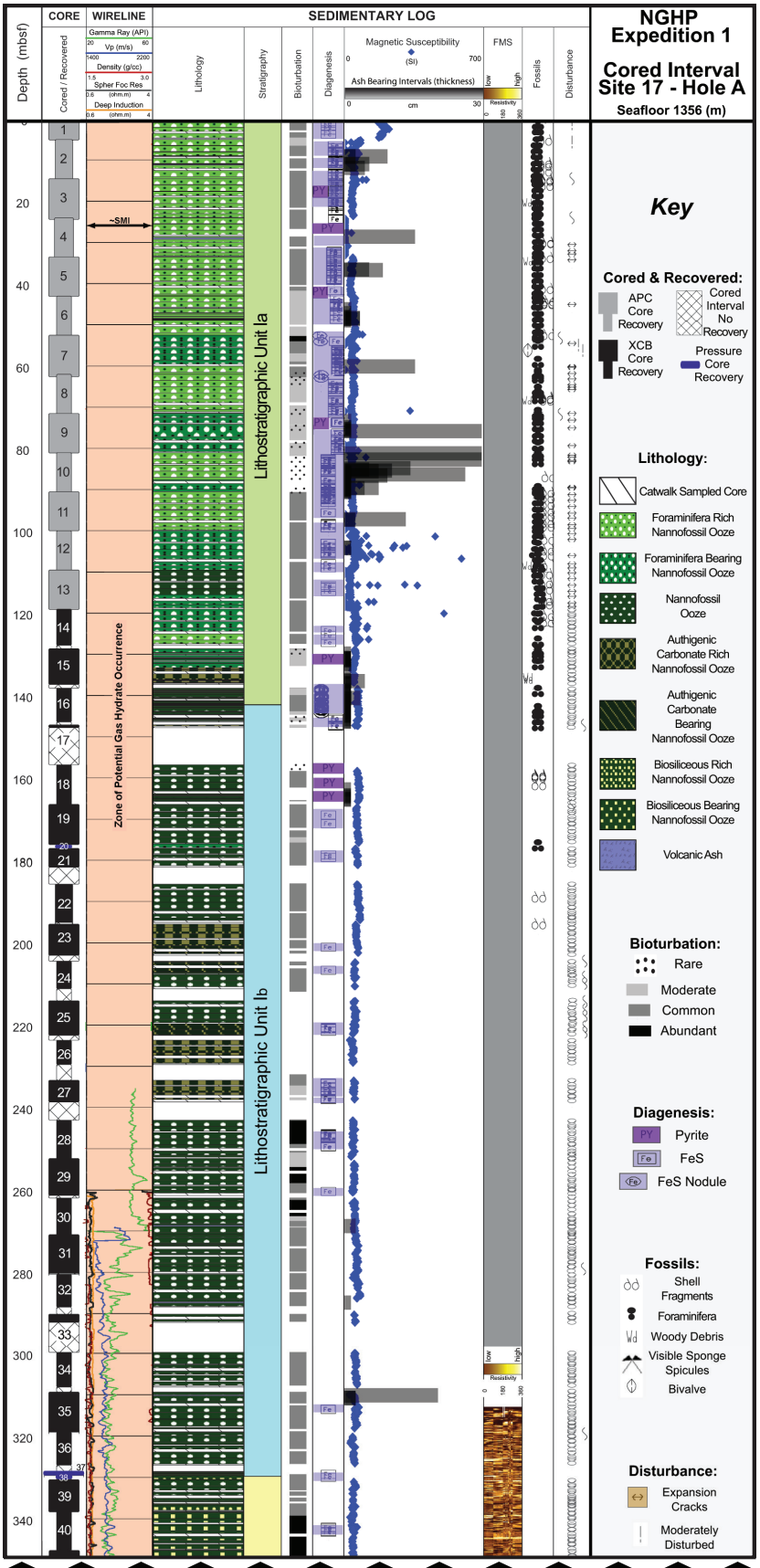
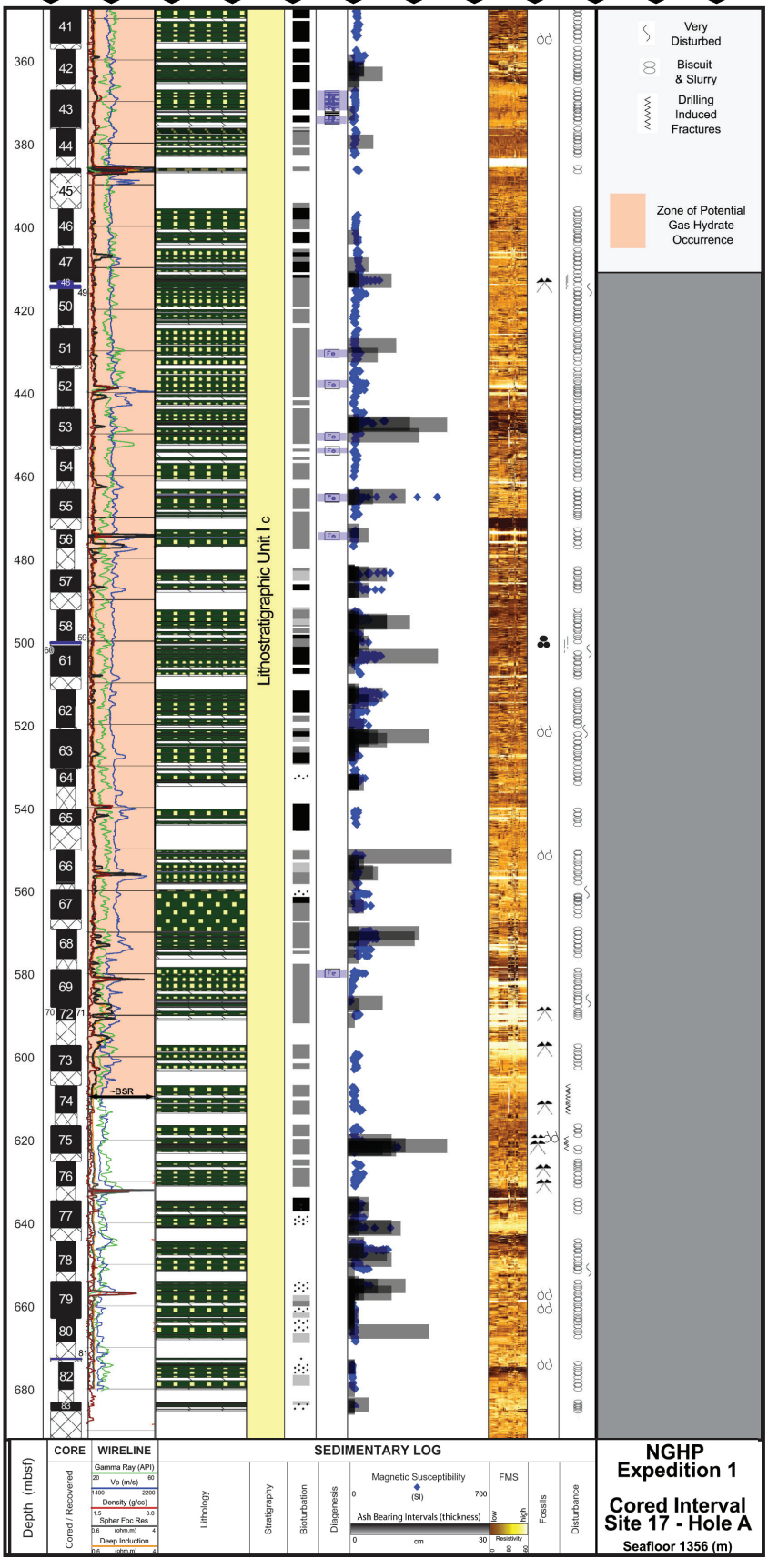


Figure 7 (facing and following pages). A, Lithostratigraphic summary of Hole NGHP-01-17A. B and C show an expanded scale of A. Note: Colored intervals exceed symbol size when there is a range in the occurrence. Center point of each symbol represents depth of occurrence; therefore, colored bars may slightly exceed core recovery; see Site NGHP-01-17 Visual Core Descriptions for the expanded scale, detailed core descriptions; see Site NGHP-01-17 Oversized Figure for the enlarged versions of this summary. [BSR, bottom-simulating reflector; FMS, formation micro scanner; RAB, resistivity-at-bit; SMI, sulfate-methane interface]



LOG CONTINUES ON NEXT PAGE

LOG CONTINUED FROM PREVIOUS PAGE



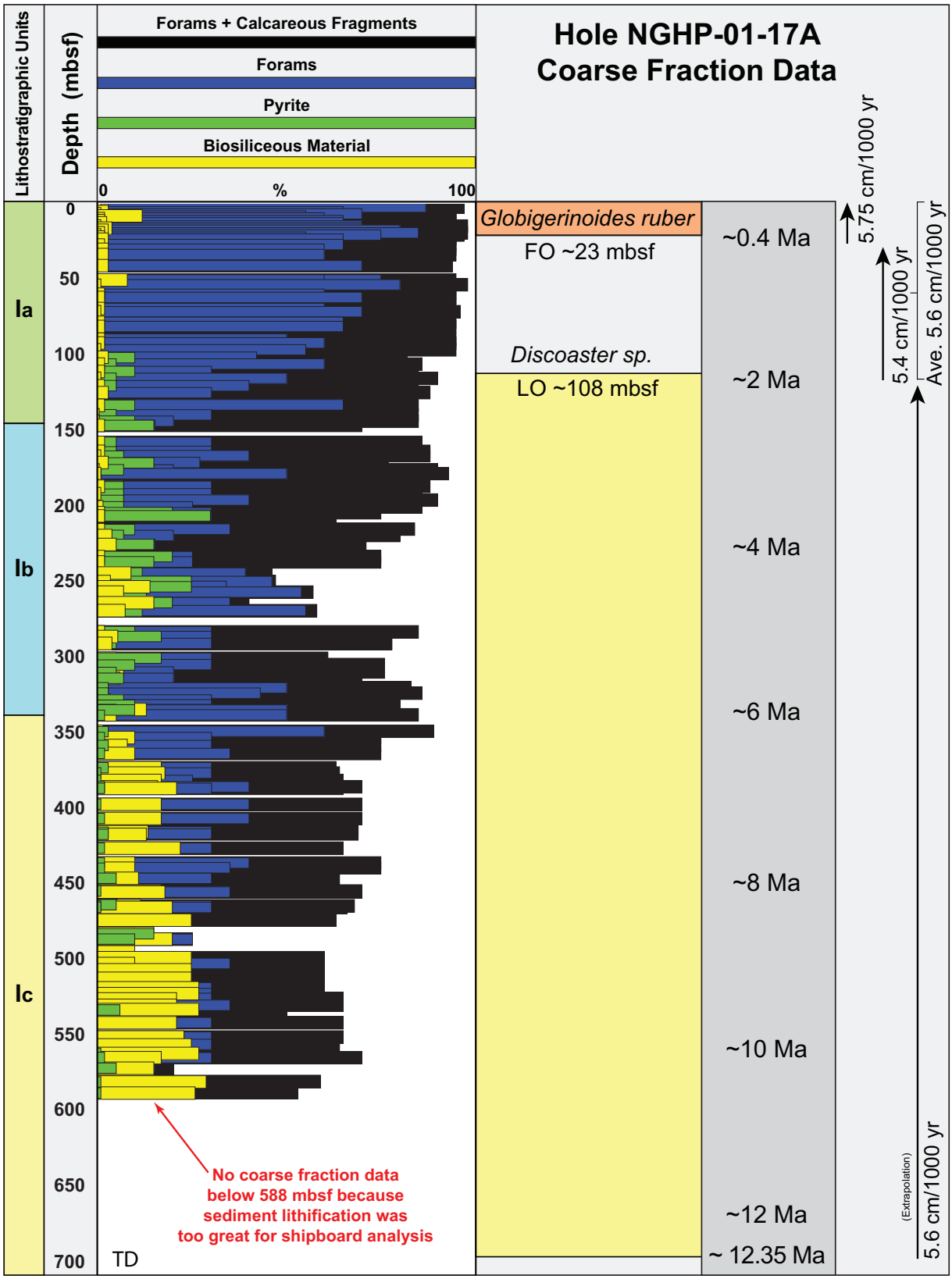


Figure 8. A, Summary plot of coarse fraction (>63 µm) showing the relative abundances of foraminifera, total calcareous and total biosiliceous materials, and pyrite at Site NGHP-01-17. The positions of the first occurrence of *Globigerinoides ruber* and the last occurrence of *Discoaster* spp. and the calculated sedimentation rates are also shown. We extrapolate the ages to the bottom of the hole using the average sedimentation rate constrained by the last occurrence of *Discoaster* spp. and the first occurrence of *Globigerinoides ruber*. B, Coarse fraction results plotted individually with depth.

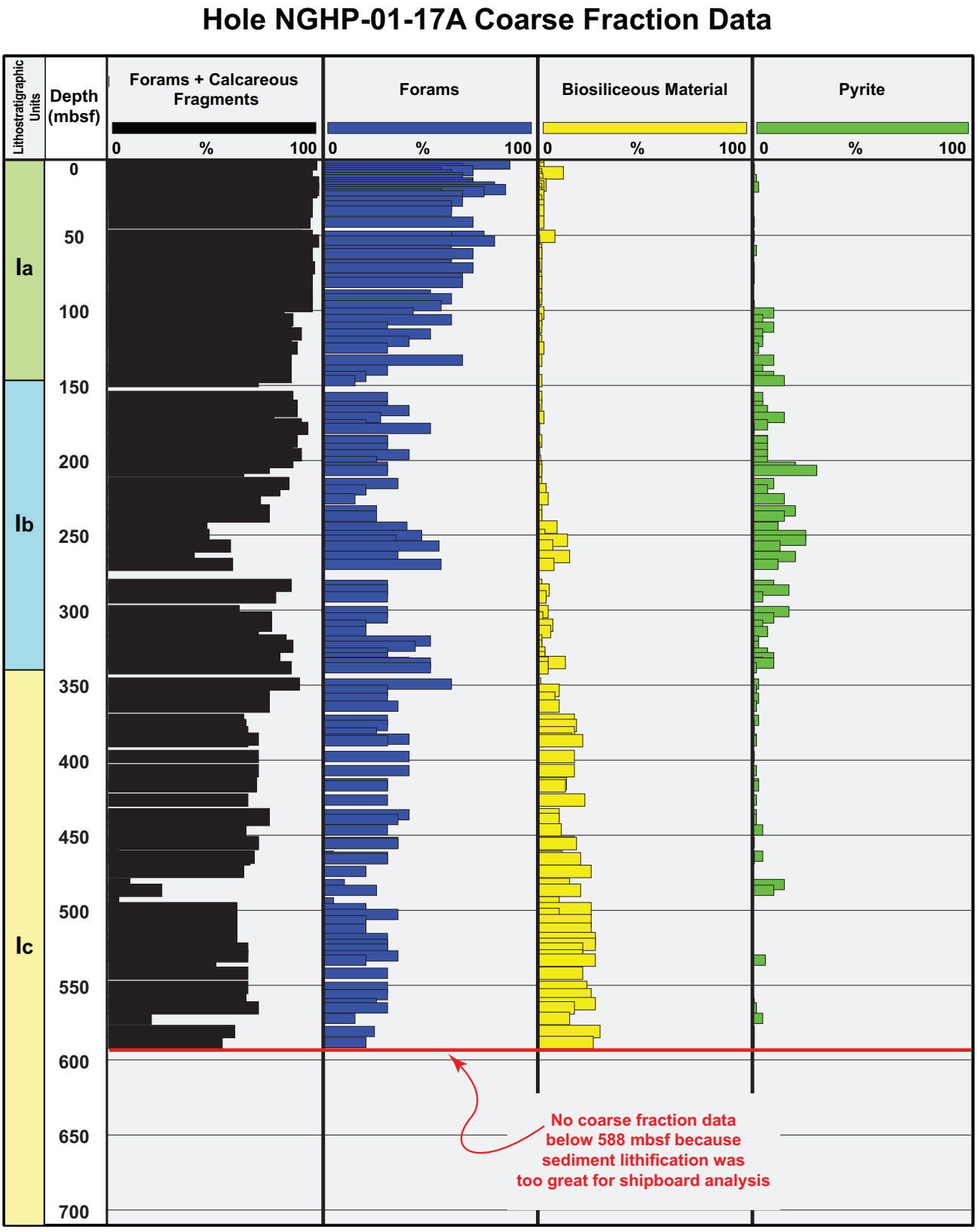


Figure 8. A, Summary plot of coarse fraction (>63 µm) showing the relative abundances of foraminifera, total calcareous and total biosiliceous materials, and pyrite at Site NGHP-01-17. The positions of the first occurrence of *Globigerinoides ruber* and the last occurrence of *Discoaster* spp. and the calculated sedimentation rates are also shown. We extrapolate the ages to the bottom of the hole using the average sedimentation rate constrained by the last occurrence of *Discoaster* spp. and the first occurrence of *Globigerinoides ruber.* B, Coarse fraction results plotted individually with depth.—Continued

Table 1. Smear slide data for Hole NGHP-01-17A.

Sample reference		Texture			Mineral										
Core, section, depth (cm, in section)	Lithology	Sand	Silt	Clay	Quartz	Feld-spar	Mica	Heavy minerals	Clay minerals	Volcanic glass	Opaques	Iron sulfides	Fram-boidal pyrite	Rock fragments	Authigenic carbonates
NGHP-01-17A															
1H-2, 60	D		30	70						2					1
2H-2, 80	D		20	80		trace	trace			2					
2H-3, 85	D		15	85		1	1			2					
2H-3, 90	M		100		5	3	7			82					
2H-3, 109	M		70	30		1	3			37					
2H-4, 133	M		20	80	trace	trace				5					
2H-5, 80	D		15	85		trace	trace	1		1					
3H-2, 80	D		15	85		trace	trace			1					
3H-6, 80	D		20	80											
4H-4, 70	D		15	85	trace		trace			trace			1		
4H-4, 104	M		100		2	1	1			96		trace			
4H-4, 139	M		10	90	trace		trace			35					
4H-6, 80	D		10	90											
5H-2, 80	D		10	90	trace										
5H-3, 82	M	60	40							5		85			
5H-6, 80	D	8		92											
6H-1, 82	D		10	90						3		1			
6H-6, 64	D		5	95	1		1								
7H-2, 52	D		15	85											
7H-6, 60	D		7	93											
7H-4, 50	M	5	80	15								85			
8H-1, 66	D		3	97	5			3				2		3	
8H-6, 60	D		3	97	3			3							2
9H-1, 80	D		5	95											
9H-6, 70	D		3	97											
10H-1, 95	D		8	92	1										
10H-5, 34	D		5	95	1										
10H-5, 28	D		3	97											
10H-6, 88	M		90	10						79			1		
10H-7, 40	D		2	98											
11H-2, 77	D		15	85			trace			2					
11H-2, 63	M		20	80		1	1			5					
11H-5, 75	D		15	85			trace			1					
12H-2, 90	D		10	90			trace			1					
12H-6, 70	D		7	93			trace			1					
12H-7, 24	M		65	35			1			1					
13H-2, 70	D		5	95	1	1	trace			trace		trace		trace	
13H-5, 70	D		5	95	2	trace						trace			
14X-2, 70	D		7	93	3	2						trace			
14X-5, 70	D		15	85	5	5	trace					trace		trace	
15X-1, 60	D		20	80			trace			trace			trace		
15X-5, 73	D		7	93						1			trace		40
16X-2, 70	D		1	99	trace	trace				trace					
16X-5, 55	D		2	98									trace		
17X-1, 21	D		1	99	1				10				1		7
18X-2, 43	D		5	95						trace		2			3
18X-6, 88	D		3	97			trace			trace					trace
19X-2, 70	D		2	98						trace		trace			
19X-5, 70	D		2	98						trace		trace			trace
20Y-1, 51	M		10	90									trace		
20Y-1, 61	D		3	97	trace	trace									

Table 1. Smear slide data for Hole NGHP-01-17A.—Continued

Sample reference		Biogenic									
Core, section, depth (cm, in section)	Lithology	Foraminifera	Nannofossils	Carbonate shell fragments	Diatoms	Radiolarians	Silicoflagellates	Siliceous shell fragments	Sponge spicules	Plant debris	Comments
NGHP-01-17A—Continued											
1H-2, 60	D	10	75	10					2		Trace discoasters
2H-2, 80	D	12	82	3			trace		1		Trace discoasters, altered pyroxene
2H-3, 85	D	6	82	5				2	1		Trace apatite, trace discoasters
2H-3, 90	M	trace	3								From ash, trace altered olivine
2H-3, 109	M	5	50	3					1		Trace tourmaline
2H-4, 133	M	4	85	5					1		Trace discoasters, trace tourmaline
2H-5, 80	D	10	75	12					1		Trace discoasters, trace tourmaline
3H-2, 80	D	7	85	5				1	1	trace	Trace discoasters, trace tourmaline
3H-6, 80	D	15	84						1		
4H-4, 70	D	10	87	1					1		Trace discoasters
4H-4, 104	M										
4H-4, 139	M	5	60						trace		Trace discoasters
4H-6, 80	D	30	70								Trace discoasters, many broken
5H-2, 80	D	30	69						1		Trace discoasters
5H-3, 82	M	10									
5H-6, 80	D	20	80								Trace discoasters
6H-1, 82	D	60	32						2	2	Trace discoasters
6H-6, 64	D	20	70						3	5	Trace discoasters
7H-2, 52	D	7	93								Trace discoasters
7H-6, 60	D	15	85						trace		Trace discoasters
7H-4, 50	M	15									Trace discoasters
8H-1, 66	D	20	62						2	3	Trace discoasters
8H-6, 60	D	20	70						2		Trace discoasters
9H-1, 80	D	10	90								Trace discoasters
9H-6, 70	D	5	94						1		Trace discoasters
10H-1, 95	D	33	65						1		Trace discoasters
10H-5, 34	D	10	89						trace		Trace discoasters
10H-5, 28	D	5	95						trace		Trace discoasters, possible fish remains
10H-6, 88	M	20									
10H-7, 40	D	10	90						trace		Trace discoasters
11H-2, 77	D	5	81	10					2		Trace discoasters
11H-2, 63	M	5	77	10			trace		1		Trace discoasters
11H-5, 75	D	7	83	7			trace		2		Trace discoasters
12H-2, 90	D	3	90	3				1	2	trace	Trace discoasters
12H-6, 70	D	4	91	3					1		Trace discoasters, trace tourmaline, trace olivine
12H-7, 24	M	trace	37	1						60	First appearance of substantial discoasters, 1% of nannofossils
13H-2, 70	D	1	97						trace		Polycrystalline quartz and feldspar lithic fragments, 1-2% discoasters
13H-5, 70	D	5	93						trace		Feldspars are altering, discoasters 1.5% of nannofossils
14X-2, 70	D	7	88						trace		Foraminifera silt and clay sized, trace discoasters
14X-5, 70	D	10	80						trace		Foraminifera silt and clay sized, 1% discoasters, polycrystalline quartz
15X-1, 60	D	3	86	10	trace	trace			1		Trace dolomite or calcite rhombs., discoasters 20% of nannofossils
15X-5, 73	D	2	52	5					trace		Discoasters 20% of nannofossils, authigenic carbonate is calcite
16X-2, 70	D	3	97								Trace discoasters, polycrystalline quartz
16X-5, 55	D	3	97								Foraminifera mostly in fragments
17X-1, 21	D		81								Discoasters 1.5% of nannofossils, authigenic carbonate is calcite
18X-2, 43	D	3	85	7							Trace dolomite or calcite rhombs., discoasters 20% of nannofossils
18X-6, 88	D	trace	97	3				trace			Discoasters 20% of nannofossils
19X-2, 70	D	trace	98	2				trace			Discoasters 30% of nannofossils
19X-5, 70	D	trace	98	2				trace	trace		
20Y-1, 51	M	99	1								From concentration of foraminifera
20Y-1, 61	D	7	93								Discoasters 1% of nannofossils

Table 1. Smear slide data for Hole NGHP-01-17A.—Continued

Sample reference		Texture			Mineral										
Core, section, depth (cm, in section)	Lithology	Sand	Silt	Clay	Quartz	Feld-spar	Mica	Heavy minerals	Clay minerals	Volcanic glass	Opaques	Iron sulfides	Fram-boidal pyrite	Rock fragments	Authigenic carbonates
NGHP-01-17A—Continued															
20Y-1, 70	D		3	97		trace									
21X-2, 39	D		30	70						10					
21X-2, 70	D		6	94						1					
22X-2, 70	D		4	96						trace		trace			
22X-6, 70	D		7	93						trace					
22X-1, 53	M		20	80						3					
22X-2, 10	M		10	90						2					7
22X-6, 64	M		7	93						4					
23X-2, 38	D		7	93						1		trace			
23X-2, 70	D		2	98						2		trace			40
23X-5, 70	D		2	98						trace					9
24X-2, 70	D		2	98	1	1									8
24X-4, 25	D		3	97	1	1			1						2
25X-2, 70	D		1	99	trace	trace							1		3
25X-5, 70	D		2	98	2	trace				trace		trace			8
25X-6, 37	M		2	98	1	1			10	trace		50			5
26X-2, 110	D		10	90											40
27X-1, 87	D		5	95	trace					trace		5		trace	15
27X-4, 22	D		5	95	trace					trace		trace			30
28X-2, 67	D		10	90											
28X-6, 17	M		1	99					5	5					
29X-2, 54	D		1	99						trace		trace			
29X-5, 21	D		1	99					1	trace		trace			
30X-3, 59	D		1	99						trace					
30X-5, 64.5	M		3	97						trace					
30X-7, 129	D		2	98						trace		trace			
31X-2, 53	D		2	98						trace					
31X-5, 90	D		2	98				trace		trace					
32X-3, 38	D		2	98				trace		trace					
32X-6, 36	M		15	85		1	1			8					
32X-6, 66	M		20	80		trace			trace	10					
33X-2, 12	D		2	98						trace					
34X-2, 28	D		1	99						trace					
35X-2, 61	D		1	99					1						
35X-5, 60	D		2	98	1	trace			1	trace					2
36X-5, 68	D		10	90	trace	trace			2						
36X-2, 99	D		9	91	trace	trace			1						
37P-1, 66	D		7	93		trace				trace				2	
38Y-1, 38	D		15	85						1				2	
39X-2, 38	D		8	92	1	1									
39X-4, 34	D		24	76	1	1									trace
39X-6, 13	D		20	80	trace	trace									trace
40X-2, 56	D		20	80						trace					
40X-7, 50	D		10	90						trace					
41X-2, 54	D		10	90											
41X-5, 37	D		3	97						trace					
42X-2, 65	M		7	93						90					
42X-2, 84	D		7	93						trace					
42X-6, 49	D		5	95						trace					
42X-7, 24	M		2	98						98		trace			
43X-2, 46	D		5	95	trace					trace		trace			10
43X-7, 37	D		9	95						trace		trace			5
43X-7, 84	D		10	90	trace					trace					10
44X-5, 89	D		5	95	trace					trace		trace			5
45X-1, 34	D		10	90	trace							5			25

Table 1. Smear slide data for Hole NGHP-01-17A.—Continued

Sample reference		Biogenic									
Core, section, depth (cm, in section)	Lithology	Foraminifera	Nannofossils	Carbonate shell fragments	Diatoms	Radiolarians	Silicoflagellates	Siliceous shell fragments	Sponge spicules	Plant debris	Comments
NGHP-01-17A—Continued											
20Y-1, 70	D	5	95								Trace discoasters, foraminifera in tests and fragments
21X-2, 39	D	1	86	3							Discoasters 20% of nannofossils
21X-2, 70	D	1	93	5				trace			Discoasters 20% of nannofossils
22X-2, 70	D	1	97	2				trace			Discoasters 20% of nannofossils
22X-6, 70	D	trace	97	3				trace	trace		Discoasters 20% of nannofossils
22X-1, 53	M	1	91	5					trace		Discoasters 20% of nannofossils
22X-2, 10	M	1	85	5	trace			trace		trace	Discoasters 20% of nannofossils
22X-6, 64	M	1	89	5			trace	1	trace		Discoasters 20% of nannofossils
23X-2, 38	D	trace	95	3				1			Discoasters 20% of nannofossils
23X-2, 70	D		57	1				trace	trace		Authigenic carbonate is dolomite or calcite rhombs, discoasters 20% of nannofossils
23X-5, 70	D		90	trace				1			Authigenic carbonate is dolomite or calcite rhombs, discoasters 20% of nannofossils
24X-2, 70	D	trace	89		trace	trace	trace		1	trace	Discoasters 1% of nannofossils
24X-4, 25	D	trace	94						1		Authigenic carbonate is dolomite or calcite rhombs, discoasters 20% of nannofossils
25X-2, 70	D	trace	92		2				2		Authigenic carbonate is dolomite or calcite rhombs, discoasters 20% of nannofossils
25X-5, 70	D	trace	86		1	trace			3	trace	Discoasters 4% of nannofossils
25X-6, 37	M	trace	32						1	trace	Authigenic carbonate is dolomite or calcite rhombs, discoasters 1% of nannofossils
26X-2, 110	D		57		1				2		Authigenic carbonate is dolomite or calcite rhombs, discoasters 2.5% of nannofossils
27X-1, 87	D	3	57		5		5		10		
27X-4, 22	D	trace	62		trace		5		3	trace	Discoasters 6.5% of nannofossils
28X-2, 67	D		98	trace	1				1		
28X-6, 17	M		84		2	1			3		Discoasters 1% of nannofossils
29X-2, 54	D		89		6				5		Discoasters 3.5% of nannofossils
29X-5, 21	D	trace	94		2				3		Discoasters 2.5% of nannofossils
30X-3, 59	D		98		1		trace		1		Discoasters 3% of nannofossils
30X-5, 64.5	M	trace	98		1				1		From lighter colored burrow, discoasters 1% of nannofossils
30X-7, 129	D		97		1		trace		2		Discoasters 5% of nannofossils
31X-2, 53	D	1	97			trace			2		Discoasters present
31X-5, 90	D	1	99				trace		trace		Discoasters present
32X-3, 38	D	1	98			trace			1		Discoasters present
32X-6, 36	M	1	88			trace			1		Trace pyroxene
32X-6, 66	M		89						1		
33X-2, 12	D	trace	98		trace	trace			2		Discoasters present
34X-2, 28	D	trace	99			trace			1		Discoasters present
35X-2, 61	D		96		1	1			1		Trace discoasters
35X-5, 60	D		95		1	trace			trace		Trace discoasters
36X-5, 68	D	1	87		3	3	1		3		Discoasters 1% of nannofossils
36X-2, 99	D	1	90		2	2	1		3		Discoasters 1% of nannofossils
37P-1, 66	D	trace	89	3	1		trace	3	2		Discoasters 15% of nannofossils
38Y-1, 38	D	1	77		5	trace		2	12		Discoasters 20% of nannofossils
39X-2, 38	D	trace	93		1	2	trace		2		Discoasters 1% of nannofossils
39X-4, 34	D		77		5	5	1		10		Discoasters 1% of nannofossils
39X-6, 13	D		82		4	4	2		8		Discoasters 1% of nannofossils
40X-2, 56	D	trace	88		5				7		Discoasters 2.5% of nannofossils
40X-7, 50	D		86		7		trace		7		Discoasters 1% of nannofossils
41X-2, 54	D		89		5	1			5		Discoasters 5.5% of nannofossils
41X-5, 37	D		81		5	trace			14		Discoasters 4% of nannofossils
42X-2, 65	M				5	trace			5		From ash
42X-2, 84	D	trace	89		5	1			5		Discoasters 2% of nannofossils
42X-6, 49	D		92		5	trace	trace		3		Discoasters 3% of nannofossils
42X-7, 24	M		2								From ash, nice glass-mostly unaltered
43X-2, 46	D	trace	75		5	trace	5		5		
43X-7, 37	D		80		10	trace	trace		5		
43X-7, 84	D	trace	80		5	trace	trace		5		
44X-5, 89	D	trace	75		10	trace	trace		10		
45X-1, 34	D		55		5	trace	trace		10	trace	

Table 1. Smear slide data for Hole NGHP-01-17A.—Continued

Sample reference		Texture			Mineral										
Core, section, depth (cm, in section)	Lithology	Sand	Silt	Clay	Quartz	Feld-spar	Mica	Heavy minerals	Clay minerals	Volcanic glass	Opaques	Iron sulfides	Fram-boidal pyrite	Rock fragments	Authigenic carbonates
NGHP-01-17A—Continued															
46X-2, 82	D		5	95								1			
46X-6, 78	D		2	98						trace					
47X-2, 38	D			100						trace					
47X-6, 108	D			100						trace					trace
47X-6, 120	M		20	80		trace				15					
47X-6, 103	M									75					
48P-1, 75	D		2	98						trace		trace			
48P-1, 87	M		100												
49E-1, 70	D		5	95		trace			trace	1					
50X-3, 58	D		1	99						trace					
50X-6, 15	D		2	98						trace		trace			
51X-2, 72	D			100						1					
51X-4, 105	D		1	99						1					
52X-2, 77	D		2	98		trace				trace		trace			
52X-3, 75	D		1	99						trace					trace
52X-5, 18	D		1	99						trace					
53X-2, 70	D		30	70	trace	trace				trace					trace
53X-3, 106	M		80	20	5	1	trace			89					
53X-3, 8	M	5	25	70	7	3		15		4					
53X-6, 15	D		43	57						1					2
54X-2, 84	D	trace	13	87	1	trace									2
54X-3, 21	D	1													1
55X-1, 89	M	1	14	85	1	1				1					
55X-3, 24	D		9	97						trace					
55X-4, 90	D		7	93						trace					
55X-3, 8	M		90	10	trace					90					
56X-2, 43	D		7	93											
57X-2, 21	M	10	80	10	trace					87	8				5
57X-5, 15	D		20	80											
58X-3, 25	D			100								trace			trace
58X-6, 41	D			100								trace			trace
59P-1, 31	M		52	48	2	1				30			10		
59P-1, 23	D		2	98											
60Y-1, 60	D		13	87						trace					
60Y-1, 46	M		20	80	3	7	trace	10		45					
61X-2, 58	D		5	95								trace			5
61X-3, 28	M		15	85						17		trace			trace
61X-5, 54	D		5	95						trace		trace			5
62X-2, 96	D			100						trace		4			trace
62X-6, 81	D			100						trace		trace			3
63X-2, 114	D		2	98						trace					
63X-5, 11	D		10	90											
64X-1, 29	D		20	80											
64X-3, 60	D		10	90											
65X-2, 50	D		2	98											
66X-6, 120	D		1	99						trace					
66X-2, 112	D		2	98						trace					trace
67X-1, 97	D		1	99						trace					1
68X-1, 67	M		3	97						35		trace			
68X-3, 120	D		1	99						trace			trace		
67X-4, 60	D		4	96						trace					
68X-1, 67	M		55	45				3		50		3			trace
68X-3, 120	D		10	90				trace		1					
69X-2, 90	D			100						3			2		
69X-7, 69	M		85	15						85		trace			
69X-5, 85	D		6	94						1					
72X-1, 74	D		5	95				trace		2		trace			
73X-5, 36	D		5	95				trace		1		trace			trace

Table 1. Smear slide data for Hole NGHP-01-17A.—Continued

Sample reference		Biogenic									
Core, section, depth (cm, in section)	Lithology	Foraminifera	Nannofossils	Carbonate shell fragments	Diatoms	Radiolarians	Silicoflagellates	Siliceous shell fragments	Sponge spicules	Plant debris	Comments
NGHP-01-17A—Continued											
46X-2, 82	D	trace	85		7	trace	trace		7		Discoasters 2% of nannofossils
46X-6, 78	D	trace	90		5				5		Discoasters 2% of nannofossils
47X-2, 38	D	trace	70	1	12	1	1		15		Discoasters 15% of nannofossils
47X-6, 108	D	trace	69		13	1	2		15		Discoasters 15% of nannofossils
47X-6, 120	M	trace	55	1	15	2			12		From ash
47X-6, 103	M		20		2	trace			3		From ash
48P-1, 75	D		82		8	trace	trace		10		
48P-1, 87	M								100		
49E-1, 70	D	1	95						3		Trace discoasters
50X-3, 58	D	trace	71	trace	12	1	1		15		Microtektite found
50X-6, 15	D	trace	70		8	2	5		15		
51X-2, 72	D	trace	58	trace	10	2	4		25		Discoasters 15% of nannofossils
51X-4, 105	D	trace	68	trace	5	1	5		20		Discoasters 10% of nannofossils
52X-2, 77	D	trace	59	trace	15	1	5		20		Discoasters 15% of nannofossils, microtektite found
52X-3, 75	D	trace	66	trace	10	1	3		20		Discoasters 15% of nannofossils
52X-5, 18	D	trace	70	trace	7	1	2		20		Discoasters 15% of nannofossils
53X-2, 70	D		70		10	5	7		8		Discoasters 1% of nannofossils
53X-3, 106	M		2			1	1		1		From black ash, trace discoasters
53X-3, 8	M	trace	70		trace	trace	trace		1		
53X-6, 15	D	1	58		10	8	5		15		Discoasters 1% of nannofossils
54X-2, 84	D	2	87		2	2	1		3		Trace discoasters, trace polycrystalline quartz
54X-3, 21	D	1	87		2	2	2		5		Trace discoasters, trace polycrystalline quartz
55X-1, 89	M	1	85		2	2	2		5		Trace discoasters
55X-3, 24	D	trace	87		5		trace		8		Discoasters 1% of nannofossils
55X-4, 90	D	1	85		5	trace	1		8		Trace discoasters
55X-3, 8	M		10		trace		trace				From dark ash, 10% of glass is altered
56X-2, 43	D	trace	85		7		3		5		Discoasters 1% of nannofossils
57X-2, 21	M										From ash, volcan glass and pumice, auth. carbonate is dolomite or calcite rhombs.
57X-5, 15	D	trace	79		10	1	trace		10		
58X-3, 25	D		85		5	trace	trace		10		
58X-6, 41	D	trace	85		5	trace	trace		10		
59P-1, 31	M		48		5	trace	trace		4		From black ash, highly altered glass, trace discoasters
59P-1, 23	D	trace	86		7	trace	trace		7		Discoasters 2% of nannofossils
60Y-1, 60	D	trace	88		2	2	3		5		Discoasters 1% of nannofossils
60Y-1, 46	M		35								From ash, trace discoasters
61X-2, 58	D	trace	75		5	5	trace		10		
61X-3, 28	M	trace	65		5	trace			13		
61X-5, 54	D	trace	75		5	trace	trace		15		
62X-2, 96	D	trace	81		5	trace	trace		10		
62X-6, 81	D	trace	82		5	trace	trace		10		
63X-2, 114	D	trace	82		7	trace	1		10		Discoasters 1% of nannofossils
63X-5, 11	D	1	74		5				20		Discoasters 1% of nannofossils
64X-1, 29	D	1	77		10	1	1		10		
64X-3, 60	D	trace	82		7	1	trace		10		Discoasters present
65X-2, 50	D	trace	85		5	trace	trace		10		
66X-6, 120	D	trace	69		12	2	2		15		
66X-2, 112	D		70		12	2	1		15		Discoasters 10% of nannofossils, authigenic carbonate is calcite rhombs.
67X-1, 97	D		96		trace				3		Discoasters 10% of nannofossils, authigenic carbonate is calcite rhombs.
68X-1, 67	M		54		3		1		3		From ash, discoasters 10% of nannofossils
68X-3, 120	D		73	trace	5	1	1		20		Discoasters 15% of nannofossils
67X-4, 60	D		62	trace	5	1	7		25		Discoasters 15% of nannofossils
68X-1, 67	M		37		3	trace	1		3		Trace discoasters
68X-3, 120	D	2	87		3	trace	2		5		Trace discoasters
69X-2, 90	D		77		3	1			14		Discoasters 15% of nannofossils
69X-7, 69	M		15								Nearly pure glass
69X-5, 85	D		69	trace	7	1	2		20		
72X-1, 74	D	trace	84		6	trace	2		6		Trace discoasters, trace blue diatoms
73X-5, 36	D	1	74		5	1	3		15		Trace discoasters

Table 1. Smear slide data for Hole NGHP-01-17A.—Continued

Sample reference		Texture			Mineral										
Core, section, depth (cm, in section)	Lithology	Sand	Silt	Clay	Quartz	Feld-spar	Mica	Heavy minerals	Clay minerals	Volcanic glass	Opaques	Iron sulfides	Fram-boidal pyrite	Rock fragments	Authigenic carbonates
NGHP-01-17A—Continued															
74X-2, 5	D		10	90						1		trace			1
74X-4, 10	D		5	95						2		trace			1
75X-2, 56	D		9	91				trace		1		trace			1
75X-4, 40	D		5	95	trace					1		trace			1
75X-4, 57	M		70	30				5		67		3			1
76X-2, 34	D		10	90								1			
76X-4, 98	D		10	90						trace			1		2
77X-2, 54	D		5	95						trace		1			3
77X-6, 4	D		5	95						trace					
78X-2, 53	D		2	98						1					
78X-4, 43	D		3	97						1			1		
79X-1, 130	D		3	97									3		
79X-3, 90	D		5	95											1
80X-1, 10	D		10	90									1		
80X-3, 61	D		2	80								2			
81E-1, 6	D		3	97						trace			1		
82X-5, 104	D		3	97									1		
82X-2, 112	D		5	95											
83X-1, 67	D		1	99									1		

Table 2. Coarse fraction (>63 mm) sieve data for Hole NGHP-01-17A.

Sample reference		Mineral										
Core, section, depth (cm, in section)	MBSF	Quartz	Feldspar	Mica	Heavy minerals	Volcanic glass	Pyrite	Iron sulfides	Framboidal pyrite	Rock fragments	Pumice	Authigenic carbonates
NGHP-01-17A												
1H-1, 30	0.3				1				2			
1H-1, 60	0.6				1				2			
1H-1, 90	0.9			2	2		trace					
1H-2, 60	2.1				2		trace					
1H-2, 90	2.4	trace		1	trace				1			
2H-1, 90	5.4				2		1					
2H-2, 90	6.9				3		1					
2H-3, 85	8.35			2	1							
2H-4, 90	9.9			2	1							
2H-5, 90	11.4			1	2		trace					
2H-6, 90	12.9			trace	1		2					
3H-1, 90	14.9				1							
3H-2, 90	16.4				1							
3H-3, 90	17.9				1		3					
3H-4, 90	19.4				trace		trace					
3H-5, 90	20.9				2		trace					
3H-6, 90	22.4				3							
4H-1, 30	23.8				2							
4H-3, 90	27.4				3							
4H-5, 90	30.4				2							
5H-1, 85	33.85				2		trace					
5H-6, 85	41.35				2		1					
6H-6, 86	50.8				2							
6H-6, 64	50.58				1		1					
7H-2, 52	54.02				1		trace					
7H-6, 60	60.1				1		2					

Table 1. Smear slide data for Hole NGHP-01-17A.—Continued

Sample reference		Biogenic									Comments
Core, section, depth (cm, in section)	Lithology	Foraminifera	Nannofossils	Carbonate shell fragments	Diatoms	Radiolarians	Silicoflagellates	Siliceous shell fragments	Sponge spicules	Plant debris	
NGHP-01-17A—Continued											
74X-2, 5	D	2	77		7	trace	2		10		Trace discoasters
74X-4, 10	D	trace	85		5	1	1		5		Trace discoasters
75X-2, 56	D	3	83		3		1		8		Trace discoasters
75X-4, 40	D	1	88		3	trace	1	5			Trace discoasters
75X-4, 57	M		20		2	trace	1		1		From ash, trace discoasters, trace blue diatoms
76X-2, 34	D	trace	82		7				10		Discoasters 1% of nannofossils
76X-4, 98	D	trace	80		7				10		Trace discoasters, authigenic carbonate is calcite rhombs.
77X-2, 54	D	trace	81		5		trace		10		Trace discoasters
77X-6, 4	D	trace	88		5		trace		7		Trace discoasters
78X-2, 53	D	trace	89		5	trace	trace		5		
78X-4, 43	D	trace	88		5	trace			5		Trace discoasters
79X-1, 130	D	trace	86		5	1			5		Discoasters 1% of nannofossils
79X-3, 90	D	trace	85		7		trace		7		Trace discoasters
80X-1, 10	D	1	81		7	trace	trace		10		
80X-3, 61	D	2	76		10	trace	trace		10		Trace discoasters
81E-1, 6	D	trace	89		5				5		Trace discoasters
82X-5, 104	D	trace	89		5	trace			5		Trace discoasters
82X-2, 112	D	trace	80		10	trace	trace		10		Trace discoasters
83X-1, 67	D	1	84		5	trace	trace		9		Trace discoasters

Note: M = minor lithology, D = dominant lithology.

Table 2. Coarse fraction (>63 mm) sieve data for Hole NGHP-01-17A.—Continued

Sample reference		Biogenic									Comments
Core, section, depth (cm, in section)	MBSF	Foraminifera	Carbonate shell fragments	Diatoms	Radiolarians	Silicoflagellates	Siliceous shell fragments	Sponge spicules	Other biogenic	Plant debris	
NGHP-01-17A—Continued											
1H-1, 30	0.3	80	15					2			Mostly planktonic, pink G. ruber present
1H-1, 60	0.6	80	15					2			Mostly planktonic, pink G. ruber present
1H-1, 90	0.9	86	10					trace		trace	1% pink G. ruber
1H-2, 60	2.1	85	10					3			Mostly planktonic, pink G. ruber present
1H-2, 90	2.4	87	10					1			1% pink G. ruber
2H-1, 90	5.4	65	29					3			Pink G. ruber present, shell fragments mostly bivalves
2H-2, 90	6.9	70	25					1			Mostly planktonic, pink G. ruber present
2H-3, 85	8.35	55	30				10	2			Pink G. ruber present
2H-4, 90	9.9	60	35				1	1			Pink G. ruber common
2H-5, 90	11.4	65	30				1	1			Pink G. ruber present
2H-6, 90	12.9	65	30				trace	2			Pink G. ruber present
3H-1, 90	14.9	70	28					1			Pink G. ruber present
3H-2, 90	16.4	70	25					4			Mostly planktonic, pink G. ruber present
3H-3, 90	17.9	80	13					3			Mostly planktonic, pink G. ruber present
3H-4, 90	19.4	85	13					2			Mostly planktonic, pink G. ruber present
3H-5, 90	20.9	75	22					1			Mostly planktonic, pink G. ruber present
3H-6, 90	22.4	55	40					2			Mostly planktonic, pink G. ruber present
4H-1, 30	23.8	65	30					3			Mostly planktonic, pink G. ruber NOT present
4H-3, 90	27.4	65	30					2			
4H-5, 90	30.4	60	35					3			Mostly planktonic
5H-1, 85	33.85	60	35					3			Pyritized foraminifera
5H-6, 85	41.35	70	24					3			
6H-6, 86	50.8	60	30					8			Pyritized foraminifera
6H-6, 64	50.58	75	20					3			
7H-2, 52	54.02	80	18					1			Mostly planktonic
7H-6, 60	60.1	60	35					2			Pyritized foraminifera

Table 2. Coarse fraction (>63 mm) sieve data for Hole NGHP-01-17A.—Continued

Sample reference		Mineral										
Core, section, depth (cm, in section)	MBSF	Quartz	Feldspar	Mica	Heavy minerals	Volcanic glass	Pyrite	Iron sulfides	Framboidal pyrite	Rock fragments	Pumice	Authigenic carbonates
NGHP-01-17A—Continued												
8H-1, 68	62.18				3							
8H-6, 60	69.6				3							
9H-1, 80	71.8				2		1					
9H-6, 60	78.7				2		1					
10H-1, 95	81.45				3		trace					
10H-7, 40	89.84	1			2		trace					
11H-2, 75	92.25	trace			3							
11H-5, 77	96.77	trace			3		1					
12H-2, 90	101.9				5		10					
12H-5, 70	106.2			1	6		5			trace		
13H-2, 70	111.2			trace	3		10					
13H-5, 70	115.7			1	3		5					
14X-2, 70	120.7	2		1	5		5			trace		
14X-5, 70	125.2	1		2	3		3					
15X-5, 73	133.45	2	1	trace		trace	10				trace	
16X-2, 70	139.9			trace	10		5					
16X-5, 55	144.09				5		10					
17X-1, 21	146.81	3			10		15					
18X-2, 43	157.99	trace	trace	trace	7		5			trace		
18X-6, 88	164.19	trace		trace	5		5					
19X-2, 70	167.03	1	trace	trace	3		7					
19X-5, 70	171.53	trace		trace	5		15					
20Y-1, 70	176.2	trace			3		7					
21X-2, 70	178.7	1			5		1					
22X-2, 10	186.7			1	5		7					
22X-2, 70	187.3	trace		trace	3		7					
22X-5, 70	192.2	1		trace	5		7					
23X-2, 70	196.38	trace		trace	3		7					
23X-5, 70	200.78	2		1	3		7					
24X-2, 70	204.75	trace		trace	3		20					
24X-4, 10	206.65	trace		trace	5	trace	30					
25X-2, 70	215.7	1		trace	3		10					
25X-5, 70	219.8	3		1	5		7					
26X-2, 110	225.7	3		1	5		15					
27X-1, 87	233.67	trace			3		20					
27X-4, 22	237.32	trace		1	7		15			trace		
28X-2, 67	244.67	20	10				12				3	
28X-6, 17	250.17	20					25				5	
29X-2, 54	253.52	15	5	trace		trace	25				5	
29X-5, 21	257.25	15	5	trace		trace	13				4	
30X-3, 59	264.19	15	5				20				5	
30X-7, 129	269.56	15	5	trace		trace	12				3	
32X-3, 38	283.28	1	trace		3		10					
32X-6, 37	286.65	trace		trace	3		17					
33X-2, 12	290.98	10			3		5					
34X-2, 28	300.98	15			2		17					
34X-5, 47	305.31	10			2		10					
35X-2, 64	310.16	10			2		5					
35X-5, 60	314.26	15		trace	2		7					
36X-2, 99	320.38	10		1	1		3					
36X-5, 68	323.95	8		trace	1		3					
37P-1, 66	328.66	10		1	3		7					
39X-2, 38	331.88	5			2		10					
39X-4, 36	334.86	5			2		5					

Table 2. Coarse fraction (>63 mm) sieve data for Hole NGHP-01-17A.—Continued

Sample reference		Biogenic									Comments
Core, section, depth (cm, in section)	MBSF	Foraminifera	Carbonate shell fragments	Diatoms	Radiolarians	Silicoflagellates	Siliceous shell fragments	Sponge spicules	Other biogenic	Plant debris	
NGHP-01-17A—Continued											
8H-1, 68	62.18	70	25					2			Mostly planktonic
8H-6, 60	69.6	60	35					2			
9H-1, 80	71.8	70	26					1			Pyritized foraminifera
9H-6, 60	78.7	65	30					2			Pyritized foraminifera
10H-1, 95	81.45	65	30					2			
10H-7, 40	89.84	50	45					2			
11H-2, 75	92.25	60	35					2			
11H-5, 77	96.77	55	40					1			Pyritized foraminifera
12H-2, 90	101.9	42	40				1	2			Pyrite filled burrows
12H-5, 70	106.2	60	26				1	1			
13H-2, 70	111.2	30	55					2			Pyrite filled burrows
13H-5, 70	115.7	50	40					1			Pyrite filled burrows
14X-2, 70	120.7	40	45					2			
14X-5, 70	125.2	30	58					3			Pyrite filled burrows
15X-5, 73	133.45	65	20				2				Some pyritized foraminifera
16X-2, 70	139.9	30	55					trace			
16X-5, 55	144.09	20	65					trace			Mostly planktonics
17X-1, 21	146.81	15	55					2			
18X-2, 43	157.99	30	56					2			
18X-6, 88	164.19	30	58					2			
19X-2, 70	167.03	40	48					1			
19X-5, 70	171.53	27	50				1	2			
20Y-1, 70	176.2	20	70					trace			
21X-2, 70	178.7	50	43				trace	trace			
22X-2, 10	186.7	30	57					trace			Mostly planktonics
22X-2, 70	187.3	30	58					2			Mostly planktonics
22X-5, 70	192.2	30	56					1			
23X-2, 70	196.38	40	50								
23X-5, 70	200.78	25	61				trace	1			Mostly planktonics
24X-2, 70	204.75	30	45					2			
24X-4, 10	206.65	30	33					2			
25X-2, 70	215.7	35	49				1	1			Mostly planktonics
25X-5, 70	219.8	20	60				2	2			
26X-2, 110	225.7	15	56				2	3			
27X-1, 87	233.67	25	50				1	1			
27X-4, 22	237.32	25	50				1	1			
28X-2, 67	244.67	39	7	5	1		3				Pyritized foraminifera
28X-6, 17	250.17	46	1		trace		1	2	trace		Mostly pyritized burrows with some nodules and pryritized foraminifera
29X-2, 54	253.52	34	2	10	1		1	2			Mostly pyritized burrows with some nodules and pryritized foraminifera and diatoms
29X-5, 21	257.25	54	3	5	trace		1	trace			Mostly pyritized burrows with some nodules and pryritized foraminifera and diatoms
30X-3, 59	264.19	35	5	10	1		3	1			Mostly pyritized burrows with some nodules and pryritized foraminifera and diatoms
30X-7, 129	269.56	55	3	5	trace		1	1			Mostly pyritized burrows with some nodules and pryritized foraminifera and diatoms
32X-3, 38	283.28	30	55	trace	trace		1				
32X-6, 37	286.65	30	45	trace	1		2	2			
33X-2, 12	290.98	30	48		1		1	2			
34X-2, 28	300.98	30	31				2	3			
34X-5, 47	305.31	30	46		trace			2			
35X-2, 64	310.16	20	56		1		4	2			
35X-5, 60	314.26	20	50				5	1			
36X-2, 99	320.38	50	33				1	1			
36X-5, 68	323.95	43	43				1	1			
37P-1, 66	328.66	30	46		trace		2	1			
39X-2, 38	331.88	30	50		trace		2	1			
39X-4, 36	334.86	40	35	1	3		7	2			

Table 2. Coarse fraction (>63 mm) sieve data for Hole NGHP-01-17A.—Continued

Sample reference		Mineral										
Core, section, depth (cm, in section)	MBSF	Quartz	Feldspar	Mica	Heavy minerals	Volcanic glass	Pyrite	Iron sulfides	Framboidal pyrite	Rock fragments	Pumice	Authigenic carbonates
NGHP-01-17A—Continued												
40X-2, 56	338.49	5			3		2					
40X-7, 50	335.18	3			2		10					
41X-2, 54	349.34	5		trace	2		3					
41X-5, 37	353.28	10			3		2					
42X-2, 84	358.63	10			3		3			1		
42X-6, 49	363.78	10			3		2					
43X-7, 37	373.25	15			2		3					
44X-1, 81	376.91	15			2		1					
44X-5, 89	381.65	15			2		1					
45X-1, 34	386.04	10			2		2					
45X-2, 46	387.01	10			2		2					
46X-2, 82	397.46	10			2		1					
47X-2, 38	406.98	10			1		2					
50X-2, 15	415.85	10			5		3			trace		
50X-3, 58	417.28	10		trace	5		3			trace		
51X-2, 72	426.45	8			3		2					
52X-2, 77	436.27	10			3		2			trace		
52X-5, 18	439.68	10			3		2					
53X-3, 106	446.41	10		1	8		5			1		
54X-2, 84	454.83	10		trace	2		1					
54X-3, 21	455.49	10		trace	2							
55X-4, 90	465.79	10			3		1					
55X-1, 88	463.88	50			20		5				20	
55X-3, 24	464.81	10			10		1					
56X-2, 43	474.13	10		trace	2		trace			trace		
57X-2, 27	483.06	3			19		15			19	19	
57X-5, 15	486.83	5			15		10			20	5	
58X-3, 25	495.03	30			5						50	
58X-6, 41	499.14	10		5								
61X-2, 58	502.89	15			20						20	
61X-5, 54	507.02	10			5							
62X-2, 56	512.8	10		5								
62X-6, 81	518.92	10			3							
63X-2, 116	522.89	12			1							
63X-5, 111	526.16	13			1							
64X-1, 28	530.58	13			1							
64X-3, 59	533.46	10			7		6					
65X-2, 50	542	12			2							
66X-2, 112	551.62	10			2							
66X-6, 120	556.62	10			1							
67X-4, 60	562.37	10			1		1					
67X-6, 108	565.22	8			3		2					
68X-3, 120	572.06	50			10		5					
69X-2, 90	581.1	10			1		1					
72X-1, 63	588.43	15		trace	3		1			2		

Table 2. Coarse fraction (>63 mm) sieve data for Hole NGHP-01-17A.—Continued

Sample reference		Biogenic									Comments
Core, section, depth (cm, in section)	MBSF	Foraminifera	Carbonate shell fragments	Diatoms	Radiolarians	Silicoflagellates	Siliceous shell fragments	Sponge spicules	Other biogenic	Plant debris	
NGHP-01-17A—Continued											
40X-2, 56	338.49	50	35		1		2	2			
40X-7, 50	335.18	50	30		2		2	1			
41X-2, 54	349.34	60	29				trace	1			
41X-5, 37	353.28	30	45		5		3	2			
42X-2, 84	358.63	30	45		3		3	2			
42X-6, 49	363.78	35	40		5		3	2			
43X-7, 37	373.25	30	33	1	5		10	1			
44X-1, 81	376.91	30	34	1	5		10	2			
44X-5, 89	381.65	25	40	1	5		10	1			
45X-1, 34	386.04	40	30		5		10	1			
45X-2, 46	387.01	30	35	2	3		15	1			
46X-2, 82	397.46	40	30		6		10	1			
47X-2, 38	406.98	40	30	1	8		7	1			
50X-2, 15	415.85	30	39	trace	5		7	1			
50X-3, 58	417.28	30	39		5		7	1			
51X-2, 72	426.45	30	35	5	5		10	2			
52X-2, 77	436.27	40	35		5		4	1			
52X-5, 18	439.68	35	40		5		4	1			
53X-3, 106	446.41	30	34		5		5	1			
54X-2, 84	454.83	35	35	5	8		3	1			
54X-3, 21	455.49	35	35	5	8		4	1			
55X-4, 90	465.79	30	36	3	5	1	8	3			
55X-1, 88	463.88	5									From dispersed ash layer
55X-3, 24	464.81	30	38	1	5		5	trace			
56X-2, 43	474.13	20	43	4	5		15	1			
57X-2, 27	483.06	10			5		10				From ash layer, basaltic to glassy rock fragments
57X-5, 15	486.83	25			5		15				
58X-3, 25	495.03	5					10				
58X-6, 41	499.14	20	40	4	5		15	1			
61X-2, 58	502.89	35					10				
61X-5, 54	507.02	20	40	4	5		15	1			
62X-2, 56	512.8	20	40	1	7		15	2			
62X-6, 81	518.92	30	30	3	7		15	2			
63X-2, 116	522.89	30	30	3	7		15	2			
63X-5, 111	526.16	30	35	3	7		10	1			
64X-1, 28	530.58	35	30	3	7		10	1			
64X-3, 59	533.46	20	30	3	7		15	2			
65X-2, 50	542	30	35	4	6		10	1			
66X-2, 112	551.62	30	35	2	8	1	10	2			
66X-6, 120	556.62	30	34	5	8		10	2			
67X-4, 60	562.37	25	36	5	5		15	2			
67X-6, 108	565.22	30	40	2	6		8	1			
68X-3, 120	572.06	15	5		5		10				
69X-2, 90	581.1	24	35	5	10		12	2			
72X-1, 63	588.43	20	33	5	20			1			From hydrate sample #122

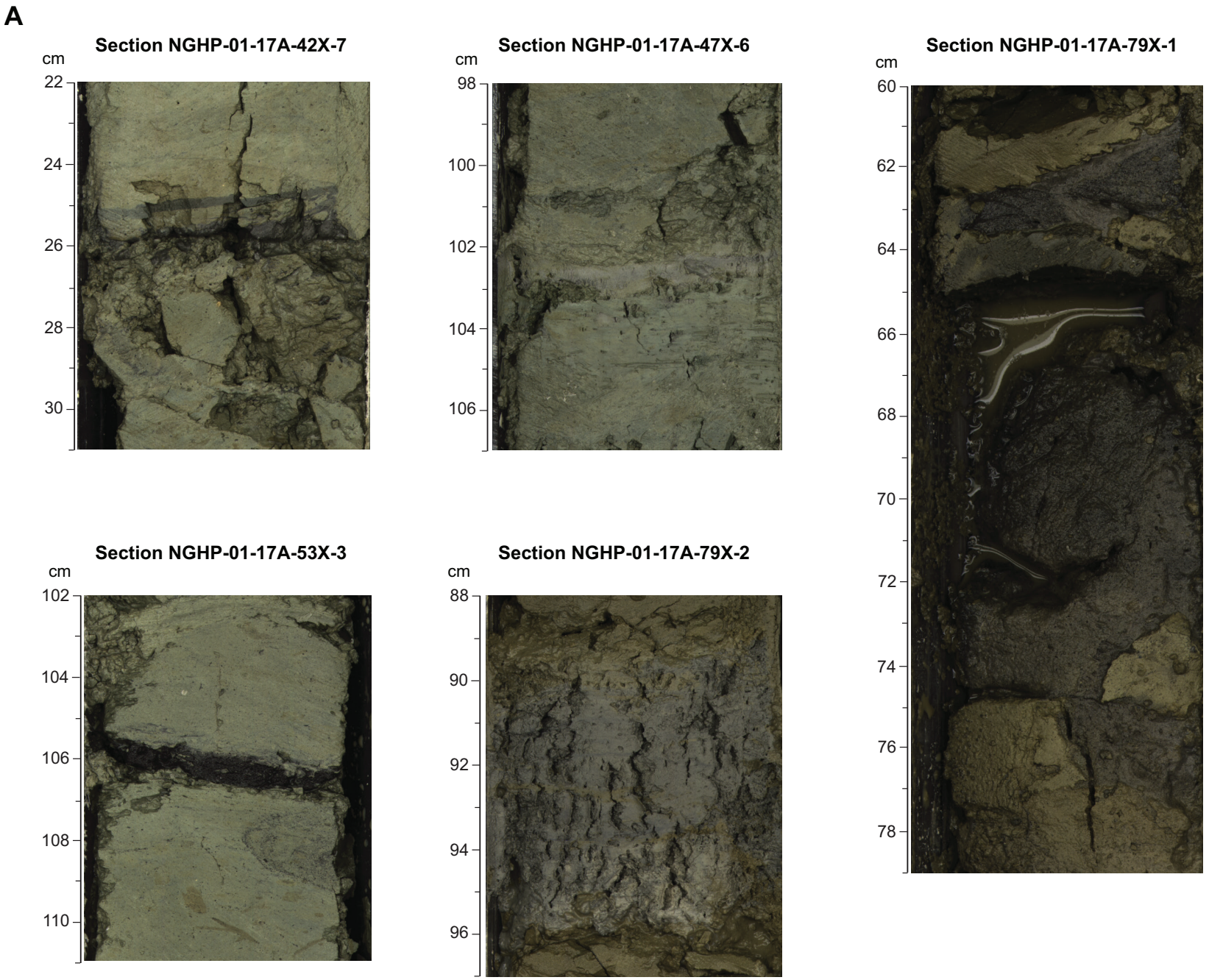


Figure 9. A, Ash beds, B, bioturbated occurrences of ash, and C, disseminated occurrences of ash observed throughout Lithostratigraphic Unit I.

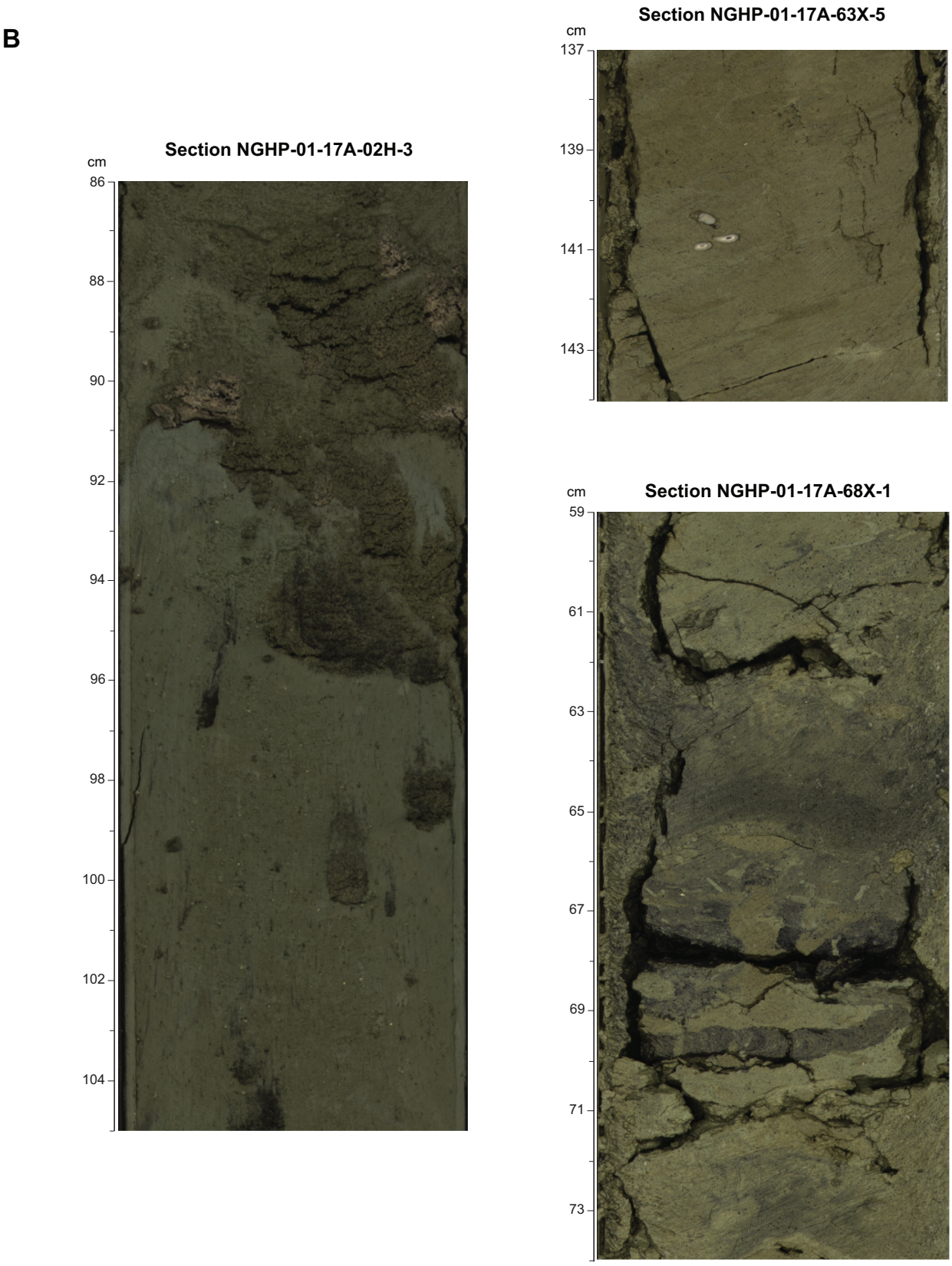


Figure 9. A, Ash beds, B, bioturbated occurrences of ash, and C, disseminated occurrences of ash observed throughout Lithostratigraphic Unit I.—Continued

C

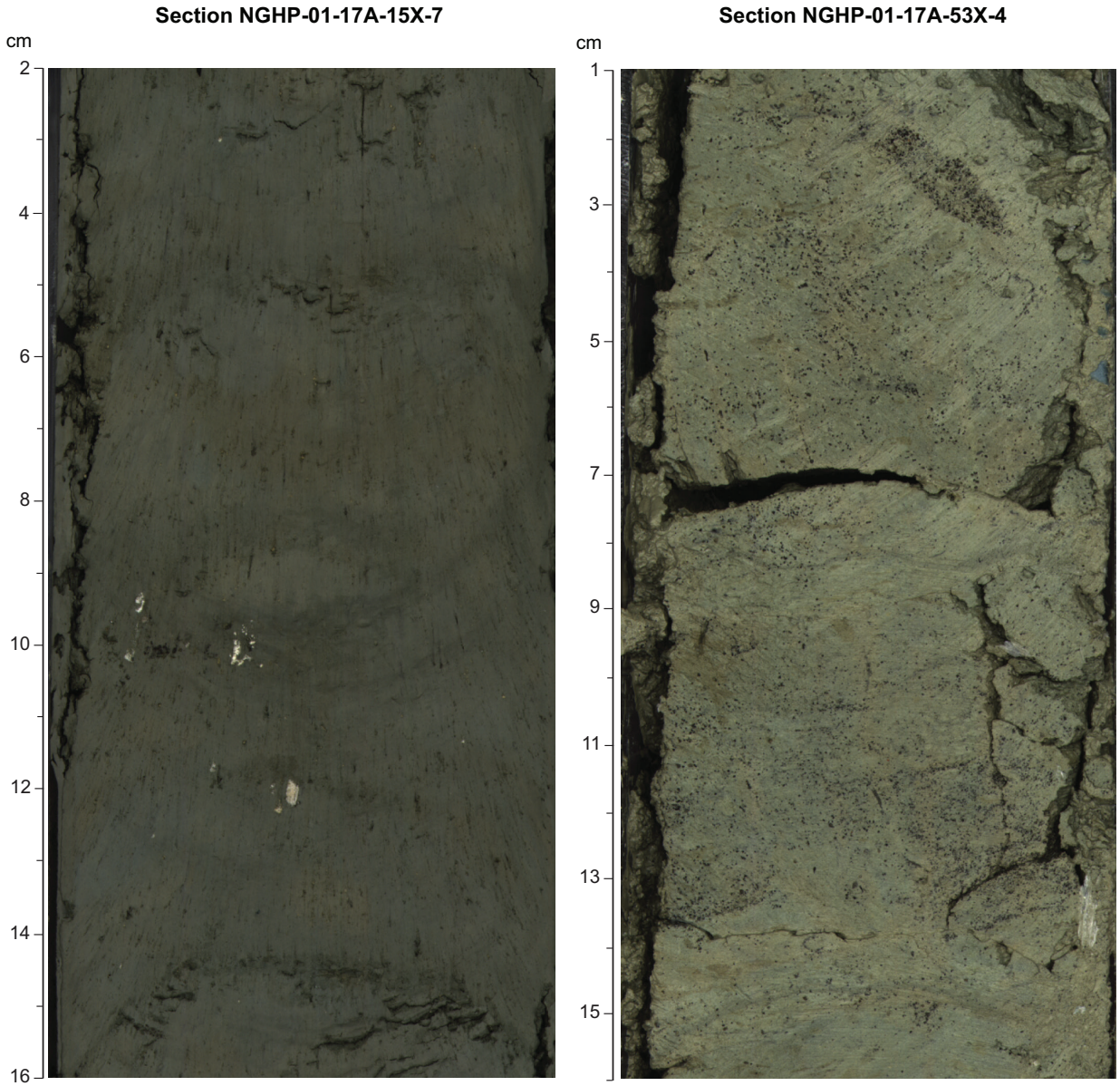


Figure 9. A, Ash beds, B, bioturbated occurrences of ash, and C, disseminated occurrences of ash observed throughout Lithostratigraphic Unit I.—Continued

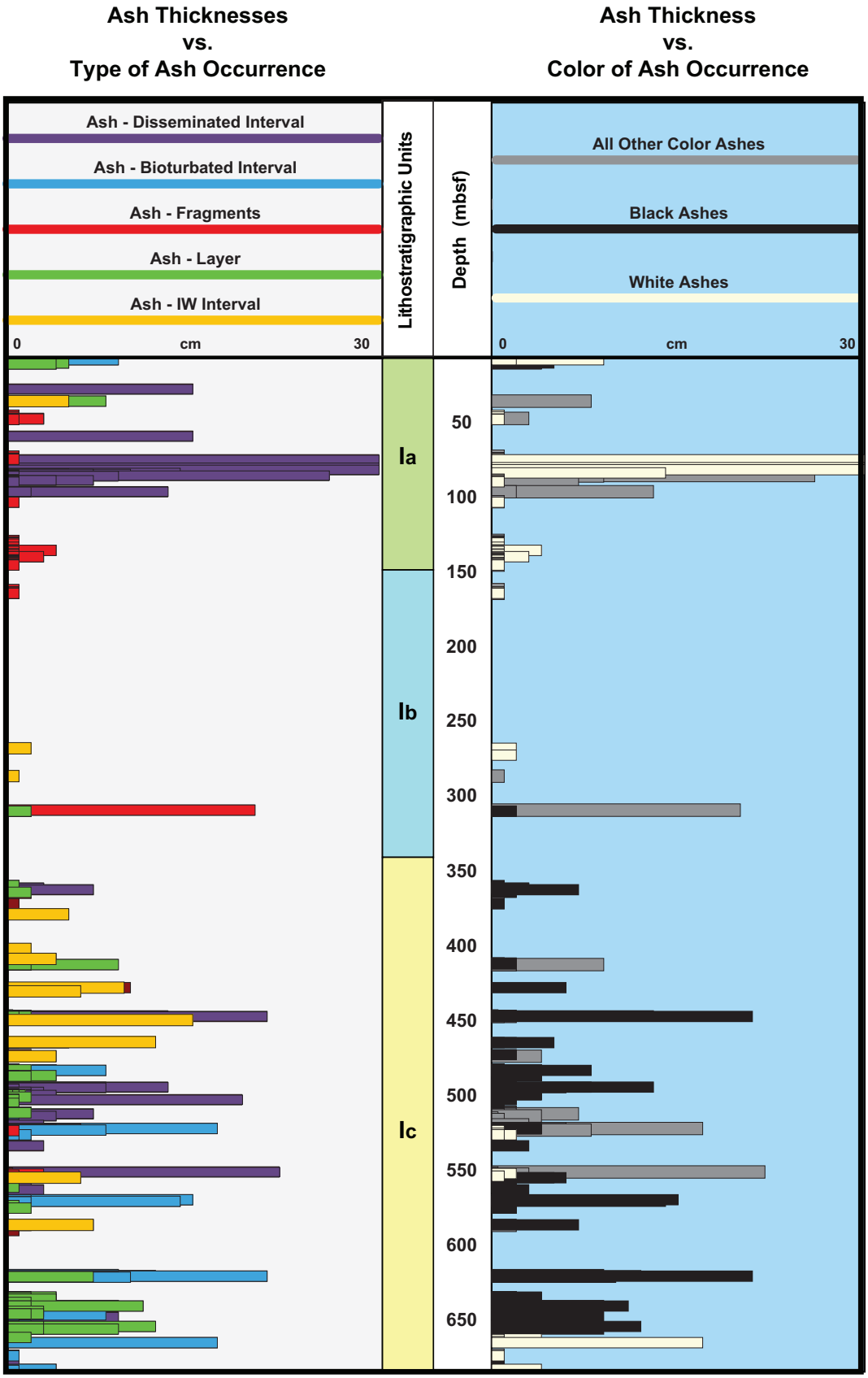


Figure 10. A, Summary of the ash types, thickness, and occurrences with depth (left) and the colors of ash versus depth (right). See also table 3. B, Ash colors plotted individually by thickness versus depth in Lithostratigraphic Unit I. C, Ash occurrences plotted individually by thickness versus depth in Unit I.



Figure 10. A, Summary of the ash types, thickness, and occurrences with depth (left) and the colors of ash versus depth (right). See also table 3. B, Ash colors plotted individually by thickness versus depth in Lithostratigraphic Unit I. C, Ash occurrences plotted individually by thickness versus depth in Unit I.—Continued

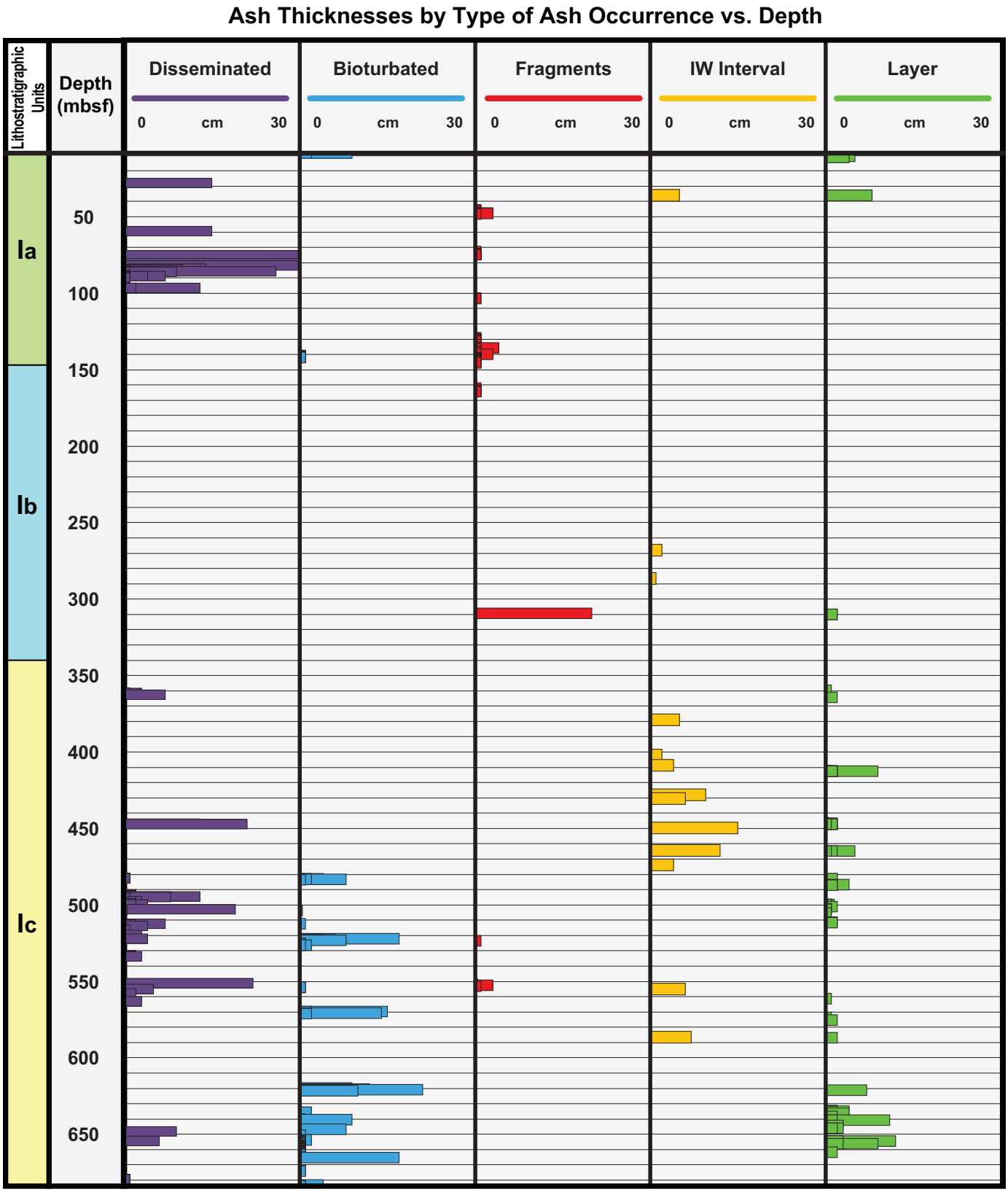


Figure 10. A, Summary of the ash types, thickness, and occurrences with depth (left) and the colors of ash versus depth (right). See also table 3. B, Ash colors plotted individually by thickness versus depth in Lithostratigraphic Unit I. C, Ash occurrences plotted individually by thickness versus depth in Unit I.—Continued

Table 3. Volcanic ash occurrences at Hole NGHP-01-17A. (To view complete table, please refer to the ASCII files.)

Core, section	Expedition	Site	Hole	Core	Core type	Section	Position start	Position end	Depth top (mbsf)	Depth base (mbsf)
					NGHP-01-17A					
2H-3	1	17	A	2	H	3	87	96	8.37	8.46
2H-3	1	17	A	2	H	3	88	90	8.38	8.4
2H-4	1	17	A	2	H	4	131	136	10.31	10.36
2H-4	1	17	A	2	H	4	133	135	10.33	10.35
2H-5	1	17	A	2	H	5	66	70	11.16	11.2
4H-3	1	17	A	4	H	3	135	150	27.85	28
5H-2	1	17	A	5	H	2	140	145	35.9	35.95
5H-3	1	17	A	5	H	3	0	8	36	36.08
5H-5	1	17	A	5	H	5	135	150	40.4	40.43
6H-3	1	17	A	6	H	3	2	3	45.46	45.47
6H-3	1	17	A	6	H	3	106	107	46.5	46.51
6H-4	1	17	A	6	H	4	48	49	47.42	47.43
6H-4	1	17	A	6	H	4	63	66	47.57	47.6
6H-4	1	17	A	6	H	4	91	92	47.85	47.86
6H-4	1	17	A	6	H	4	95	98	47.89	47.92
6H-4	1	17	A	6	H	4	130	131	48.24	48.25
7H-5	1	17	A	7	H	5	135	150	59.35	59.5
9H-2	1	17	A	9	H	2	57	58	72.67	72.68
9H-3	1	17	A	9	H	3	57	58	74.17	74.18
9H-3	1	17	A	9	H	3	60	61	74.2	74.21
9H-3	1	17	A	9	H	3	95	96	74.55	74.56
9H-3	1	17	A	9	H	3	98	99	74.58	74.59
9H-3	1	17	A	9	H	3	108	109	74.68	74.69
9H-3	1	17	A	9	H	3	136	137	74.96	74.97
9H-4	1	17	A	9	H	4	0	150	75.1	76.6
10H-1	1	17	A	10	H	1	0	150	80.5	82
10H-2	1	17	A	10	H	2	0	120	82	83.2
10H-3	1	17	A	10	H	3	56	70	84.06	84.2
10H-3	1	17	A	10	H	3	86	91	84.36	84.41
10H-3	1	17	A	10	H	3	116	126	84.66	84.76
10H-3	1	17	A	10	H	3	130	137	84.8	84.87
10H-4	1	17	A	10	H	4	10	11	85.1	85.11
10H-4	1	17	A	10	H	4	37	38	85.37	85.38
10H-4	1	17	A	10	H	4	50	51	85.5	85.51
10H-4	1	17	A	10	H	4	60	86	85.6	85.86
10H-4	1	17	A	10	H	4	91	100	85.91	86
10H-4	1	17	A	10	H	4	119	120	86.19	86.2
10H-6	1	17	A	10	H	6	30	31	88.3	88.31
10H-6	1	17	A	10	H	6	58	59	88.58	88.59
10H-6	1	17	A	10	H	6	84	85	88.84	88.85
10H-6	1	17	A	10	H	6	87	94	88.87	88.94
10H-6	1	17	A	10	H	6	88	92	88.88	88.92
10H-6	1	17	A	10	H	6	100	101	89	89.01
10H-6	1	17	A	10	H	6	114	115	89.14	89.15
10H-6	1	17	A	10	H	6	134	135	89.34	89.35
10H-7	1	17	A	10	H	7	2	3	89.46	89.47
10H-7	1	17	A	10	H	7	25	26	89.69	89.7
10H-7	1	17	A	10	H	7	43	44	89.87	89.88
11H-5	1	17	A	11	H	5	52	65	96.52	96.65
11H-5	1	17	A	11	H	5	57	59	96.57	96.59
12H-3	1	17	A	12	H	3	88	89	103.38	103.39
12H-3	1	17	A	12	H	3	100	101	103.5	103.51
15X-1	1	17	A	15	X	1	96	97	129.06	129.07
15X-3	1	17	A	15	X	3	52	53	130.24	130.25
15X-3	1	17	A	15	X	3	57	58	130.29	130.3
15X-3	1	17	A	15	X	3	62	63	130.34	130.35
15X-3	1	17	A	15	X	3	66	67	130.38	130.39
15X-3	1	17	A	15	X	3	75	76	130.47	130.48
15X-3	1	17	A	15	X	3	82	83	130.54	130.55
15X-3	1	17	A	15	X	3	90	91	130.62	130.63
15X-3	1	17	A	15	X	3	112	113	130.84	130.85
15X-4	1	17	A	15	X	4	38	39	131.6	131.61
15X-5	1	17	A	15	X	5	79	80	133.51	133.52
15X-6	1	17	A	15	X	6	134	135	135.56	135.57
15X-7	1	17	A	15	X	7	10	14	135.82	135.86

Table 3. Volcanic ash occurrences at Hole NGHP-01-17A. (To view complete table, please refer to the ASCII files.)—Continued

Core, section	Thickness (m)	Ash type	Color	Comment	
				NGHP-01-17A—Continued	
2H-3	0.09	B	W	Bioturbated ash layer	Type:
2H-3	0.02	B	W	Bioturbated ash layer	L = Layer
2H-4	0.05	L	B	Volcanic glass rich layer	D = Disseminated
2H-4	0.02	L	B	Volcanic glass rich layer	B = Bioturbated or Burrow Fill
2H-5	0.04	L	B	Volcanic glass rich layer	P = Pumice
4H-3	0.15	D		IW ash sample	F = Fragments
5H-2	0.05	IW	P	From IW sample at 135–150 cm. Exact extent within the IW interval is unknown.	"blank" = No Information
5H-3	0.08	L	W/P	White/Pink ash layer bioturbated below 8 cm down to 22 cm	IW = From IW Sample
5H-5	0.03	L	P	From IW sample at 135–150 cm. Exact extent within the IW interval is unknown.	
6H-3	0.01	F	W		
6H-3	0.01	F	W		Color:
6H-4	0.01	F	B/W		B = Black
6H-4	0.03	F	B/W		W = White
6H-4	0.01	F	W		DG = Dark gray
6H-4	0.03	F			LG = Light Gray
6H-4	0.01	F	W		G = Gray
7H-5	0.15	D		From IW sample	P = Pink
9H-2	0.01	F	LG		"blank" = No Information
9H-3	0.01	F	W		
9H-3	0.01	F	W		
9H-3	0.01	F	W		
9H-3	0.01	F	LG		
9H-3	0.01	F	W		
9H-3	0.01	F	B/LG	Volcanic glass fragments, medium to coarse grained	
9H-4	1.5	D	W	Large volcanic ash fragments disseminated throughout	
10H-1	1.5	D	W	Disseminated sparsely throughout entire section	
10H-2	1.2	D	W	Disseminated sparsely throughout entire section	
10H-3	0.14	D	W		
10H-3	0.05	D	W/LG		
10H-3	0.1	D	W/LG		
10H-3	0.07	D	G/W		
10H-4	0.01	D	G		
10H-4	0.01	D	G		
10H-4	0.01	D	G		
10H-4	0.26	D	G/W		
10H-4	0.09	D	G/W		
10H-4	0.01	D	G/W		
10H-6	0.01	D	W		
10H-6	0.01	D	W		
10H-6	0.01	D	LG/DG		
10H-6	0.07	L	B/LG		
10H-6	0.04	D			
10H-6	0.01	D	B		
10H-6	0.01	D	W/LG		
10H-6	0.01	D	W		
10H-7	0.01	D	W		
10H-7	0.01	D	W		
10H-7	0.01	D	W		
11H-5	0.13	D	DG/B	Possible foram rich ash zone	
11H-5	0.02	D	DG/B	Possible foram rich ash zone	
12H-3	0.01	F	W/LG		
12H-3	0.01	F	W		
15X-1	0.01	F	LG		
15X-3	0.01	D	LG		
15X-3	0.01	F	W		
15X-3	0.01	F	W		
15X-3	0.01	F	LG		
15X-3	0.01	F	W		
15X-3	0.01	F	W		
15X-3	0.01	F	W		
15X-3	0.01	F	W		
15X-4	0.01	F	LG		
15X-5	0.01	F	W		
15X-6	0.01	F	W		
15X-7	0.04	F	W		

Table 3. Volcanic ash occurrences at Hole NGHP-01-17A. (To view complete table, please refer to the ASCII files.)—Continued

Core, section	Expedition	Site	Hole	Core	Core type	Section	Position start	Position end	Depth top (mbsf)	Depth base (mbsf)
NGHP-01-17A—Continued										
15X-7	1	17	A	15	X	7	62	63	136.34	136.35
15X-7	1	17	A	15	X	7	69	70	136.41	136.42
16X-1	1	17	A	16	X	1	43	44	138.13	138.14
16X-1	1	17	A	16	X	1	65	66	138.35	138.36
16X-1	1	17	A	16	X	1	98	99	138.68	138.69
16X-2	1	17	A	16	X	2	73	76	139.93	139.96
16X-2	1	17	A	16	X	2	84	85	140.04	140.05
16X-2	1	17	A	16	X	2	94	95	140.14	140.15
16X-3	1	17	A	16	X	3	13	14	140.83	140.84
16X-3	1	17	A	16	X	3	22	23	140.92	140.93
16X-3	1	17	A	16	X	3	60	61	141.3	141.31
16X-3	1	17	A	16	X	3	83	84	141.53	141.54
16X-3	1	17	A	16	X	3	104	105	141.74	141.75
16X-3	1	17	A	16	X	3	127	128	141.97	141.98
16X-3	1	17	A	16	X	3	139	140	142.09	142.1
16X-4	1	17	A	16	X	4	4	5	142.24	142.25
16X-4	1	17	A	16	X	4	14	15	142.34	142.35
16X-4	1	17	A	16	X	4	20	21	142.4	142.41
16X-4	1	17	A	16	X	4	44	45	142.64	142.65
16X-4	1	17	A	16	X	4	64	65	142.84	142.85
16X-4	1	17	A	16	X	4	79	80	142.99	143
16X-4	1	17	A	16	X	4	99	100	143.19	143.2
16X-4	1	17	A	16	X	4	114	115	143.34	143.35
16X-5	1	17	A	16	X	5	43	44	143.97	143.98
16X-5	1	17	A	16	X	5	44	45	143.98	143.99
16X-5	1	17	A	16	X	5	67	68	144.21	144.22
16X-6	1	17	A	16	X	6	12	13	145.01	145.02
16X-6	1	17	A	16	X	6	14	15	145.03	145.04
16X-6	1	17	A	16	X	6	57	58	145.46	145.47
16X-6	1	17	A	16	X	6	68	69	145.57	145.58
18X-5	1	17	A	18	X	5	4	5	162.1	162.11
18X-6	1	17	A	18	X	6	18	19	163.49	163.5
18X-6	1	17	A	18	X	6	52	53	163.83	163.84
18X-6	1	17	A	18	X	6	112	113	164.43	164.44
18X-6	1	17	A	18	X	6	126	127	164.57	164.58
30X-3	1	17		30	X	3	120	150	264.8	264.82
30X-6	1	17	A	30	X	6	52	54	268.13	268.15
31X-3	1	17	A	31	X	3	30	32	272.63	272.65
32X-5	1	17	A	32	X	5	86	87	286.73	286.74
35X-2	1	17	A	35	X	2	0	20	309.52	309.72
42X-2	1	17	A	42	X	2	62	64	310.14	310.16
42X-2	1	17	A	42	X	2	64	66	310.16	310.18
42X-3	1	17	A	42	X	3	41	42	359.7	359.71
42X-4	1	17	A	42	X	4	49	50	361.28	361.29
42X-4	1	17	A	42	X	4	66	69	361.45	361.48
42X-4	1	17	A	42	X	4	89	92	361.68	361.71
42X-5	1	17	A	42	X	5	38	45	362.67	362.74
42X-7	1	17	A	42	X	7	24	25	364.19	364.2
42X-7	1	17	A	42	X	7	24	26	364.19	364.21
42X-cc	1	17	A	42	X	cc	25	27	365.13	365.15
43X-6	1	17	A	43	X	6	12	13	372.15	372.16
44X-3	1	17	A	44	X	3	40	45	379	379.05
46X-5	1	17	A	46	X	5	88	90	402.02	402.04
47X-4	1	17	A	47	X	4	94	98	408.64	408.68
47X-6	1	17	A	47	X	6	59	61	411.92	411.94
47X-6	1	17	A	47	X	6	79	80	412.12	412.13
47X-6	1	17	A	47	X	6	101	103	412.34	412.36

Table 3. Volcanic ash occurrences at Hole NGHP-01-17A. (To view complete table, please refer to the ASCII files.)—Continued

Core, section	Thickness (m)	Ash type	Color	Comment
				NGHP-01-17A—Continued
15X-7	0.01	F	W	
15X-7	0.01	F	W	
16X-1	0.01	F	LG	<1 mm
16X-1	0.01	F	W	<1 mm
16X-1	0.01	F	W	<1 mm
16X-2	0.03	F	W	<1 mm
16X-2	0.01	F	W/G	<1 mm
16X-2	0.01	F	W/G	<1 mm
16X-3	0.01	B	W	
16X-3	0.01	B	W	
16X-3	0.01	B	W	
16X-3	0.01	B	W/LG	
16X-3	0.01	B	W	
16X-3	0.01	B	W	
16X-3	0.01	B	W	
16X-4	0.01	F	W	<1 mm
16X-4	0.01	F	W	<1 mm
16X-4	0.01	F	LG	<1 mm
16X-4	0.01	F	DG	<1 mm
16X-4	0.01	F	DG/LG	<1 mm
16X-4	0.01	F	B	<1 mm
16X-4	0.01	F	DG/B	<1 mm
16X-4	0.01	F	DG/W	<1 mm
16X-5	0.01	F	W	<1 mm
16X-5	0.01	F	W/LG	<1 mm
16X-5	0.01	F	W	<1 mm
16X-6	0.01	F	W	<1 mm
16X-6	0.01	F	W	<1 mm
16X-6	0.01	F	W	<1 mm
16X-6	0.01	F	LG	<1 mm
18X-5	0.01	F	LG	<1 mm
18X-6	0.01	F	W	<1 mm
18X-6	0.01	F	W	<1 mm
18X-6	0.01	F	LG	<1 mm
18X-6	0.01	F	W	<1 mm
30X-3	0.02	L	P	From IW sample ~40 degree angle
30X-6	0.02	IW	W	IW sample, pink/white in color, 2 cm thick but exact location within IW not known
31X-3	0.02	D	W	
32X-5	0.01	IW	P	From IW sample, 1/2 cm ash rich interval, pink in color, exact location within IW not known
35X-2	0.2	F	W/LG	Pumice from IR anomaly
42X-2	0.02	L	B	ASH LAYER
42X-2	0.02	L	B	Thin laminations of ash
42X-3	0.01	L	B	Thin ash layer
42X-4	0.01	D	B	Disseminated ash in thin layer
42X-4	0.03	D	B	Disseminated ash in thin layer
42X-4	0.03	D	B	Disseminated ash in thin layer
42X-5	0.07	D	B	Disseminated and bioturbated ash
42X-7	0.01	L	DG	Thin bed of dark gray ash, ~3mm thick
42X-7	0.02	L	B	from catwalk
42X-cc	0.02	L		ASH LAYER from cc
43X-6	0.01		B	Weak ash?
44X-3	0.05	IW		From IW sample at 36–66 cm. Ash described as “sand layer” at 4–9 cm within IW sample
46X-5	0.02	IW		From IW hydrate bearing sample at 67–97 cm. Chemists location for “clear ash layer” is at 21.5 to 23.5 cm within IW sample
47X-4	0.04	IW		From IW sample at 73–103 cm. Diagonal “sandy” zone from 21–25 cm within IW sample, but Chemists indicate that some of the hydrate may have been in the background material as well
47X-6	0.02	L	B	
47X-6	0.01	L	DG	2 mm thick, dark gray ash layer
47X-6	0.02	L	DG, B, LG	2 mm thick, dark gray ash layer

Table 3. Volcanic ash occurrences at Hole NGHP-01-17A. (To view complete table, please refer to the ASCII files.)—Continued

Core, section	Expedition	Site	Hole	Core	Core type	Section	Position start	Position end	Depth top (mbsf)	Depth base (mbsf)
NGHP-01-17A—Continued										
47X-6	1	17	A	47	X	6	114	123	412.47	412.56
47X-6	1	17	A	47	X	6	116	118	412.49	412.51
47X-6	1	17	A	47	X	6	117	119	412.5	412.52
47X-6	1	17	A	47	X	6	121	123	412.54	412.56
51X-3	1	17	A	51	X	3	78	84	428.01	428.07
51X-3	1	17	A	51	X	3	89	98.5	428.12	428.215
52X-5	1	17	A	52	X	5	45	51	430.37	430.43
51X-5	1	17	A	51	X	5	120	150	431.1	431.13
53X-3	1	17	A	53	X	3	100.5	101	446.355	446.36
53X-3	1	17	A	53	X	3	105	107	446.4	446.42
53X-4	1	17	A	53	X	4	0	13	446.85	446.98
53X-4	1	17	A	53	X	4	25	27	447.1	447.12
53X-4	1	17	A	53	X	4	27	28	447.12	447.13
53X-4	1	17	A	53	X	4	37	58	447.22	447.43
53X-4	1	17	A	53	X	4	52	54	447.37	447.39
53X-4	1	17	A	53	X	4	56	57	447.41	447.42
53X-6	1	17	A	53	X	6	47	62	449.65	449.8
55X-2	1	17	A	55	X	2	35	47	464.35	464.47
55X-3	1	17	A	55	X	3	6	11	464.63	464.68
55X-3	1	17	A	55	X	3	9	11	464.66	464.68
55X-3	1	17	A	55	X	3	19	20	464.76	464.77
56X-1	1	17	A	56	X	1	3	5	472.73	472.75
56X-2	1	17	A	56	X	2	13.5	17.5	473.835	473.875
56X-2	1	17	A	56	X	2	69	99	474.4	474.41
57X-1	1	17	A	57	X	1	14	15	482.54	482.55
57X-1	1	17	A	57	X	1	15	16	482.55	482.56
57X-1	1	17	A	57	X	1	18	19	482.58	482.59
57X-1	1	17	A	57	X	1	22	23	482.62	482.63
57X-1	1	17	A	57	X	1	35	36	482.75	482.76
57X-2	1	17	A	57	X	2	16	20	482.95	482.99
57X-2	1	17	A	57	X	2	20	21	482.99	483
57X-2	1	17	A	57	X	2	21	23	483	483.02
57X-2	1	17	A	57	X	2	40	48	483.19	483.27
57X-2	1	17	A	57	X	2	61	63	483.4	483.42
57X-2	1	17	A	57	X	2	91	92	483.7	483.71
57X-5	1	17	A	57	X	5	28	29	486.96	486.97
57X-5	1	17	A	57	X	5	30	34	486.98	487.02
57X-5	1	17	A	57	X	5	34	36	487.02	487.04
57X-5	1	17	A	57	X	5	40	42	487.08	487.1
58X-1	1	17	A	58	X	1	125	127	493.25	493.27
58X-2	1	17	A	58	X	2	33	34	493.61	493.62
58X-2	1	17	A	58	X	2	57	59	493.85	493.87
58X-2	1	17	A	58	X	2	110	118	494.38	494.46
58X-2	1	17	A	58	X	2	125	126	494.53	494.54
58X-2	1	17	A	58	X	2	131	132	494.59	494.6
58X-2	1	17	A	58	X	2	137	150	494.65	494.78
58X-3	1	17	A	58	X	3	0	8	494.78	494.86
58X-3	1	17	A	58	X	3	77	78	495.55	495.56
58X-5	1	17	A	58	X	5	47	50	497.7	497.73
58X-6	1	17	A	58	X	6	5	6	498.78	498.79
58X-6	1	17	A	58	X	6	14	15	498.87	498.88
58X-6	1	17	A	58	X	6	16	17	498.89	498.9
58X-6	1	17	A	58	X	6	19	20	498.92	498.93
58X-6	1	17	A	58	X	6	23	24	498.96	498.97
58X-6	1	17	A	58	X	6	50	52	499.23	499.25
58X-6	1	17	A	58	X	6	93	97	499.66	499.7
59P-1	1	17	A	59	P	1	28.5	30	499.885	499.9
59P-1	1	17	A	59	P	1	30	31	499.9	499.91
59P-1	1	17	A	59	P	1	31	32	499.91	499.92

Table 3. Volcanic ash occurrences at Hole NGHP-01-17A. (To view complete table, please refer to the ASCII files.)—Continued

Core, section	Thickness (m)	Ash type	Color	Comment
				NGHP-01-17A—Continued
47X-6	0.09	L	DG	Extensively bioturbated, dark gray ash bed
47X-6	0.02	L	DG	Extensively bioturbated, dark gray ash bed
47X-6	0.02	L	DG	Extensively bioturbated, dark gray ash bed
47X-6	0.02	L	DG	Extensively bioturbated, dark gray ash bed
51X-3	0.06	D	B	
51X-3	0.1	IW		From IW sample at 89–119 cm. IR anomaly with ash layer at 0–9.5 cm
52X-5	0.06	IW		From IW sample at 27–57 cm. Ash mixed with sediment noted by chemists at 18–24 cm.
51X-5	0.03	D	G	
53X-3	0	L	B	discontinuous
53X-3	0.02	L	B	~1 cm thick
53X-4	0.13	D	B	
53X-4	0.02	L	B/W	1 to 2 cm thick
53X-4	0.01	L	B	1 to 2 cm thick
53X-4	0.21	D	B	
53X-4	0.02	L	B	<1cm thick
53X-4	0.01	L	B/W	<1cm thick
53X-6	0.15	IW		IW sample. Chemists noted that the IR anomaly occurred both in the ash bearing interval at 56–62 cm; adjacent clay with anomaly at 52–56 cm
55X-2	0.12	IW	W	From IW sample taken at 17–47 cm. Ash from 35–47 cm with IR anomaly. Chemists noted that this ash looks “coarser” with “more ash”?
55X-3	0.05	L	B	Black ash layer
55X-3	0.02	L	B	Black ash layer
55X-3	0.01	L	B	Black ash layer
56X-1	0.02	F	B	
56X-2	0.04	IW	DG	From IW sample at 69–99 cm. Dark “brown” ash at “Max. IR anomaly” at 13.5–17.5 cm
56X-2	0.01	F	DG	Fine grained ash, brownish in color, from IW sample
57X-1	0.01	D	B	Disseminated black ash fragments as burrow fill
57X-1	0.01	D	B	Disseminated black ash fragments as burrow fill
57X-1	0.01	D	B	Disseminated black ash fragments as burrow fill
57X-1	0.01	D	B	Disseminated black ash fragments as burrow fill
57X-1	0.01	D	B	Disseminated black ash fragments as burrow fill
57X-2	0.04	B	B	Black ash burrow fill
57X-2	0.01	L	B	Thick black ash layer
57X-2	0.02	L	B	Thick black ash layer
57X-2	0.08	B	B	Black ash burrow fill
57X-2	0.02	B	B	Black ash burrow fill
57X-2	0.01	B	B	Black ash burrow fill
57X-5	0.01	L	B	Thin black ash layer
57X-5	0.04	L	B	Thick black ash layer
57X-5	0.02	L	B	Thick black ash layer
57X-5	0.02	L	B	
58X-1	0.02	D	B	Disseminated black ash
58X-2	0.01	D	B	Disseminated black ash
58X-2	0.02	D	B	Disseminated black ash
58X-2	0.08	D	B	Disseminated black ash
58X-2	0.01	D	B	Disseminated black ash
58X-2	0.01	D	B	Disseminated black ash
58X-2	0.13	D	B	Disseminated black ash
58X-3	0.08	D	B	massive layer
58X-3	0.01	D	B	Disseminated black ash
58X-5	0.03	D	B	Disseminated black ash
58X-6	0.01	D	B	Disseminated black ash
58X-6	0.01	D	B	Disseminated black ash
58X-6	0.01	D	B	Disseminated black ash
58X-6	0.01	D	B	Disseminated black ash
58X-6	0.01	D	B	Disseminated black ash
58X-6	0.02	D	B	Disseminated black ash
58X-6	0.04	D	B	Disseminated black ash
59P-1	0.01	L	G	Gray ash layer
59P-1	0.01	L	DG	Dark gray ash layer
59P-1	0.01	L	G	Gray ash layer

Table 3. Volcanic ash occurrences at Hole NGHP-01-17A. (To view complete table, please refer to the ASCII files.)—Continued

Core, section	Expedition	Site	Hole	Core	Core type	Section	Position start	Position end	Depth top (mbsf)	Depth base (mbsf)
NGHP-01-17A—Continued										
59P-1	1	17	A	59	P	1	33.5	34	499.935	499.94
60Y-1	1	17	A	60	Y	1	13	15	500.73	500.75
60Y-1	1	17	A	60	Y	1	45	47	501.05	501.07
60Y-1	1	17	A	60	Y	1	46	48	501.06	501.08
60Y-1	1	17	A	60	Y	1	74	76	501.34	501.36
60Y-1	1	17	A	60	Y	1	75	77	501.35	501.37
61X-2	1	17	A	61	X	2	37	38	502.68	502.69
61X-2	1	17	A	61	X	2	45	46	502.76	502.77
61X-2	1	17	A	61	X	2	60	79	502.91	503.1
61X-3	1	17	A	61	X	3	26	32	503.5059222	503.5119043
61X-3	1	17	A	61	X	3	32	34	503.5119043	503.5138983
61X-3	1	17	A	61	X	3	66	67	503.5458026	503.5467996
61X-3	1	17	A	61	X	3	83	84	503.5627517	503.5637488
61X-4	1	17	A	61	X	4	39	40	505.37	505.38
62X-1	1	17	A	62	X	1	2	4	511.22	511.24
62X-1	1	17	A	62	X	1	14	15	511.34	511.35
62X-1	1	17	A	62	X	1	57	59	511.77	511.79
62X-2	1	17	A	62	X	2	0	7	512.24	512.31
62X-2	1	17	A	62	X	2	8	9	512.32	512.33
62X-2	1	17	A	62	X	2	23	24	512.47	512.48
62X-2	1	17	A	62	X	2	32	33	512.56	512.57
62X-2	1	17	A	62	X	2	35	37	512.59	512.61
62X-3	1	17	A	62	X	3	22	26	513.84	513.88
62X-4	1	17	A	62	X	4	1.5	2	515.125	515.13
62X-4	1	17	A	62	X	4	122	123	516.33	516.34
62X-7	1	17	A	62	X	7	62	65	519.73	519.76
63X-1	1	17	A	63	X	1	81	82	521.61	521.62
63X-2	1	17	A	63	X	2	35	52	522.08	522.25
63X-2	1	17	A	63	X	2	43	47	522.16	522.2
63X-2	1	17	A	63	X	2	63	67	522.36	522.4
63X-2	1	17	A	63	X	2	70	76	522.43	522.49
63X-2	1	17	A	63	X	2	114	118	522.87	522.91
63X-2	1	17	A	63	X	2	132	140	523.05	523.13
63X-3	1	17	A	63	X	3	26	27	523.49	523.5
63X-4	1	17	A	63	X	4	2	4	524.25	524.27
63X-5	1	17	A	63	X	5	13	14	525.18	525.19
63X-5	1	17	A	63	X	5	30	31	525.35	525.36
63X-5	1	17	A	63	X	5	139	141	526.44	526.46
64X-3	1	17	A	64	X	3	3	5	532.9	532.92
64X-3	1	17	A	64	X	3	9	11	532.96	532.98
64X-3	1	17	A	64	X	3	20	22	533.07	533.09
64X-3	1	17	A	64	X	3	26	28	533.13	533.15
64X-3	1	17	A	64	X	3	33	34	533.2	533.21
64X-3	1	17	A	64	X	3	36	38	533.23	533.25
64X-3	1	17	A	64	X	3	42	44	533.29	533.31
64X-3	1	17	A	64	X	3	64	66	533.51	533.53
64X-3	1	17	A	64	X	3	74	77	533.61	533.64
66X-2	1	17	A	66	X	2	57	79	551.07	551.29
66X-3	1	17	A	66	X	3	1	2	552.01	552.02
66X-3	1	17	A	66	X	3	6	9	552.32	552.33
66X-3	1	17	A	66	X	3	19	21	552.32	552.33
66X-3	1	17	A	66	X	3	24	25	552.22	552.26
66X-4	1	17	A	66	X	4	106	107	554.17	554.18
66X-4	1	17	A	66	X	4	107	108	554.18	554.19
66X-5	1	17	A	66	X	5	51	56	554.94	554.99
66X-5	1	17	A	66	X	5	75	81	555.18	555.24
66X-7	1	17	A	66	X	7	78	80	557.7	557.72
67X-3	1	17	A	67	X	3	10	11	561.5	561.51
67X-5	1	17	A	67	X	5	45	48	563.09	563.12
68X-1	1	17	A	68	X	1	60	75	569.6	569.75
68X-3	1	17	A	68	X	3	8	22	570.94	571.08
68X-3	1	17	A	68	X	3	16	18	571.02	571.04
68X-5	1	17	A	68	X	5	58	59	573.67	573.68
68X-6	1	17	A	68	X	6	63	65	575.22	575.24

Table 3. Volcanic ash occurrences at Hole NGHP-01-17A. (To view complete table, please refer to the ASCII files.)—Continued

Core, section	Thickness (m)	Ash type	Color	Comment
			NGHP-01-17A—Continued	
59P-1	0	L	G	Gray ash layer
60Y-1	0.02	D	DG/B	
60Y-1	0.02	L	B	Black ash layer
60Y-1	0.02	D	DG/B	
60Y-1	0.02	F	B	
60Y-1	0.02	L	B	
61X-2	0.01	L	B	Black ash horizon
61X-2	0.01	L	B	Black ash horizon
61X-2	0.19	D	B	Disseminated black ash
61X-3	0.01	D	B	Disseminated black ash
61X-3	0	D	B	Disseminated black ash
61X-3	0	B	B	Burrow fill, black
61X-3	0	B	B	Burrow fill, black
61X-4	0.01	L	B	Black ash horizon
62X-1	0.02	L	DG	Ash in disturbed biscuits
62X-1	0.01	L	DG	Ash in disturbed biscuits
62X-1	0.02	L	DG	Ash in disturbed biscuits
62X-2	0.07	D	DG	Dark gray zones
62X-2	0.01	B	DG	Dark gray ash burrows
62X-2	0.01	D	DG	Dark gray zones
62X-2	0.01	D	DG	Dark gray zones
62X-2	0.02	D	DG	Dark gray zones
62X-3	0.04	D	DG	Dark gray zones
62X-4	0	D	DG	Dark gray zones
62X-4	0.01	D	DG	Dark gray zones
62X-7	0.03	D	DG	Dark gray zones
63X-1	0.01	D	B	
63X-2	0.17	B	B/W	Ash filled burrows (with sponge spicules)
63X-2	0.04	D	B	Disseminated
63X-2	0.04	D	B	
63X-2	0.06	B	LG	Ash filled burrows (with sponge spicules)
63X-2	0.04	B	LG/B	Ash filled burrows (with sponge spicules)
63X-2	0.08	B	LG/B	Ash filled burrows (with sponge spicules)
63X-3	0.01	F	W	Fragment
63X-4	0.02		LG/W	
63X-5	0.01	B	W/LG	Ash filled burrows (with sponge spicules)
63X-5	0.01	B	W	Ash filled burrows (with sponge spicules)
63X-5	0.02	B	W	Ash filled burrows (with sponge spicules)
64X-3	0.02	D	B	Black ash disseminated in discrete layers/bands
64X-3	0.02	D	B	Black ash disseminated in discrete layers/bands
64X-3	0.02	D	B	Black ash disseminated in discrete layers/bands
64X-3	0.02	D	B	Black ash disseminated in discrete layers/bands
64X-3	0.01	D	B	Black ash disseminated in discrete layers/bands
64X-3	0.02	D	B	Black ash disseminated in discrete layers/bands
64X-3	0.02	D	B	Black ash disseminated in discrete layers/bands
64X-3	0.02	D	B	Black ash disseminated in discrete layers/bands
64X-3	0.03	D	B	Black ash disseminated in discrete layers/bands
66X-2	0.22	D	B/W	Disseminated in layers
66X-3	0.01	F	W/B	Glass fragments
66X-3	0.01	F	B/LG	Glass fragments
66X-3	0.01	D	W	
66X-3	0.04	F	W/B	Glass fragments
66X-4	0.01	B	W	Burrows filled with sponge spicules and ash
66X-4	0.01	B	W	Burrows filled with sponge spicules and ash
66X-5	0.05	D	B	Disseminated
66X-5	0.06	IW	B	From IW sample at 69–99 cm. Distinct black ash at 6–12 cm within IW interval
66X-7	0.02	D	B	Disseminated
67X-3	0.01	L	B	Black ash layer
67X-5	0.03	D	B	Black volcanic glass rich zone
68X-1	0.15	B	B	Black ash in Zoophycus burrow
68X-3	0.14	B	B	Black ash in Zoophycus burrow
68X-3	0.02	B	B	Black ash in Zoophycus burrow
68X-5	0.01	L	B	Black ash layer
68X-6	0.02	L	B	Black ash layer

Table 3. Volcanic ash occurrences at Hole NGHP-01-17A. (To view complete table, please refer to the ASCII files.)—Continued

Core, section	Expedition	Site	Hole	Core	Core type	Section	Position start	Position end	Depth top (mbsf)	Depth base (mbsf)
NGHP-01-17A—Continued										
69X-6	1	17	A	69	X	6	71	78	586.41	586.48
69X-7	1	17	A	69	X	7	20	22	586.9	586.92
72X-CC	1	17	A	72	X	CC	0	0.01	590.56	590.57
75X-3	1	17	A	75	X	3	38	47	619.65	619.74
75X-3	1	17	A	75	X	3	138	150	620.65	620.77
75X-4	1	17	A	75	X	4	0	21	620.77	620.98
75X-4	1	17	A	75	X	4	53	60	621.3	621.37
75X-4	1	17	A	75	X	4	71	80	621.48	621.57
75X-4	1	17	A	75	X	4	86	96	621.63	621.73
77X-1	1	17	A	77	X	1	26	28	634.66	634.68
77X-1	1	17	A	77	X	1	43	47	634.83	634.87
77X-1	1	17	A	77	X	1	80	82	635.2	635.22
77X-2	1	17	A	77	X	2	40	42	635.64	635.66
77X-2	1	17	A	77	X	2	91	95	636.15	636.19
77X-4	1	17	A	77	X	4	44	46	638.22	638.24
77X-5	1	17	A	77	X	5	72	73	640	640.01
77X-5	1	17	A	77	X	5	89	89	640.17	640.17
77X-6	1	17	A	77	X	6	6	15	640.34	640.43
77X-6	1	17	A	77	X	6	39	50	640.67	640.78
77X-6	1	17	A	77	X	6	45	47	640.73	640.75
78X-1	1	17	A	78	X	1	35	38	644.45	644.48
78X-1	1	17	A	78	X	1	35	37	644.45	644.47
78X-2	1	17	A	78	X	2	84	87	646.05	646.08
78X-2	1	17	A	78	X	2	89	91	646.1	646.12
78X-3	1	17	A	78	X	3	6	14	646.77	646.85
78X-4	1	17	A	78	X	4	3	12	648.24	648.33
78X-5	1	17	A	78	X	5	94	95	650.65	650.66
79X-1	1	17	A	79	X	1	10	12	653.9	653.92
79X-1	1	17	A	79	X	1	29	30	654.09	654.1
79X-1	1	17	A	79	X	1	58	59	654.38	654.39
79X-1	1	17	A	79	X	1	61	64	654.41	654.44
79X-1	1	17	A	79	X	1	66	78	654.46	654.58
79X-1	1	17	A	79	X	1	80	83	654.6	654.63
79X-1	1	17	A	79	X	1	127	128	655.07	655.08
79X-1	1	17	A	79	X	1	129	130	655.09	655.1
79X-1	1	17	A	79	X	1	136	137	655.16	655.17
79X-1	1	17	A	79	X	1	146	147	655.26	655.27
79X-2	1	17	A	79	X	2	3	4	655.33	655.34
79X-2	1	17	A	79	X	2	7	8	655.37	655.38
79X-2	1	17	A	79	X	2	10	11	655.4	655.41
79X-2	1	17	A	79	X	2	28	29	655.58	655.59
79X-2	1	17	A	79	X	2	46	47	655.76	655.77
79X-2	1	17	A	79	X	2	51	52	655.81	655.82
79X-2	1	17	A	79	X	2	59	60	655.89	655.9
79X-2	1	17	A	79	X	2	65	66	655.95	655.96
79X-2	1	17	A	79	X	2	70	71	656	656.01
79X-2	1	17	A	79	X	2	87	96	656.17	656.26
79X-2	1	17	A	79	X	2	90	92	656.2	656.22
79X-2	1	17	A	79	X	2	92	95	656.22	656.25
79X-3	1	17	A	79	X	3	6	7	656.86	656.87
79X-3	1	17	A	79	X	3	18	19	656.98	656.99
79X-3	1	17	A	79	X	3	34	35	657.14	657.15
79X-3	1	17	A	79	X	3	38	39	657.18	657.19
79X-3	1	17	A	79	X	3	42	43	657.22	657.23
79X-3	1	17	A	79	X	3	48	49	657.28	657.29
79X-3	1	17	A	79	X	3	58	59	657.38	657.39
79X-3	1	17	A	79	X	3	69	70	657.49	657.5
79X-3	1	17	A	79	X	3	77	78	657.57	657.58
79X-3	1	17	A	79	X	3	82	83	657.62	657.63
79X-3	1	17	A	79	X	3	93	94	657.73	657.74
79X-3	1	17	A	79	X	3	127	128	658.07	658.08
79X-3	1	17	A	79	X	3	130	131	658.1	658.11

Table 3. Volcanic ash occurrences at Hole NGHP-01-17A. (To view complete table, please refer to the ASCII files.)—Continued

Core, section	Thickness (m)	Ash type	Color	Comment
				NGHP-01-17A—Continued
69X-6	0.07	IW	B	From IW sample at 55–85 cm. IR anomaly at 16 to 23 cm within sample Ash sampled from this for JJA
69X-7	0.02	L	LG/B	
72X-CC	0.01	CC		bottom of CC
75X-3	0.09	B	B	Black ash, bioturbated up and down
75X-3	0.12	B	B	Black ash, bioturbated up and down
75X-4	0.21	B	B	Black ash bioturbated upand down, very coarse grained
75X-4	0.07	L	B	Layer, half of vertical section other shared w/ WGS
75X-4	0.09	B	B	Black ash bioturbated upand down, very coarse grained
75X-4	0.1	B	B	Black ash bioturbated upand down, coarse and fine grained
77X-1	0.02	L	B	Black ash rich layer, speckled ash/pumice/volcanic fragments
77X-1	0.04	L	B	Black ash rich layer, speckled ash/pumice/volcanic fragments
77X-1	0.02	L	B	Black ash rich layer, speckled ash/pumice/volcanic fragments
77X-2	0.02	B	B	Black ash filled burrows
77X-2	0.04	L	B	Black ash rich layer
77X-4	0.02	L	B	Black ash rich layer
77X-5	0.01	B	B	Burrows filled with sponge spicules and ash
77X-5	0	B	B	Burrows filled with sponge spicules and ash
77X-6	0.09	B	B	Burrows filled with sponge spicules and ash
77X-6	0.11	L	B	Black ash bed
77X-6	0.02	L	B	Black ash bed
78X-1	0.03	L	B	Black ash bed
78X-1	0.02	L	B	Black ash bed
78X-2	0.03	L	B	Black ash bed
78X-2	0.02	L	B	Black ash bed
78X-3	0.08	B	B	Burrows filled with sponge spicules and ash
78X-4	0.09	D	B	Black ash rich zone
78X-5	0.01	B	B	Burrows filled with sponge spicules and ash
79X-1	0.02	B	B	Burrows filled with sponge spicules and ash
79X-1	0.01	B	B	Burrows filled with sponge spicules and ash
79X-1	0.01	B	B	Burrows filled with sponge spicules and ash
79X-1	0.03	L	B	Black ash bed
79X-1	0.12	L	B	Black ash bed
79X-1	0.03	L	B	Black ash bed
79X-1	0.01	B	B	Burrows filled with sponge spicules and ash
79X-1	0.01	B	B	Burrows filled with sponge spicules and ash
79X-1	0.01	B	B	Burrows filled with sponge spicules and ash
79X-1	0.01	B	B	Burrows filled with sponge spicules and ash
79X-2	0.01	B	B	Burrows filled with sponge spicules and ash
79X-2	0.01	B	B	Burrows filled with sponge spicules and ash
79X-2	0.01	B	B	Burrows filled with sponge spicules and ash
79X-2	0.01	B	B	Burrows filled with sponge spicules and ash
79X-2	0.01	B	B	Burrows filled with sponge spicules and ash
79X-2	0.01	B	B	Burrows filled with sponge spicules and ash
79X-2	0.01	B	B	Burrows filled with sponge spicules and ash
79X-2	0.01	B	B	Burrows filled with sponge spicules and ash
79X-2	0.09	L	B	Black ash bed
79X-2	0.02	L	DG	darker gray ash layer
79X-2	0.03	L	LG	light gray ash layer
79X-3	0.01	B	B	Burrows filled with sponge spicules and ash
79X-3	0.01	B	B	Burrows filled with sponge spicules and ash
79X-3	0.01	B	B	Burrows filled with sponge spicules and ash
79X-3	0.01	B	B	Burrows filled with sponge spicules and ash
79X-3	0.01	B	B	Burrows filled with sponge spicules and ash
79X-3	0.01	B	B	Burrows filled with sponge spicules and ash
79X-3	0.01	B	B	Burrows filled with sponge spicules and ash
79X-3	0.01	B	B	Burrows filled with sponge spicules and ash
79X-3	0.01	B	B	Burrows filled with sponge spicules and ash
79X-3	0.01	B	B	Burrows filled with sponge spicules and ash
79X-3	0.01	B	B	Burrows filled with sponge spicules and ash

Table 3. Volcanic ash occurrences at Hole NGHP-01-17A. (To view complete table, please refer to the ASCII files.)—Continued

Core, section	Expedition	Site	Hole	Core	Core type	Section	Position start	Position end	Depth top (mbsf)	Depth base (mbsf)
NGHP-01-17A—Continued										
79X-3	1	17	A	79	X	3	145	146	658.25	658.26
79X-4	1	17	A	79	X	4	6	7	658.36	658.37
79X-4	1	17	A	79	X	4	18	19	658.48	658.49
79X-4	1	17	A	79	X	4	34	35	658.64	658.65
79X-4	1	17	A	79	X	4	38	39	658.68	658.69
79X-4	1	17	A	79	X	4	42	43	658.72	658.73
79X-4	1	17	A	79	X	4	48	49	658.78	658.79
79X-4	1	17	A	79	X	4	58	59	658.88	658.89
79X-4	1	17	A	79	X	4	69	70	658.99	659
79X-4	1	17	A	79	X	4	77	78	659.07	659.08
79X-4	1	17	A	79	X	4	82	83	659.12	659.13
79X-4	1	17	A	79	X	4	93	94	659.23	659.24
79X-4	1	17	A	79	X	4	127	128	659.57	659.58
79X-4	1	17	A	79	X	4	130	131	659.6	659.61
79X-4	1	17	A	79	X	4	145	146	659.75	659.76
79X-5	1	17	A	79	X	5	21	22	660.01	660.02
79X-5	1	17	A	79	X	5	54	55	660.34	660.35
79X-5	1	17	A	79	X	5	93	94	660.73	660.74
79X-5	1	17	A	79	X	5	113	114	660.93	660.94
79X-5	1	17	A	79	X	5	119	120	660.99	661
79X-5	1	17	A	79	X	5	131	132	661.11	661.12
79X-6	1	17	A	79	X	6	24	25	661.54	661.55
79X-6	1	17	A	79	X	6	35	37	661.65	661.67
79X-6	1	17	A	79	X	6	39	40	661.69	661.7
79X-6	1	17	A	79	X	6	47	48	661.77	661.78
79X-6	1	17	A	79	X	6	54	55	661.84	661.85
79X-6	1	17	A	79	X	6	59	60	661.89	661.9
79X-6	1	17	A	79	X	6	66	67	661.96	661.97
79X-6	1	17	A	79	X	6	70	71	662	662.01
79X-6	1	17	A	79	X	6	74	75	662.04	662.05
79X-6	1	17	A	79	X	6	91	92	662.21	662.22
79X-6	1	17	A	79	X	6	106	107	662.36	662.37
80X-1	1	17	A	80	X	1	16	20	662.86	662.9
80X-2	1	17	A	80	X	2	19	20	663.2	663.21
80X-2	1	17	A	80	X	2	20	21	663.21	663.22
80X-2	1	17	A	80	X	2	22	23	663.23	663.24
80X-3	1	17	A	80	X	3	10	11	664.56	664.57
80X-4	1	17	A	80	X	4	5	22	665.47	665.64
82X-2	1	17	A	82	X	2	38	39	673.88	673.89
82X-2	1	17	A	82	X	2	64	65	674.14	674.15
82X-6	1	17	A	82	X	6	39	40	679.46	679.47
82X-6	1	17	A	82	X	6	41	42	679.48	679.49
82X-6	1	17	A	82	X	6	43	44	679.5	679.51
82X-6	1	17	A	82	X	6	44	45	679.51	679.52
83X-1	1	17	A	83	X	1	17	21	683.07	683.11
83X-1	1	17	A	83	X	1	51	52	683.41	683.42
83X-1	1	17	A	83	X	1	93	94	683.83	683.84

Table 3. Volcanic ash occurrences at Hole NGHP-01-17A. (To view complete table, please refer to the ASCII files.)—Continued

Core, section	Thickness (m)	Ash type	Color	Comment
			NGHP-01-17A—Continued	
79X-3	0.01	B	B	Burrows filled with sponge spicules and ash
79X-4	0.01	B	B	Burrows filled with sponge spicules and ash
79X-4	0.01	B	B	Burrows filled with sponge spicules and ash
79X-4	0.01	B	B	Burrows filled with sponge spicules and ash
79X-4	0.01	B	B	Burrows filled with sponge spicules and ash
79X-4	0.01	B	B	Burrows filled with sponge spicules and ash
79X-4	0.01	B	B	Burrows filled with sponge spicules and ash
79X-4	0.01	B	B	Burrows filled with sponge spicules and ash
79X-4	0.01	B	B	Burrows filled with sponge spicules and ash
79X-4	0.01	B	B	Burrows filled with sponge spicules and ash
79X-4	0.01	B	B	Burrows filled with sponge spicules and ash
79X-4	0.01	B	B	Burrows filled with sponge spicules and ash
79X-4	0.01	B	B	Burrows filled with sponge spicules and ash
79X-4	0.01	B	B	Burrows filled with sponge spicules and ash
79X-5	0.01	B	B	Burrows filled with sponge spicules and ash
79X-5	0.01	B	B	Burrows filled with sponge spicules and ash
79X-5	0.01	B	B	Burrows filled with sponge spicules and ash
79X-5	0.01	B	B	Burrows filled with sponge spicules and ash
79X-5	0.01	B	B	Burrows filled with sponge spicules and ash
79X-5	0.01	B	B	Burrows filled with sponge spicules and ash
79X-6	0.01	B	B	Burrows filled with sponge spicules and ash
79X-6	0.02	L	B	Black ash bed
79X-6	0.01	B	B	Burrows filled with sponge spicules and ash
79X-6	0.01	B	B	Burrows filled with sponge spicules and ash
79X-6	0.01	B	B	Burrows filled with sponge spicules and ash
79X-6	0.01	B	B	Burrows filled with sponge spicules and ash
79X-6	0.01	B	B	Burrows filled with sponge spicules and ash
79X-6	0.01	B	B	Burrows filled with sponge spicules and ash
79X-6	0.01	B	B	Burrows filled with sponge spicules and ash
79X-6	0.01	B	B	Burrows filled with sponge spicules and ash
79X-6	0.01	B	B	Burrows filled with sponge spicules and ash
80X-1	0.04	B	W	Burrows filled with sponge spicules and ash
80X-2	0.01	B	W	Burrows filled with sponge spicules and ash
80X-2	0.01	D	W	Burrows filled with sponge spicules and ash
80X-2	0.01	B	W	Burrows filled with sponge spicules and ash
80X-3	0.01	B	W	Burrows filled with sponge spicules and ash
80X-4	0.17	B	W	Burrows filled with sponge spicules and ash
82X-2	0.01	B	W/LG	Burrows filled with sponge spicules and ash
82X-2	0.01	B	W	Burrows filled with sponge spicules and ash
82X-6	0.01	D	B	disseminated ash
82X-6	0.01	D	LG	disseminated ash
82X-6	0.01	D	LG	disseminated ash
82X-6	0.01	D	LG	disseminated ash
83X-1	0.04	B	W	Burrows filled with sponge spicules and ash
83X-1	0.01	B	LG	Burrows filled with sponge spicules and ash
83X-1	0.01	B	LG	Burrows filled with sponge spicules and ash

Total thickness of ash bearing layers within the GHOZ: 7.65.

The major lithologies of Lithostratigraphic Subunit Ib determined from smear slides consist primarily of clay-sized (70–99 percent) grains with minor amounts of silt-sized grains (up to 30 percent; table 1). Minor lithologies described in smear slide included volcanic ash and glass-rich and authigenic-carbonate-rich zones. Non-biogenic components identified in smear slide of Lithostratigraphic Subunit Ia are generally present in small amounts (trace to 5 percent; table 1) with the exception of pyrite, which occurs in amounts larger than 5 percent, primarily in the coarse fraction (table 2). The biogenic component of the sediment is dominated by calcareous nannofossils, which comprise 80 percent to 98 percent of the total (biogenic and non-biogenic) sediment grains (table 1). Foraminifera occur (trace to 7 percent) in smear slides, and comprise 15 percent to 50 percent of the sediment coarse fraction (table 2). Authigenic carbonate precipitates were observed in smear slides in several places within Subunit Ib (see above and table 1). We tentatively assign an age of Late Miocene to Late Pliocene to Subunit Ib by extrapolating the average sedimentation rate of 5.6 cm/kyr, from Subunit Ia, to the bottom of Subunit Ib.

Subunit Ic

Intervals: Hole NGHP-01-17A, Sections NGHP-01-17A-39X-3 to NGHP-01-17A-83X-CC

Depth: Hole NGHP-01-17A, 334.5–691.6 mbsf

Age: Middle Miocene to Late Miocene

Lithostratigraphic Subunit Ic is composed of diatom-bearing-to-rich and sponge spicule-bearing to-rich nannofossil ooze that ranges in color from greenish grey (10GY 5/1) to dark greenish grey (10Y 4/1 and 5GY 5/1; figs. 7A and 7C, and Site NGHP-01-17 Visual Core Descriptions). The siliceous components in the coarse fraction and smear slide samples occur consistently in a greater abundance (trace to 20 percent in both coarse fraction and smear slide) throughout Subunit Ic, as compared to the overlying units. In particular, sponge spicules and diatoms are more abundant than silicoflagellates and radiolarians (tables 1 and 2). By extrapolation of the average sedimentation rate from Subunit Ia (5.6 cm/kyr), the estimated age at the bottom of Subunit Ic is ~12 Ma.

Shell fragments and sponge spicules are visible on the split core surface sporadically throughout Subunit Ic (figs. 7A and 7C, and Site NGHP-01-17 Visual Core Descriptions), consistent with their presence in smear slide and coarse fraction (tables 1 and 2). Authigenic carbonates (likely calcite or dolomite crystals) are observed in significant abundance in the clay to silt size fraction in smear slides from Cores NGHP-01-17A-45X and NGHP-01-17A-67X (figs. 7A, 7C, Site NGHP-01-17 Visual Core Descriptions and table 1). These precipitates appear to have significantly cemented the surrounding sediments, producing more lithified sediments that were more difficult to drill and core (see “Operations”). Bioturbation is abundant throughout Subunit Ic. Iron sulfide and pyrite precipitates are observed sporadically on the split core surface to 475 mbsf (figs. 7A and 7C, and Site NGHP-01-17 Visual Core Descriptions). Smear slides throughout the Subunit document iron sulfides present as trace to 5 percent, particularly from Core NGHP-01-17A-42X to TD (table 1).

Volcanic ash, present either as beds, bioturbated beds, burrow fills, or disseminated through sediments, occurs sporadically throughout Subunit Ic (figs. 9 and 10, and table 3). The abundance of ash is greater than in previous Subunits and is dominated by the occurrence of black ashes. Grey ashes are also present, whereas white ashes are the least abundant (fig. 10). This contrasts with Subunits Ia and Ib, which are dominated by white and grey ashes, with only a few black ashes (figs. 9 and 10). Magnetic susceptibility (figs. 7A and 7C) remains generally low throughout Subunit Ic, however, there are several sharp but low magnitude peaks in susceptibility that appear to correlate with the occurrences of many of the ashes (figs. 7A and 7C). The presence of ferrimagnetic metastable iron monosulfides (gregite or pyrrhotite) may also contribute to this signal, however, the decreased abundance of any iron sulfide precipitates (pyrite, pyrrhotite, or gregite) in the core below Core NGHP-01-17A-57X, and the increase in the occurrences of ash, suggests the magnetic susceptibility highs are most likely related to the ashes (figs. 7A and 7C).

The major lithologies of Lithostratigraphic Subunit Ic were determined from smear slides and consist primarily of clay-sized (76–99 percent) grains with minor amounts of silt-sized grains (up to 24 percent; table 1). Minor lithologies described in smear slide include volcanic ashes, iron sulfide-rich zones, and organic-rich intervals. Non-biogenic components identified in smear slides are present in low amounts (trace to 5 percent) in the major lithologies, but increase in the ashes (table 1). The total biogenic component of the sediment is dominated by calcareous nannofossils, which comprise 74 percent to 99 percent of the total (biogenic and non-biogenic) sediment grains of the major lithology (table 1). Foraminifera occur (trace to 3 percent) in smear slides, and are more abundant (trace to 60 percent) in the coarse fractions of the sediments (table 2). We tentatively assign an age of Middle to Late Miocene to Unit Ic by extrapolating a sedimentation rate 5.6 cm/ky to the bottom of the Subunit (see above).

Sedimentary Environment

At Site NGHP-01-17, a remarkably uniform 691.6 m thick sediment sequence of predominantly nannofossil ooze was deposited at an estimated sedimentation rate of ~5.6 cm/ky (see above). This rate is unusually high for this lithology (see, for example, Mix and others, 2003). As a first

order estimate, if the average sedimentation rate of 5.6 cm/kyr for the upper 108 m is extrapolated to the base of the hole it results in an estimated total age of 12.35 Ma for the deepest stratigraphy encountered at Site NGHP-01-17. It is important to note, however, that extrapolation of the uphole average rate to the rate of sedimentation for deeper and likely more compacted sediments is problematic. Vertical differences in loss of water content and associated compaction of sediments during burial can influence the estimation of sedimentation rates. Further caution is warranted as the extrapolation described above assumes constant sedimentation (that is, no significant quiescent or erosional events).

The terrigenous sediment contribution is low at Site NGHP-01-17, indicating that both suspended material from the Irrawady River to the N and from the Andaman Islands to the W and NW, are not major sources of sediment at this location. Minor biogenic components, such as biosiliceous grains (that is, spicules, diatoms) or foraminifera, are variable downhole and provide the basis for subunit classification (fig. 7A). After ~2.5 Ma (~130 mbsf), unbroken foraminifera tests in the coarse fraction (figs. 8A and 8B) show a relatively rapid increase to ~90 percent at present, after being relatively stable at ~40 percent, since ~11 Ma (that is, bottom of the hole). On the other hand, the total calcareous fragments (including foraminifera) show a more gradual and steady increase since ~11 Ma (fig. 8A). Simultaneous with these changes in the calcareous biogenic components, there is a gradual but steady decrease in biosiliceous grains from ~11 Ma (fig. 8), from up to 30 percent of the coarse fraction in the lower part of the section to a minor component (trace to a few percent in the coarse fraction) by ~4 Ma (~220 mbsf). This pattern could be the result of a change from a more diverse ecosystem favoring both siliceous and calcareous test-building plankton in the Miocene to a calcareous test-building dominated ecosystem in the Early Pliocene to present. Some of these ecosystem changes could be related to the Late Miocene-Early Pliocene "biogenic bloom" observed throughout the tropical Indo-Pacific (for example, Farrell and others, 1995; Dickens and Owen, 1999; Hermoyian and Owen, 2001). In particular, at Site NGHP-01-17, minor authigenic components such as carbonate and pyrite increase significantly in the ~2–6 Ma interval (fig. 10A). This increase could be related to an elevated organic matter input leading to more intense redox diagenesis during the Miocene-Pliocene biogenic bloom. Alternatively or complementarily, these changes could reflect the availability of nutrients brought into the Bay of Bengal by rivers under a variable monsoonal intensity since Miocene (for example, Clift, 2006). It is interesting to note that environmental conditions appear to have been particularly favorable for foraminifera development in the Quaternary, which could be related to the global cooling during this period and(or) to the parallel intensification of the monsoon (Clift, 2006 and references therein).

The sediment sequence drilled at Site NGHP-01-17 also contains a remarkable record of the volcanic activity in Andaman region since the Miocene (fig. 10A and table 3). The sequence contains 382 horizons of recognized pyroclastic materials, including layers and patches of white, gray and black ash, white pumice fragments, and dispersed black ash and rare scoria of lapilli size (fig. 10A). The presence of these pyroclastic materials may explain the suspected elevated sedimentation rates determine from microfossils alone, as described above. The presence of separate horizons dominated by white, gray, and black ash suggests that the volcaniclastic material originated from multiple sources or types of volcanism. Black ashes dominate at the bottom of the sequence in the time interval estimated from ~12 Ma to ~6 Ma, whereas white ashes are dominant in the top of the sequence since ~3 Ma (fig. 10B). This trend may suggest an evolution from more mafic to more felsic volcanism in the Andaman region since the Miocene. During the transition between the types of volcanism, a potential period of eruptive quiescence is suggested by the absence of ash between ~6 Ma and ~3 Ma (fig. 10). Alternatively, a significant change in sedimentation rate across this interval may explain the apparent lack of ashes. Additional biostratigraphy and radiometric dating of the ashes will aid in the further interpretation of this record.

Gas-Hydrate Occurrence

Gas hydrate was inferred and detected from several IR and porewater chloride anomalies at Site NGHP-01-17 (see "Inorganic Geochemistry" and "Physical Properties"). These anomalies are first observed in Core NGHP-01-17A-26X and are present sporadically in the ash beds and ash rich zones (fig. 10; table 3) from Core NGHP-01-17A-30X to the BSR (610 mbsf). Comparison of the IR anomalies with the occurrence of ashes and the wire-line gamma ray, *P*-wave velocity, density, and resistivity is shown in figure 11. There is good correlation between the IR anomalies, the highs in *P*-wave velocity and various resistivity logs (fig. 11), and the occurrence of ashes in several locations between Cores NGHP-01-17A-30X and the BSR (~610 mbsf). These data confirm gas hydrate was present in these intervals, although there was no visible gas hydrate observed on the catwalk. Because the thickness of ashes is small (cm scale) compared to the spatial resolution of the downhole tools, the downhole tools tend to average the *in situ* gas hydrate induced character over a larger depth interval. For this reason, not all of the ashes (particularly the thinner ones) are accurately resolved in the well log data. It is also important to note that the IR camera scans are taken on the catwalk before the voids are collapsed during core curation. Therefore, the locations of the IR anomalies may be slightly shifted relative to the depths of the ash bearing beds as recorded on well logs.

Once the voids (orange to yellow colors on the IR images) are removed, a better depth correlation can be made (see "Physical Properties").

In most of the pressure cores collected at this site, gas hydrate was not detected or recovered and there were no ash beds or ash rich zones observed (see "Pressure Coring"). Abundant methane was recovered, however, in Pressure Core NGHP-01-17A-70P, but due to low recovery in that core, it was difficult to interpret if this was due to gas hydrate (see "Pressure Coring"). In addition, Pressure Core NGHP-01-17A-81E, contained abundant methane, but that core was collected beneath the BSR and thus the methane was interpreted as free gas rather than dissociated from gas hydrate. Moussey and soupy textures were not observed in any of the split cores described on the sedimentology table; however, abundant ash beds and ash rich zones were observed (figs. 10A and 11), suggesting not all of the ash occurrences contained or were associated with gas hydrate.

Inorganic Geochemistry

The main objectives of the inorganic geochemistry program at this site were to: (1) constrain the depth distribution and abundance of gas hydrate detected by infrared (IR) anomalies and based on dissolved chloride concentrations, (2) evaluate the geologic and/structural controls on the distribution of the gas hydrate, and (3) determine the biogeochemical reactions associated with subsurface gas hydrate. Geochemical characterization of this site will allow the comparison of processes that control gas-hydrate occurrence in this accretionary prism/back arc basin transition setting with those in the sedimentary fan deposits of the eastern continental margin of India. The inorganic geochemistry data are tabulated in tables 4 and 5, and illustrated in figures 12, 14, and 15.

A total of 140 whole-round samples were collected for interstitial water (IW) analyses at Site NGHP-01-17 in a bathymetric trough (Narcondam Trough), east of the Andaman Islands, in coordination with both the organic geochemistry and microbiology sampling programs. These include all the conventional cores plus four pressure cores (Cores NGHP-01-17A-37P, -38Y, -48P and -49E). The pressure core X-ray images (see "Pressure Coring") suggested a homogeneous sediment core, therefore, just one subsample per pressure core was processed for geochemistry. Whole-round lengths for the conventional core samples ranged from 10 to 30 cm, with longer sections subsampled from cores recovered deeper within the hole. The higher resolution sampling, of 16 whole rounds in the upper 32 mbsf, was aimed at characterizing the sulfate-methane interface (SMI) and providing supporting data and samples for studies on the microbial dynamics of the SMI. From two cores below the SMI to about 330 mbsf and two cores above and below the expected level of the BSR two whole-round background samples were obtained per core; below 330 mbsf to TD (691.6 mbsf) one background sample per core was obtained.

In addition to the background whole-round sampling scheme, when the IR scan on the catwalk revealed presence of an inferred gas hydrate, whole-round samples collected with an IR anomaly were immediately transferred to the chemistry laboratory, and imaged with mounted IR and hand-held digital cameras (fig. 13). Sections showing different IR signals were separated from the whole-round sample and squeezed individually to examine the original percent of sediment pore space occupied by gas hydrate and lithological controls on gas-hydrate distribution. Two to three subsamples were processed from each whole round based on its IR profile, for an additional 28 IW samples. At this site a total of 168 samples were processed.

Interstitial Water Chloride and Salinity

Chloride concentrations were measured by titration with $AgNO_3$, with an average deviation of 0.2 percent of duplicates and salinity was determined by refractometry. The chloride concentration and salinity data are presented in table 5 and illustrated in figure 12.

The salinity depth profile mimics that of Cl^- below ~180 mbsf. The lower than seawater salinity values at 20–140 mbsf (fig. 12B), most likely reflect the loss of sulfate and some of the major seawater cations, primarily Ca^{2+} and Mg^{2+}, by biogeochemical reactions that reduce sulfate and produce alkalinity, hence, induce authigenic carbonate formation (the cations will be analyzed post cruise). The cross plot of Cl^- versus salinity (fig. 12C) clearly demonstrates the distinct behavior of salinity and Cl^- in the upper sediment section versus their coherent behavior below ~180 mbsf.

The Cl^- concentration depth profile (fig. 12A) shows a distinct minor increase in Cl^-, by 2–4 mM (by 0.4–0.7 percent), between 21–28 mbsf, that probably represents diffusion of interglacial lower Cl^- water into the sediment, also implying no vertical fluid advection at this site during the last 18,000 years. Deeper in the section below ~260 mbsf, the Cl^- distribution is primarily controlled by gas-hydrate dissociation, hence Cl^- concentration can be used as a proxy for gas-hydrate concentration, assuming knowledge of the background Cl^-.

Figure 11 (following page). Core temperature and catwalk infrared camera imagery compared to the occurrences of ashes and several downhole logging data sets. Lithostratigraphic Unit I subunits are also shown. Infrared anomaly shifts relative to observed ash layers exist because of gap reductions on catwalk; see Site NGHP-01-17. Oversized Figure for the enlarged versions of this summary.

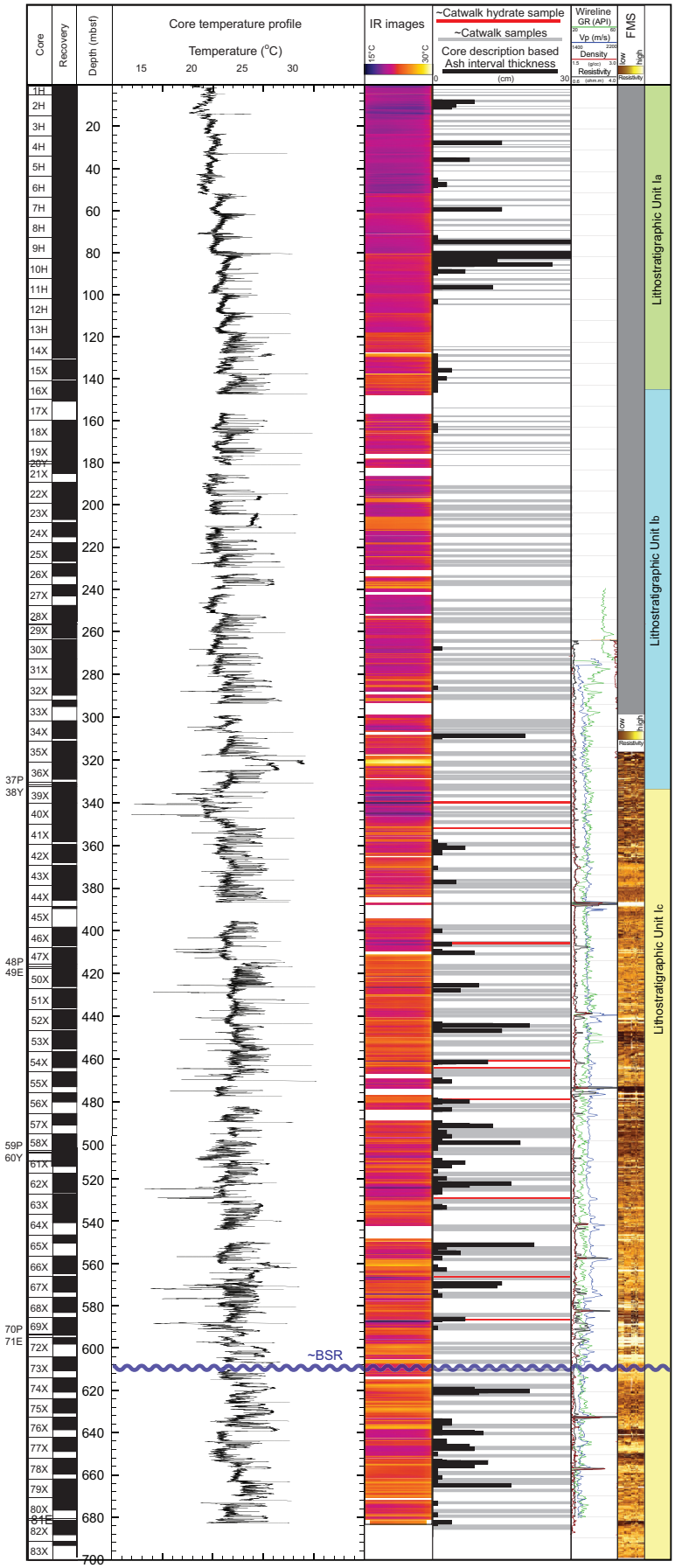

Core
Recovery
Depth (mbsf)
Core temperature profile
Temperature (°C)
15
20
25
30
IR images
15°C
30°C
~Catwalk hydrate sample
~Catwalk samples
Core description based
Ash interval thickness
(cm)
0
30
Wireline
GR (API)
Vp (m/s)
Density
Resistivity
FMS
low
high
Resistivity
Lithostratigraphic Unit Ia
Lithostratigraphic Unit Ib
Lithostratigraphic Unit Ic
~BSR
1H
2H
3H
4H
5H
6H
7H
8H
9H
10H
11H
12H
13H
14X
15X
16X
17X
18X
19X
20Y
21X
22X
23X
24X
25X
26X
27X
28X
29X
30X
31X
32X
33X
34X
35X
36X
37P
38Y
39X
40X
41X
42X
43X
44X
45X
46X
47X
48P
49E
50X
51X
52X
53X
54X
55X
56X
57X
58X
59P
60Y
61X
62X
63X
64X
65X
66X
67X
68X
69X
70P
71E
72X
73X
74X
75X
76X
77X
78X
79X
80X
81E
82X
83X
20
40
60
80
100
120
140
160
180
200
220
240
260
280
300
320
340
360
380
400
420
440
460
480
500
520
540
560
580
600
620
640
660
680
700

Table 4. Interstitial-water data for Hole NGHP-01-17A.

[Note that a dash indicates the value was not determined. The gas-hydrate-bearing samples are designated by "HY" and the neighboring samples by "BK." The samples that were corrected for drill-water contamination are marked by bold data in the sulfate concentration column]

Sample name	Depth (mbsf)	Vol. (mL)	pH	Alk (mM)	Salinity	Titr Cl^- (mM)	Br^- (mM)	SO_4^{2-} (mM)	Comments*
1H-1 140-150	1.4	55.0	7.6	3.56	34.8	556	0.87	26.91	Fine green-gray clay with shells and forams
1H-2 140-150	2.9	45.0	7.7	4.69	34.8	556	0.87	25.88	Fine green-gray clay with shells and forams
1H-3 113-123	4.1	45.0	7.6	5.04	34.8	553	0.86	24.51	Fine green-gray clay with shells and forams
2H-1 140-150	5.9	45.0	7.5	5.42	34.8	553	0.88	24.47	Fine green-gray clay with shells and forams
2H-2 140-150	7.4	47.0	7.6	5.75	34.5	552	0.86	26.06	Fine green-gray clay with shells and forams
2H-3 140-150	8.9	50.0	7.5	5.01	34.5	555	0.84	21.58	Fine green-gray clay with shells and forams
2H-5 140-150	11.9	47.0	7.6	6.91	34.5	555	0.85	18.81	Fine green-gray clay with shells and forams
2H-7 63-73	14.1	43.0	7.6	7.91	34.5	557	0.86	17.04	Fine green-gray clay with shells and forams. Stiff. H2S smell
3H-1 135-150	15.4	53.0	7.6	8.88	34.0	557	0.90	16.76	Fine green-gray clay with more shells and forams. Some H_2S Smell. Carbonates
3H-3 135-150	18.4	47.0	7.6	10.93	33.8	556	0.86	10.91	Lighter color, perhaps more calcareous, more forams and shells. Black sulfides, H_2S smell.
3H-5 135-150	21.4	42.0	7.7	14.39	33.0	560	0.94	5.73	First methane
3H-7 62-77	23.1	50.0	7.6	16.74	32.5	561	0.94	2.23	Forams and sulfide
4H-1 135-150	24.9	33.0	7.8	16.85	32.0	559	0.91	0.23	Sulfide. Carbonate not visible. Stiff green-gray clay
4H-3 135-150	27.9	65.0	7.6	14.67	31.5	560	0.95	0.10	Few forams, sulfides, stiff clay
4H-5 135-150	30.9	47.0	–	–	31.5	555	0.99	0.07	Sulfide smell. Stiff and sticky clay. Few forams
4H-7 69-84	32.7	46.0	7.7	12.65	31.5	555	1.00	0.04	Stiff clay. No sulfide smell
5H-2 135-150	35.9	62.0	7.9	12.61	31.5	553	0.98	**0.33**	Coarse-grained pink ash layer (at least 2–3 cm thick)
5H-5 135-150	40.4	40.0	7.8	11.41	31.0	548	0.99	0.05	Coarse-grained pink ash layer
6H-2 135-150	45.3	56.0	7.6	12.69	30.5	550	1.07	0.05	Lots of calcareous shells.
6H-5 135-150	49.8	38.0	7.9	12.80	30.5	548	1.03	0.00	Lots of calcareous shells .
7H-2 135-150	54.9	42.0	7.7	13.32	30.2	546	1.11	0.06	Brittle sediments. Lots of calcareous shells, sometimes in layers.
7H-5 135-150	59.4	43.0	7.9	13.13	30.2	547	1.13	0.05	Brittle sediments. Lots of calcareous shells, sometimes in layers.
8H-5 130-150	68.8	40.0	7.8	16.07	30.2	548	1.15	0.06	No IR anomalies. Stiff Clay with forams.
8H-7 57-87	70.6	46.0	7.9	14.95	30.2	550	1.11	0.06	Sample significantly colder than rest of core. No difference in lithology. Silty clay with forams
9H-2 130-150	73.4	42.0	7.8	17.64	30.2	551	1.13	0.00	Brittle clays similar to above
9H-5 130-150	77.9	44.0	8.2	16.55	30.0	548	1.15	0.06	Brittle clays similar to above
10H-2 130-150	83.3	39.0	8.2	–	30.0	547	1.18	0.05	Silty clay with forams
10H-5 130-150	87.8	44.0	8.2	18.85	30.0	558	1.18	0.00	Silty clay with forams
11H-2 130-150	92.8	44.0	8.2	19.66	30.2	550	1.25	0.00	Silty clay with forams
11H-5 130-150	97.3	41.0	8.1	19.42	30.0	557	1.25	0.05	Silty clay with forams
12H-2 130-150	102.3	40.0	8.1	20.64	30.2	554	1.20	0.06	Silty clay with forams.
12H-5 130-150	106.8	43.0	8.0	20.86	30.2	555	1.21	0.00	Silty clay with forams
13H-2 130-150	111.8	41.0	8.4	–	30.0	553	1.28	0.11	Silty clay with forams
13H-5 130-150	116.3	41.0	8.2	21.26	30.2	552	1.29	0.00	Silty clay with forams
14X-2 125-150	121.3	38.0	8.1	22.04	30.2	554	1.25	0.08	Silty clay with forams.Not well-developed biscuits
14X-4 125-150	124.3	38.5	8.2	22.23	30.2	552	1.26	0.11	Silty clay with forams.Not well-developed biscuits
15X-2 37-62	129.5	13.0	–	–	31.0	553	1.32	0.08	Small IR anomaly. Very messy sample, no good biscuits
15X-5 125-150	134.0	37.0	8.2	22.84	30.5	553	1.56	0.07	Silty clay with forams. Biscuits not well-developed
16X-2 125-150	140.5	22.0	8.3	23.52	31.0	551	1.29	0.06	Silty clay with forams. Few, small biscuits
16X-5 110-135	144.6	18.0	–	–	31.0	552	1.35	0.07	Silty clay with forams. Few, small biscuits
18X-2 125-150	158.8	23.0	8.2	25.28	31.0	551	1.37	0.06	Silty clay with forams. Few, small biscuits

Table 4. Interstitial-water data for Hole NGHP-01-17A.—Continued

[Note that a dash indicates the value was not determined. The gas-hydrate-bearing samples are designated by "HY" and the neighboring samples by "BK." The samples that were corrected for drill-water contamination are marked by bold data in the sulfate concentration column]

Sample name	Depth (mbsf)	Vol. (mL)	pH	Alk (mM)	Salinity	Titr Cl^- (mM)	Br^- (mM)	SO_4^{2-} (mM)	Comments*
18X-5 100-125	163.1	12.0	–	–	31.0	563	1.36	**0.14**	Silty clay with forams. Few, small biscuits
19X-3 125-150	169.1	17.0	8.0	–	30.8	554	1.28	0.06	Silty clay with forams. Few, small biscuits
19X-5 125-150	172.1	18.0	8.0	25.86	31.0	556	1.33	0.08	Silty clay with forams. Few, small biscuits
21X-2 120-150	179.2	15.0	7.8	28.42	32.0	551	1.35	0.10	Silty clay with forams. Few, small biscuits
22X-1 105-140	186.3	38.0	7.9	27.79	31.8	551	1.34	**0.18**	Silty clay with forams. Few, small biscuits
22X-5 99-129	192.1	25.0	7.9	28.16	31.8	553	1.47	0.00	No IR anomaly. Regular core sample
23X-3 110-150	198.3	12.0	–	–	32.0	551	1.43	0.07	Large void in sample. Highly disturbed
23X-5 120-130	201.3	16.0	–	–	32.0	555	1.38	0.11	Very few biscuits. Highly disturbed
24X-2 120-150	205.3	17.0	–	–	33.0	555	1.28	0.08	Very few biscuits. Highly disturbed
25X-1 120-150	214.7	44.0	7.6	29.76	31.8	556	1.18	**0.34**	Very few biscuits. Highly disturbed
25X-4 80-110	218.8	46.0	7.5	30.98	32.0	557	1.35	**0.38**	Very few biscuits. Highly disturbed
26X-1 120-150	224.3	40.0	7.5	33.33	32.2	555	1.15	**0.47**	Disturbed biscuits
26X-3 106-136	227.2	47.0	7.4	34.10	32.0	547	1.36	**0.22**	Disturbed biscuits
27X-1 120-150	234.0	22.0	7.6	36.88	32.5	560	1.43	**0.19**	Very few biscuits. Highly disturbed
27X-3 100-130	236.8	54.0	7.5	38.68	32.5	563	1.32	**0.22**	Highly disturbed fractured clay
28X-2 120-150	245.2	36.0	7.6	41.78	32.5	561	1.34	0.10	Highly disturbed fractured clay
28X-5 120-150	249.7	54.0	7.8	40.75	32.5	555	1.38	**0.16**	Highly disturbed fractured clay
29X-3 120-150	255.2	44.0	7.6	42.73	32.0	558	1.36	**0.23**	Highly disturbed fractured clay
29X-5 120-150	258.2	34.0	7.6	43.37	32.5	555	1.36	**0.12**	Highly disturbed fractured clay
30X-3 120-150	264.8	42.5	7.7	43.41	33.0	557	1.35	**0.23**	No IR anomaly. Regular core sample
30X-6 36-66 HY	268.0	9.9	–	–	24.8	444	1.06	**0.54**	IR anomaly. Clearly visible 2cm pink ash layer at ~40 degree angle. Relatively easy to separate, may contain some clay. Potential contamination
30X-6 36-66 BK	268.0	27.0	7.8	44.92	32.0	554	1.35	**0.12**	IR anomaly background
31X-3 120-150	273.5	35.0	7.7	42.54	32.0	559	1.34	**0.25**	No IR anomaly. Regular core sample
31X-5 35-50	275.2	22.0	8.0	41.80	31.0	533	1.35	0.09	Larger IR Anomaly. Core extruded out of whole round sample due to gas pressure. No apparent lithological constraint to anomaly
31X-5 50-85	275.3	26.0	7.9	43.80	32.0	553	1.36	0.06	If there was a gas hydrate in this sample, it was in a fracture & water released may have been missed by cleaning
32X-3 107-137	284.0	44.0	7.5	44.92	32.5	559	1.37	**0.13**	No IR anomaly. Regular core sample. Good biscuits
32X-5 71-101 HY	286.0	15.0	–	–	19.0	350	0.83	**0.58**	IR Anomaly. Gas hydrate in pink, glassy layer; ~0.5 cm and not continuous Hard to sample; some clay mixed in with ash sample
32X-5 71-101 BK	286.0	28.0	7.9	41.38	30.0	517	1.23	0.08	IR anomaly background. Nice biscuits
33X-1 96-126	290.6	41.0	7.7	43.74	32.8	558	1.37	**0.18**	No IR anomalies in Core 33X. Small core
34X-4 84-114 HY	303.4	5.0	–	–	27.5	540	1.14	0.09	IR Anomaly—No visual indication of gas hydrate, uniform lithology. Sample was highly fractured (small slivers), poorly developed biscuits
34X-4 84-114 BK	303.4	6.0	–	–	30.2	540	1.34	0.06	IR anomaly background
34X-3 120-150	304.5	36.0	7.7	43.00	32.5	557	1.38	0.09	No IR anomaly. Regular core sample. Good biscuits
35X-3 84-114	311.9	46.0	7.5	45.19	32.5	554	1.35	**0.14**	No IR anomaly. Regular core sample. Good biscuits
35X-7 69-99 HY	317.1	23.0	7.6	43.11	30.0	503	1.23	0.06	IR anomaly. No apparent lithological control.
35X-7 69-99 BK	317.1	21.0	7.7	44.56	32.0	550	1.36	0.08	IR anomaly background. No apparent lithological control.

Table 4. Interstitial-water data for Hole NGHP-01-17A.—Continued

[Note that a dash indicates the value was not determined. The gas-hydrate-bearing samples are designated by "HY" and the neighboring samples by "BK." The samples that were corrected for drill-water contamination are marked by bold data in the sulfate concentration column]

Sample name	Depth (mbsf)	Vol. (mL)	pH	Alk (mM)	Salinity	Titr Cl^- (mM)	Br^- (mM)	SO_4^{2-} (mM)	Comments*
36X-3 65-78 HY	321.5	22.0	7.9	31.57	23.0	396	0.96	**0.60**	Medium IR anomaly across the 13 cm sample. Took sub-samples for resistivity
36X-3 78-95 BK	321.5	32.0	7.7	38.99	28.0	485	1.15	**0.26**	Medium IR anomaly background. Pore water came out easily and quickly
36X-4 113-143	323.0	42.0	7.4	44.37	33.5	555	1.36	**0.18**	No IR anomaly. Regular core sample
37P-1 50-60		20.0	–	–	32.5	556	1.30	0.06	Sample had 1.5 liters of gas
38Y-1 50-65	329.5	23.0	–	–	33.5	558	1.41	0.00	Pressure core with ~2 liter of methane, close to saturation of methane hydrate
39X-5 31-71 HY	334.2	35.0	7.6	35.81	26.0	475	1.12	0.11	IR anomaly
39X-5 31-71 BK	334.2	46.0	7.3	42.66	30.5	514	1.27	**0.36**	IR anomaly background
39X-3 120-150	335.4	22.0	7.3	45.75	32.5	538	1.37	0.08	No IR anomaly. Regular core sample
40X-5 110-140	343.4	41.0	7.2	46.42	33.2	558	1.49	0.09	No IR anomaly. Regular core sample
40X-7 60-90 HY	345.3	45.0	7.6	33.30	24.5	416	1.06	**0.22**	IR anomaly. Sample had fracture
40X-7 60-90 BK	345.3	23.0	7.6	38.07	28.5	479	1.21	**0.12**	IR anomaly background
41X-2 120-150	350.0	52.0	7.3	46.30	33.0	556	1.63	**0.20**	Calcareous sample
42X-3 120-150	360.5	51.0	7.2	46.14	33.0	554	1.40	**0.19**	Calcareous sample. Very good biscuits
43X-5 53-83 HY	371.7	28.0	7.3	36.48	26.0	442	1.14	0.09	Considerably strong IR anomaly. Lithology seems homogeneous. Some micro-fractures
43X-5 53-83 BK	371.7	49.0	7.1	45.37	31.0	522	1.35	0.10	IR anomaly background
43X-8 110-140	375.0	30.0	7.3	44.30	33.2	557	1.67	**0.12**	No IR anomaly. Regular core sample
44X-3 36-66 HY	379.0	2.0	–	–	13.5	236	0.61	**0.37**	Clearly constrained IR Anomaly in 5cm ash layer, easily separated from surrounding sediment
44X-3 36-66 BK	379.0	44.0	7.1	46.47	33.0	544	1.40	**0.21**	IR anomaly background
44X-4 120-150	380.5	53.0	7.2	43.72	33.5	554	1.43	0.08	No IR anomaly. Regular core sample
45X-1 55-85	386.3	50.0	7.1	44.34	33.5	552	1.38	**0.44**	Collected as a "regular" sample, but when opened noted bubbly, mousy texture suggesting that gas hydrate may have been present. No IR anomaly
46X-4 120-150	400.8	50.0	7.4	48.25	33.2	553	1.41	0.11	No IR anomaly. Regular core sample
46X-5 67-97 HY	401.8	2.0	–	–	15.0	256	0.63	**1.78**	IR anomaly
46X-5 67-97 BK	401.8	50.0	7.2	49.03	33.5	553	1.42	**0.20**	IR anomaly background
47X-5 120-150	409.5	54.0	7.3	46.32	33.0	554	1.36	**0.57**	No IR anomaly. Regular core sample
47X-4 73-103 HY	411.0	8.0	–	–	11.0	209	0.45	**3.12**	Very large IR anomaly in catwalk. Nice ash layer
47X-4 73-103 BK	411.0	50.0	7.2	49.13	34.0	550	1.40	**0.30**	IR anomaly background
48P-1 18-30	412.9	22.0	–	–	33.0	556	1.32	0.10	Sample had 2.5 liters of gas
49E-1 45-60	414.2	21.0	7.2	45.36	33.0	558	1.35	**0.76**	Sample had 1.9 liters of gas
50X-4 120-150	419.4	50.0	7.2	47.33	33.5	554	1.39	**0.25**	No IR anomaly. Regular core sample
50X-7, 75-105 HY	422.1	48.0	7.5	31.62	22.5	389	0.97	0.10	IR anomaly. No apparent lithological control
50X-7 75-105 BK	–	55.0	7.5	–	27.0	457	1.14	**0.47**	IR anomaly background
51X-3 89-119 HY	428.1	23.0	8.0	11.79	10.0	165	0.36	**1.81**	IR Anomaly. Spectacular 9.5cm ash layer
51X-3 89-119 BK	428.1	58.0	7.7	29.00	24.5	402	1.00	**1.06**	IR anomaly background in direct contact with ash layer
51X-5 120-150	431.1	55.0	7.5	44.42	32.0	553	1.45	**0.20**	No IR anomaly, but contained a 1.5cm brownish ash layer.
52X-5 27-57 HY	439.8	21.0	7.7	27.33	19.0	342	0.77	**0.87**	IR anomaly. The cold spot matched a zone of mixed ash and clay. Not easy to separate
52X-5 27-57 BK	439.8	45.0	7.4	48.86	32.5	552	1.38	**0.34**	IR anomaly background is indurated clay as above

Table 4. Interstitial-water data for Hole NGHP-01-17A.—Continued

[Note that a dash indicates the value was not determined. The gas-hydrate-bearing samples are designated by "HY" and the neighboring samples by "BK." The samples that were corrected for drill-water contamination are marked by bold data in the sulfate concentration column]

Sample name	Depth (mbsf)	Vol. (mL)	pH	Alk (mM)	Salinity	Titr Cl^- (mM)	Br^- (mM)	SO_4^{2-} (mM)	Comments*
52X-6 120-150	441.3	49.0	7.3	43.26	32.5	547	1.44	**0.44**	No IR anomaly. Regular core sample
53X-4 103-133	447.9	59.0	7.2	43.23	32.0	554	1.38	**0.44**	No IR anomaly. Regular core sample
53X-6 47-62 HY	449.7	2.0	–	–	7.0	150	0.71	**1.25**	IR Anomaly. Sample 3 zones: No anomaly on one side; max anomaly at other end corresponds to an ash layer
53X-6 47-62 HY-INT	449.7	9.0	–	–	16.0	284	0.43	**0.55**	Intermediate IR anomaly does not look lithologically different from the background
53X-6 47-62 BK	449.7	9.0	–	–	30.5	528	1.36	**0.81**	IR anomaly background is not lithologically different than Intermediate zone
54X-3 116-146	456.4	37.0	7.2	54.05	33.0	554	1.41	0.09	No IR anomaly. Regular core sample
55X-2 17-47 HY2	464.2	14.0	–	–	10.0	201	0.47	**1.97**	IR anomaly. Almost a pure white fine-grained ash
55X-2 17-47 BK2	464.2	21.0	7.2	49.39	33.0	553	1.45	0.08	IR anomaly background, lithologically distinct from gas hydrate sample. Clay with carbonate
55X-7 46-66 HY1	468.9	9.0	–	–	27.0	450	1.15	**1.19**	IR anomaly, had some ash in It
56X-2 69-99 HY	474.4	9.0	–	–	12.0	226	0.49	**3.04**	IR anomaly, brown, distinct ash, rather fine-grained
56X-2 69-99 BK	474.4	42.0	7.1	50.12	32.5	548	1.46	0.09	IR anomaly background. Clayey and calcareous
56X-3 120-150	475.9	51.0	7.0	49.94	33.0	549	1.64	**0.13**	No IR anomaly. Regular core sample
57X-3 120-150	485.4	38.0	7.2	47.56	33.5	552	1.45	0.11	No IR anomaly. Regular core sample
58X-4 115-145 HY	496.9	20.0	7.4	30.20	21.0	362	0.89	**0.54**	IR anomaly. No obvious ash in sample portion with max anomaly
58X-4 115-145 BK	496.9	39.0	7.2	47.10	30.0	436	1.35	**0.12**	IR anomaly background
58X-5 120-150	498.4	50.0	7.2	47.85	33.0	552	1.42	**0.17**	No IR anomaly. Regular core sample
61X-4 120-150	506.2	39.0	7.1	49.94	33.5	554	1.45	**0.21**	No IR anomaly. Regular core sample
62X-5 120-150	517.8	50.0	7.2	45.83	33.5	552	1.75	**0.39**	No IR anomaly. Regular core sample
63X-3 70-100	529.2	45.0	7.1	47.14	33.5	552	1.47	**0.13**	No IR anomaly. Regular core sample
63X-7 115-145 HY	523.9	23.0	7.4	37.45	20.5	439	1.37	**0.14**	IR anomaly. No apparent lithological or structural control
63X-7 115-145 BK	523.9	48.0	7.3	40.92	29.5	498	1.32	**0.17**	IR anomaly background
64X-1 77-107	531.1	30.0	7.4	–	33.5	493	1.33	0.11	No IR Anomaly in core, but lots of gas. Lost some sediments due to rapid expansion. Only 2 good biscuits
65X-2 110-140	542.6	50.0	7.3	45.80	33.0	553	1.50	**0.21**	No IR anomaly in core. Low recovery
66X-3 81-111	552.8	39.0	7.2	44.91	32.5	548	1.42	**0.42**	No IR anomaly. Regular core sample
66X-5 69-99 HY	555.1	2.6	–	–	14.0	229	0.73	**2.37**	IR Anomaly. ~6cm zone of ash interbedded with clay. Very small amount of "clean" ash
66X-5 69-99 BK	555.1	46.0	7.3	42.66	30.0	511	1.35	**0.19**	IR anomaly background
67X-6 67-97	564.8	43.0	7.1	38.95	32.0	545	1.62	**0.45**	No IR anomaly. Regular core sample
67X-7 80-110 HY	565.9	22.0	7.6	5.56	24.0	405	1.24	**0.24**	IR anomaly. No obvious lithological changes at different IR Intensities
67X-7 80-110 BK1	565.9	19.0	7.5	5.49	25.5	448	1.37	**0.35**	IR anomaly background 1
67X-7 80-110 BK2	565.9	20.0	7.4	34.83	29.0	492	1.29	**0.46**	IR anomaly background 2
68X-4 62-92 HY	572.8	32.0	7.7	23.93	20.0	362	1.12	**0.21**	IR anomaly. No obvious lithological changes at different IR Intensities
68X-4 62-92 BK	572.8	19.0	7.1	44.25	31.0	518	1.61	**0.23**	IR anomaly background
68X-5 120-150	574.3	34.0	7.0	42.06	32.0	547	1.47	0.11	No IR anomaly. Regular core sample
69X-4 120-150	584.4	44.0	7.1	42.25	32.5	548	1.64	**0.52**	No IR anomaly. Regular core sample

Table 4. Interstitial-water data for Hole NGHP-01-17A.—Continued

[Note that a dash indicates the value was not determined. The gas-hydrate-bearing samples are designated by "HY" and the neighboring samples by "BK." The samples that were corrected for drill-water contamination are marked by bold data in the sulfate concentration column]

Sample name	Depth (mbsf)	Vol. (mL)	pH	Alk (mM)	Salinity	Titr Cl^- (mM)	Br^- (mM)	SO_4^{2-} (mM)	Comments*
69X-6 55-85 HY	586.3	9.0	–	–	19.0	342	1.10	**1.44**	IR anomaly. Highest IR anomaly section showed browninsh coloring not present in the adjacent sediment with low IR intensities. During cleaning IR anomaly section behaved like ash
69X-6 55-85 BK	586.3	41.0	6.9	40.66	30.0	510	1.51	**0.54**	IR anomaly background
72X-1 10-53 HY	587.9	27.0	6.5	21.31	20.0	352	1.12	**0.96**	IR Anomaly. Very hard sample reminiscent of limestone
72X-1 10-53 BK1	587.9	44.0	6.5	21.40	20.0	366	1.12	**0.62**	IR anomaly background 1 considerably softer and with larger pore fluid volume that the HY sample
72X-1 10-53 BK2	587.9	29.0	6.4	18.75	20.0	353	1.15	**0.30**	IR anomaly background 2 considerably softer and with larger pore fluid volume that the HY sample
72X-3 65-95	590.3	39.0	7.3	33.71	26.0	469	1.42	**0.72**	No IR anomaly. Regular core sample
73X-2 0-25 HY	598.5	31.0	6.9	36.69	26.0	461	1.42	**0.54**	IR anomaly. No apparent lithological or structural control
73X-2 0-25 BK	598.5	15.0	–	–	32.0	544	1.67	0.11	IR anomaly background
73X-3 110-140	601.1	39.0	7.0	40.54	33.0	549	1.69	**0.24**	No IR anomaly. Regular core sample
74X-2 120-150	609.4	40.0	6.9	42.65	33.0	550	1.68	**0.35**	No IR anomalies in this core. Likely below the BSR
74X-3 120-150	610.9	40.0	7.0	42.97	33.5	553	1.49	**0.19**	No IR anomalies in this core. Likely below the BSR
75X-2 120-150	619.0	36.0	7.0	43.59	33.0	549	1.43	**0.64**	No IR anomalies in this core. Likely below the BSR
76X-2 87-117	626.7	25.0	7.3	41.27	33.5	555	1.48	**0.13**	No IR anomalies in this core. Likely below the BSR
77X-3 120-150	637.5	39.0	7.0	43.42	33.5	549	1.70	**0.43**	No IR anomalies in this core. Likely below the BSR
78X-3 120-150	647.9	26.0	7.1	43.41	33.5	551	1.69	**0.46**	No IR anomalies in this core. Likely below the BSR
79X-4 120-150	659.5	41.0	6.9	46.14	33.0	554	1.54	**0.13**	Homogeneous lithology as above. Still much pore water recovered
80X-2 115-145	664.2	27.0	7.1	43.59	33.0	552	1.49	**0.24**	Homogeneous lithology as above. Still much pore water recovered
82X-1 0-20	673.3	13.0	–	–	33.0	552	1.52	**0.19**	IR Anomaly. No evidence in lithology as to reason for this anomaly. Three hard rock pieces preserved
82X-4 120-150	677.4	20.0	7.3	42.05	33.0	551	1.81	**0.62**	No IR anomalies in this Core. Only a few thin biscuits
83X-2 37-67	684.3	23.0	7.1	42.06	33.0	552	1.72	**1.21**	Only thin biscuits. Sample is highly fractured

*From Core 5H to total depth, most of the samples had some heavy organic smell.

Table 5. Interstitial-water data corrected for drill-water contamination based on sulfate concentration, for Hole NGHP-01-17A.

[Note that a dash indicates the value was not determined. The gas hydrate bearing samples are designated by "HY" and the neighboring samples by "BK." The samples that were corrected for drill-water contamination are marked by bold data in the sulfate concentration column]

Sample name	Depth (mbsf)	V Samp (mL)	pH	Alk (mM)	Salinity	Titr Cl^- (mM)	Br^- (mM)	Br^-/Cl^-	SO_4^{2-} (mM)
1H-1 140-150	1.4	55.0	7.6	3.56	34.8	556	0.87	0.0016	26.91
1H-2 140-150	2.9	45.0	7.7	4.69	34.8	556	0.87	0.0016	25.88
1H-3 113-123	4.1	45.0	7.6	5.04	34.8	553	0.86	0.0016	24.51
2H-1 140-150	5.9	45.0	7.5	5.42	34.8	553	0.88	0.0016	24.47
2H-2 140-150	7.4	47.0	7.6	5.75	34.5	552	0.86	0.0016	26.06
2H-3 140-150	8.9	50.0	7.5	5.01	34.5	555	0.84	0.0015	21.58
2H-5 140-150	11.9	47.0	7.6	6.91	34.5	555	0.85	0.0015	18.81
2H-7 63-73	14.1	43.0	7.6	7.91	34.5	557	0.86	0.0015	17.04
3H-1 135-150	15.4	53.0	7.6	8.88	34.0	557	0.90	0.0016	16.76
3H-3 135-150	18.4	47.0	7.6	10.93	33.8	556	0.86	0.0015	10.91
3H-5 135-150	21.4	42.0	7.7	14.39	33.0	560	0.94	0.0017	5.73
3H-7 62-77	23.1	50.0	7.6	16.74	32.5	561	0.94	0.0017	2.23
4H-1 135-150	24.9	33.0	7.8	16.85	32.0	559	0.91	0.0016	0.23
4H-3 135-150	27.9	65.0	7.6	14.67	31.5	560	0.95	0.0017	0.10
4H-5 135-150	30.9	47.0	–	–	31.5	555	0.99	0.0018	0.07
4H-7 69-84	32.7	46.0	7.7	12.65	31.5	555	1.00	0.0018	0.04
5H-2 135-150	35.9	62.0	7.9	12.58	31.1	547	0.97	0.0018	**0.00**
5H-5 135-150	40.4	40.0	7.8	11.41	31.0	548	0.99	0.0018	0.05
6H-2 135-150	45.3	56.0	7.6	12.69	30.5	550	1.07	0.0019	0.05
6H-5 135-150	49.8	38.0	7.9	12.80	30.5	548	1.03	0.0019	0.00
7H-2 135-150	54.9	42.0	7.7	13.32	30.2	546	1.11	0.0020	0.06
7H-5 135-150	59.4	43.0	7.9	13.13	30.2	547	1.13	0.0021	0.05
8H-5 130-150	68.8	40.0	7.8	16.07	30.2	548	1.15	0.0021	0.06
8H-7 57-87	70.6	46.0	7.9	14.95	30.2	550	1.11	0.0020	0.06
9H-2 130-150	73.4	42.0	7.8	17.64	30.2	551	1.13	0.0020	0.00
9H-5 130-150	77.9	44.0	8.2	16.55	30.0	548	1.15	0.0021	0.06
10H-2 130-150	83.3	39.0	8.2	–	30.0	547	1.18	0.0022	0.05
10H-5 130-150	87.8	44.0	8.2	18.85	30.0	558	1.18	0.0021	0.00
11H-2 130-150	92.8	44.0	8.2	19.66	30.2	550	1.25	0.0023	0.00
11H-5 130-150	97.3	41.0	8.1	19.42	30.0	557	1.25	0.0022	0.05
12H-2 130-150	102.3	40.0	8.1	20.64	30.2	554	1.20	0.0022	0.06
12H-5 130-150	106.8	43.0	8.0	20.86	30.2	555	1.21	0.0022	0.00
13H-2 130-150	111.8	41.0	8.4	–	30.0	553	1.28	0.0023	0.11
13H-5 130-150	116.3	41.0	8.2	21.26	30.2	552	1.29	0.0023	0.00
14X-2 125-150	121.3	38.0	8.1	22.04	30.2	554	1.25	0.0023	0.08
14X-4 125-150	124.3	38.5	8.2	22.23	30.2	552	1.26	0.0023	0.11
15X-2 37-62	129.5	13.0	–	–	31.0	553	1.32	0.0024	0.08
15X-5 125-150	134.0	37.0	8.2	22.84	30.5	553	1.56	0.0028	0.07
16X-2 125-150	140.5	22.0	8.3	23.52	31.0	551	1.29	0.0023	0.06
16X-5 110-135	144.6	18.0	–	–	31.0	552	1.35	0.0025	0.07
18X-2 125-150	158.8	23.0	8.2	25.28	31.0	551	1.37	0.0025	0.06
18X-5 100-125	163.1	12.0	–	–	30.8	560	1.35	0.0024	**0.00**
19X-3 125-150	169.1	17.0	8.0	–	30.8	554	1.28	0.0023	0.06
19X-5 125-150	172.1	18.0	8.0	25.86	31.0	556	1.33	0.0024	0.08
21X-2 120-150	179.2	15.0	7.8	28.42	32.0	551	1.35	0.0025	0.10
22X-1 105-140	186.3	38.0	7.9	27.78	31.6	547	1.34	0.0024	**0.00**
22X-5 99-129	192.1	25.0	7.9	28.16	31.8	553	1.47	0.0027	0.00
23X-3 110-150	198.3	12.0	–	–	32.0	551	1.43	0.0026	0.07
23X-5 120-130	201.3	16.0	–	–	32.0	555	1.38	0.0025	0.11
24X-2 120-150	205.3	17.0	–	–	33.0	555	1.28	0.0023	0.08
25X-1 120-150	214.7	44.0	7.6	29.73	31.4	549	1.17	0.0021	**0.00**
25X-4 80-110	218.8	46.0	7.5	30.95	31.5	550	1.34	0.0024	**0.00**
26X-1 120-150	224.3	40.0	7.5	33.29	31.6	546	1.14	0.0021	**0.00**
26X-3 106-136	227.2	47.0	7.4	34.08	31.7	543	1.36	0.0025	**0.00**
27X-1 120-150	234.0	22.0	7.6	36.86	32.3	556	1.42	0.0026	**0.00**
27X-3 100-130	236.8	54.0	7.5	38.66	32.2	559	1.32	0.0024	**0.00**
28X-2 120-150	245.2	36.0	7.6	41.78	32.5	561	1.34	0.0024	0.10
28X-5 120-150	249.7	54.0	7.8	40.74	32.3	552	1.38	0.0025	**0.00**

Table 5. Interstitial-water data corrected for drill-water contamination based on sulfate concentration, for Hole NGHP-01-17A.—Continued

[Note that a dash indicates the value was not determined. The gas hydrate bearing samples are designated by "HY" and the neighboring samples by "BK." The samples that were corrected for drill-water contamination are marked by bold data in the sulfate concentration column]

Sample name	Depth (mbsf)	V Samp (mL)	pH	Alk (mM)	Salinity	Titr Cl^- (mM)	Br^- (mM)	Br^-/Cl^-	SO_4^{2-} (mM)
29X-3 120-150	255.2	44.0	7.6	42.71	31.7	554	1.36	0.0025	**0.00**
29X-5 120-150	258.2	34.0	7.6	43.36	32.4	553	1.36	0.0025	**0.00**
30X-3 120-150	264.8	42.5	7.7	43.39	32.7	553	1.34	0.0024	**0.00**
30X-6 36-66 HY	268.0	9.9	–	–	24.1	433	1.04	0.0024	**0.00**
30X-6 36-66 BK	268.0	27.0	7.8	44.91	31.9	552	1.35	0.0024	**0.00**
31X-3 120-150	273.5	35.0	7.7	42.52	31.7	554	1.33	0.0024	**0.00**
31X-5 35-50	275.2	22.0	8.0	41.80	31.0	533	1.35	0.0025	0.09
31X-5 50-85	275.3	26.0	7.9	43.80	32.0	553	1.36	0.0025	0.06
32X-3 107-137	284.0	44.0	7.5	44.91	32.3	556	1.36	0.0025	**0.00**
32X-5 71-101 HY	286.0	15.0	–	–	18.2	339	0.81	0.0024	**0.00**
32X-5 71-101 BK	286.0	28.0	7.9	41.38	30.0	517	1.23	0.0024	0.08
33X-1 96-126	290.6	41.0	7.7	43.73	32.6	554	1.36	0.0025	**0.00**
34X-4 84-114 HY	303.4	5.0	–	–	27.5	540	1.14	0.0021	0.09
34X-4 84-114 BK	303.4	6.0	–	–	30.2	540	1.34	0.0025	0.06
34X-3 120-150	304.5	36.0	7.7	43.00	32.5	557	1.38	0.0025	0.09
35X-3 84-114	311.9	46.0	7.5	45.18	32.3	551	1.35	0.0024	**0.00**
35X-7 69-99 HY	317.1	23.0	7.6	43.11	30.0	503	1.23	0.0025	0.06
35X-7 69-99 BK	317.1	21.0	7.7	44.56	32.0	550	1.36	0.0025	0.08
36X-3 65-78 HY	321.5	22.0	7.9	31.52	22.3	384	0.95	0.0025	**0.00**
36X-3 78-95 BK	321.5	32.0	7.7	38.97	27.7	480	1.15	0.0024	**0.00**
36X-4 113-143	323.0	42.0	7.4	44.36	33.3	551	1.36	0.0025	**0.00**
37P-1 50-60	–	20.0	–	–	32.5	556	1.30	0.0023	0.06
38Y-1 50-65	329.5	23.0	–	–	33.5	558	1.41	0.0025	0.00
39X-5 31-71 HY	334.2	35.0	7.6	35.81	26.0	475	1.12	0.0024	0.11
39X-5 31-71 BK	334.2	46.0	7.3	42.63	30.1	507	1.26	0.0025	**0.00**
39X-3 120-150	335.4	22.0	7.3	45.75	32.5	538	1.37	0.0025	0.08
40X-5 110-140	343.4	41.0	7.2	46.42	33.2	558	1.49	0.0027	0.09
40X-7 60-90 HY	345.3	45.0	7.6	33.28	24.2	412	1.06	0.0026	**0.00**
40X-7 60-90 BK	345.3	23.0	7.6	38.06	28.4	477	1.21	0.0025	**0.00**
41X-2 120-150	350.0	52.0	7.3	46.28	32.8	552	1.62	0.0029	**0.00**
42X-3 120-150	360.5	51.0	7.2	46.12	32.8	550	1.40	0.0025	**0.00**
43X-5 53-83 HY	371.7	28.0	7.3	36.48	26.0	442	1.14	0.0026	0.09
43X-5 53-83 BK	371.7	49.0	7.1	45.37	31.0	522	1.35	0.0026	0.10
43X-8 110-140	375.0	30.0	7.3	44.29	33.1	555	1.67	0.0030	**0.00**
44X-3 36-66 HY	379.0	2.0	–	–	13.1	229	0.60	0.0026	**0.00**
44X-3 36-66 BK	379.0	44.0	7.1	46.45	32.7	540	1.40	0.0026	**0.00**
44X-4 120-150	380.5	53.0	7.2	43.72	33.5	554	1.43	0.0026	0.08
45X-1 55-85	386.3	50.0	7.1	44.30	33.0	544	1.37	0.0025	**0.00**
46X-4 120-150	400.8	50.0	7.4	48.25	33.2	553	1.41	0.0025	0.11
46X-5 67-97 HY	401.8	2.0	–	–	12.8	222	0.58	0.0026	**0.00**
46X-5 67-97 BK	401.8	50.0	7.2	49.01	33.3	549	1.41	0.0026	**0.00**
47X-5 120-150	409.5	54.0	7.3	46.27	32.3	543	1.34	0.0025	**0.00**
47X-4 73-103 HY	411.0	8.0	–	–	7.2	149	0.35	0.0024	**0.00**
47X-4 73-103 BK	411.0	50.0	7.2	49.11	33.6	544	1.39	0.0026	**0.00**
48P-1 18-30	412.9	22.0	–	–	33.0	556	1.32	0.0024	0.10
49E-1 45-60	414.2	21.0	7.2	45.30	32.1	543	1.33	0.0024	**0.00**
50X-4 120-150	419.4	50.0	7.2	47.31	33.2	549	1.38	0.0025	**0.00**
50X-7 75-105 HY	422.1	48.0	7.5	31.62	22.5	389	0.97	0.0025	0.10
50X-7 75-105 BK	–	55.0	7.5	–	26.4	448	1.12	0.0025	**0.00**
51X-3 89-119 HY	428.1	23.0	8.0	11.64	7.8	130	0.31	0.0024	**0.00**
51X-3 89-119 BK	428.1	58.0	7.7	28.92	23.2	382	0.97	0.0025	**0.00**
51X-5 120-150	431.1	55.0	7.5	44.40	31.8	549	1.45	0.0026	**0.00**
52X-5 27-57 HY	439.8	21.0	7.7	27.26	17.9	325	0.74	0.0023	**0.00**
52X-5 27-57 BK	439.8	45.0	7.4	48.83	32.1	545	1.37	0.0025	**0.00**

Table 5. Interstitial-water data corrected for drill-water contamination based on sulfate concentration, for Hole NGHP-01-17A.—Continued

[Note that a dash indicates the value was not determined. The gas hydrate bearing samples are designated by "HY" and the neighboring samples by "BK." The samples that were corrected for drill-water contamination are marked by bold data in the sulfate concentration column]

Sample name	Depth (mbsf)	V Samp (mL)	pH	Alk (mM)	Salinity	Titr Cl^- (mM)	Br^- (mM)	Br^-/Cl^-	SO_4^{2-} (mM)
52X-6 120-150	441.3	49.0	7.3	43.22	32.0	538	1.42	0.0026	**0.00**
53X-4 103-133	447.9	59.0	7.2	43.19	31.5	545	1.37	0.0025	**0.00**
53X-6 47-62 HY	449.7	2.0	–	–	5.5	126	0.39	0.0031	**0.00**
53X-6 47-62 HY-INT	449.7	9.0	–	–	15.3	273	0.69	0.0025	**0.00**
53X-6 47-62 BK	449.7	9.0	–	–	29.5	512	1.34	0.0026	**0.00**
54X-3 116-146	456.4	37.0	7.2	54.05	33.0	554	1.41	0.0025	0.09
55X-2 17-47 HY2	464.2	14.0	–	–	7.6	163	0.41	0.0025	–
55X-2 17-47 BK2	464.2	21.0	7.2	49.39	33.0	553	1.45	0.0026	0.08
55X-7 46-66 HY1	468.9	9.0	–	–	25.6	427	1.11	0.0026	**0.00**
56X-2 69-99 HY	474.4	9.0	–	–	8.3	167	0.40	0.0024	**0.00**
56X-2 69-99 BK	474.4	42.0	7.1	50.12	32.5	548	1.46	0.0027	0.09
56X-3 120-150	475.9	51.0	7.0	49.93	32.8	546	1.63	0.0030	**0.00**
57X-3 120-150	485.4	38.0	7.2	47.56	33.5	552	1.45	0.0026	0.11
58X-4 115-145 HY	496.9	20.0	7.4	30.16	20.3	352	0.87	0.0025	**0.00**
58X-4 115-145 BK	496.9	39.0	7.2	47.09	29.9	434	1.35	0.0031	**0.00**
58X-5 120-150	498.4	50.0	7.2	47.84	32.8	549	1.42	0.0026	**0.00**
61X-4 120-150	506.2	39.0	7.1	49.92	33.2	550	1.44	0.0026	**0.00**
62X-5 120-150	517.8	50.0	7.2	45.80	33.0	544	1.73	0.0032	**0.00**
63X-3 70-100	529.2	45.0	7.1	47.13	33.3	550	1.47	0.0027	**0.00**
63X-7 115-145 HY	523.9	23.0	7.4	37.44	20.3	436	1.36	0.0031	**0.00**
63X-7 115-145 BK	523.9	48.0	7.3	40.91	29.3	495	1.31	0.0026	**0.00**
64X-1 77-107	531.1	30.0	7.4	–	33.5	493	1.33	0.0027	0.11
65X-2 110-140	542.6	50.0	7.3	45.78	32.7	549	1.49	0.0027	**0.00**
66X-3 81-111	552.8	39.0	7.2	44.88	32.0	540	1.41	0.0026	**0.00**
66X-5 69-99 HY	555.1	2.6	–	–	11.1	183	0.66	0.0036	**0.00**
66X-5 69-99 BK	555.1	46.0	7.3	42.65	29.8	507	1.34	0.0026	**0.00**
67X-6 67-97	564.8	43.0	7.1	38.91	31.5	536	1.61	0.0030	**0.00**
67X-7 80-110 HY	565.9	22.0	7.6	5.54	23.7	400	1.23	0.0031	**0.00**
67X-7 80-110 BK1	565.9	19.0	7.5	5.46	25.1	441	1.35	0.0031	**0.00**
67X-7 80-110 BK2	565.9	20.0	7.4	34.79	28.4	483	1.27	0.0026	**0.00**
68X-4 62-92 HY	572.8	32.0	7.7	23.91	19.7	358	1.11	0.0031	**0.00**
68X-4 62-92 BK	572.8	19.0	7.1	44.23	30.7	514	1.60	0.0031	**0.00**
68X-5 120-150	574.3	34.0	7.0	42.06	32.0	547	1.47	0.0027	0.11
69X-4 120-150	584.4	44.0	7.1	42.21	31.9	538	1.62	0.0030	**0.00**
69X-6 55-85 HY	586.3	9.0	–	–	17.3	314	1.06	0.0034	**0.00**
69X-6 55-85 BK	586.3	41.0	6.9	40.62	29.4	500	1.50	0.0030	**0.00**
72X-1 10-53 HY	587.9	27.0	6.5	21.23	18.8	333	1.09	0.0033	**0.00**
72X-1 10-53 BK1	587.9	44.0	6.5	21.35	19.2	354	1.10	0.0031	**0.00**
72X-1 10-53 BK2	587.9	29.0	6.4	18.73	19.6	347	1.14	0.0033	**0.00**
72X-3 65-95	590.3	39.0	7.3	33.65	25.1	455	1.40	0.0031	**0.00**
73X-2 0-25 HY	598.5	31.0	6.9	36.65	25.3	451	1.40	0.0031	**0.00**
73X-2 0-25 BK	598.5	15.0	–	–	32.0	544	1.67	0.0031	0.11
73X-3 110-140	601.1	39.0	7.0	40.52	32.7	544	1.69	0.0031	**0.00**
74X-2 120-150	609.4	40.0	6.9	42.62	32.6	543	1.67	0.0031	**0.00**
74X-3 120-150	610.9	40.0	7.0	42.95	33.3	549	1.49	0.0027	**0.00**
75X-2 120-150	619.0	36.0	7.0	43.54	32.2	537	1.41	0.0026	**0.00**
76X-2 87-117	626.7	25.0	7.3	41.26	33.3	552	1.47	0.0027	**0.00**
77X-3 120-150	637.5	39.0	7.0	43.39	33.0	541	1.69	0.0031	**0.00**
78X-3 120-150	647.9	26.0	7.1	43.37	32.9	542	1.68	0.0031	**0.00**
79X-4 120-150	659.5	41.0	6.9	46.13	32.8	551	1.53	0.0028	**0.00**
80X-2 115-145	664.2	27.0	7.1	43.57	32.7	547	1.48	0.0027	**0.00**
82X-1 0-20	673.3	13.0	–	–	32.8	548	1.52	0.0028	**0.00**
82X-4 120-150	677.4	20.0	7.3	42.00	32.2	539	1.80	0.0033	**0.00**
83X-2 37-67	684.3	23.0	7.1	41.96	31.5	529	1.68	0.0032	**0.00**

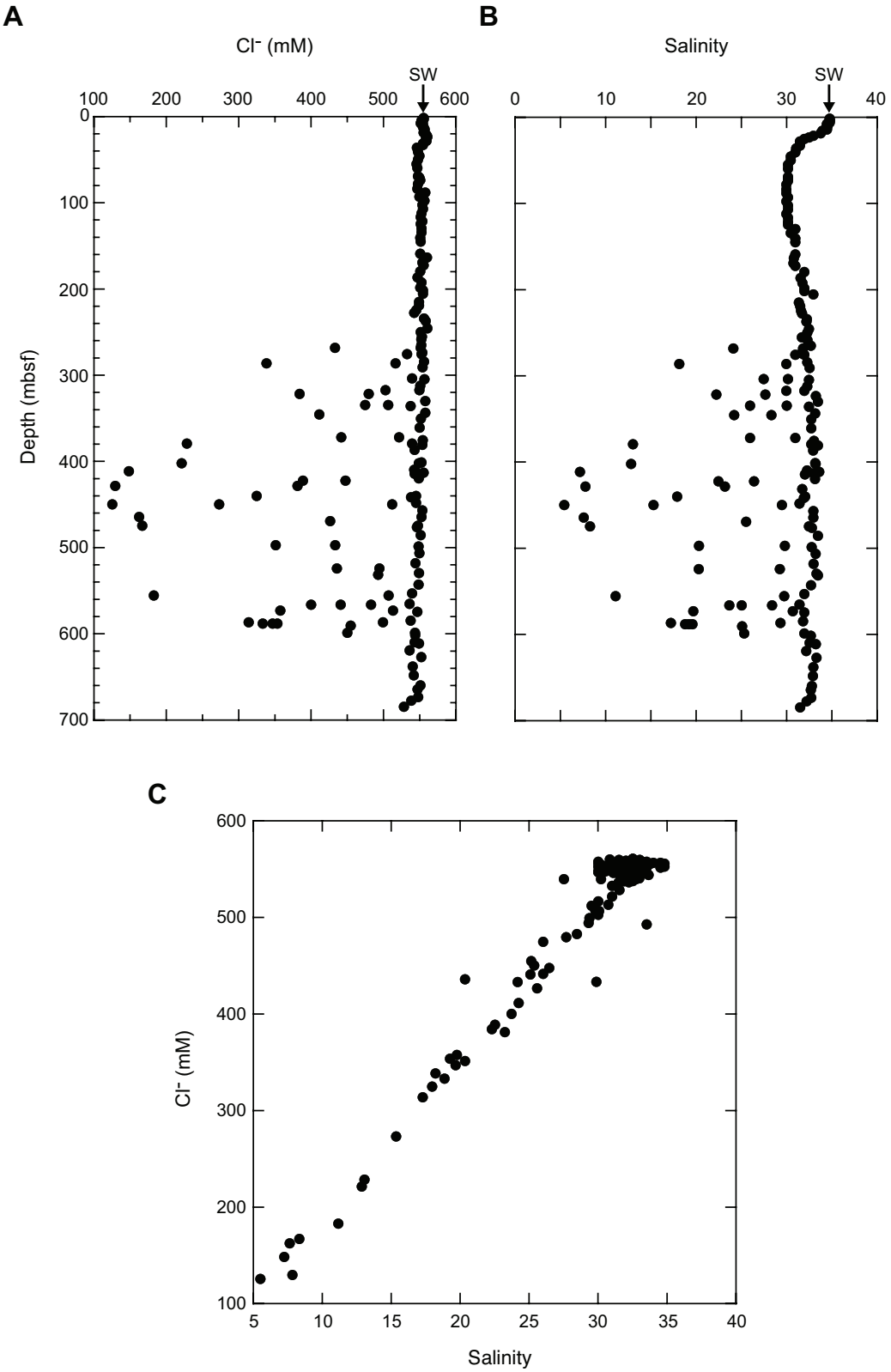


Figure 12. Concentration-depth profiles of A, chloride and B, salinity at Hole NGHP-01-17A. C, Cross plot between dissolved chloride concentration and salinity, showing a good correspondence for samples deeper than 180 mbsf, where both parameters are primarily influenced by dilution of the fluids by hydrate dissociation. Seawater value is designated as "sw" in A and B. [mbsf, meters below sea floor]

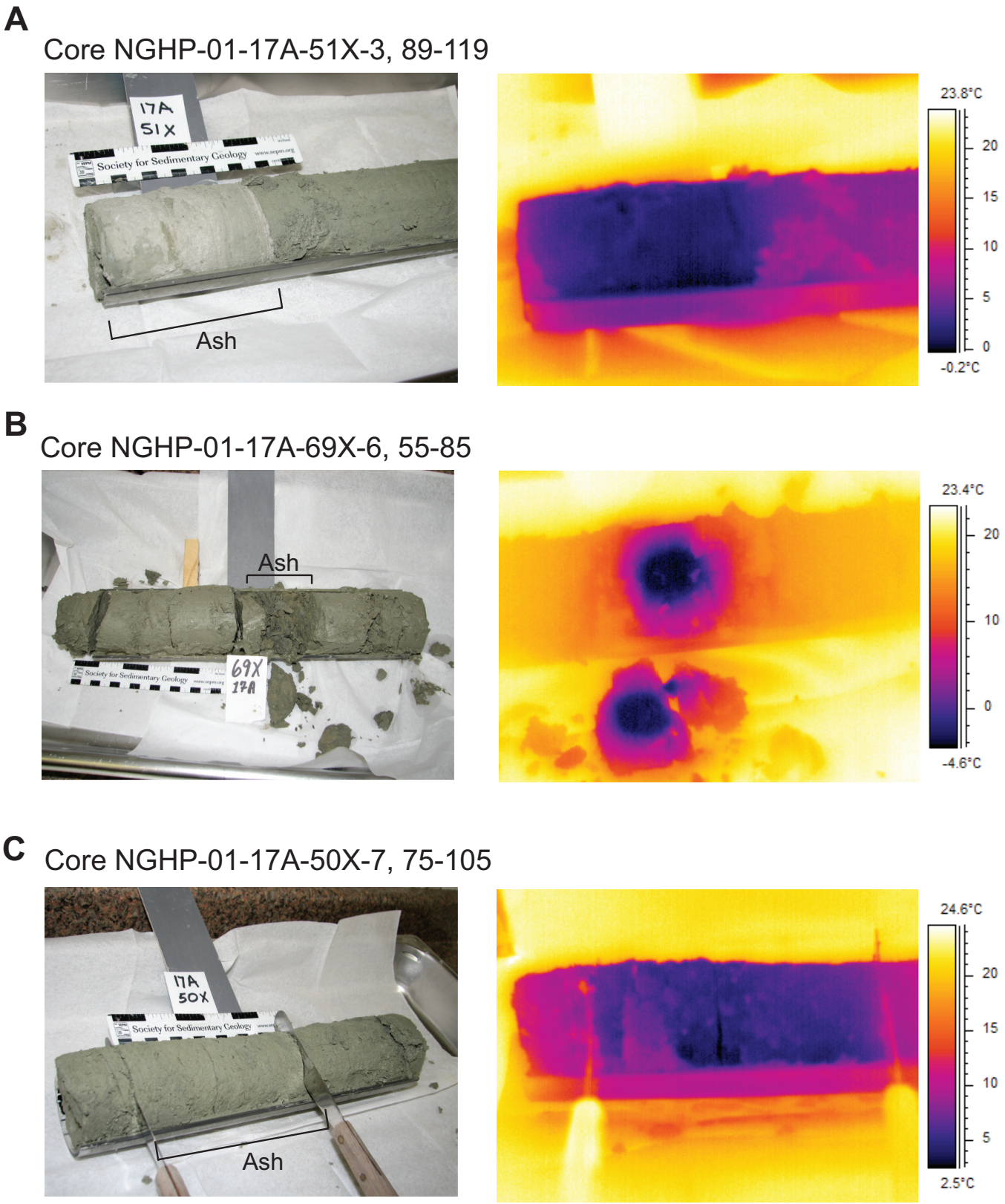


Figure 13. A and B, Visual and infrared (IR) images of core samples with ash-bearing hydrate layers. C, Visual and IR images of a core with no apparent lithologic control of the IR signal.

Gas-Hydrate Distribution

The interstitial Cl^- concentrations at Site NGHP-01-17 show clear excursions to low chlorinities against a relatively constant background concentration. These excursions reflect gas-hydrate dissociation during core recovery and processing. The gas-hydrate occurrence zone (GHOZ) as defined by the presence of chlorinity anomalies extends from ~265 to ~600 mbsf (Core NGHP-01-17A-30X to top of Core NGHP-01-17A-73X, respectively), showing a maximum in gas-hydrate abundance between ~400 and 500 mbsf. The sediment section showing Cl^- anomalies is consistent with inferences of gas-hydrate presence based on IR scans of the cores, which at this site show IR anomalies attributed to gas-hydrate dissociation between ~224 and ~600 mbsf (see "Physical Properties"). The upper limit of this zone is probably controlled by the methane concentration, such that above 265 mbsf there is not enough methane present to stabilize the gas hydrate. The lower boundary approximately corresponds to the base of the gas-hydrate stability zone. Using 600 mbsf (last dissolved chloride anomaly), and thermodynamic estimates for the stability of pure methane hydrate, the data suggest a geothermal gradient of about 2.1°C/100 m. This depth is close to that estimated for the bottom simulating reflector (BSR) in regional seismic data.

To estimate gas-hydrate abundance from Cl^- data requires a knowledge of the *in situ* dissolved Cl^- concentration. At Hole NGHP-01-17A, the dissolved Cl^- concentration above the gas-hydrate stability zone averages 554 ± 4 mM, and beneath the hydrate stability zone, the dissolved Cl^- values average 551 ± 2 mM. In addition, at this site, the dissolved Cl^- concentration in sediments recovered under pressure in Cores NGHP-01-17A-37P, -38Y, -48P and -49E (at 328, 329, 413, and 441 mbsf, respectively) were measured. Degassing analyses of these pressure cores provided between 1.5 to 2.5 L methane, indicating that no gas hydrate was present in these cores. Thus, these samples can be used as reliable proxies for the background Cl^- in the gas-hydrate-bearing sediment section. The dissolved Cl^- concentration in these four core samples is extremely consistent, with an average of 557± 1 mM. This value is consistent with the average concentration in the upper 200 mbsf, and provides a robust constraint on the background Cl^- values against which hydrate concentrations can be estimated from Cl^- data. The Cl^- data beneath the gas-hydrate stability zone (GHSZ), of 551± 2 mM, are slightly lower than the above mentioned average background value. Although small, the difference is significant.

Based on these results, the amount of disseminated gas hydrate present in the background sediment samples within the gas-hydrate stability zone can be determined with confidence; the detection threshold for background disseminated gas hydrate by IR imaging is as yet undetermined. At this site, the background Cl^- between 260 to 440 mbsf is 555 ± 2 mM. This value is very close to the background Cl^- value of 557 ± 1 mM obtained with the pressure cores, indicating the absence of background disseminated gas hydrate in this depth interval. Deeper in the section, between ~440 to the base of the GHSZ, the background Cl^- value is slightly lower (550 ± 3 mM), suggesting that a small amount (<1 percent) of disseminated gas hydrate occupies the pore space. This depth interval corresponds to the zone of the highest discrete Cl^- anomalies, which reflect the maximum amounts of gas hydrate present in discrete horizons.

The Cl^- concentration depth profile at this site reveals that gas hydrate is distributed heterogeneously, with intervals of high gas-hydrate content causing the observed discrete anomalous freshening. This is consistent with the IR scan records of the cores that imaged the presence of gas hydrate in distinct intervals of the cores. In 11 of the 25 samples recovered from zones displaying IR anomalies, the gas hydrate was hosted within medium-to-coarser grain volcanic ash layers (figs. 13A and 13B); these occurrences yielded the largest dissolved Cl^- anomalies, with a minimum value of 126 mM (~23 percent at background) at 450 mbsf (in Core NGHP-01-17A-53X-6). The sediment in immediate contact with the ash layers had in general lower Cl^- than background samples, with the lowest value having 347 mM (62 percent at background), but the remaining samples ranged from 537 to 557 mM (96–99 percent at background). These data indicate a preferential formation of gas hydrate in the medium to coarser-grained sediment intervals, as previously observed in samples recovered from northern Cascadia Margin during IODP Expedition 311 (Riedel and others, 2006). No Cl^- or IR anomalies were observed in the volcanic ash horizon below 600 mbsf, supporting the suggestion that the base of the GHSZ is in the vicinity of 600 mbsf. (For a compilation of volcanic ash distribution with depth at this site see "Lithostratigraphy").

In general, the samples with no apparent lithologic control on the location of the IR anomaly, show no pronounced difference in dissolved Cl^- between the sections of the core displaying colder signals in the IR scan and the adjacent sediment (fig. 3C). These samples show Cl^- values ranging from 352 to 540 mM, and the corresponding paired samples from the non-IR anomaly sections of the whole rounds range from 353 to 554 mM. In some of the samples, based on sediment color and(or) physical behavior during the cleaning operation, the maximum IR anomaly interval having slightly higher gas-hydrate concentration seemed to be controlled by disseminated volcanic ash. In others, it may have been controlled by the presence of fractures or microfractures in the formation. Indeed, the anomalies in Sections 34X-4 and 52X-5 occur in sediment samples with fractures probably are original formation features and not induced by drilling.

In summary, at this site the Cl^- and salinity data indicate that, (1) volcanic ash hosts the largest concentrations of gas hydrate, and (2) in the calcareous-siliceous-clayey sediment gas hydrate occurs disseminated in much lower concentrations and is distributed over larger sections of the core.

Sulfate and Alkalinity Concentrations: Characterization of the SMI

The primary objectives of the higher resolution sampling in the upper 32 m of the sediment section were to delineate and characterize the sulfate-methane interface (SMI) for future geochemical modeling of methane fluxes and to provide supporting data and samples for studies on the microbial dynamics of the SMI. At Site NGHP-01-17, the sulfate-methane interface is located at 25 mbsf, as illustrated in figure 14B. Alkalinity shows a maximum of just 16.8 mM at the SMI depth (fig. 14A). This value is significantly lower, about 1/3 of the alkalinity production value by bacterial SO_4^{2-} reduction (Equation 1), and about half of the production value by anaerobic methane oxidation (Equation 2), indicating a significant loss of alkalinity most likely by authigenic carbonate formation. The non-linear decrease in SO_4^{2-} and increase in alkalinity reflect that these depth-concentration profiles are controlled by the combined reactions of bacterial sulfate reduction and anaerobic methane oxidation coupled to sulfate reduction.

1. $2CH_2O + SO_4^{2-} \rightarrow 2HCO_3^- + H_2S$

2. $CH_4 + SO_4^{2-} \rightarrow HCO_3^- + HS^- + H_2O$

The sulfate profile will be carefully modeled to compute the vertical component of the methane flux at this site, and the Ca^{2+} and Mg^{2+} concentration profiles will be used to calculate total alkalinity loss by authigenic carbonate formation. Below the SMI, SO_4^{2-} concentrations remain zero throughout this sediment section; the few somewhat higher than 0.10 mM sulfate values, reported in table 4, most likely indicate contamination by drill-water. The most difficult samples to clean from drill-water contamination were the ash layers and the samples from the first few XCB cores. The sulfate concentrations in these samples were used to calculate the amount of drill-water contamination, and the salinity, alkalinity, Cl^-, and Br^- concentrations were corrected for the contamination. The corrected concentration values are listed in table 5.

From the SMI to ~200 mbsf alkalinity values gradually increase at a rate of ~1 mM/10 m, and between 200 and 260 mbsf, the depth of the first recovered gas-hydrate sample, the rate of alkalinity increase more than doubles (2.3 mM/10 m). The change in slope at ~200 mbsf corresponds with a change in lithology, from a foraminiferal ooze to a mostly coccolith ooze (see "Lithostratigraphy"). The lithological change may have been accompanied by a change in the percent and(or) type of organic matter that could influence alkalinity production. Within the gas-hydrate zone, in the background samples the alkalinity values remain rather constant at 40–50 mM, suggesting a steady-state between alkalinity production and utilization by carbonate and methane formation. The discrete lower alkalinity values within the gas-hydrate zone, seen in figure 14A, represent dilution by gas-hydrate dissociation.

Bromide Concentrations

Pore water samples were analyzed for dissolved Br^- by the ion chromatograph used for SO_4^{2-} determinations. Bromide concentrations are primarily influenced by marine organic matter diagenesis, such that the Br^- concentration increases with organic matter decomposition. The concentration depth profile of Br^- may also be utilized to evaluate variations in the input of terrestrial organic matter, thus the dilution of marine organic matter by terrestrial organic matter, as the diagenesis of the latter does not contribute much Br^- to the pore fluids. When normalized to Cl^- the influence of gas-hydrate dissociation on the Br^- depth profile is eliminated, shown in figure 15A (seawater normalized value is 0.00154). The bromide concentrations and Br^-/Cl^- ratios increase steeply with depth to ~200 mbsf (fig. 15A) from seawater value of 0.86 to 1.38, and from 0.00154 to 0.00249, respectively (by ~60 percent), indicating intense marine organic matter diagenesis. Below 200 mbsf to total depth the concentration ratios steadily and gradually increase only by ~20 percent, suggesting that both the organic matter content and the terrestrial versus marine organic matter input did not greatly fluctuate over time. Primarily below ~350 mbsf, the higher than the background interstitial water Br^-/Cl^- values, correspond with ash layers that hosted gas hydrate, as identified by IR imaging, implying that the Br^-/Cl^- in the volcanic ashes is higher than in seawater.

Organic Geochemistry

The organic geochemistry program at Site NGHP-01-17 (ANGH-01) included analysis of the composition of volatile hydrocarbons including methane, ethane, and propane (C_1–C_3) and fixed natural gases (that is, O_2, CO_2, and N_2+Ar) from headspace, void gas, and pressure core sampler (PCS) degassing experiments. In general, these analyses indicate that the predominant hydrocarbon gas found in the cores at Site NGHP-01-17 was methane; however ethane was measurable in headspace samples below 585 mbsf. Ethane was also observed in nearly all void gases and pressure core samples. Propane was detected at low levels (<300 ppmv) in void gases below 563 mbsf, likely indicating the presence of thermogenic hydrocarbons. The samples taken above the sulfate-methane interface (SMI, 0–18 mbsf) were depleted in methane. Conversely, methane and ethane were relatively enriched below the SMI and above the seismically-inferred bottom-simulating reflector (BSR). Methane and ethane concentrations were consistently elevated below the SMI, likely due to presence of gas hydrate in these cores.

Headspace gas analyses were performed on 135 samples from NGHP-01-17A, ranging in depth from 1.35 to 684.1 meters below seafloor (mbsf). The concentrations given here represent minimum proxy measurements of the actual concentrations due to limitations of the gas headspace method (Kvenvolden and Lorenson, 2000). The sediment

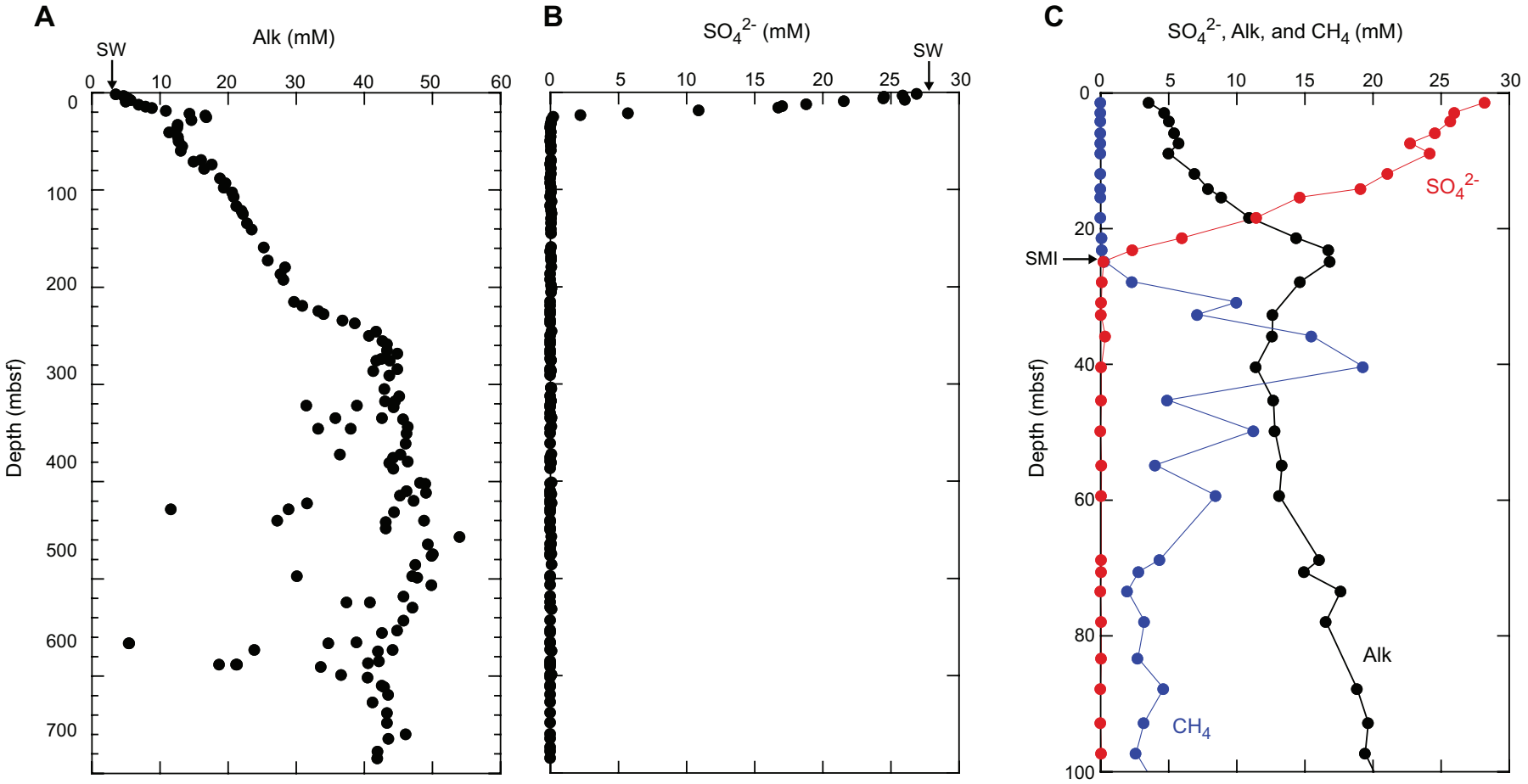


Figure 14. Concentration-depth profiles of A, alkalinity; B, sulfate; and C, sulfate, methane, and alkalinity. Note the alkalinity maximum at the SMI depth, at 25 mbsf, and the steep increase in methane concentration below the SMI. Seawater value is designated as "sw" in A and B. [SMI, sulfate-methane interface; mbsf, meters below sea floor]

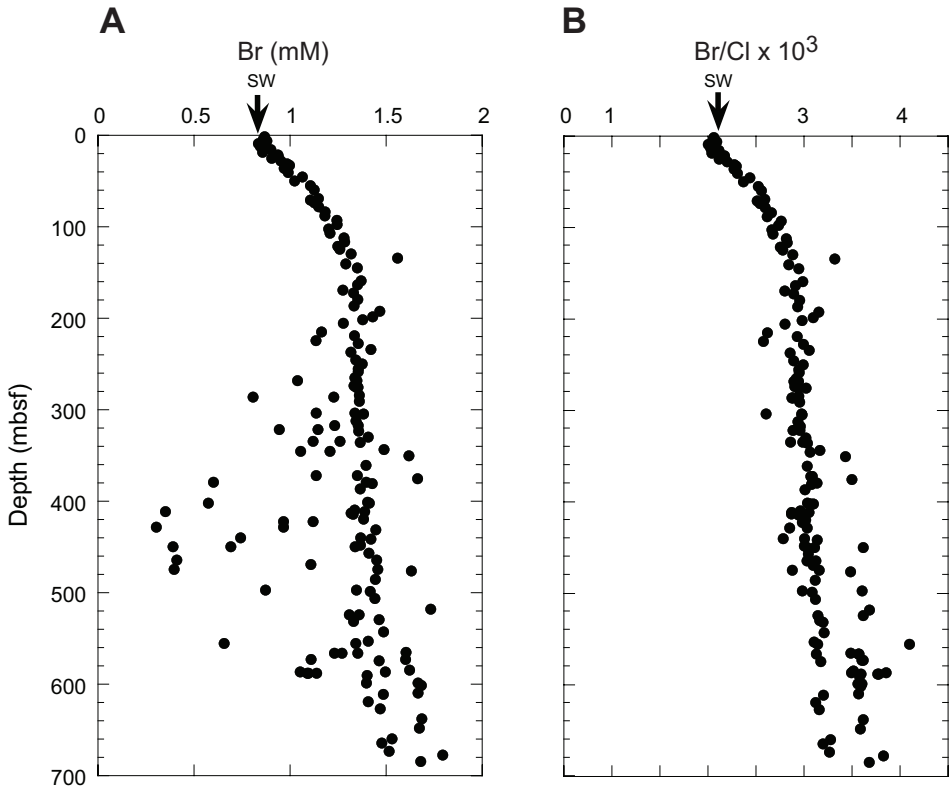


Figure 15. A, Concentration-depth profile of dissolved bromide, and B, depth profile of Br^-/Cl^- ratios at Hole NGHP-01-17A. Seawater value is designated as "sw" in each of the figures.

pore water contained methane at concentrations ranging from non-detectable near the surface to 25.9 mM at ~360 mbsf (table 6). Theoretical methane saturation in pore water under site-specific physical conditions, calculated using the Duan and others, (1992) and Xu (2002, 2004) methodologies, ranges from 54.7 mM at the seafloor to 162.2 mM near the borehole completion depth of 680 mbsf (fig. 16). Headspace samples in NGHP-01-17A indicated the presence of C_2 gas at depths of greater than 585 mbsf, ranging from 0.004 to 0.014 mM; however no C_3 or higher carbon number gases were present above detection limits, despite presence of propane in void gas samples below 563 mbsf. The presence of elevated levels of C_1 gas and only limited detection of ethane gas in headspace samples suggests hydrocarbon gases result from microbial methanogenesis. Further analysis of C_1 isotopic signatures will help to clarify the nature of hydrocarbon gas production at Site NGHP-01-17.

Methane concentrations increase step-wise from non-detectable near the surface to nearly 10 mM between 18 and 30.4 mbsf. The noted transition near the top of this interval provides constants to the depths of the sulfate-methane interface (SMI) (see "Inorganic Geochemistry"). Methane concentrations below the SMI range from 0.19 to 25.9 mM, with relative enrichment between the intervals ~30–110 mbsf, 210–310 mbsf, and from ~360 mbsf through the BSR (fig. 16). This is likely to be due to the presence of distinct gas-hydrate layers, as other proxy measurements indicate extensive occurrence of gas hydrate in these intervals of up to 20 percent pore volume beginning at 224 mbsf through the BSR. (see "Inorganic geochemistry", "Physical Properties" and "Downhole Logging"). Pressure core samples from NGHP-01-17A indicate elevated methane gas in the same depth ranges (discussed below and in detail in "Pressure Coring"). The presence of methane at elevated concentrations below the BSR may imply the presence of methane gas bubbles or pockets in this interval (fig. 16). Results from PCS core NGHP-01-17-18E confirm the presence of free gas below the BSR (see "Pressure Coring").

Carbon dioxide (CO_2) concentrations ranged from 0.15 to 42.4 mM in pore water contained within the sediment. An equivalent concentration expression of gas volume to sediment volume ranges from 1850 to nearly 321,200 microL CO_2/L wet sediment (table 6). There is a consistent, increasing trend in the CO_2 concentration with depth, however concentrations tend to alternate between high and low at depths greater than ~350 mbsf. The lowest concentrations are found in the upper 25 mbsf, above the SMI. The apparent gas-hydrate enrichment zones are also highlighted where the methane to carbon dioxide ratio for headspace is elevated (values near and above 2) (fig. 17). Air gases are present in all samples as the result of core plugs being degassed in an air headspace. The air gases (N_2+Ar), and O_2 were the sample balance gases, however the (N_2+Ar)/O_2 ratios were typically greater than air reflecting the ratio in sediment and may also indicate some oxygen has likely dissolved preferentially into the sediment porewater from air during sampling compared to N_2.

Table 6. Headspace gas composition for Site NGHP-01-17.

Sample	Site	Hole	Core	Section	Interval (cm)	Sed wt. (g)	Sample depth (mbsf)	CO_2	C_1	C_2	C_3
								(ppmv)			
17A-1H1-135-140	17	A	1	1	135–140	8.8	1.35	3,500	nd	nd	nd
17A-1H2-95-100	17	A	1	2	95–100	8.9	2.45	8,300	nd	nd	nd
17A-1H3-108-113	17	A	1	3	108–113	10.2	4.08	2,900	nd	nd	nd
17A-2H1-135-140	17	A	2	1	135–140	11.0	5.85	7,400	nd	nd	nd
17A-2H2-135-140	17	A	2	2	135–140	9.6	7.35	4,900	nd	nd	nd
17A-2H3-105-110	17	A	2	3	105–110	7.3	8.55	7,700	nd	nd	nd
17A-2H5-95-100	17	A	2	5	95–100	9.7	11.45	12,200	nd	nd	nd
17A-2H7-58-63	17	A	2	7	58–63	6.0	14.08	4,500	nd	nd	nd
17A-3H1-130-135	17	A	3	1	130–135	5.5	15.30	1,100	nd	nd	nd
17A-3H3-100-105	17	A	3	3	100–105	7.8	18.00	10,700	nd	nd	nd
17A-3H5-90-95	17	A	3	5	90–95	5.3	20.90	6,300	300	nd	nd
17A-3H7-57-62	17	A	3	7	57–62	7.4	23.07	1,900	400	nd	nd
17A-4H1-130-135	17	A	4	1	130–135	10.0	24.80	900	1,700	nd	nd
17A-4H3-100-105	17	A	4	3	100–105	10.3	27.50	3,300	14,000	nd	nd
17A-4H5-90-95	17	A	4	5	90–95	10.4	30.40	17,700	60,100	nd	nd
17A-4H7-64-69	17	A	4	7	64–69	9.4	32.64	6,500	36,700	nd	nd
17A-5H2-120-125	17	A	5	2	120–125	7.4	35.70	9,400	57,700	nd	nd
17A-5H5-90-95	17	A	5	5	90–95	7.1	39.90	10,500	66,900	nd	nd
17A-6H2-120-125	17	A	6	2	120–125	8.8	45.14	10,100	21,900	nd	nd
17A-6H5-90-95	17	A	6	5	90–95	7.3	49.34	9,700	38,900	nd	nd
17A-7H2-120-125	17	A	7	2	120–125	8.0	54.70	5,800	15,300	nd	nd
17A-7H5-90-95	17	A	7	5	90–95	9.1	58.90	4,000	37,800	nd	nd
17A-8H5-85-90	17	A	8	5	85–90	7.0	68.35	17,300	13,600	nd	nd
17A-8H7-52-57	17	A	8	7	52–57	7.5	70.52	17,300	9,500	nd	nd
17A-9H2-115-120	17	A	9	2	115–120	7.7	73.25	10,100	6,800	nd	nd
17A-9H5-85-90	17	A	9	5	85–90	8.0	77.45	12,000	11,600	nd	nd
17A-10H2-115-120	17	A	10	2	115–120	5.4	83.15	6,000	6,100	nd	nd
17A-10H5-85-90	17	A	10	5	85–90	6.3	87.35	8,600	12,200	nd	nd
17A-11H2-115-120	17	A	11	2	115–120	8.6	92.65	8,800	12,200	nd	nd
17A-11H5-85-90	17	A	11	5	85–90	7.0	96.85	9,500	7,700	nd	nd
17A-12H2-115-120	17	A	12	2	115–120	7.9	102.15	8,600	13,900	nd	nd
17A-12H5-85-90	17	A	12	5	85–90	6.5	106.35	9,800	13,100	nd	nd
17A-13H2-115-120	17	A	13	2	115–120	6.9	111.65	5,200	9,100	nd	nd
17A-13H5-85-90	17	A	13	5	85–90	6.5	115.85	5,200	8,800	nd	nd
17A-14X2-110-115	17	A	14	2	110–115	10.9	121.10	4,800	8,800	nd	nd
17A-14X4-80-85	17	A	14	5	80–85	8.0	123.80	4,200	5,900	nd	nd
17A-15X2-32-37	17	A	15	2	32–37	8.1	129.42	6,600	10,300	nd	nd
17A-15X5-80-85	17	A	15	5	80–85	8.0	133.52	5,500	7,400	nd	nd
17A-16X2-110-115	17	A	16	2	110–115	8.4	140.30	6,000	9,300	nd	nd
17A-16X5-65-70	17	A	16	5	65–70	7.7	144.19	7,900	6,100	nd	nd
17A-18H2-110-115	17	A	18	2	110–115	14.3	158.66	4,500	5,300	nd	nd
17A-18H5-55-60	17	A	18	5	55–60	11.5	162.61	23,300	10,100	nd	nd
17A-19X3-110-115	17	A	19	3	110–115	9.8	168.93	3,400	4,300	nd	nd
17A-19X5-80-85	17	A	19	5	80–85	11.1	171.63	13,700	6,000	nd	nd
17A-21X2-75-80	17	A	21	2	75–80	9.4	178.75	16,900	5,100	nd	nd
17X-22X1-100-105	17	A	22	1	100–105	12.7	186.20	7,700	9,200	nd	nd
17X-22X5-54-59	17	A	22	5	54–59	9.7	191.64	17,400	3,400	nd	nd
17A-23X3-105-110	17	A	23	3	105–110	9.9	198.23	28,400	10,300	nd	nd
17A-23X5-75-80	17	A	23	5	75–80	11.4	200.83	9,100	1,500	nd	nd
17A-24X2-75-80	17	A	24	2	75–80	12.0	204.80	2,200	1,000	nd	nd
17A-25X1-75-80	17	A	25	1	75–80	7.0	214.25	20,900	10,900	nd	nd
17A-25X4-75-80	17	A	25	4	75–80	9.1	218.75	16,800	14,100	nd	nd
17A-26X1-115-120	17	A	26	1	115–120	8.7	224.25	15,600	18,900	nd	nd
17A-26X3-61-66	17	A	26	3	61–66	9.2	226.71	13,100	22,000	nd	nd
17A-27X1-115-120	17	A	27	1	115–120	9.7	233.95	29,700	21,500	nd	nd
17A-27X3-55-60	17	A	27	3	55–60	10.1	236.35	21,700	15,400	nd	nd
17A-28X2-110-115	17	A	28	2	110–115	8.6	245.15	18,300	12,300	nd	nd

Table 6. Headspace gas composition for Site NGHP-01-17.—Continued

Sample	O_2	N2+Ar	H_2S	C1 (mL/L WS)	C1 (mM PW)	CO_2 (mL/L WS)	CO_2 (mM PW)	C_1/CO_2
	(ppmv)							
17A-1H1-135-140	196,200	773,400	nd	nd	nd	8,900	0.4	–
17A-1H2-95-100	190,800	784,900	nd	nd	nd	21,200	1.1	–
17A-1H3-108-113	190,000	760,500	nd	nd	nd	6,000	0.3	–
17A-2H1-135-140	192,300	790,500	nd	nd	nd	13,700	0.8	–
17A-2H2-135-140	187,500	767,400	nd	nd	nd	11,200	0.7	–
17A-2H3-105-110	192,500	772,500	nd	nd	nd	25,700	1.5	–
17A-2H5-95-100	182,500	767,300	nd	nd	nd	27,300	1.7	–
17A-2H7-58-63	189,500	766,200	nd	nd	nd	19,200	1.2	–
17A-3H1-130-135	191,900	741,700	nd	nd	nd	5,100	0.3	–
17A-3H3-100-105	189,600	761,500	nd	nd	nd	32,400	2.1	–
17A-3H5-90-95	189,900	756,400	nd	1,300	0.1	30,900	2.0	0.0
17A-3H7-57-62	190,700	748,100	nd	1,400	0.1	6,100	0.4	0.2
17A-4H1-130-135	192,000	741,000	nd	3,600	0.2	1,800	0.1	1.9
17A-4H3-100-105	184,900	734,200	nd	28,800	2.0	6,800	0.5	4.2
17A-4H5-90-95	168,100	746,100	nd	121,900	8.5	35,800	2.5	3.4
17A-4H7-64-69	178,400	743,200	nd	86,200	6.1	15,300	1.1	5.6
17A-5H2-120-125	178,000	732,400	nd	187,800	13.2	30,500	2.1	6.1
17A-5H5-90-95	163,600	743,800	nd	229,800	16.4	36,000	2.6	6.4
17A-6H2-120-125	186,900	744,000	nd	56,500	4.1	26,200	1.9	2.2
17A-6H5-90-95	178,600	730,200	nd	129,100	9.4	32,000	2.3	4.0
17A-7H2-120-125	185,500	752,700	nd	45,100	3.3	17,100	1.3	2.6
17A-7H5-90-95	179,800	739,200	nd	93,100	7.0	9,900	0.7	9.5
17A-8H5-85-90	182,700	756,200	nd	47,500	3.6	60,400	4.6	0.8
17A-8H7-52-57	184,600	754,500	nd	30,400	2.3	55,300	4.2	0.5
17A-9H2-115-120	190,400	749,500	nd	21,100	1.6	31,200	2.4	0.7
17A-9H5-85-90	186,400	749,700	nd	34,200	2.6	35,200	2.7	1.0
17A-10H2-115-120	191,800	745,200	nd	29,200	2.2	29,000	2.2	1.0
17A-10H5-85-90	190,500	752,100	nd	48,800	3.8	34,200	2.7	1.4
17A-11H2-115-120	182,800	766,700	nd	32,400	2.6	23,400	1.8	1.4
17A-11H5-85-90	190,000	750,300	nd	26,800	2.1	33,300	2.6	0.8
17A-12H2-115-120	176,900	762,200	nd	41,400	3.3	25,800	2.1	1.6
17A-12H5-85-90	185,000	755,100	nd	50,400	4.0	37,600	3.0	1.3
17A-13H2-115-120	187,000	742,000	nd	32,300	2.6	18,600	1.5	1.8
17A-13H5-85-90	190,800	747,500	nd	34,000	2.7	20,000	1.6	1.7
17A-14X2-110-115	178,100	760,200	nd	16,500	1.4	9,100	0.8	1.8
17A-14X4-80-85	189,700	753,000	nd	17,200	1.4	12,500	1.0	1.4
17A-15X2-32-37	179,900	737,400	nd	29,600	2.4	19,100	1.6	1.6
17A-15X5-80-85	184,700	737,200	nd	21,600	1.8	16,100	1.3	1.3
17A-16X2-110-115	187,100	743,700	nd	25,500	2.1	16,500	1.4	1.6
17A-16X5-65-70	185,000	741,100	nd	18,900	1.6	24,500	2.0	0.8
17A-18H2-110-115	176,700	738,900	nd	6,400	0.6	5,400	0.5	1.2
17A-18H5-55-60	154,500	767,000	nd	17,600	1.5	40,500	3.5	0.4
17A-19X3-110-115	183,100	737,700	nd	9,500	0.8	7,600	0.6	1.3
17A-19X5-80-85	163,900	763,800	nd	11,000	1.0	25,100	2.2	0.4
17A-21X2-75-80	176,200	728,500	nd	11,900	1.0	39,700	3.3	0.3
17X-22X1-100-105	182,400	743,600	nd	13,600	1.3	11,400	1.1	1.2
17X-22X5-54-59	173,900	747,100	nd	7,600	0.8	39,200	4.1	0.2
17A-23X3-105-110	154,700	778,200	nd	22,500	2.5	61,900	6.9	0.4
17A-23X5-75-80	181,500	758,400	nd	2,700	0.3	16,000	2.0	0.2
17A-24X2-75-80	191,300	737,900	nd	1,600	0.2	3,500	0.3	0.5
17A-25X1-75-80	180,100	741,500	nd	38,000	2.8	73,200	5.3	0.5
17A-25X4-75-80	169,500	746,100	nd	34,800	2.7	41,400	3.3	0.8
17A-26X1-115-120	180,000	742,300	nd	49,500	4.0	41,000	3.3	1.2
17A-26X3-61-66	174,600	747,400	nd	53,400	4.2	31,700	2.5	1.7
17A-27X1-115-120	151,000	760,900	nd	48,200	3.4	66,800	4.8	0.7
17A-27X3-55-60	163,900	767,400	nd	32,500	2.4	46,000	3.4	0.7
17A-28X2-110-115	174,800	759,900	nd	32,600	2.4	48,700	3.5	0.7

Table 6. Headspace gas composition for Site NGHP-01-17.—Continued

Sample	Site	Hole	Core	Section	Interval (cm)	Sed wt. (g)	Sample depth (mbsf)	CO_2	C_1	C_2	C_3
								(ppmv)			
17A-28X5-75-80	17	A	28	5	75–80	9.7	249.25	15,700	14,800	nd	nd
17A-29X2-110-115	17	A	29	2	110–115	9.1	254.79	22,400	13,200	nd	nd
17A-29X5-75-80	17	A	29	5	75–80	7.8	258.19	18,200	12,900	nd	nd
17A-30X3-75-80	17	A	30	3	75–80	6.3	264.35	19,400	10,500	nd	nd
17A-30X6-31-36	17	A	30	6	31–36	9.7	267.92	22,800	10,000	nd	nd
17A-31X3-75-80	17	A	31	3	75–80	6.2	273.08	19,600	8,600	nd	nd
17A-31X5-30-35	17	A	31	5	30–35	8.6	275.13	19,500	11,500	nd	nd
17A-32X2-75-80	17	A	32	2	62–67	8.7	283.52	20,200	15,800	nd	nd
17A-32X5-30-35	17	A	32	5	66–71	9.4	285.93	14,400	26,000	nd	nd
17A-33X1-51-56	17	A	33	1	51–56	6.5	290.11	20,200	12,200	nd	nd
17A-34X3-75-80	17	A	34	3	75–80	5.6	302.95	23,300	7,000	nd	nd
17A-34X4-79-84	17	A	34	4	79–84	5.1	304.49	21,400	17,000	nd	nd
17A-35X3-75-80	17	A	35	3	75–80	7.0	311.41	25,700	10,100	nd	nd
17A-35X7-64-69	17	A	35	7	64–69	7.4	317.04	26,600	10,800	nd	nd
17A-36X3-60-65	17	A	36	3	60–65	7.4	321.49	12,500	12,400	nd	nd
17A-36X4-68-73	17	A	36	4	68–73	7.3	322.52	17,800	8,100	nd	nd
17A-37P-10-15	17	A	37	P	10–15	7.9	328.10	19,000	6,200	nd	nd
17A-37P-45-50	17	A	37	P	45–50	11.3	328.45	25,000	8,900	nd	nd
17A-38Y-45-50	17	A	38	Y	45–50	9.4	329.45	22,500	2,000	nd	nd
17A-39X3-75-80	17	A	39	3	75–80	10.7	333.75	49,200	13,200	nd	nd
17A-39X5-26-31	17	A	39	5	26–31	12.1	335.33	6,100	4,500	nd	nd
17A-40X5-65-70	17	A	40	5	65–70	10.3	342.93	5,500	3,900	nd	nd
17A-40X7-55-60	17	A	40	7	55–60	11.7	345.23	17,000	3,300	nd	nd
17A-41X2-75-86	17	A	41	2	75–86	9.8	349.55	15,400	12,300	nd	nd
17A-42X3-75-80	17	A	42	3	75–80	9.5	360.04	91,300	89,100	nd	nd
17A-43X5-48-53	17	A	43	5	48–53	9.5	371.68	41,800	16,700	nd	nd
17A-43X8-65-70	17	A	43	8	65–70	8.3	374.52	73,200	22,500	nd	nd
17A-44X3-31-36	17	A	44	3	31–36	11.9	378.91	58,900	14,300	nd	nd
17A-44X4-75-80	17	A	44	4	75–80	11.4	380.01	52,100	14,400	nd	nd
17A-45X1-50-55	17	A	45	1	50–55	10.9	386.20	50,100	25,400	nd	nd
17A-46X4-75-80	17	A	46	4	75–80	8.6	400.39	31,300	8,400	nd	nd
17A-46X5-62-67	17	A	46	5	62–67	10.8	401.76	49,800	16,300	nd	nd
17A-47X4-68-73	17	A	47	4	68–73	8.6	409.48	35,000	9,700	nd	nd
17A-47X5-75-80	17	A	47	5	75–80	7.7	410.58	33,000	11,300	nd	nd
17A-48P-15-18	17	A	48	P	15–18	6.3	412.85	70,300	7,000	nd	nd
17A-49E1-40-45	17	A	49	E	40–45	8.0	414.10	17,900	5,300	nd	nd
17A-50X4-75-80	17	A	50	4	75–80	8.6	418.95	52,100	19,600	nd	nd
17A-50X7-70-75	17	A	50	7	70–75	8.5	422.06	40,600	11,400	nd	nd
17A-51X3-84-89	17	A	51	3	84–89	7.4	428.07	36,800	16,600	nd	nd
17A-51X5-75-80	17	A	51	5	75–80	8.4	430.67	34,100	8,100	nd	nd
17A-52X5-22-27	17	A	52	5	22–27	9.3	439.72	48,300	15,500	nd	nd
17A-52X6-75-80	17	A	52	6	75–80	8.8	440.82	59,100	19,300	nd	nd
17A-53X4-58-63	17	A	53	4	58–63	10.3	447.43	63,700	9,200	nd	nd
17A-53X6-42-47	17	A	53	6	42–47	12.8	449.60	85,000	14,400	nd	nd
17A-54X3-71-76	17	A	54	3	71–76	8.2	455.99	76,200	7,200	nd	nd
17A-55X2-12-17	17	A	55	2	12–17	9.8	464.12	25,900	6,600	nd	nd
17A-55X7-41-46	17	A	55	7	41–46	8.7	468.87	13,500	3,700	nd	nd
17A-56X2-64-69	17	A	56	2	64–69	8.3	474.34	36,500	6,300	nd	nd
17A-56X3-75-80	17	A	56	3	75–80	12.4	475.44	115,700	13,300	nd	nd
17A-57X3-75-80	17	A	57	3	75–80	8.5	484.93	106,900	10,300	nd	nd
17A-58X4-80-85	17	A	58	4	80–85	10.2	496.58	53,200	12,000	nd	nd
17A-58X5-75-80	17	A	58	5	75–80	8.9	497.98	18,100	5,100	nd	nd
17A-61X4-75-80	17	A	61	4	75–80	7.9	505.73	42,800	6,300	nd	nd
17A-62X5-75-80	17	A	62	5	75–80	7.9	517.36	49,500	9,100	nd	nd
17A-63X3-25-30	17	A	63	3	25–30	9.2	523.48	61,800	10,600	nd	nd
17A-64X1-32-37	17	A	64	1	32–37	7.3	530.62	57,700	10,900	nd	nd
17A-65X2-75-80	17	A	65	2	75–80	6.4	542.15	60,900	8,300	nd	nd
17A-66X3-36-41	17	A	66	3	36–41	7.6	552.36	44,200	10,400	nd	nd
17A-66X5-64-69	17	A	66	5	64–69	7.2	555.07	35,300	11,200	nd	nd
17A-67X6-22-27	17	A	67	6	22–27	10.8	564.36	97,300	18,500	nd	nd

Table 6. Headspace gas composition for Site NGHP-01-17.—Continued

Sample	O_2	N2+Ar	H_2S	C1	C1	CO_2	CO_2	C_1/CO_2
		(ppmv)		(mL/L WS)	(mM PW)	(mL/L WS)	(mM PW)	
17A-28X5-75-80	173,300	757,100	nd	33,400	2.5	35,300	2.6	0.9
17A-29X2-110-115	168,200	754,200	nd	32,600	2.4	55,200	4.0	0.6
17A-29X5-75-80	168,800	765,500	nd	39,300	2.6	55,200	3.6	0.7
17A-30X3-75-80	179,600	732,900	nd	42,000	2.7	77,600	5.0	0.5
17A-30X6-31-36	182,200	756,200	nd	22,400	1.5	51,200	3.4	0.4
17A-31X3-75-80	178,300	749,600	nd	34,900	2.4	79,800	5.5	0.4
17A-31X5-30-35	171,300	764,300	nd	30,700	2.2	52,000	3.8	0.6
17A-32X2-75-80	151,600	773,200	nd	41,300	2.9	52,900	3.7	0.8
17A-32X5-30-35	165,200	732,800	nd	61,200	4.3	33,900	2.4	1.8
17A-33X1-51-56	185,200	739,500	nd	46,800	3.0	77,700	4.9	0.6
17A-34X3-75-80	182,000	744,200	nd	32,300	2.2	107,700	7.4	0.3
17A-34X4-79-84	173,200	756,300	nd	88,100	6.9	110,600	8.7	0.8
17A-35X3-75-80	181,000	728,700	nd	35,200	2.5	89,800	6.3	0.4
17A-35X7-64-69	175,200	723,900	nd	35,200	2.6	86,700	6.3	0.4
17A-36X3-60-65	160,500	739,800	nd	40,400	2.4	40,700	2.4	1.0
17A-36X4-68-73	129,400	781,000	nd	27,000	1.9	58,900	4.2	0.5
17A-37P-10-15	174,500	737,900	nd	18,600	1.4	56,800	4.2	0.3
17A-37P-45-50	162,100	733,700	nd	15,900	1.2	44,700	3.4	0.4
17A-38Y-45-50	170,600	717,900	nd	4,700	0.3	52,900	3.9	0.1
17A-39X3-75-80	133,600	723,500	nd	25,700	1.9	95,600	6.9	0.3
17A-39X5-26-31	175,600	744,100	nd	7,200	0.5	9,800	0.7	0.7
17A-40X5-65-70	182,900	741,100	nd	8,100	0.6	11,400	0.8	0.7
17A-40X7-55-60	147,700	745,600	nd	5,600	0.4	28,800	2.1	0.2
17A-41X2-75-86	146,400	739,800	nd	27,300	1.9	34,100	2.4	0.8
17A-42X3-75-80	113,800	723,900	nd	206,400	14.6	211,500	15.0	1.0
17A-43X5-48-53	159,400	748,600	nd	38,700	2.7	96,900	6.7	0.4
17A-43X8-65-70	159,300	734,000	nd	62,800	4.5	204,700	14.6	0.3
17A-44X3-31-36	155,500	754,200	nd	23,500	1.6	97,100	6.4	0.2
17A-44X4-75-80	158,100	757,400	nd	25,400	1.8	91,900	6.5	0.3
17A-45X1-50-55	170,500	720,500	nd	48,000	3.3	94,600	6.5	0.5
17A-46X4-75-80	183,100	757,200	nd	22,400	1.5	83,500	5.4	0.3
17A-46X5-62-67	167,100	756,000	nd	31,200	2.2	95,400	6.8	0.3
17A-47X4-68-73	171,800	750,400	nd	25,700	2.4	93,100	8.8	0.3
17A-47X5-75-80	174,400	754,400	nd	34,900	2.3	102,000	6.6	0.3
17A-48P-15-18	138,500	748,100	nd	27,900	1.8	281,200	18.5	0.1
17A-49E1-40-45	168,200	743,900	nd	15,400	1.1	52,500	3.6	0.3
17A-50X4-75-80	171,300	729,600	nd	52,200	3.6	138,600	9.7	0.4
17A-50X7-70-75	180,900	732,300	nd	30,800	2.1	109,900	7.6	0.3
17A-51X3-84-89	185,600	730,600	nd	54,000	3.6	119,800	7.9	0.5
17A-51X5-75-80	178,800	747,400	nd	22,400	1.5	93,700	6.3	0.2
17A-52X5-22-27	158,000	752,000	nd	37,000	2.7	115,300	8.3	0.3
17A-52X6-75-80	160,700	734,300	nd	49,900	3.2	152,400	9.7	0.3
17A-53X4-58-63	161,700	753,400	nd	19,000	1.4	131,000	9.7	0.1
17A-53X6-42-47	151,800	732,500	nd	21,000	1.5	124,200	8.7	0.2
17A-54X3-71-76	154,700	745,700	nd	20,300	1.5	216,400	15.6	0.1
17A-55X2-12-17	154,400	728,700	nd	14,600	0.9	57,400	3.7	0.3
17A-55X7-41-46	169,300	745,100	nd	9,700	0.7	35,500	2.4	0.3
17A-56X2-64-69	154,500	731,400	nd	17,500	1.2	102,100	6.8	0.2
17A-56X3-75-80	120,800	746,700	nd	20,500	1.4	178,100	12.3	0.1
17A-57X3-75-80	134,500	711,600	nd	28,000	2.1	289,400	21.2	0.1
17A-58X4-80-85	121,800	711,700	nd	25,000	1.6	111,100	7.1	0.2
17A-58X5-75-80	161,300	748,700	nd	13,100	0.9	45,900	3.0	0.3
17A-61X4-75-80	179,400	726,500	nd	18,900	1.3	127,800	8.8	0.1
17A-62X5-75-80	175,000	718,700	nd	27,100	1.9	147,800	10.4	0.2
17A-63X3-25-30	173,700	725,300	nd	25,600	1.8	149,700	10.3	0.2
17A-64X1-32-37	173,300	733,500	nd	36,100	2.5	191,300	13.4	0.2
17A-65X2-75-80	176,900	736,700	nd	32,700	1.5	238,900	11.0	0.1
17A-66X3-36-41	166,400	754,100	nd	32,800	2.3	139,000	9.6	0.2
17A-66X5-64-69	164,200	757,600	nd	37,700	2.7	119,200	8.6	0.3
17A-67X6-22-27	150,400	711,900	nd	35,500	4.2	186,400	22.0	0.2

Table 6. Headspace gas composition for Site NGHP-01-17.—Continued

Sample	Site	Hole	Core	Section	Interval (cm)	Sed wt. (g)	Sample depth (mbsf)	CO_2	C_1	C_2	C_3
								(ppmv)			
17A-68X4-57-62	17	A	68	4	57–62	6.6	572.74	85,100	14,400	nd	nd
17A-68X5-75-80	17	A	68	5	75–80	8.0	573.84	90,700	10,900	nd	nd
17A-69X4-75-80	17	A	69	4	75–80	9.5	583.95	44,900	9,600	nd	nd
17A-69X6-50-55	17	A	69	6	50–55	7.4	586.20	92,700	12,900	10	nd
17A-72X2-0-5	17	A	72	2	0–5	9.8	588.83	52,800	19,500	20	nd
17A-72X3-20-25	17	A	72	3	20–25	11.0	589.81	35,100	15,800	20	nd
17A-73X3-65-70	17	A	73	3	65–70	7.8	600.65	33,400	11,400	50	nd
17A-74X2-75-80	17	A	74	2	75–80	12.2	608.95	82,900	18,400	30	nd
17A-74X3-115-120	17	A	74	3	115–120	8.4	610.85	49,600	13,100	30	nd
17A-75X2-75-80	17	A	75	2	75–80	7.1	618.52	44,700	11,600	20	nd
17A-76X2-42-47	17	A	76	2	42–47	8.6	626.20	47,800	18,100	20	nd
17A-77X3-75-80	17	A	77	3	75–80	7.3	637.03	48,500	15,000	30	nd
17A-78X3-75-80	17	A	78	3	75–80	7.0	647.46	52,200	19,300	30	nd
17A-79X4-75-80	17	A	79	4	75–80	8.7	659.05	80,300	15,000	10	nd
17A-80X2-70-75	17	A	80	2	70–75	9.5	663.71	78,100	19,300	30	nd
17A-82X2-0-5	17	A	82	2	0–5	8.1	673.50	78,300	29,800	30	nd
17A-82X4-75-80	17	A	82	4	75–80	8.3	676.92	86,600	23,000	30	nd
17A-83X2-17-22	17	A	83	2	17–22	7.4	684.07	92,500	21,900	30	nd

Void gas samples were collected from 89 different locations ranging in depth from 43.7 to 684.5 mbsf. Methane concentrations within voids averaged nearly 84.5 percent (±23 percent with one extreme outlier). The void gas samples primarily contained methane, although ethane was also detected in nearly all samples with increasing concentration at depth, as noted in table 7. Propane was also detectable at levels up to 280 ppmv in samples obtained below 590 mbsf. Higher molecular weight hydrocarbon gases (C_4+) were not detected; however samples had a strong organic odor. Taken together these observations suggest that thermogenic hydrocarbons may be migrating from depth. Shore-based analyses will confirm presence or absence of C_4+ gases and(or) sediment bound hydrocarbons common in oil and gas reservoirs.

Carbon dioxide concentrations ranged from 1,635 to 138,560 ppmv and are tabulated with other gas data in table 7. The methane to carbon dioxide ratios are highest just below the SMI and show a general decreasing trend to ~450 mbsf, where they stabilize with depth through the BSR (fig. 18). These generally low and decreasing trends in C_1/CO_2 may be due to production of gas hydrates—the presence/weathering of volcanic ash layers and(or) diagenesis of organic material over geologic time with depth (see "Lithostratigraphy" and "Inorganic Geochemistry"). This trend occurs in headspace gas samples although the magnitude of the ratios is at least 1 order of magnitude less due to the preferential loss of volatile methane by the headspace sample method. Typically, the PCS C_1/CO_2 gas ratio is one order of magnitude greater than void gas samples, however in the interval between ~325 to 425 the disparity between magnitudes is quite low (fig. 18). The response of this ratio with depth also corroborates with the general increase in CO_2 concentrations with depth through the BSR (~610 mbsf). This may indicate that these void gas samples are of high quality, or the CO_2 was preferentially stripped from PCS samples via degassing through water. The air gases N_2+Ar, and O_2 composed the balance gases and represent air contamination plus concentrations in the sediment.

Gas was collected from six pressure core sampler (PCS) cores in NGHP-01-17A. The gas concentration results showed similar trends as the void gas results (tables 7 and 8); however, CO_2 concentrations were approximately 1 order of magnitude lower. The decrease in concentration can be attributed to the sampling method, whereby gas must first pass through the water-filled PCS chamber and into a water-filled inverted graduated cylinder. PCS core gas analysis contained C_2 with concentrations ranging from 60 to 460 ppmv. Ratio values for C_1 to C_2 gases ranged from ~830 to ~13,000 and showed apparent ethane enrichment zones below ~560 mbsf through the BSR depth, corresponding to temperatures ~16°C (fig. 19). The anomalously low C_1/C_2 values reflect the presence of minor concentrations of thermogenically-derived ethane and propane. Ethane enrichment within the zone of gas-hydrate occurrence is likely due to scavenging of ethane into the gas-hydrate structure. Post cruise studies of the isotopic character of hydrocarbon gases will assist in determination of microbial versus thermogenic sources for evaluation of drilling hazards. The C_1/C_2 ratios trend toward "normal" with depth (fig. 19); however, a collective reduction of the C_1/C_2 ratio below 565 mbsf signals the presence of thermogenic hydrocarbon input. Though several samples fell within the 'anomalous' subdivision, potential drilling hazards were not considered critical since propane and heavier hydrocarbons did not exhibit a comparable increase in magnitude.

Microbiology

Hole NGHP-01-17A

Analysis of all microbiological samples will be shore-based. Seventy-three samples were collected for cell enumeration (CEL), 71 for hydrogenase activity analysis (SPH), 24 samples for detailed microbiological studies (MAF, MAG, MAR), and

Table 6. Headspace gas composition for Site NGHP-01-17.—Continued

Sample	O_2	N2+Ar	H_2S	C1	C1	CO_2	CO_2	C_1/CO_2
		(ppmv)		(mL/L WS)	(mM PW)	(mL/L WS)	(mM PW)	
17A-68X4-57-62	153,500	737,800	nd	54,200	3.8	321,200	22.6	0.2
17A-68X5-75-80	153,400	713,200	nd	32,100	2.3	266,500	19.2	0.1
17A-69X4-75-80	129,600	744,900	nd	22,200	1.4	104,000	6.4	0.2
17A-69X6-50-55	92,600	796,000	nd	42,100	2.7	302,000	19.3	0.1
17A-72X2-0-5	147,100	718,200	nd	43,200	3.0	116,900	8.2	0.4
17A-72X3-20-25	152,000	740,200	nd	29,400	2.0	65,500	4.4	0.5
17A-73X3-65-70	171,100	742,200	nd	34,500	2.3	101,500	6.8	0.3
17A-74X2-75-80	152,200	711,900	nd	29,100	1.9	131,100	8.6	0.2
17A-74X3-115-120	158,600	745,600	nd	36,000	2.7	136,500	10.1	0.3
17A-75X2-75-80	167,800	725,300	nd	39,700	2.5	153,700	9.5	0.3
17A-76X2-42-47	150,100	738,000	nd	48,100	3.2	127,200	8.6	0.4
17A-77X3-75-80	155,600	763,800	nd	49,800	3.6	160,600	11.5	0.3
17A-78X3-75-80	154,600	758,300	nd	67,600	4.9	182,600	13.3	0.4
17A-79X4-75-80	92,100	797,200	nd	39,300	3.0	210,500	16.0	0.2
17A-80X2-70-75	26,800	836,600	nd	44,700	3.4	180,700	13.8	0.2
17A-82X2-0-5	141,300	703,800	nd	86,100	6.4	226,100	16.9	0.4
17A-82X4-75-80	153,500	733,500	nd	64,400	4.0	242,100	15.1	0.3
17A-83X2-17-22	160,500	710,200	nd	71,200	4.8	301,400	20.1	0.2

Notes: nd = not detected. WS = Wet sediment. PW = porewater. Approximate detection limits are about 15 ppmv for methane, 30 ppmv for ethane, 50 ppmv for propane, and 20 ppmv for hydrogen sulfide.

15 samples for background section (MBF, MBG, MBR) (table 9). Additional microbiological samples were taken (Lab code JUD, 73 samples; Lab code JAN, 71 samples).

Physical Properties

Whole-round cores at NGHP Expedition 01, Site 17 were imaged using an IR camera on the catwalk to determine the location of temperature anomalies on the surface of core liners and enable sections containing potential gas hydrate to be quickly removed, preserved, and studied. After IR imaging was finished, nondestructive measurements were conducted on temperature-equilibrated whole-round core sections with the MSCL. Thermal conductivity measurements were also conducted on whole-round cores. Various tests were performed on split cores including: electrical resistivity by use of a Wenner array, *P*-wave velocity by inserted spades, and shear strength by mini-vane, Torvane, and Pocket Penetrometer. Core subsamples were placed in 10-mL beakers and dried at 105 °C for at least 24 hr to determine water content. Subsequently, the dried samples were analyzed for grain density using gas pycnometers and other sediment parameters were then calculated. See the "Physical Properties" section of the "Methods" chapter for more details.

The physical properties program at Site NGHP-01-17A focused primarily on Hole NGHP-01-17A located in about 1325 m of water. The borehole was drilled about 55 km off the east coast of Little Andaman Island at the southern end of the Great Andaman uplifted accretionary island complex. Hole NGHP-01-17A was continuously cored to 691.6 mbsf and had an overall core recovery of 81.5 percent. IR anomalies indicative of gas hydrate were present from approximately 224 to 596 mbsf. Gas hydrate probably existed throughout the section in low concentrations but was more prevalent in volcanic ash layers.

Infrared Imaging

Environmental Conditions

The catwalk environment was monitored during the entire drilling operation at Site NGHP-01-17. Temperature on the catwalk was ~29 °C, ranging from 27 to 31 °C during the drilling operation (fig. 20). There was one downward spike to 26 °C during a rainstorm mid-day on July 26. Relative humidity ranged from 72 to 84 percent (fig. 20), which is consistent with a marine environmental setting of the Andaman Sea. During the last two days of drilling, the diurnal temperature and humidity variation was damped with temperature slightly lower and humidity slightly higher than the earlier average. No adverse environmental conditions such as thunderstorms, rough seas, lightning, or high winds, persisted during drilling operations at this site. Occasional rain squalls occurred, typically lasting less than 30 min, but none of the changes are expected to have a major impact on the IR images, particularly not on the DT's estimated from IR temperature data.

Infrared Images

All APC and XCB cores from Site NGHP-01-17 were systematically scanned upon arrival on the catwalk using the track-mounted IR camera described in the "Physical Properties" section of the "Methods" chapter. IR anomalies, commonly referred to as "cold spots," indicate gas-hydrate dissociation during core recovery, which subsequently provides guidance to catwalk sampling. Summary digital maps of the scans of all cores are available on the data DVD that accompanies this report and listings of the image files are presented in tables 10 and 11. Temperature arrays in text-formatted files were exported from the IR camera software and then concatenated for each core. The

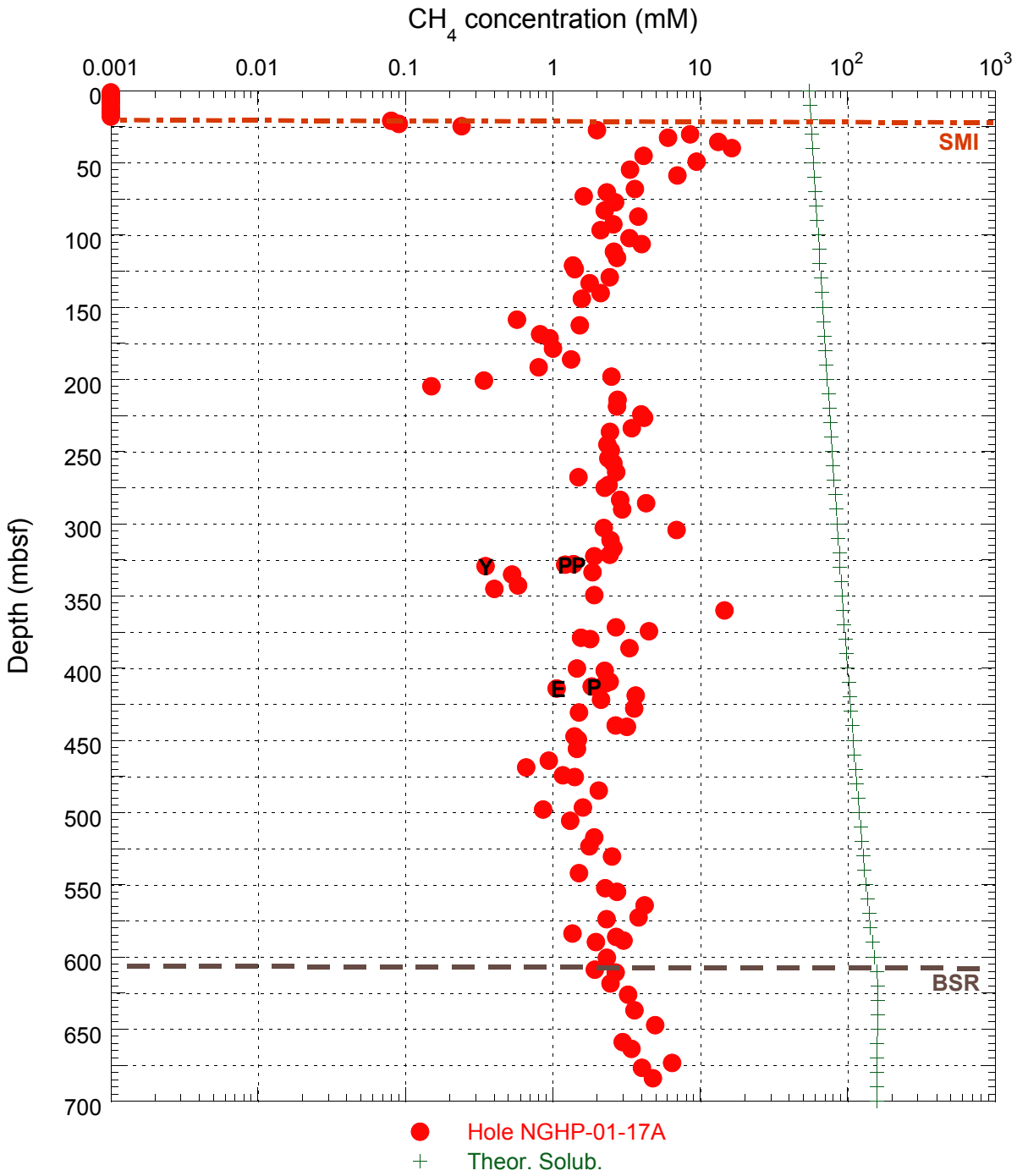


Figure 16. Plot of headspace methane gas concentration (mM) with depth for Hole NGHP-01-17A. Note the apparent peak in methane below the SMI, from 210–310 mbsf, and from 360 mbsf through the BSR. Text inside a symbol denotes special coring tool (E, HRC; P, PCS; Y, FPC). Theoretical solubility of methane calculated using the Duan and others (1992) and Xu (2002, 2004) methodologies. [SMI, sulfate-methane interface; mbsf, meters below sea floor; BSR, bottom-simulating reflector]

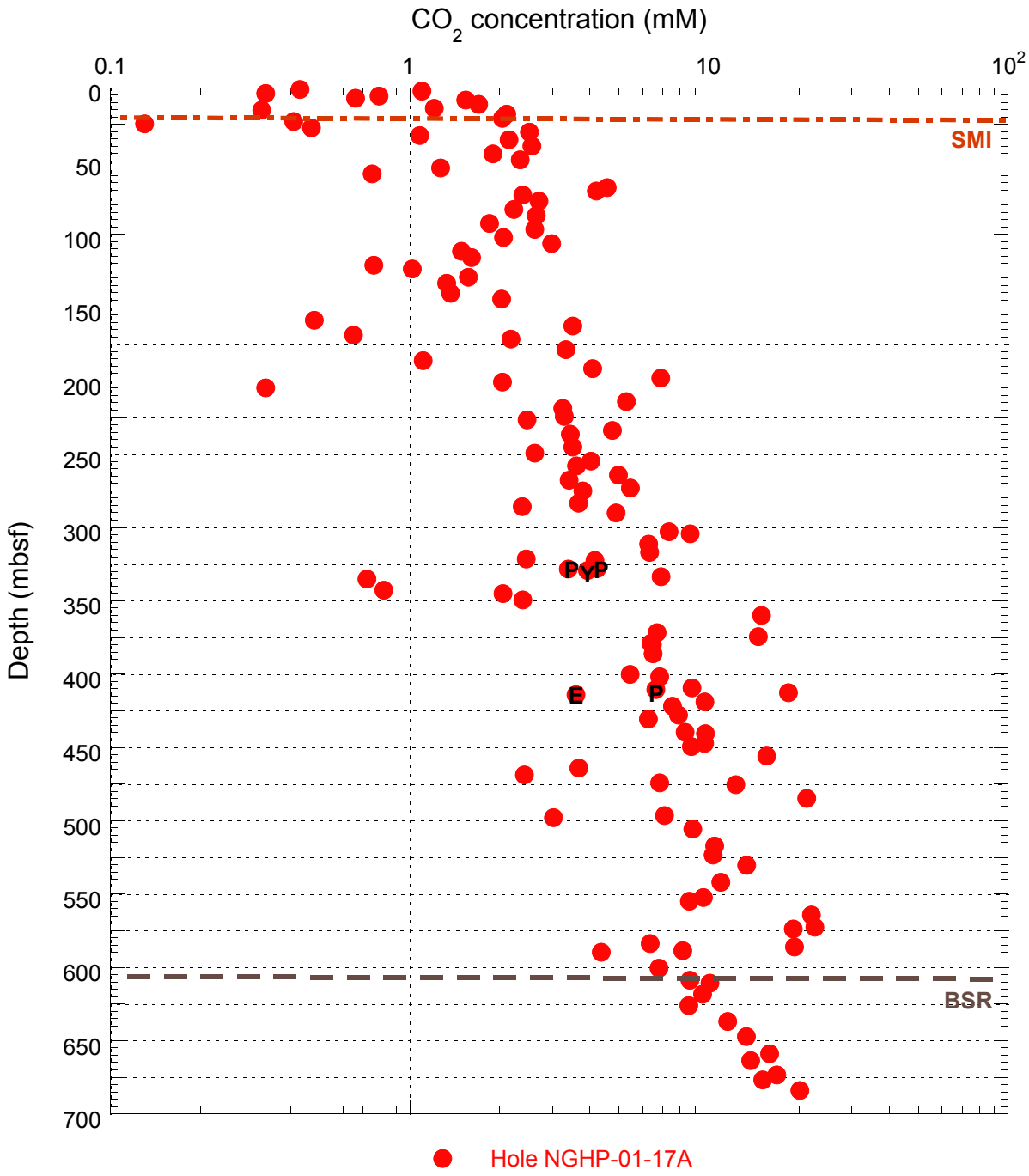


Figure 17. Plot of headspace carbon dioxide gas concentration (mM) with depth for Hole NGHP-01-17A. Note the increasing trend in data and high degree of variation between samples with depth at this site. Text inside a symbol denotes special coring tool (E, HRC; P, PCS; Y, FPC).

Table 7. Void gas composition for Site NGHP-01-17.

Sample	Site	Hole	Core	Section	Interval (cm)	Sample depth (mbsf)	CO_2	C_1	C_2	C_3	O_2	N_2+Ar	H_2S	C_1/CO_2	C_1/C_2
							(ppmv) normalized to nitrogen+argon								
17A-6H1-123	17	A	6	1	123	43.73	7,800	948,000	10	nd	5,100	39,100	nd	120	94,800
17A-6H2-76	17	A	6	2	76	44.7	5,500	800,400	80	nd	32,700	161,200	nd	150	10,000
17A-7H1-1	17	A	7	1	1	52.01	5,400	739,500	80	nd	22,700	232,300	nd	140	9,200
17A-7H1-101	17	A	7	1	101	53.01	4,900	876,300	90	nd	8,300	110,400	nd	180	9,700
17A-8H1-56	17	A	8	1	56	62.06	8,800	958,400	100	nd	3,600	29,000	nd	110	9,600
17A-8H7-65	17	A	8	7	65	70.65	9,100	742,800	80	nd	47,600	200,500	nd	80	9,300
17A-9H1-25	17	A	9	1	25	71.25	9,600	962,000	100	nd	6,100	22,200	nd	100	9,600
17A-9H7-5	17	A	9	7	5	79.65	5,600	980,600	80	nd	1,900	11,700	nd	180	12,300
17A-10H1-85	17	A	10	1	85	81.35	6,100	976,700	90	nd	2,200	15,000	nd	160	10,900
17A-11H3-41	17	A	11	3	41	93.41	1,600	986,100	90	nd	1,700	10,500	nd	620	11,000
17A-12H2-6	17	A	12	2	6	101.06	3,900	986,500	90	nd	1,000	8,500	nd	250	11,000
17A-13H2-1	17	A	13	2	1	110.51	7,500	979,700	100	nd	1,200	11,500	nd	130	9,800
17A-14X3-41	17	A	14	3	41	121.91	6,200	986,000	110	nd	1,200	6,500	nd	160	9,000
17A-14X5-26	17	A	14	5	26	124.76	6,500	986,500	90	nd	1,000	6,000	nd	150	11,000
17A-15X3-57	17	A	15	3	57	130.29	10,900	952,600	120	nd	10,000	26,300	nd	90	7,900
17A-16X2-146	17	A	16	2	146	139.16	6,900	986,300	100	nd	1,000	5,700	nd	140	9,900
17A-16X5-42	17	A	16	5	42	143.96	7,600	976,900	90	nd	3,800	11,600	nd	130	10,900
17A-18X4-17	17	A	18	4	17	160.73	8,000	982,000	90	nd	2,000	7,900	nd	120	10,900
17A-18X6-150	17	A	18	6	150	164.81	9,700	976,900	80	nd	3,100	10,200	nd	100	12,200
17A-19X6-180	17	A	19	6	180	173.53	5,000	871,300	30	nd	27,200	96,500	nd	170	29,000
17A-19X7-28	17	A	19	7	28	174.11	2,700	791,200	20	nd	41,700	164,400	nd	290	39,600
17A-22X2-1	17	A	22	2	1	186.61	3,700	982,100	70	nd	2,500	11,500	nd	270	14,000
17A-22X6-1	17	A	22	6	1	192.4	13,600	976,200	90	nd	2,000	8,100	nd	70	10,800
17A-23X3-118	17	A	23	3	118	198.36	23,200	882,400	110	nd	4,900	89,400	nd	40	8,000
17A-24X1-1	17	A	24	1	1	204.06	4,700	956,300	30	nd	10,200	28,800	nd	200	31,900
17A-24X2-25	17	A	24	2	25	204.3	1,800	426,700	10	nd	125,500	445,900	nd	240	42,700
17A-25X3-20	17	A	25	3	20	216.7	13,900	979,300	100	nd	900	5,700	nd	70	9,800
17A-25X5-38	17	A	25	5	38	219.48	26,400	966,800	100	nd	1,300	5,500	nd	40	9,700
17A-26X3-23	17	A	26	3	23	226.33	28,400	966,700	250	nd	900	3,800	nd	30	3,900
17A-27X2-1	17	A	27	2	1	234.31	11,800	983,200	260	nd	900	3,900	nd	80	3,800
17A-29X3-52	17	A	29	3	52	254.56	16,500	976,900	90	nd	1,000	5,600	nd	60	10,900
17A-29X6-10	17	A	29	6	10	258.64	28,400	965,700	90	nd	900	4,900	nd	30	10,700
17A-30X5-84	17	A	30	5	84	267.12	20,600	973,500	110	nd	900	4,900	nd	50	8,900
17A-31X3-125	17	A	31	3	125	273.58	15,700	978,400	110	nd	800	5,000	nd	60	8,900
17A-31X8-38	17	A	31	8	38	278.33	11,400	981,900	80	nd	1,000	5,600	nd	90	12,300
17A-32X4-1	17	A	32	4	1	284.28	22,400	972,300	160	nd	900	4,200	nd	40	6,100
17A-33X2-1	17	A	33	2	1	290.87	23,600	970,400	80	nd	700	5,200	nd	40	12,100
17A-35X5-52	17	A	35	5	52	314.18	16,200	978,400	150	nd	700	4,500	nd	60	6,500
17A-36X5-49	17	A	36	5	49	323.76	45,500	948,100	60	nd	1,200	5,200	nd	20	15,800
17A-39X5-1	17	A	39	5	1	335.08	36,800	950,900	350	nd	3,300	8,600	nd	30	2,700
17A-40X4-133	17	A	40	4	133	342.17	60,300	925,800	170	nd	3,700	10,100	nd	20	5,400
17A-40X6-4	17	A	40	6	4	343.72	3,600	61,100	nd	nd	189,700	745,600	nd	20	-
17A-41X3-78	17	A	41	3	78	351.08	3,900	208,200	nd	nd	161,700	626,200	nd	50	-
17A-41X5-1	17	A	41	5	1	352.92	15,700	463,800	170	nd	105,500	414,900	nd	30	2,700
17A-41X5-52	17	A	41	5	52	353.43	27,000	894,100	310	nd	20,100	58,600	nd	30	2,900
17A-42X2-37	17	A	42	2	37	358.16	33,000	920,500	70	nd	12,800	33,700	nd	30	13,200
17A-42X4-106	17	A	42	4	106	361.85	7,100	143,000	nd	nd	173,300	676,600	nd	20	-
17A-42X5-1	17	A	42	5	1	362.3	98,200	871,700	100	nd	8,700	21,300	nd	10	8,700
17A-43X3-135	17	A	43	3	135	370.05	60,000	928,800	150	nd	2,900	8,100	nd	20	6,200
17A-43X4-77	17	A	43	4	77	370.97	19,500	470,400	140	nd	103,600	406,400	nd	20	3,400
17A-43X7-31	17	A	43	7	31	373.44	119,000	831,100	110	nd	13,700	36,100	nd	10	7,600
17A-44X4-50	17	A	44	4	50	379.76	71,500	921,000	180	nd	1,800	5,600	nd	10	5,100
17A-44X5-1	17	A	44	5	1	380.77	59,700	930,500	160	nd	2,500	7,200	nd	20	5,800
17A-46X3-1	17	A	46	3	1	398.15	67,200	886,600	140	nd	12,600	33,400	nd	10	6,300
17A-46X3-143	17	A	46	3	143	399.57	65,800	929,200	150	nd	900	4,000	nd	10	6,200
17A-47X2-55	17	A	47	2	55	407.15	23,100	973,200	420	nd	800	2,400	nd	40	2,300
17A-50X4-33	17	A	50	4	33	418.53	108,200	881,900	110	nd	1,300	8,500	nd	10	8,000
17A-50X7-1	17	A	50	7	1	421.37	52,600	939,500	160	nd	1,100	6,600	nd	20	5,900
17A-51X1-50	17	A	51	1	50	424.8	68,400	900,700	140	nd	8,800	22,000	nd	10	6,400
17A-52X3-99	17	A	52	3	99	437.99	119,400	876,000	170	nd	1,000	3,500	nd	10	5,200
17A-53X3-41	17	A	53	3	41	445.76	95,100	665,500	220	nd	48,900	190,200	nd	10	3,000
17A-53X5-57	17	A	53	5	57	448.75	138,600	767,700	140	nd	22,900	70,700	nd	10	5,500
17A-54X2-94	17	A	54	2	94	454.93	3,200	10,500	nd	nd	199,500	786,900	nd	0	-

Table 7. Void gas composition for Site NGHP-01-17.—Continued

Sample	Site	Hole	Core	Section	Interval (cm)	Sample depth (mbsf)	CO_2	C_1	C_2	C_3	O_2	N_2+Ar	H_2S	C_1/CO_2	C_1/C_2
							(ppmv) normalized to nitrogen+argon								
17A-55X5-5	17	A	55	5	5	466.44	131,100	858,400	280	nd	3,000	7,200	nd	10	3,100
17A-56X3-26	17	A	56	3	26	474.95	133,700	806,600	120	nd	16,000	43,600	nd	10	6,700
17A-57X3-146	17	A	57	3	146	485.64	93,600	725,400	180	nd	37,900	142,900	nd	10	4,000
17A-58X1-122	17	A	58	1	122	493.22	136,500	846,000	230	nd	5,100	12,200	nd	10	3,700
17A-61X3-35	17	A	61	3	35	503.83	34,300	958,500	200	nd	1,100	5,800	nd	30	4,800
17A-62X4-35	17	A	62	4	35	515.46	116,300	875,400	150	nd	2,100	6,100	nd	10	5,800
17A-63X5-86	17	A	63	5	86	525.91	70,200	925,500	220	nd	700	3,300	nd	10	4,200
17A-64X2-1	17	A	64	2	1	531.38	58,200	936,900	190	nd	800	3,900	nd	20	4,900
17A-66X6-1	17	A	66	6	1	555.43	54,900	941,000	290	nd	600	3,200	nd	20	3,200
17A-67X5-1	17	A	67	5	1	562.65	62,100	933,200	860	30	1,200	2,700	nd	20	1,100
17A-68X3-131	17	A	68	3	131	572.17	67,700	912,400	630	nd	5,800	13,400	nd	10	1,400
17A-68X5-9	17	A	68	5	9	573.18	18,600	159,300	180	nd	166,500	655,400	nd	10	900
17A-69X3-23	17	A	69	3	23	581.93	82,100	894,300	730	nd	5,800	17,000	nd	10	1,200
17A-69X4-89	17	A	69	4	89	584.09	37,800	163,600	100	nd	160,200	638,300	nd	0	1,600
17A-72X3-68	17	A	72	3	68	590.29	81,700	902,400	1,640	70	4,300	9,900	nd	10	600
17A-73X3-1	17	A	73	3	1	600.01	28,400	966,200	1,250	60	700	3,300	nd	30	800
17A-74X3-118	17	A	74	3	118	610.88	76,000	918,100	1,150	110	1,000	3,600	nd	10	800
17A-75X2-1	17	A	75	2	1	617.78	33,000	961,800	1,010	90	700	3,400	nd	30	1,000
17A-76X4-1	17	A	76	4	1	628.01	51,300	942,300	1,040	170	1,000	4,300	nd	20	900
17A-77X2-1	17	A	77	2	1	635.25	49,900	944,800	1,160	140	700	3,400	nd	20	800
17A-78X2-1	17	A	78	2	1	645.22	36,300	958,500	890	90	700	3,600	nd	30	1,100
17A-79X2-73	17	A	79	2	73	656.03	76,400	915,200	1,120	130	1,800	5,300	nd	10	800
17A-80X4-1	17	A	80	4	1	665.43	38,300	915,500	580	60	12,800	32,800	nd	20	1,600
17A-82X4-1	17	A	82	4	1	676.18	90,400	901,800	1,170	270	1,300	5,100	nd	10	800
17A-82X5-25	17	A	82	5	25	677.92	36,100	953,200	1,130	110	2,200	7,300	nd	30	800
17A-83X2-63	17	A	83	2	63	684.53	55,400	309,200	490	120	133,900	501,000	nd	10	600

Notes: nd= not detected. nr = not recorded. Approximate detection limits are about 15 ppmv for methane, 30 ppmv for ethane, 50 ppmv for propane, and 20 ppmv for hydrogen sulfide.

arrays were then further concatenated for all cores available in a given borehole. Down-core temperatures were averaged for each pixel row in the array, excluding pixels ~1 cm from the edge of the image and 2 cm along the midline of the image. Exclusion of these pixels minimized the effects caused by major thermal artifacts in the images. This processing enabled us to measure the average amplitude of the cold anomalies and identify warm anomalies due to voids from the background temperature field.

IR track imaging at Site NGHP-01-17A consisted of 80 scans for a total scanned core length of ~640 m. The complete set of IR images collected for Hole NGHP-01-17A is presented in figure 21 along with the corresponding down-core temperatures. The core temperature extracted from the IR images for Hole NGHP-01-17A ranged from a high of ~26 °C on core liner in the lower third of the hole, to a low of ~12 °C at two locations where the strongest IR anomalies occurred (~340 and 345 mbsf). As shown in figure 21, IR anomalies occur between ~224 mbsf and ~596 mbsf. Cool zones above ~224 mbsf probably represent cooler cores near the seafloor or zones of drillwater intrusion during drilling. The characteristics of these cool zones are not typical of those associated with gas hydrate. The deepest strong IR anomaly occurs at ~588 mbsf. Minor IR anomalies occurred below the BSR (~609 mbsf, estimated based on seismic data), but these are attributed to either adiabatic gas expansion or drilling fluid impacts. A single anomaly at 673.3 mbsf was sampled for interstitial water and showed no chlorinity anomaly.

Also notice in figures 21A and 21B that strong artificial thermal gradients appear in many APC and XCB cores. This trend is more pronounced between 50 and 120 mbsf, perhaps related to uniform lithology and high core recovery, than at other depths in this hole. Cores that are warmer at the top is the opposite trend from that observed in cores from more temperate regions such as Hydrate Ridge or offshore Vancouver Island. At these sites, the temperatures were typically cooler at the top, warming toward the bottom, not warmer at the top as is characteristic of NGHP Expedition 01 cores. We attribute this difference to the warm surface waters (~29 °C) at all sites drilled on NGHP Expedition 01. Near-surface seawater is used for drilling fluid and likely does not equilibrate with deeper water as it travels down the drill pipe. For sites drilled on NGHP Expedition 01, this means that the upper part of the cores are exposed to relatively warm water for a longer period of time after it enters the core barrel than the lower parts of the core. For sites drilled at Hydrate Ridge and offshore Vancouver Island, the near-surface seawater is much cooler, on the order of 15 °C. Consequently, the upper parts of a core are cooled preferentially relative to the lower parts, in direct relation to their time of thermal exposure to drilling fluids, hence the observed gradient. Note that absolute temperatures are not critical. It is the relative temperatures of drilling fluid and core that drive the development of the temperature gradient that persist on the catwalk where IR measurements are made. Cores that do not exhibit a strong thermal gradient can be explained by slower drilling or retrieval (fig. 21A, 180 to 240 mbsf). Post-cruise data analysis

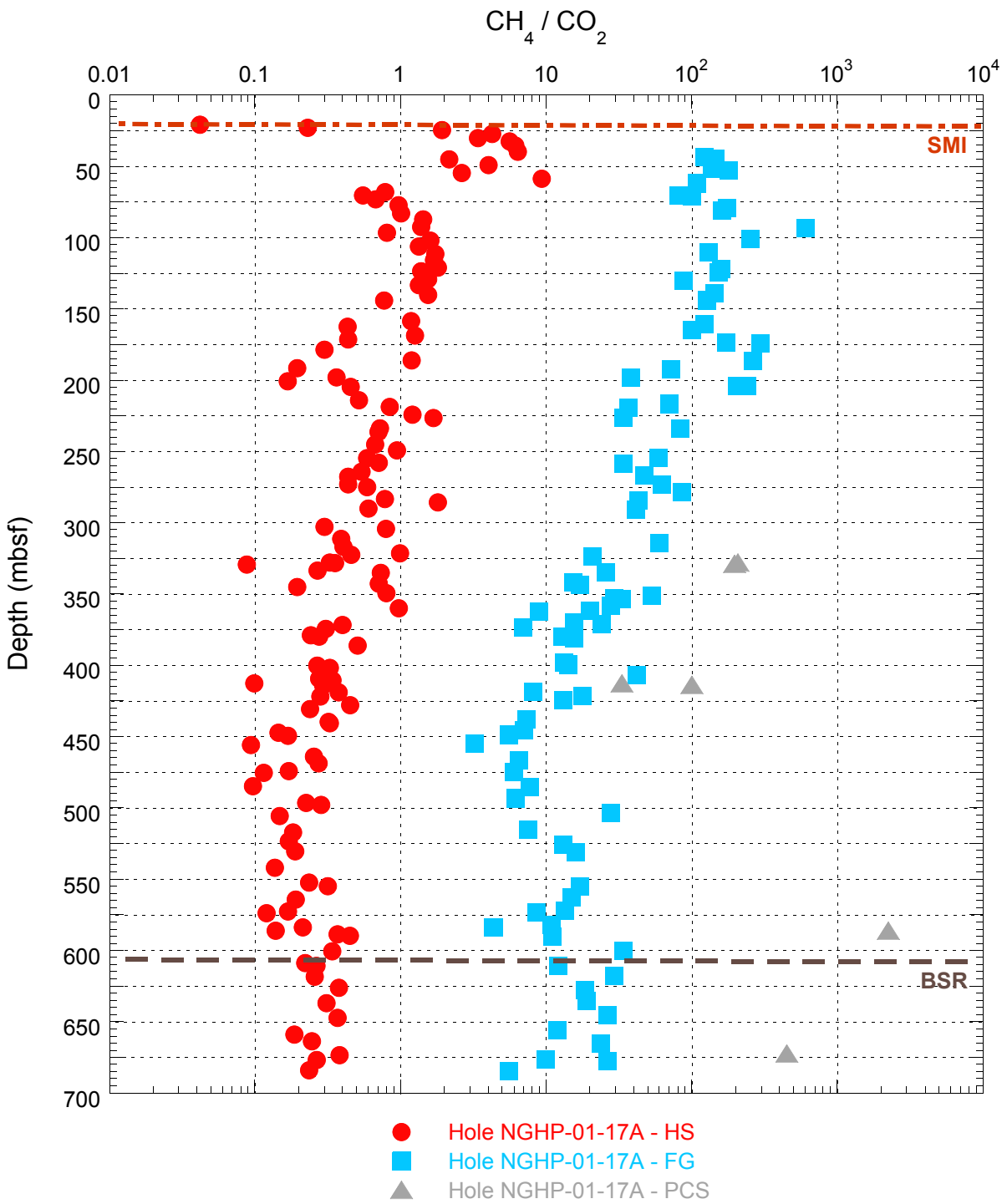


Figure 18. Plot of headspace and free/void gas methane to carbon dioxide gas ratio with depth for Hole NGHP-01-17A. Note the spikes in magnitude are a general indicator of strata with higher concentrations of methane, perhaps indicating elevated levels of gas hydrate.

Table 8. Pressure Core Sampler gas composition for Site NGHP-01-17.

Sample	Site	Hole	Core	Section	Sample depth (mbsf)	Time	Gas vol. (ml)	CO_2	C_1	C_2	C_3	O_2	N_2+Ar	H_2S	C_1/CO_2	C_1/C_2
								(ppmv) normalized to nitrogen+argon								
17A-37P-t1	17	A	37	P	328	1	-	2,900	944,000	80	nd	11,400	41,600	nd	300	11,800
17A-37P-t2	17	A	37	P	328	2	-	11,300	964,900	80	nd	3,300	20,400	nd	100	12,100
17A-38Y-t1	17	A	38	Y	329	1	-	4,100	813,800	70	nd	27,600	154,400	nd	200	11,600
17A-48P-t1	17	A	48	P	412.7	1	-	28,800	956,000	130	nd	3,000	12,100	nd	0	7,400
17A-49E-t1	17	A	49	E	413.7	1	-	8,800	886,600	70	nd	21,100	83,400	nd	100	12,700
17A-70P-t1	17	A	70	P	586.3	1	-	300	736,300	460	nd	12,900	250,000	nd	2,500	1,600
17A-81E-t1	17	A	81	E	672.3	1	-	200	66,700	60	nd	103,700	829,300	nd	300	1,100
17A-81E-t2	17	A	81	E	672.3	2	-	200	119,700	140	nd	100,600	779,400	nd	600	900
17A-81E-t3	17	A	81	E	672.3	3	-	500	364,800	440	50	269,500	364,800	nd	700	800
17A-81E-t4	17	A	81	E	672.3	4	-	1,800	361,600	430	nd	274,500	361,600	nd	200	800

Notes: nd = not detected. Approximate detection limits are about 15 ppmv for methane, 30 ppmv for ethane, 50 ppmv for propane, and 20 ppmv for hydrogen sulfide.

will include an assessment of the drilling and retrieval times of individual cores to determine if differences in down-core thermal gradients are consistent with available drilling information. The occurrence of gas hydrate also impacts the thermal gradient of cores and is alternate explanation for cores that do not exhibit a consistent artificial thermal gradient.

IR anomalies occurred preferentially in ash layers, but also occurred in sediment without ash and, in at least one case, in sediment adjacent to ash (NGHP-01-17A-53X-6, 47–62, 449.7 mbsf). Importantly, observation of cores exhibiting IR anomalies indicates that all gas hydrate in Hole NGHP-01-17A occur as pore-filling hydrate. No lenses or nodules of gas hydrate were observed, nor were there significant occurrences of moussey sediment (see "Lithostratigraphy") that would indicate large concentrations of gas hydrate as discrete mesoscopic features.

IR images of the ends of core sections were acquired with a hand-held IR camera on the catwalk during core sectioning. Figure 22 shows two section-end IR images, one away from an IR anomaly (NGHP-01-17A-66X-5 ~557 mbsf), and one adjacent to an IR anomaly (NGHP-01-17A-67X-6 ~569 mbsf). Temperature profiles extracted from the core-end images show the expected colder temperature of the core adjacent to the IR anomaly and a relatively flat temperature profile indicative of a thermal perturbation within the core as opposed to conductive thermal equilibration (see fig. 17 in "Site NGHP-01-16" or a typical conductive equilibration profile). Note that while the core away from any obvious IR anomalies is warmer than the one near an anomaly, its thermal profile also is flat, suggesting that minor amounts (background) of gas hydrate may have been present to modify the profile. Core end thermal images and associated thermal profiles will be analyzed more extensively post-cruise.

In addition to the IR core end images, a similar technique was used to identify cold anomalies in the sediment selected for interstitial water samples. Whole-round samples were removed from the core on the catwalk and taken to the chemical laboratory for extrusion from the core liner and immediate interstitial water sampling. After extruding the sediment from the liner or opening a cut liner, IR imaging with a hand held camera was used to identify gas hydrate or "cold spots" in the sediment and provide guidance for detailed sediment sampling. Figures 23, 24, 25, and 26 provide an example of IR imaging performed on Core NGHP-01-17A-53X-6, 47–62. The temperature profile and the IR image observed on the catwalk for this sample are shown in figure 23 . The difference in time from the catwalk scan is ~5.3 °C. Figures 24A through 24D show IR images with progressive dissection of the sample, starting with the catwalk image and a DT (4.8 °C) based on a single line of pixels instead of the averaged values extracted from the catwalk IR images (fig. 24A). The IW sample with split liner still in place and IR imaged in the geochemistry lab shows a DT of 8.5 °C (fig. 24B). An increasing DT shows that during the time between catwalk IR imaging and initial IR imaging in the core lab (~10 to 15 min), additional gas-hydrate dissociation occurred, indicating that gas hydrate was present at the time the cores were scanned on the catwalk. Samples placed in LN_2 on the catwalk thus have a significant chance of containing preserved gas hydrate. Based on the apparent absence of mesoscale gas-hydrate lenses or fracture fillings, these samples may contain exclusively residual pore-filling gas hydrate. Figure 24C and 24D show the core after the liner is removed and after the core is split open, respectively. The interior of this sample is as cold as –3.9 °C. Co-registration of IR and visible images (fig. 25) enables the determination of which specific lithologies and parts of the core contained gas hydrate. In the case of IW sample NGHP-01-17A-53X-6, 47–62, gas hydrate is restricted to the lower two-thirds of the sample and occurs in both a white volcanic ash and in adjacent sediment (fig. 26). It does not, however, occur throughout the ash layer. Instead, the gas hydrate is restricted to one side of the ash, clearly showing why the original IR anomaly in the catwalk scans was localized on one side of the core liner. Chlorinity values for three subsampled areas of the core (see "Inorganic Geochemistry") show that the upper, warm end of the core (to the right in fig. 26) has near background chlorinity (512 mM), the cold sediment layer adjacent to the ash layer has intermediate chlorinity (273 mM) and the ash layer has low chlorinity (126 mM). These results precisely match the IR data and indicate that greater concentration of gas hydrate occurs in at least part of the ash than occurs in adjacent sediment. This observation is consistent with the porosities for ash and sediment discussed later in this chapter.

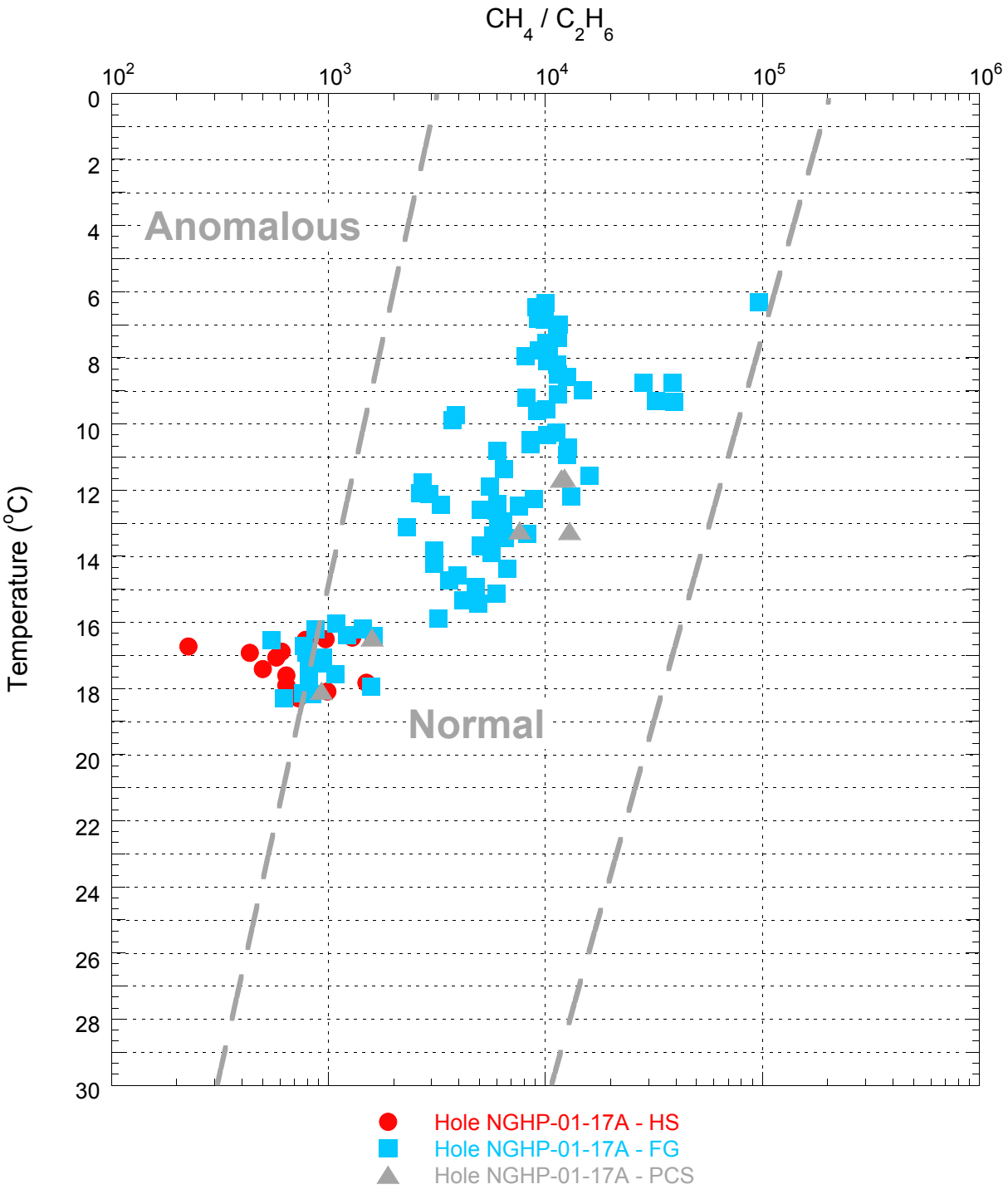


Figure 19. Plot of free gas and PCS gas methane to ethane ratio with temperature at increasing depths for Hole NGHP-01-17A. Note the apparent enrichment of ethane leading to borderline anomalous hydrocarbon occurrence. However, levels appear to trend toward "normal" with decreasing depth/temperature. The elevated levels likely represent ethane enrichment due to gas hydrate and(or) minor thermogenic gas migration. [PCS, pressure core sampler]

Table 9. List of microbiological samples taken for Site NGHP-01-07. (To view the complete table, please see the ASCII files.)

Sample reference						Comments
Core, section	Sample code	Top (cm)	Bottom (cm)	Depth (mbsf)	Volume (cc)	
NGHP-01-17A						
1H-2	CEL	95	100	2.45	5	
2H-5	CEL	95	100	11.45	5	
3H-5	CEL	90	95	20.9	5	
4H-5	CEL	90	95	30.4	5	
5H-5	CEL	90	95	39.9	5	
6H-5	CEL	90	95	49.34	5	
7H-5	CEL	90	95	58.9	5	
8H-5	CEL	85	90	68.35	5	
9H-5	CEL	85	90	77.45	5	
10H-5	CEL	85	90	87.35	5	
11H-5	CEL	85	90	96.85	5	
12H-5	CEL	85	90	106.35	5	
13H-5	CEL	85	90	115.85	5	
14X-4	CEL	80	85	123.8	5	
15X-5	CEL	80	85	133.52	5	
16X-5	CEL	65	70	144.19	5	
18X-5	CEL	55	60	162.61	5	
19X-5	CEL	80	85	171.63	5	
21X-2	CEL	75	80	178.75	5	
22X-5	CEL	54	59	191.64	5	
23X-5	CEL	75	80	200.83	5	
24X-2	CEL	75	80	204.8	62	WR TAKEN
25X-1	CEL	75	80	214.25	5	
26X-3	CEL	61	66	226.71	5	
27X-3	CEL	55	60	236.35	5	
28X-5	CEL	75	80	249.25	5	
29X-3	CEL	75	80	254.79	5	
30X-3	CEL	75	80	264.35	5	
31X-3	CEL	75	80	273.08	5	
32X-3	CEL	62	67	283.52	5	
33X-1	CEL	51	56	290.11	5	
34X-3	CEL	75	80	302.95	5	
35X-3	CEL	39	44	311.41	5	
36X-4	CEL	68	73	322.52	5	
39X-3	CEL	75	80	333.75	5	
40X-5	CEL	65	70	342.93	5	
41X-2	CEL	75	80	349.55	5	
42X-3	CEL	75	80	360.04	5	
43X-8	CEL	65	70	374.52	5	
44X-4	CEL	75	80	380.01	5	
45X-1	CEL	50	55	386.2	5	
46X-4	CEL	75	80	400.39	5	
47X-4	CEL	68	73	409.48	62	WR TAKEN
47X-5	CEL	75	80	410.58	5	
50X-4	CEL	75	80	418.95	5	
51X-5	CEL	75	80	430.67	5	
52X-6	CEL	75	80	440.82	5	
53X-4	CEL	58	63	447.43	5	
54X-3	CEL	71	76	455.99	5	
55X-7	CEL	41	46	468.87	5	
56X-3	CEL	75	80	475.44	5	
57X-3	CEL	75	80	484.93	5	
58X-5	CEL	75	80	497.98	5	
61X-4	CEL	75	80	505.73	5	
62X-5	CEL	75	80	517.36	5	
63X-3	CEL	25	30	523.48	5	
64X-1	CEL	32	37	530.62	5	
65X-2	CEL	65	70	542.15	5	
66X-3	CEL	36	41	552.36	5	

Table 9. List of microbiological samples taken for Site NGHP-01-07. (To view the complete table, please see the ASCII files.)—Continued

Sample reference						Comments
Core, section	Sample code	Top (cm)	Bottom (cm)	Depth (mbsf)	Volume (cc)	
NGHP-01-17A—Continued						
67X-6	CEL	22	27	564.36	5	
68X-5	CEL	75	80	573.84	5	
69X-4	CEL	75	80	583.95	5	
72X-3	CEL	20	25	589.81	5	
73X-3	CEL	65	70	600.65	5	
74X-2	CEL	75	80	608.95	5	
75X-2	CEL	75	80	618.52	5	
76X-2	CEL	42	47	626.2	5	
77X-3	CEL	75	80	637.03	5	
78X-3	CEL	75	80	647.46	5	
79X-4	CEL	75	80	659.05	5	
80X-2	CEL	70	75	663.71	5	
82X-4	CEL	75	80	676.92	5	
83X-2	CEL	17	22	684.07	5	
1H-2	JAN	105	110	2.55	187	
2H-5	JAN	105	110	11.55	187	
3H-5	JAN	100	105	21	187	
4H-5	JAN	100	105	30.5	187	
5H-5	JAN	100	105	40	187	
6H-5	JAN	100	105	49.44	187	
7H-5	JAN	100	105	59	187	
8H-5	JAN	95	100	68.45	187	
9H-5	JAN	95	100	77.55	187	
10H-5	JAN	95	100	87.45	187	
11H-5	JAN	95	100	96.95	187	
12H-5	JAN	95	100	106.45	187	
13H-5	JAN	95	100	115.95	187	
14X-4	JAN	90	95	123.9	187	
15X-5	JAN	90	95	133.62	187	
16X-5	JAN	75	80	144.29	187	
18X-5	JAN	65	70	162.71	187	
19X-5	JAN	90	95	171.73	187	
21X-2	JAN	85	90	178.85	187	
22X-5	JAN	64	69	191.74	187	
23X-5	JAN	85	90	200.93	187	
24X-2	JAN	85	90	204.9	187	
25X-1	JAN	85	90	214.35	187	
26X-3	JAN	71	76	226.81	187	
27X-3	JAN	65	70	236.45	187	
28X-5	JAN	85	90	249.35	187	
29X-3	JAN	85	90	254.89	187	
30X-3	JAN	85	90	264.45	187	
31X-3	JAN	85	90	273.18	187	
32X-3	JAN	72	77	283.62	187	
33X-1	JAN	61	66	290.21	187	
34X-3	JAN	85	90	303.05	187	
34X-5	JAN	140	141	306.24	37	
35X-3	JAN	49	54	311.51	187	
36X-4	JAN	78	83	322.62	187	
39X-3	JAN	85	90	333.85	187	
40X-5	JAN	75	80	343.03	187	
41X-2	JAN	85	90	349.65	187	
42X-3	JAN	85	90	360.14	187	
43X-8	JAN	75	80	374.62	187	
44X-4	JAN	85	90	380.11	187	
46X-4	JAN	85	90	400.49	187	
47X-5	JAN	85	90	410.68	187	
50X-4	JAN	85	90	419.05	187	
51X-5	JAN	85	90	430.77	187	

Table 9. List of microbiological samples taken for Site NGHP-01-07. (To view the complete table, please see the ASCII files.)—Continued

Sample reference						Comments
Core, section	Sample code	Top (cm)	Bottom (cm)	Depth (mbsf)	Volume (cc)	
NGHP-01-17A—Continued						
52X-6	JAN	85	90	440.92	187	
53X-4	JAN	68	73	447.53	187	
54X-3	JAN	81	86	456.09	187	
55X-6	JAN	65	70	468.11	187	
56X-3	JAN	85	90	475.54	187	
57X-3	JAN	85	90	485.03	187	
58X-5	JAN	85	90	498.08	187	
61X-4	JAN	85	90	505.83	187	
62X-5	JAN	85	90	517.46	187	
63X-3	JAN	35	40	523.58	187	
64X-1	JAN	42	47	530.72	187	
65X-2	JAN	75	80	542.25	187	
66X-3	JAN	46	51	552.46	187	
67X-6	JAN	32	37	564.46	187	
68X-5	JAN	85	90	573.94	187	
69X-4	JAN	85	90	584.05	187	
72X-3	JAN	30	35	589.91	187	
73X-3	JAN	75	80	600.75	187	
74X-2	JAN	85	90	609.05	187	
75X-2	JAN	85	90	618.62	187	
76X-2	JAN	52	57	626.3	187	
77X-3	JAN	85	90	637.13	187	
78X-3	JAN	85	90	647.56	187	
79X-4	JAN	85	90	659.15	187	
80X-2	JAN	80	85	663.81	187	
82X-4	JAN	85	90	677.02	187	
1H-2	JUD	120	130	2.7	374	
2H-3	JUD	120	130	8.7	374	
2H-5	JUD	120	130	11.7	374	
3H-3	JUD	115	125	18.15	374	
3H-5	JUD	115	125	21.15	374	
4H-3	JUD	115	125	27.65	374	
4H-5	JUD	115	125	30.65	374	
5H-5	JUD	115	125	40.15	374	
6H-5	JUD	115	125	49.59	374	
7H-5	JUD	115	125	59.15	374	
8H-5	JUD	110	120	68.6	374	
9H-5	JUD	110	120	77.7	374	
10H-5	JUD	110	120	87.6	374	
11H-5	JUD	110	120	97.1	374	
12H-5	JUD	110	120	106.6	374	
13H-5	JUD	110	120	116.1	374	
14X-4	JUD	105	115	124.05	374	
15X-5	JUD	105	115	133.77	374	
16X-5	JUD	90	100	144.44	374	
18X-5	JUD	80	90	162.86	374	
19X-5	JUD	105	115	171.88	374	
21X-2	JUD	100	110	179	374	
22X-5	JUD	79	89	191.89	374	
23X-5	JUD	100	110	201.08	374	
24X-2	JUD	100	110	205.05	374	
25X-1	JUD	100	110	214.5	374	
26X-3	JUD	86	96	226.96	374	
27X-3	JUD	80	90	236.6	374	
28X-5	JUD	100	110	249.5	374	
29X-3	JUD	100	110	255.04	374	
30X-3	JUD	100	110	264.6	374	
31X-3	JUD	100	110	273.33	374	
32X-3	JUD	87	97	283.77	374	

Table 9. List of microbiological samples taken for Site NGHP-01-07. (To view the complete table, please see the ASCII files.)—Continued

Sample reference						Comments
Core, section	Sample code	Top (cm)	Bottom (cm)	Depth (mbsf)	Volume (cc)	
NGHP-01-17A—Continued						
33X-1	JUD	76	86	290.36	374	
34X-3	JUD	100	110	303.2	374	
35X-3	JUD	64	74	311.66	374	
36X-4	JUD	93	103	322.77	374	
39X-3	JUD	100	110	334	374	
40X-5	JUD	90	100	343.18	374	
41X-2	JUD	100	110	349.8	374	
42X-3	JUD	100	110	360.29	374	
43X-8	JUD	90	100	374.77	374	
44X-4	JUD	100	110	380.26	374	
46X-4	JUD	100	110	400.64	374	
47X-5	JUD	100	110	410.83	374	
50X-4	JUD	100	110	419.2	374	
51X-5	JUD	100	110	430.92	374	
52X-6	JUD	100	110	441.07	374	
53X-4	JUD	83	93	447.68	374	
54X-3	JUD	96	106	456.24	374	
55X-6	JUD	80	90	468.26	374	
56X-3	JUD	100	110	475.69	374	
57X-3	JUD	100	110	485.18	374	
58X-5	JUD	100	110	498.23	374	
61X-4	JUD	100	110	505.98	374	
62X-5	JUD	100	110	517.61	374	
63X-3	JUD	50	60	523.73	374	
64X-1	JUD	57	67	530.87	374	
65X-2	JUD	90	100	542.4	374	
66X-3	JUD	61	71	552.61	374	
67X-6	JUD	47	57	564.61	374	
68X-5	JUD	100	110	574.09	374	
69X-4	JUD	100	110	584.2	374	
72X-3	JUD	45	55	590.06	374	
73X-3	JUD	90	100	600.9	374	
74X-2	JUD	100	110	609.2	374	
75X-2	JUD	100	110	618.77	374	
76X-2	JUD	67	77	626.45	374	
77X-3	JUD	100	110	637.28	374	
78X-3	JUD	100	110	647.71	374	
79X-4	JUD	100	110	659.3	374	
80X-2	JUD	95	105	663.96	374	
82X-4	JUD	100	110	677.17	374	
34X-5	MAF	121	131	306.05	374	
43X-6	MAF	35	45	372.38	374	MBIO ANOMALY
47X-3	MAF	100	110	408.6	374	
54X-2	MAF	109	119	455.08	187	MBIO ANOMALY
58X-4	MAF	95	105	496.73	374	
63X-7	MAF	99	107	529.04	299	
72X-1	MAF	78	83	588.58	187	MBIO ANOMALY1
72X-1	MAF	93	98	588.73	187	MBIO ANOMALY2
34X-5	MAG	131	140	306.15	374	
43X-6	MAG	45	55	372.48	374	MBIO ANOMALY
47X-3	MAG	110	120	408.7	374	
54X-2	MAG	119	129	455.18	187	MBIO ANOMALY
58X-4	MAG	105	115	496.83	374	
63X-7	MAG	107	115	529.12	299	
72X-1	MAG	83	88	588.63	187	MBIO ANOMALY1
72X-1	MAG	98	103	588.78	187	MBIO ANOMALY2
34X-5	MAR	111	121	305.95	374	
43X-6	MAR	23	35	372.26	374	MBIO ANOMALY
47X-3	MAR	90	100	408.5	374	

Table 9. List of microbiological samples taken for Site NGHP-01-07. (To view the complete table, please see the ASCII files.)—Continued

Sample reference						Comments
Core, section	Sample code	Top (cm)	Bottom (cm)	Depth (mbsf)	Volume (cc)	
NGHP-01-17A—Continued						
54X-2	MAR	99	109	454.98	187	MBIO ANOMALY
58X-4	MAR	85	95	496.63	374	
63X-7	MAR	91	99	528.96	299	
72X-1	MAR	73	78	588.53	187	MBIO ANOMALY1
72X-1	MAR	88	93	588.68	187	MBIO ANOMALY2
39X-2	MBF	110	120	332.6	374	MBIO BACKGROUND
43X-6	MBF	65	75	372.68	374	MBIO BACKGROUND
52X-1	MBF	130	140	435.3	374	MBIO BACKGROUND
54X-6	MBF	52	62	460.26	374	MBIO BACKGROUND
66X-4	MBF	122	127	554.33	187	MBIO BACKGROUND
39X-2	MBG	120	130	332.7	374	MBIO BACKGROUND
43X-6	MBG	75	85	372.78	374	MBIO BACKGROUND
52X-1	MBG	140	150	435.4	374	MBIO BACKGROUND
54X-6	MBG	62	72	460.36	374	MBIO BACKGROUND
66X-4	MBG	127	132	554.38	187	MBIO BACKGROUND
39X-2	MBR	100	110	332.5	374	MBIO BACKGROUND
43X-6	MBR	55	65	372.58	374	MBIO BACKGROUND
52X-1	MBR	120	130	435.2	374	MBIO BACKGROUND
54X-6	MBR	42	52	460.16	374	MBIO BACKGROUND
66X-4	MBR	117	122	554.28	187	MBIO BACKGROUND
1H-2	SPH	100	105	2.5	187	
2H-5	SPH	100	105	11.5	187	
3H-5	SPH	95	100	20.95	187	
4H-5	SPH	95	100	30.45	187	
5H-5	SPH	95	100	39.95	187	
6H-5	SPH	95	100	49.39	187	
7H-5	SPH	95	100	58.95	187	
8H-5	SPH	90	95	68.4	187	
9H-5	SPH	90	95	77.5	187	
10H-5	SPH	90	95	87.4	187	
11H-5	SPH	90	95	96.9	187	
12H-5	SPH	90	95	106.4	187	
13H-5	SPH	90	95	115.9	187	
14X-4	SPH	85	90	123.85	187	
15X-5	SPH	85	90	133.57	187	
16X-5	SPH	70	75	144.24	187	
18X-5	SPH	60	65	162.66	187	
19X-5	SPH	85	90	171.68	187	
21X-2	SPH	80	85	178.8	187	
22X-5	SPH	59	64	191.69	187	
23X-5	SPH	80	85	200.88	187	
24X-2	SPH	80	85	204.85	187	
25X-1	SPH	80	85	214.3	187	
26X-3	SPH	66	71	226.76	187	
27X-3	SPH	60	65	236.4	187	
28X-5	SPH	80	85	249.3	187	
29X-3	SPH	80	85	254.84	187	
30X-3	SPH	80	85	264.4	187	
31X-3	SPH	80	85	273.13	187	
32X-3	SPH	67	72	283.57	187	
33X-1	SPH	56	61	290.16	187	
34X-3	SPH	80	85	303	187	
35X-3	SPH	44	49	311.46	187	
36X-4	SPH	73	78	322.57	187	
39X-3	SPH	80	85	333.8	187	
40X-5	SPH	70	75	342.98	187	
41X-2	SPH	80	85	349.6	187	
42X-3	SPH	80	85	360.09	187	
43X-8	SPH	70	75	374.57	187	

Table 9. List of microbiological samples taken for Site NGHP-01-07. (To view the complete table, please see the ASCII files.)—Continued

Sample reference						Comments
Core, section	Sample code	Top (cm)	Bottom (cm)	Depth (mbsf)	Volume (cc)	
NGHP-01-17A—Continued						
44X-4	SPH	80	85	380.06	187	
46X-4	SPH	80	85	400.44	187	
47X-5	SPH	80	85	410.63	187	
50X-4	SPH	80	85	419	187	
51X-5	SPH	80	85	430.72	187	
52X-6	SPH	80	85	440.87	187	
53X-4	SPH	63	68	447.48	187	
54X-3	SPH	76	81	456.04	187	
55X-6	SPH	60	65	468.06	187	
56X-3	SPH	80	85	475.49	187	
57X-3	SPH	80	85	484.98	187	
58X-5	SPH	80	85	498.03	187	
61X-4	SPH	80	85	505.78	187	
62X-5	SPH	80	85	517.41	187	
63X-3	SPH	30	35	523.53	187	
64X-1	SPH	37	42	530.67	187	
65X-2	SPH	70	75	542.2	187	
66X-3	SPH	41	46	552.41	187	
67X-6	SPH	27	32	564.41	187	
68X-5	SPH	80	85	573.89	187	
69X-4	SPH	80	85	584	187	
72X-3	SPH	25	30	589.86	187	
73X-3	SPH	70	75	600.7	187	
74X-2	SPH	80	85	609	187	
75X-2	SPH	80	85	618.57	187	
76X-2	SPH	47	52	626.25	187	
77X-3	SPH	80	85	637.08	187	
78X-3	SPH	80	85	647.51	187	
79X-4	SPH	80	85	659.1	187	
80X-2	SPH	75	80	663.76	187	
82X-4	SPH	80	85	676.97	187	
83X-2	SPH	22	27	684.12	187	

Core-End Temperature Readings

Core-end temperature readings were taken on most cores immediately following the IR track imaging (table 12). Typically four temperature probes were inserted approximately 8 cm into the end of each core and allowed to remain there until the core was completely processed and removed from the catwalk. Temperatures from the center position probes are typically 5 to 10 °C less than the IR temperatures as expected since the IR images measure the liner temperature which has warmed closer to ambient temperatures than the center of the core, except where significant gas hydrate is present.

Index Properties

Water content, porosity, bulk density, and shear strength vary downhole such that three physical-property units can be defined with boundaries at 20 and 200 mbsf (fig. 27). However, electrical resistivity and magnetic susceptibility do not exhibit any variation at 200 mbsf (fig. 28). The change in some physical behavior at 200 mbsf agrees with the Lithostratigraphic description at this site that shows the presence of an authigenic carbonate layer separating mainly foraminifera-rich nannofossil ooze in the upper section from nannofossil ooze below (see "Lithostratigraphy"). Although the porosity and density wire-line logs agree with the physical properties measured below 260 m, valid log readings do not extend above that depth.

The water content (168 percent) (related to solids) in the uppermost part of the core (table 13) is higher than at most previous sites. Porosity varies from about 82 percent at the top of the hole to 43 percent at the bottom of Physical Property Unit 2. Porosity increases abruptly to about 62 percent at a depth between 200 and 220 mbsf. Interestingly, the porosity is essentially constant from 220 mbsf to the bottom of the hole, with one offset at 562 mbsf where the porosity decreases to about 40–47 percent. This roughly coincides with the presence of gas hydrate in this hole and may be the result of early-emplaced gas hydrate reducing the natural compaction process (Winters, 2000). Except from 280 to 295 mbsf, and for a few thin offsets, bulk density data from wire-line logging are in close agreement with MAD and MSCL values (fig. 27). Surprisingly, water contents from both alternating intact biscuits and infilling slurry agree within 3 percentage points in Core NGHP-01-17A-61X. Grain density varies from 2.44 to 2.81 g/cm^3 (average value of 2.66 g/cm^3) and continuously decreases with depth to the BSR at 609 mbsf. The decrease with depth probably is a result of the increasing siliceous content of the sediment with depth.

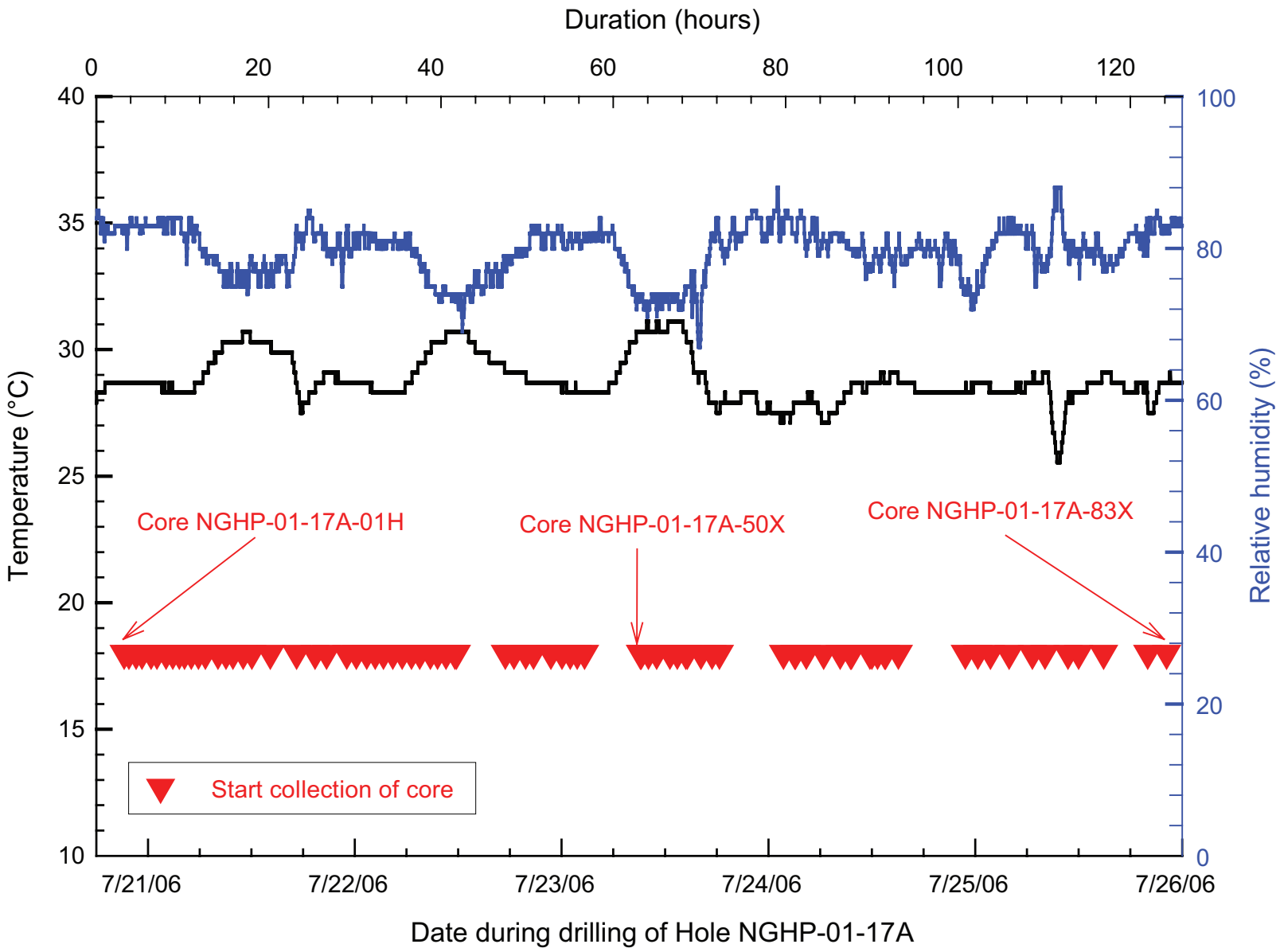


Figure 20. Catwalk temperature and humidity measurements as a function of time during drilling operations at Site NGHP-01-17.

Table 10. List of infrared images collected from Hole NGHP-01-17A.

Site:	NGHP-01-17			NGHP Expedition 01		
Hole:	A			Infrared Thermal Imaging Track		
Core	Imaging length (cm)	First run	Date	Start time	Temperature (start/end) (°C)	Comments
1H	430	x	7/20	21:14	28.7/28.7	
2H	970	x	7/20	21:48	28.7/28.7	
3H	930	x	7/20	22:38	28.7/28.7	
4H	940	x	7/20	23:19	28.7/28.7	
5H	970	x	7/21	0:22	28.7/28.7	
6H	970	x	7/21	1:03	28.7/28.7	
7H	970	x	7/21	2:06	28.7/28.7	
8H	970	x	7/21	2:53	28.3/28.3	
9H	950	x	7/21	3:38	28.3/28.3	
10H	970	x	7/21	4:15	28.3/28.3	
11H	930	x	7/21	5:02	28.3/28.3	
12H	960	x	7/21	5:51	28.3/28.3	
13H	940	x	7/21	6:40	28.7/28.7	
14X	930	x	7/21	8:07	29.5/29.5	
15X	950	x	7/21	9:03	29.9/29.9	
16X	950	x	7/21	9:52	30.3/30.3	
17X	40	x	7/21	11:03	30.3/30.3	
18X	950	x	7/21	12:04	30.7/30.7	Gas voids but no hydrate (cold spots)
19X	950	x	7/21	14:12	30.3/30.3	Check time, slight cool spot by crack
21X	440	x	7/21	17:15	29.9/29.5	Fluid present, poor liner contact
22X	950	x	7/21	19:23	28.3/28.3	Bubbly fluid, overall cool core?
23X	950	x	7/21	20:43	28.7/28.7	Large voids
24X	950	x	7/21	23:04	28.7/28.7	Much of core blown out of liner
25X	950	x	7/22	0:10	28.7/28.7	
26X	640	x	7/22	1:23	28.7/28.7	
27X	700	x	7/22	2:22	28.7/28.7	
28X	890	x	7/22	3:20	28.3/28.3	
29X	870	x	7/22	4:25	28.3/28.3	
30X	930	x	7/22	5:30	28.3/28.3	
31X	940	x	7/22	6:35	28.7/28.7	
32X	830	x	7/22	7:32	29.1/29.1	
33X	390	x	7/22	8:46	29.9/29.9	
34X	800	x	7/22	9:36	30.3/30.3	
35X	950	x	7/22	10:35	30.3/30.3	
36X	950	x	7/22	11:37	30.7/30.7	
36aX	350	x	7/22	11:47	30.7/30.7	
39X	760	x	7/22	17:28	29.5/29.5	
40X	950	x	7/22	18:28	29.1/29.1	
41X	950	x	7/22	19:50	29.1/29.1	Lost core from top of liner, hydrate?
42X	950	x	7/22	20:45	29.1/29.1	Lost core from top of liner, hydrate?
43X	950	x	7/22	22:46	28.7/28.7	Some core lost from top
44X	950	x	7/23	0:02	28.7/28.7	1 cold spot
45X	100	x	7/23	1:00	28.7/28.7	
46X	950	x	7/23	1:49	28.3/28.3	
47X	860	x	7/23	2:40	28.3/28.3	Hydrate
50X	950	x	7/23	9:08	30.3/30.3	IR anomaly (IW)
50aX	220	x	7/23	9:15	30.3/30.3	Top of 50X
51X	950	x	7/23	10:05	30.7/30.7	Hydrate
52X	950	x	7/23	11:01	30.7/30.7	
53X	950	x	7/23	12:34	30.7/30.8	Hydrate at 715
54X	950	x	7/23	13:25	31.1/31.1	
55X	570	x	7/23	14:24	31.1/31.1	
55aX	200	x	7/23	14:35	31.1/31.1	From blown out top of core 55X
56X	470	x	7/23	16:10	29.1/29.1	Partial core, barrel jammed off
57X	720	x	7/23	17:28	28.3/28.3	Cold spot in blown out core (blk ash)
58X	820	x	7/23	18:18	27.9/27.9	2 cold spots

Table 10. List of infrared images collected from Hole NGHP-01-17A.—Continued

Site:	NGHP-01-17			NGHP Expedition 01		
Hole:	A			Infrared Thermal Imaging Track		
Core	Imaging length (cm)	First run	Date	Start time	Temperature (start/end) (°C)	Comments
61X	950	x	7/24	1:45	27.5/27.5	
62X	950	x	7/24	3:03	27.1/27.1	
62aX	200	x	7/24	3:08	27.5/27.5	Top of 62X
63X	860	x	7/24	4:23	27.9/27.9	
64X	960	x	7/24	6:25	27.5/27.5	
65X	390	x	7/24	8:20	27.5/27.5	
66X	950	x	7/24	9:32	28.3/28.3	
66aX	90	x	7/24	9:38	28.3/28.3	Top of core 66X
67X	950	x	7/24	11:46	28.3/28.3	
67aX	120	x	7/24	12:00	28.3/28.3	Top of core 67X
67bX	270	x	7/24	12:40	29.1/29.1	Second top of core 67X
68X	950	x	7/24	13:29	28.7/29.1	Hydrate at 720 cm
68aX	190	x	7/24	13:36	29.1/29.1	Top of 68X
69X	950	x	7/24	15:05	29.1/29.1	
72X	950	x	7/24	22:50	28.3/28.3	Some core blown out bottom
73X	950	x	7/25	0:18	28.7/28.7	
74X	950	x	7/25	1:46	28.7/28.7	
75X	950	x	7/25	3:55	28.7/28.7	
76X	950	x	7/25	6:37	28.7/28.7	
77X	950	x	7/25	8:05	28.7/28.7	
78X	950	x	7/25	10:45	26.7/26.7	
79X	950	x	7/25	11:59	28.3/28.3	
80X	950	x	7/25	14:54	28.7/28.7	
82X	950	x	7/25	20:00	28.7/28.3	
83X	180	x	7/25	22:12	28.7	Half diameter core at upper end

Strength

Shear strength increases uniformly and linearly to 20 mbsf, then increases at a much slower rate (tables 14, 15, and 16, and fig. 27). The boundary between APC and XCB coring is about 75 mbsf. Below that depth, slightly more variation exists, illustrating the effect of disturbance caused by rotary coring on sediment. Although testing was to be restricted to intact biscuits, it was occasionally difficult to differentiate between biscuits and adjacent disturbed sediment. The strength of the sediment below 330 m exceeded the measuring limit of the Pocket Penetrometer.

The measured shear strengths were normalized to the effective vertical stress (σ'_v) (fig. 29) to provide qualitative information on the stress history of the sediment. The strength/effective vertical stress ranges from approximately 2.1 at the top of the hole to an average of about 0.1 near the bottom of the hole. Most of these values are in overall agreement with a number of other normally consolidated clays (Holtz and Kovacs, 1981). Hunt (1984) states that the strength/effective vertical stress ratio typically is between 0.4 and 0.16. The wide scatter in the results at the top of the hole reflect the dependency of this ratio on the stress path as well as the test method (Bjerrum, 1972; Ladd and others, 1977). Because many values at the top of the hole are greater than 0.4, the implication is that the sediment at this location is overconsolidated. However, this does not agree with the high water content found at the top of the hole. The discrepancy may be explained by the fact that the previous studies probably were not conducted in sediment with such a high biogenic component.

The peak (Sv) and remolded (Srem) vane shear strengths clearly increase with subbottom depth (fig. 30) and the sensitivity (St), which equals Sv/Srem, typically varies between 2.5 and 3, (with two outliers). Sensitivity values represent the amount of strength loss after remolding and in extreme examples can reach values of 500 (Lambe and Whitman, 1969). This sediment has low to medium sensitivity (Holtz and Kovacs, 1981). High values of sensitivity are indicative of good quality core recovery because the sediment has not been highly disturbed.

Electrical Resistivity

Strong agreement exists between electrical resistivity values produced by wire-line logging, MSCL, and the Wenner array below 260 m. Above this depth, hole conditions prohibited reliable wire-line logging. The resistivity values determined using the Wenner array on split cores are on the low side of the MSCL data (fig. F28), in part because the Wenner measurements are conducted on intact core material, rather than a wider portion of core that may contain voids, small expansion cracks, or slurry. Lower MSCL values are more representative of undisturbed sediment as they are less impacted by the presence of such micro voids caused by gas expansion.

Table 11. List of infrared image files collected on section ends from Hole NGHP-01-17A.

Site:	NGHP-01-17			Date	NGHP Expedition 01		
Hole:	A				Infrared Section-end Images (Catwalk)		
Core	Section	Top	Bottom		Time	Image#	Comments
1H	3		x	7/20	21:29	G0720-03, 04	IMG file odd numbers, BMP even #'s
1H	3	x		7/20	21:29	G0720-05, 06	numbers 07, 08 are test images
2H	3	x		7/20	22:00	G0720-09, 10	
3H	4	x		7/20	22:55	G0720-11, 12	
4H	2	x		7/20	23:28	G0720-13, 14	
4H	2		x	7/20	23:28	G0720-15, 16	
5H	3	x		7/21	0:34	G0721-01, 02	
6H	3	x		7/21	1:23	G0721-03, 04	
7H	3	x		7/21	2:25	G0721-05, 06	
8H	3	x		7/21	3:10	G0721-07, 08	
9H	3	x		7/21	4:00	G0721-09, 10	
10H	3	x		7/21	4:30	G0721-11, 12	
11H	3	x		7/21	5:18	G0721-13, 14	
12H	3	x		7/21	6:11	G0721-15, 16	
13H	3	x		7/21	6:55	G0721-17, 18	
14X	3	x		7/21	8:20	G0721-19, 20	
15X	3	x		7/21	9:20	G0721-21, 22	
16X	3	x		7/21	10:11	G0721-23, 24	
18X	3	x		7/21	12:20	G0721-25, 26	
19X	3	x		7/21	13:29	G0721-27, 28	
21X	3	x		7/21	17:25	G0721-29, 30	
22X	3		x	7/21	19:35	G0721-31, 32	
22X	3	x		7/21	19:35	G0721-33, 34	
23X	2	x		7/21	19:54	G0721-35, 36	
24X	3		x	7/21	23:22	G0721-37, 38	
25X	3	x		7/22	0:25	G0722-01, 02	
26X	3	x		7/22	1:38	G0722-03, 04	
27X	2	x		7/22	2:40	G0722-05, 06	
28X	3	x		7/22	3:30	G0722-07, 08	
29X	4	x		7/22	4:47	G0722-09, 10	
30X	6		x	7/22	5:55	G0722-11, 12	IR anomaly
31X	3	x		7/22	6:56	G0722-13, 14	
32X	3	x		7/22	7:49	G0722-15, 16	
33X	3	x		7/22	8:59	G0722-17, 18	
34X	3	x		7/22	9:47	G0722-19, 20	
35X	5	x		7/22	10:51	G0722-21, 22	
36X	3		x	7/22	12:06	G0722-23, 24	
39X	see note		x	7/22	17:36	G0722-25, 26	Short section just above Hyd 105
39X	see note	x		7/22	17:37	G0722-27, 28	Short section just above Hyd 105
40X	Last	x		7/22	18:34	G0722-29, 30	Good image adjacent to IW at core bottom
41X	2	x		7/22	20:10	G0722-31, 32	
42X	2	x		7/22	20:56	G0722-33, 34	
43X	3		x	7/22	22:57	G0722-35, 36	
44X	4	x		7/23	0:20	G0723-01, 02	
45X				7/23			Short core, no core end images
46X	3	x		7/23	2:12	G0723-03, 04	
47X	3		x	7/23	2:50	G0723-05, 06	
47X	6	x		7/23	3:00	G0723-07, 08	70 cm IR anomaly (hydrate?)
50X	3	x		7/23	9:30	G0723-09, 10	IR anomaly (IW)
51X	4		x	7/23	10:25	G0723-11, 12	Hydrate
52X	2		x	7/23	11:14	G0723-13, 14	
52X	3	x		7/23	11:20	G0723-15, 16	
53X	3		x	7/23	12:49	G0723-17, 18	
54X	3		X	7/23	13:42	G0723-19, 20	
55X	Last	X		7/23	14:35	G0723-21, 22	
55X	3		x	7/23	14:43	G0723-23, 24	
56X	4	x		7/23	16:28	G0723-25, 26	
57X	4		x	7/23	17:47	G0723-27, 28	Fresh cut

Table 11. List of infrared image files collected on section ends from Hole NGHP-01-17A.—Continued

Site:	NGHP-01-17				NGHP Expedition 01		
Hole:	A			Date	Infrared Section-end Images (Catwalk)		
Core	Section	Top	Bottom		Time	Image#	Comments
58X	6	x		7/23	18:31	G0723-29, 30	Fresh cut
61X	3	x		7/24	2:03	G0724-01, 02	
62X	3	x		7/24	3:25	G0724-03, 04	
63X	4	x		7/24	4:42	G0724-05, 06	Hydrate
64X	2	x		7/24	6:33	G0724-07, 08	
65X	3	x		7/24	8:29	G0724-09, 10	
66X	5		x	7/24		G0724-11, 12	Hydrate (scan above IR anomaly)
67X	Last		x	7/24	11:54	G0724-13, 14	IR/hydrate anomaly
68X	3	x		7/24	13:49	G0724-15, 16	
69X	3	x		7/24	15:20	G0724-17, 18	
72X	2		x	7/24	23:01	G0724-19, 20	
73X	2		x	7/25	0:33	G0725-01, 02	
74X	2	x		7/25	2:02	G0725-03, 04	
75X	3	x		7/25	4:10	G0725-05, 06	
76X	3	x		7/25	6:56	G0725-07, 08	
77X	4	x		7/25	8:20	G0725-09, 10	
78X	4		x	7/25	11:00	G0725-11, 12	
79X	3		x	7/25	12:15	G0725-13, 14	
80X	3	x		7/25	15:05	G0725-15, 16	
82X	3		x	7/25	20:15	G0725-17, 18	Low T is hole in end of core
83X							No core end IR, too broken

Unlike other holes, for example, NGHP-01-10B, the low wire-line resistivity values do not reflect exceptionally high zones of gas-hydrate concentration in Hole NGHP-01-17A. Resistivity determined using both MSCL and the Wenner array on split cores (table 17) increase between 24 and 28 mbsf, which is near the depth of the Sulfate-methane interface (SMI) (24 mbsf). A possible explanation for this agreement is that methane is produced below the SMI and this gas expands upon core recovery disrupting the sediment structure.

The apparent formation factor is the ratio of the resistivity of a saturated sediment to the resistivity of the pore fluid and provides an indication of the relationships between sediment structure, void space, tortuosity, and other factors, and the ability of fluid to flow through the formation. Because pore water salinity typically varies a small amount in the recovered sediment and is similar to that of seawater (see "Inorganic geochemistry"), we have normalized the measured Wenner resistivity values by that of seawater (approximately 0.2 W×m) (table 17). Values range from about 2.0 at the top of the core to 6.0 at the bottom, with a spike between 375 and 390 mbsf (fig. 31). The spike is related to a layer of authigenic carbonate rich nannofossil ooze that also produced an electrical resistivity spike in the well log. Other equations and methods exist for calculating formation factor; however, they require the use of empirical constants that have not yet been determined for the sediments at this location.

Electrical resistivity values were determined at select locations downcore to study their sensitivity to macro sediment property changes. For example, electrical resistivity in the softer top of FPC NGHP-01-17A-38Y recovered with 167 bars of pressure but without gas hydrate, had an average electrical resistivity of 0.417 Ω.m. However, the more intact sediment at the base of the core had an average resistivity of 0.602 W×m, an increase of 44 percent. This is in contrast with Hyace Core NGHP-01-17A-49E, which had similar ER (0.752 W×m) in disturbed sediment at the top of the core compared with intact sediment at the bottom of the core (0.748 W×m). In XCB Core NGHP-01-17A-77X, electrical resistivity values in biscuits averaged 1.116 W×m, an increase of 33 percent over infilling material that had an electrical resistivity of 0.841 W×m.

P-Wave Velocity

P-wave velocity (V_p) measured with the MSCL increased slightly from 1.47 km/s in the top of the hole (fig. 28) to 1.58 km/s at a subbottom depth of 28 m, which represents the depth where gas and voids present in the sediment prevented further valid measurements from being logged. The contact V_P values of 1.48 to 1.55 km/s (table 18) are in agreement with the MSCL values. Valid contact V_p measurements could not be determined below 24.05 mbsf. Both techniques are adversely affected by the SMI located at about 24 mbsf (see "Organic Geochemistry" and "Inorganic Geochemistry"). Methane, which is typically produced below the SMI, may come out of solution if present in a high enough concentration and attenuate acoustic signals.

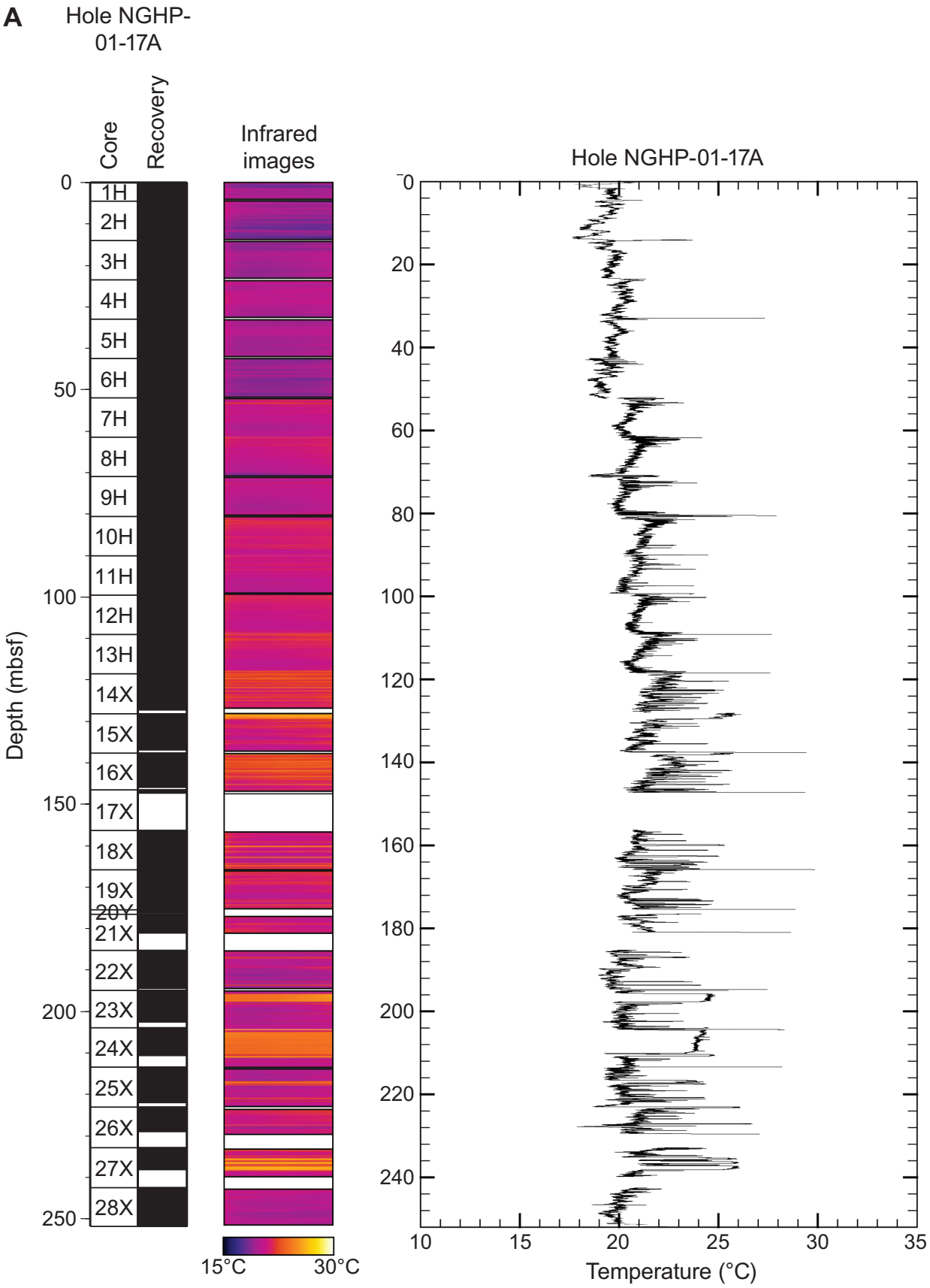


Figure 21. Infrared track imaging and the derived downhole temperature profile for Hole NGHP-01-17A in three sections (A, 0 to 250 mbsf; B, 250 to 500 mbsf; C, 500 to 700 mbsf). [mbsf, meters below sea floor]

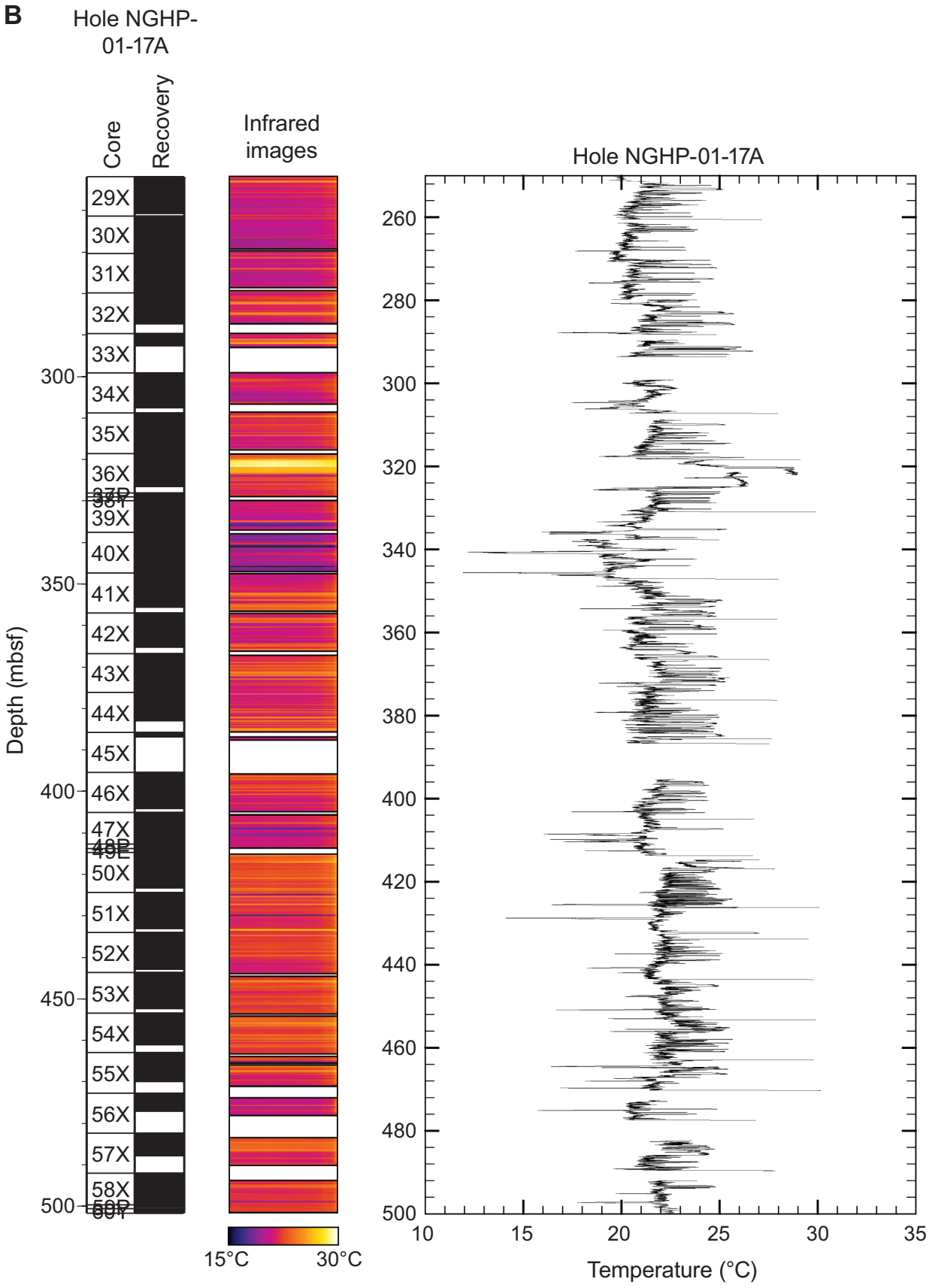


Figure 21. Infrared track imaging and the derived downhole temperature profile for Hole NGHP-01-17A in three sections (A, 0 to 250 mbsf; B, 250 to 500 mbsf; C, 500 to 700 mbsf). [mbsf, meters below sea floor]—Continued

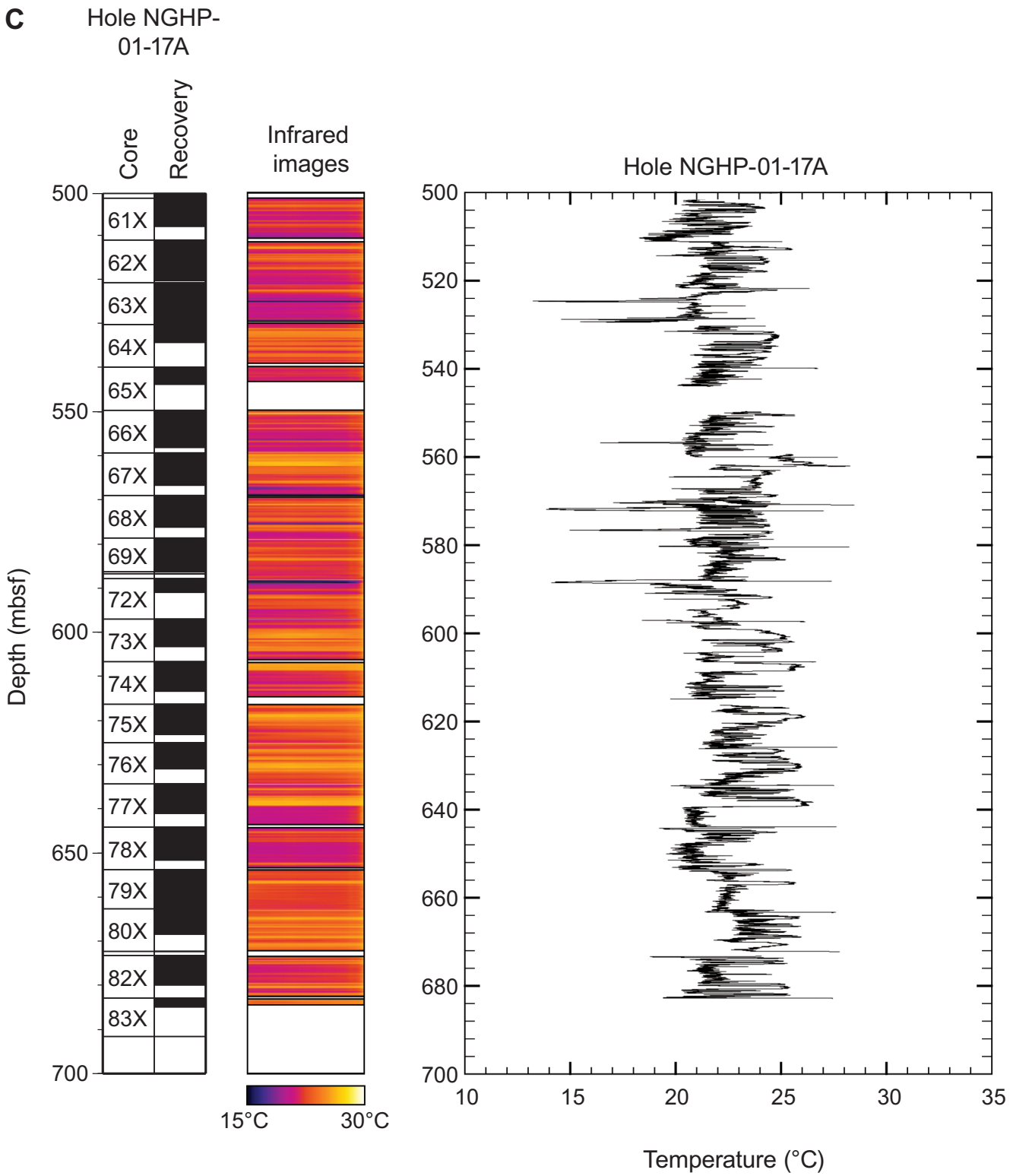


Figure 21. Infrared track imaging and the derived downhole temperature profile for Hole NGHP-01-17A in three sections (A, 0 to 250 mbsf; B, 250 to 500 mbsf; C, 500 to 700 mbsf). [mbsf, meters below sea floor]—Continued

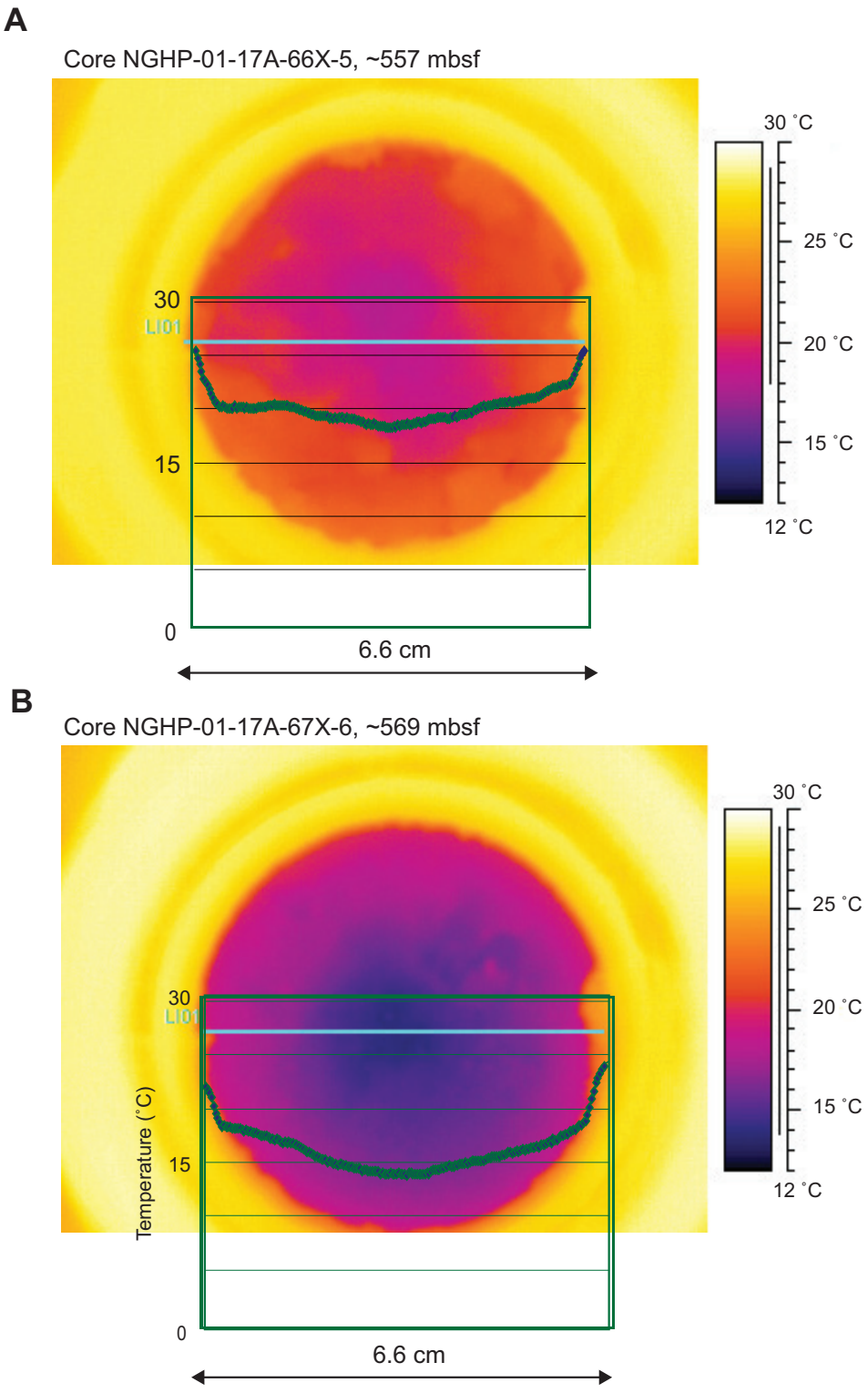


Figure 22. Comparison of core end infrared (IR) images from adjacent to an IR anomaly and away from an IR anomaly: A, Core NGHP-01-17A-66X-5 ~557 mbsf (away from IR anomaly); B, Core NGHP-01-17A-67X-6 ~569 mbsf (adjacent to an IR anomaly).

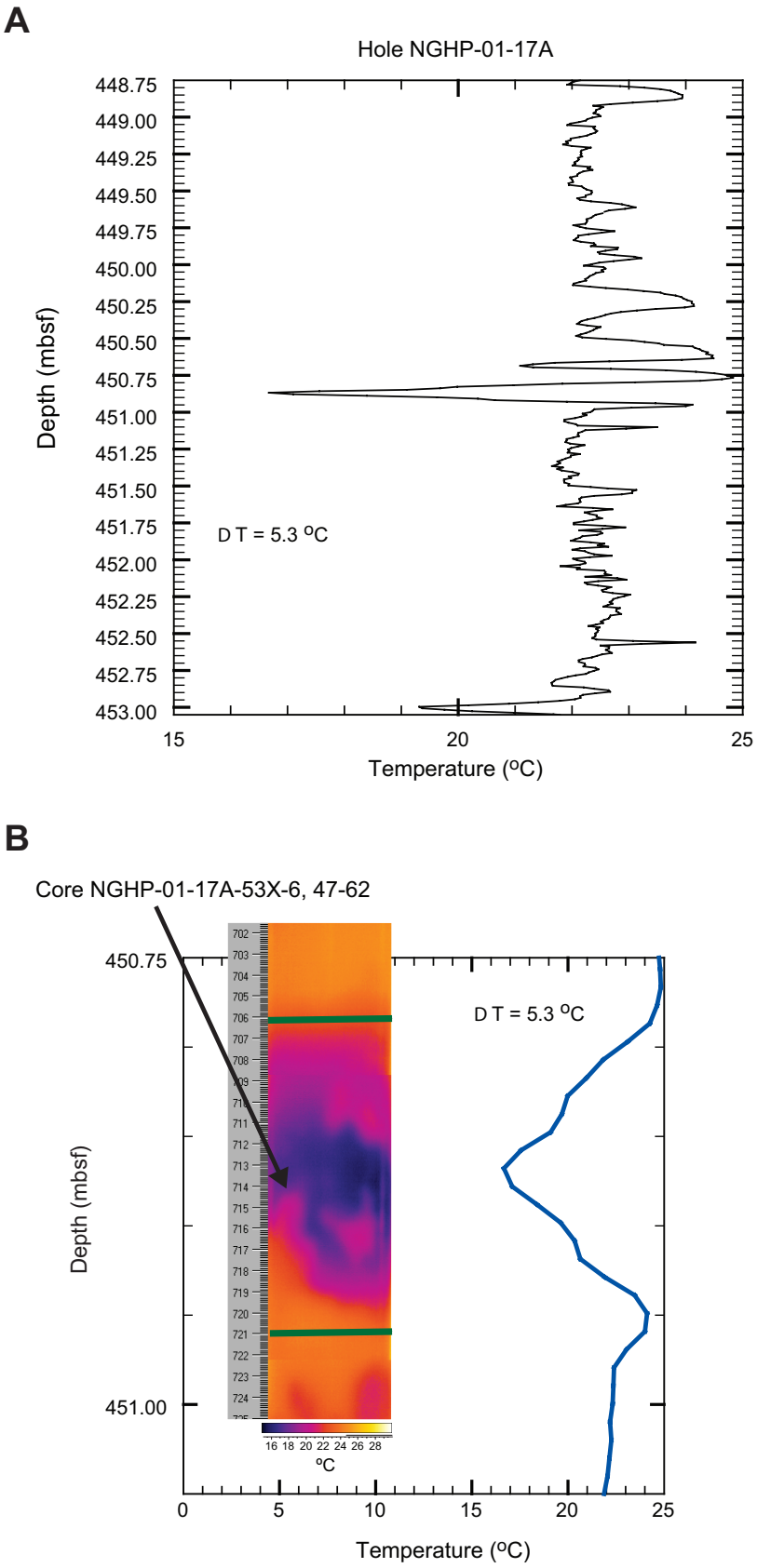


Figure 23. Detailed example of infrared (IR) anomaly (Section NGHP-01-17A-53X-6, 47–62). A, Down-core temperature plot; B, IR image from IR track and detailed down-core temperature plot.

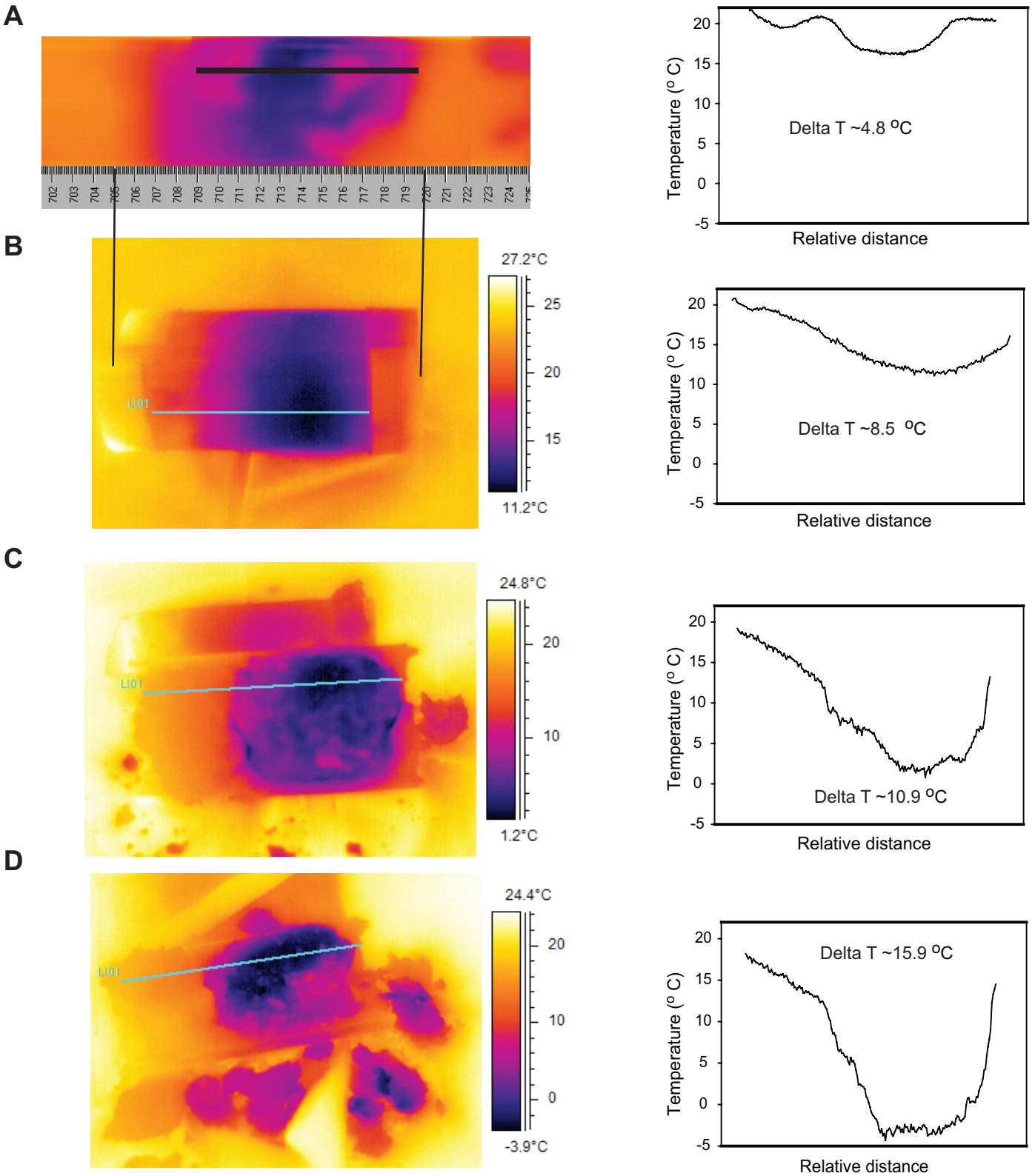


Figure 24. Sequence of infrared (IR) images and Delta T's during processing of an interstitial water sample containing an IR anomaly for IW sample NGHP-01-17A-53X-6, 47–62 cm after splitting. A, IR track image and single line estimate of Delta T; B, IR image and Delta T of IW sample still in core liner in chemistry lab; C, IR image and Delta T of IW sample after removal of core liner; D, IR image and Delta T after splitting of core.

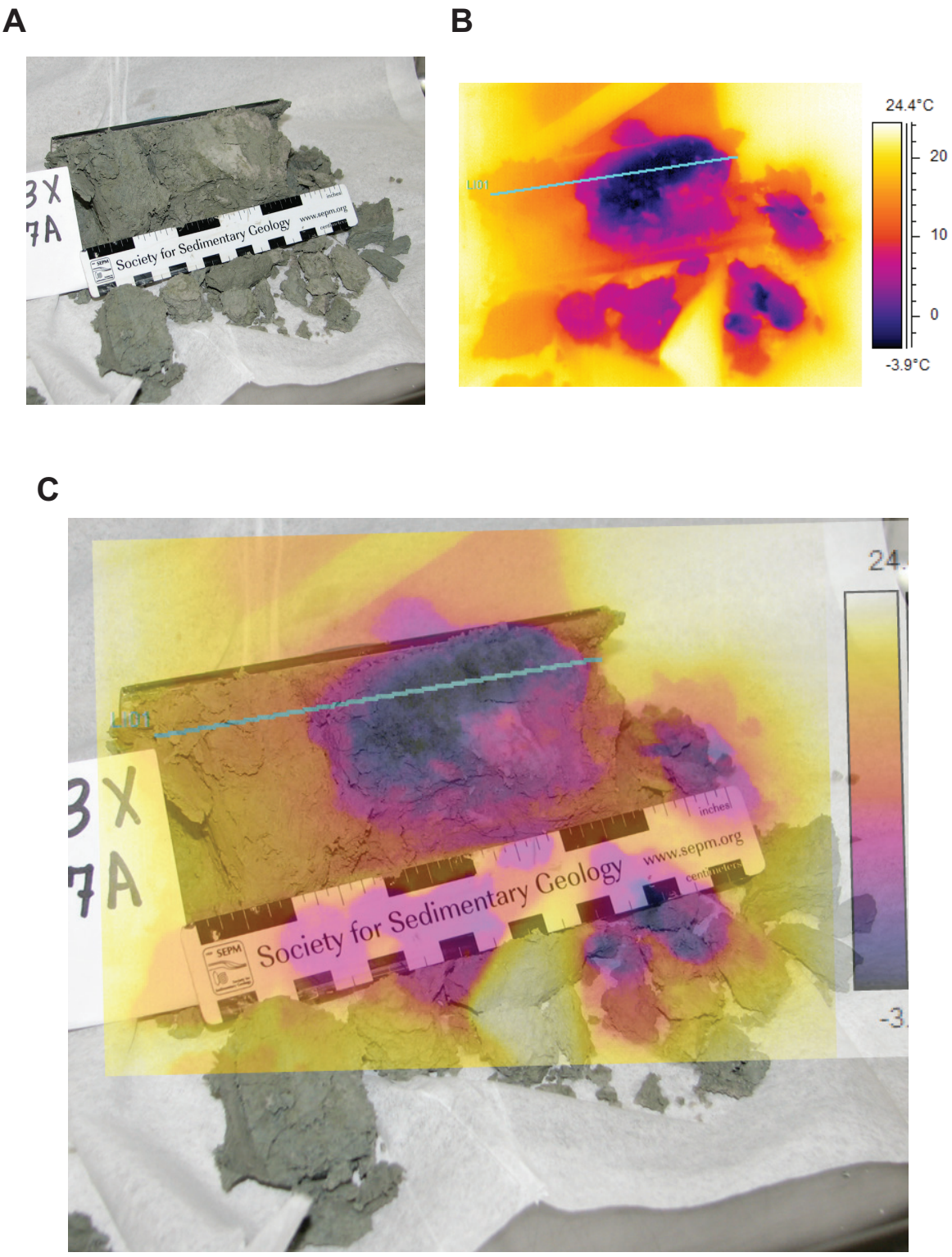


Figure 25. A, Digital image of interstitial water (IW) sample NGHP-01-17A-53X-6, 47–62 cm after splitting; B, IR image of IW sample NGHP-01-17A-53X-6, 47–62 cm after splitting; C, Merged visible and IR images of IW sample NGHP-01 17A-53X-6, 47–62 cm after splitting, showing location of cold anomaly on the split sample and in relationship to sample lithology.

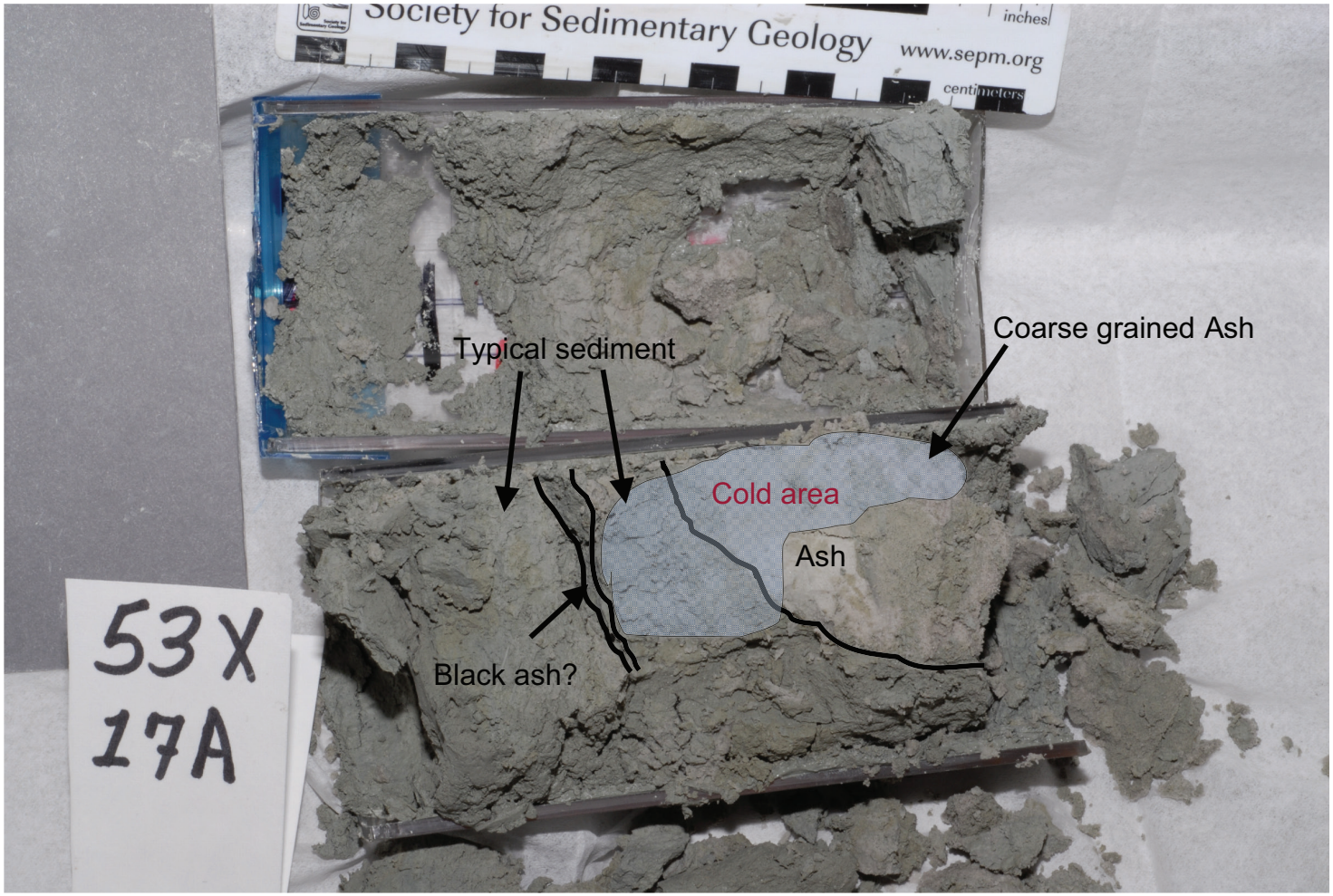


Figure 26. Digital visible image of interstitial water sample NGHP-01-17A-53X-6, 47–62 after splitting, showing lithology, cold anomaly, and resulting chlorinity values (see "Inorganic Geochemistry").

Table 12. List of temperature-probe data collected at bottom of cores from Hole NGHP-01-17A.

Core	Section	Bottom	Date	In time	Out time	Temperature probe #	Comments
1H	3	x	7/20	21:20	21:28	F-1, F-2, F-3, F-4	Used standard pattern(1, 4 on edge 90 deg apart, 3 center, 2 between 1 and 3 (until core 5H)
2H	last	x	7/20	21:50	22:08	F-1, F-2, F-3, F-4	
3H	last	x	7/20	22:47	23:01	F-1, F-2, F-3, F-4	
4H	last	x	7/20	23:20	23:34	F-1, F-2, F-3, F-4	
5H	last	x	7/21	0:23	0:35	F-1, F-2, F-3, F-4	Alternate pattern to core 18X, probe 2 center, 1 up, 3 down 4 side.
6H	last	x	7/21	1:04	1:23	F-1, F-2, F-3, F-4	
7H	last	x	7/21	2:07	2:25	F-1, F-2, F-3, F-4	
8H	last	x	7/21	2:54	3:10	F-1, F-2, F-3, F-4	
9H	last	x	7/21	3:39	4:00	F-1, F-2, F-3, F-4	
10H	last	x	7/21	4:15	4:30	F-1, F-2, F-3, F-4	
11H	last	x	7/21	5:03	5:18	F-1, F-2, F-3, F-4	
12H	last	x	7/21	5:52	6:11	F-1, F-2, F-3, F-4	
13H	last	x	7/21	6:40	6:55	F-1, F-2, F-3, F-4	
14X	last	x	7/21	8:08	8:28	F-1, F-2, F-3, F-4	
15X	last	x	7/21	9:03	9:18	F-1, F-2, F-3, F-4	
16X	last	x	7/21	9:53	10:11	F-1, F-2, F-3, F-4	Inadequate time for probe deployment
17X	last	x	7/21				Low recovery, no probes
18X	last	x	7/21	12:09	12:22	F-1, F-2, F-3, F-4	Same pattern, per note on Core 1H to core 25X. Void, pulled back.
19X	last	x	7/21	12:16	13:30	F-1, F-2, F-3, F-4	
21X	last	x	7/21	19:18	19:24	F-1, F-2, F-3, F-4	
22X	last	x	7/21	19:27	19:44	F-1, F-2, F-3, F-4	Indurated
23X	last	x	7/21	20:45	21:00	F-1, F-2, F-3, F-4	
24X	last	x	7/21	23:10	23:20	F-1, F-2, F-3, F-4	
25X	last	x	7/22	0:10	0:25	F-1, F-2, F-3, F-4	
26X	last	x	7/22	1:24	1:38	F-1, F-2, F-3, F-4	
27X	last	x	7/22	2:23	2:40	F-1, F-2, F-3, F-4	
28X	last	x	7/22	3:21	3:28	F-1, F-2, F-3, F-4	
29X	last	x	7/22	4:25	4:47	F-1, F-2, F-3, F-4	
30X	last	x	7/22	5:30	5:46	F-1, F-2, F-3, F-4	
31X	last	x	7/22	6:36	6:55	F-1, F-2, F-3, F-4	
32X	last	x	7/22	7:35	7:49	F-1, F-2, F-3, F-4	Probes at IR anomaly
33X	last	x	7/22	8:47	8:56	F-1, F-2, F-3, F-4	
34X	last	x	7/22	9:37	9:47	F-1, F-2, F-3, F-4	
35X	last	x	7/22	10:36	10:57	F-1, F-2, F-3, F-4	
36X	last	x	7/22	11:38	12:05	F-1, F-2, F-3, F-4	
39X	last	x	7/22	17:33	17:49	F-1, F-2, F-3, F-4	Return to 1H insertion pattern
40X	last	x	7/22	18:00	18:47	F-1, F-2, F-3, F-4	
41X	last	x	7/22	19:53	20:10	F-1, F-2, F-3, F-4	
42X	last	x	7/22	20:52	21:03	F-1, F-2, F-3, F-4	
43X	last	x	7/22	22:50	23:09	F-1, F-2, F-3, F-4	
44X	last	x	7/22	0:05	0:18	F-1, F-2, F-3, F-4	
45X			7/23				No temperature probe measurement
46X	last	x	7/23	1:50	2:11	F-1, F-2, F-3, F-4	Alternate probe mode, this shift
47X	last	x	7/23	2:40	2:58	F-1, F-2, F-3, F-4	IR anomaly and hydrates
50X	last	x	7/23	9:10	9:30	F-1, F-2, F-3, F-4	IR anomaly (IW)
51X	last	x	7/23	10:06	10:24	F-1, F-2, F-3, F-4	
52X	last	x	7/23	11:03	11:21	F-1, F-2, F-3, F-4	
53X	last	x	7/23	12:37	12:55	F-1, F-2, F-3, F-4	Hydrate 25 cm away from probes (up core)
54X	last	x	7/23	13:30	13:46	F-1, F-2, F-3, F-4	
55X	last	x	7/23	14:27	14:52	F-1, F-2, F-3, F-4	
56X			7/23				No temperature probes, too hard and flakey
57X			7/23				No temperature probes, too hard and flakey
58X			7/23				No temperature data, logger launch failure
61X			7/24				No temperature data, logger launch failure
62X			7/24				No temperature data, logger launch failure
63X			7/24				No temperature data, logger launch failure
64X			7/24				No temperature data, logger launch failure
65X			7/24				No temperature data, logger launch failure
66X			7/24				No temperature data, logger launch failure

Table 12. List of temperature-probe data collected at bottom of cores from Hole NGHP-01-17A.—Continued

Core	Section	Bottom	Date	In time	Out time	Temperature probe #	Comments
67X			7/24				No temperature data, logger launch failure
68X			7/24				No temperature data, logger launch failure
69X			7/24				No probes, too hard
72X			7/25				No probes, mostly empty liner
73X	last	x	7/25	0:20		F-1, F-2, F-3, F-4	
74X			7/25			F-1, F-2, F-3, F-4	No probes, too hard
75X	last	x	7/25	3:47	4:10	F-1, F-2, F-3, F-4	
76X	last	x	7/25	6:38	6:56	F-1, F-2, F-3, F-4	
77X			7/25				No probes, too hard
78X	last	x	7/25	10:46	10:55	F-1, F-2, F-3, F-4	
79X	last	x	7/25	12:03	12:21	F-1, F-4	F-1, F-4 only, two hard for 2, and 3.
80X			7/25				No probes, core mostly gone
82X	last	x	7/25	20:03	20:12	F-1, F-2, F-3, F-4	Solid probe insertion
83X			7/25				No temperature probes, too fractured

Magnetic Susceptibility

Magnetic susceptibility is uniform and low at this site compared to previous holes drilled during NGHP Expedition 01. These measurements reflect the primary biogenic nature of the sediment and indicate that a lack of terrigenous magnetic minerals is present (fig. 28; see "Lithostratigraphy"). Lower in the hole, magnetic susceptibility increases at black ash layers because the darker colored grains contain ferromagneticminerals.

Thermal Conductivity

Thermal conductivities vary between 0.602 and 1.059 W/(m×K) and decrease slightly with subbottom depth (table 19 and fig. 28). Such values are well within the range of marine sediments (for example, Novosel and others, 2007), although they are all lower than values determined by Davis and others (1990) for sediment from Cascadia and the Nankai Trough.

Downhole Temperature Measurements

A number of different tools are available for determining downhole sediment temperature (see "Physical Properties" section of "Methods" chapter). At Site NGHP-01-17, eleven attempts were made to measure *in situ* temperture, and nine provided usable *in situ* temperature data (table 20). The maximum depth attained, 664 mbsf, is over three times deeper than at other sites during this expedition. The seafloor temperature intercept was determined to be 5.6 ± 0.2 °C and the geothermal gradient was determined to be 19 ± 2 °C per km (fig. 32). The base of gas-hydrate stability is predicted at 620 mbsf assuming pure methane and porewater salinity of 35 ppt (Sloan, 1998), similar to the BSR depth of 608 mbsf. The exceptionally low thermal gradient here is probably due to a very rapid sedimentation rate in the Andaman Sea. This very low thermal gradient leads to a very thick gas-hydrate stability zone (shipboard calculated seafloor temperature 5.5 °C, geothermal gradient 20 °C per km).

Pressure Coring

The main objectives of pressure coring during NGHP Expedition 01 were to quantify natural gas composition and concentration in sediments and to determine the nature and distribution of gas hydrate and free gas within the sediment matrix. Secondary objectives were to obtain measurements of physical properties on gas-hydrate-bearing sediments under *in situ* conditions, which can be used to help interpret regional seismic data, and obtain samples under full pressure for shore-based studies. To achieve these objectives, we conducted depressurization experiments and captured resultant gas to calculate gas-hydrate quantity, made nondestructive measurements (X-ray imaging, *P*-wave velocity, gamma density) at *in situ* pressures and during depressurization to examine gas-hydrate habit within sediments, and archived gas-hydrate-bearing sediments at *in situ* pressures for more comprehensive investigations on shore.

The BSR at Site NGHP-01-17, located in the Andaman Sea, had an estimated depth of 609 mbsf, which was extremely deep compared to other sites drilled on this expedition. There was no LWD data for this site. A specific objective at Site NGHP-01-17 was to determine whether or not the BSR was a gas-hydrate-related feature.

Pressure Core Operations and Measurements

Pressure coring tools were deployed ten times at Site NGHP-01-17 (table 21); four PCS cores, three FPC cores, and three HRC cores. Figures 33 and 34 show the pressure and temperature history of the cores during deployment, coring, recovery, and chilling (in the ice shuck) of the pressure coring tools. Figures 35 and 36 show the measurements made on the six successful cores at full pressure and during depressurization. Figures 37 and 38 show the gas and fluid released from the successful cores and the character of the pressure decrease during depressurization.

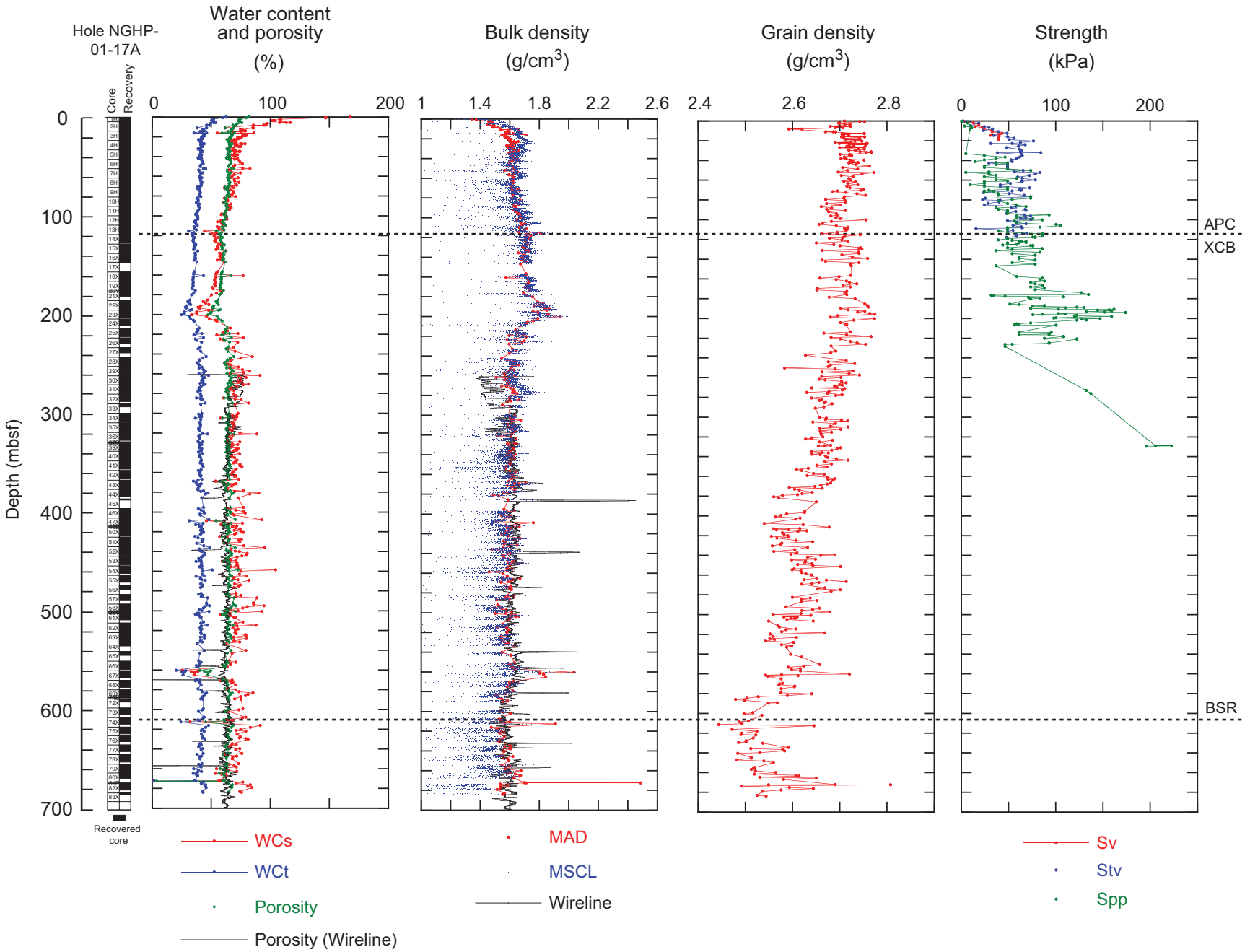


Figure 27. Profiles of core recovery, index, and strength properties for Hole NGHP-01-17A.

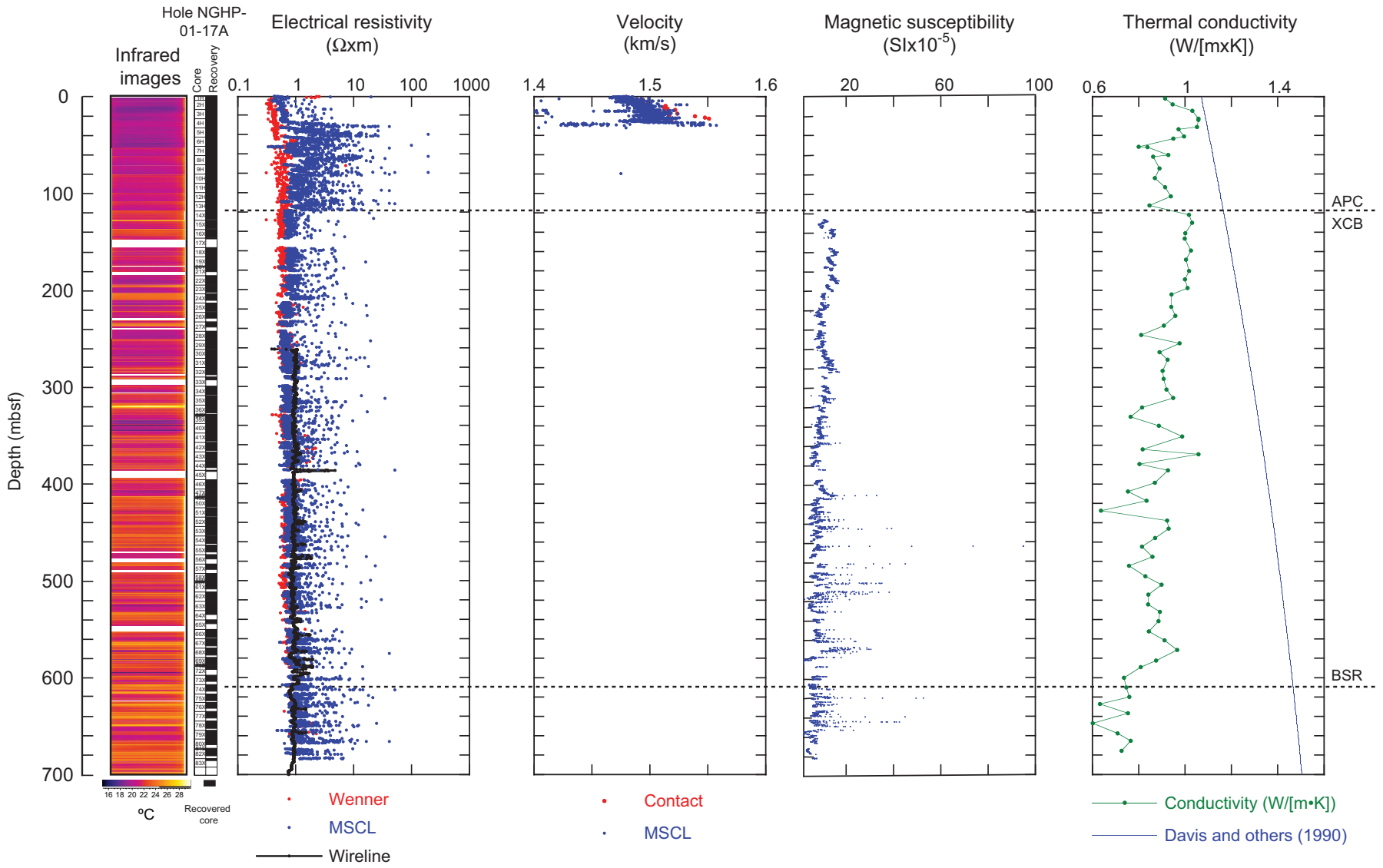


Figure 28. Profiles of infrared images, core recovery, electrical resistivity, acoustic *P*-wave velocity, magnetic susceptibility, and thermal conductivity for Hole NGHP-01-17A.

Table 13. Moisture and density (MAD) physical properties for Hole NGHP-01-17A. (To view the complete table, please see the ASCII files.)

Core, section	Depth, int, from (cm)	Depth, int, to (cm)	Depth (mbsf)	WCt (%)	WCs (%)	Grain density (g/cm³)	Bulk density (g/cm³)	Dry bulk density (g/cm³)	Porosity (%)	Void ratio	Unit weight (kN/m³)
NGHP-01-17A											
1H-1	17	19	0.17	62.65	167.76	2.71	1.34	0.50	82.03	4.57	13.16
1H-1	79	81	0.79	59.54	147.14	2.75	1.37	0.56	79.80	3.95	13.48
1H-1	79	81	0.79	59.51	146.98	2.75	1.37	0.56	79.78	3.95	13.48
1H-1	82	84	0.82	59.49	146.85	2.74	1.37	0.56	79.71	3.93	13.47
1H-2	78	79	2.28	52.14	108.95	2.70	1.46	0.70	74.14	2.87	14.30
1H-2	78	79	2.28	51.94	108.07	2.70	1.46	0.70	73.99	2.84	14.32
1H-2	82	83	2.32	51.99	108.30	2.70	1.47	0.71	74.64	2.94	14.43
1H-3	57	58	3.57	50.47	101.89	2.72	1.48	0.73	73.01	2.70	14.54
1H-3	57	58	3.57	51.00	104.09	2.72	1.48	0.72	73.43	2.76	14.47
1H-3	59	61	3.59	50.83	103.37	2.71	1.48	0.73	73.21	2.73	14.48
2H-1	114	116	5.64	53.92	117.00	2.68	1.45	0.67	76.12	3.19	14.19
2H-1	114	116	5.64	53.21	113.71	2.68	1.46	0.68	75.59	3.10	14.28
2H-1	117	119	5.67	51.93	108.02	2.72	1.46	0.70	74.15	2.87	14.36
2H-2	85	87	6.85	49.30	97.25	2.69	1.49	0.76	71.85	2.55	14.65
2H-2	85	87	6.85	49.30	97.23	2.69	1.49	0.76	71.85	2.55	14.65
2H-2	88	90	6.88	49.37	97.53	2.71	1.50	0.76	72.03	2.58	14.67
2H-3	77	79	8.27	48.55	94.38	2.62	1.49	0.77	70.64	2.41	14.63
2H-3	77	79	8.27	48.95	95.89	2.62	1.49	0.76	70.97	2.44	14.58
2H-3	80	82	8.30	46.22	85.94	2.59	1.52	0.82	68.48	2.17	14.90
2H-5	68	70	11.18	38.25	61.94	2.69	1.66	1.02	61.88	1.62	16.26
2H-5	68	70	11.18	46.22	85.94	2.69	1.54	0.83	69.29	2.26	15.07
2H-5	71	73	11.21	46.01	85.23	2.67	1.54	0.83	68.94	2.22	15.06
2H-6	68	70	12.68	43.26	76.24	2.75	1.59	0.90	67.18	2.05	15.61
2H-6	68	70	12.68	42.84	74.96	2.75	1.60	0.91	66.80	2.01	15.68
2H-6	71	73	12.71	43.12	75.80	2.71	1.59	0.90	66.67	2.00	15.54
2H-7	45	47	13.95	43.48	76.93	2.72	1.58	0.89	67.11	2.04	15.52
2H-7	45	47	13.95	44.16	79.09	2.72	1.57	0.88	67.72	2.10	15.42
2H-7	48	50	13.98	43.85	78.10	2.70	1.57	0.88	67.33	2.06	15.44
3H-1	80	82	14.80	42.87	75.05	2.71	1.59	0.91	66.46	1.98	15.59
3H-1	83	85	14.83	40.65	68.49	2.71	1.62	0.96	64.40	1.81	15.93
3H-2	57	59	16.07	35.51	55.06	2.70	1.71	1.10	59.22	1.45	16.77
3H-2	60	62	16.10	46.31	86.26	2.75	1.55	0.83	69.85	2.32	15.16
3H-3	82	84	17.82	44.17	79.11	2.71	1.57	0.88	67.64	2.09	15.40
3H-3	82	84	17.82	44.38	79.79	2.71	1.57	0.87	67.83	2.11	15.37
3H-3	85	87	17.85	44.21	79.24	2.74	1.58	0.88	67.95	2.12	15.45
3H-4	52	54	19.02	43.35	76.52	2.74	1.59	0.90	67.16	2.04	15.58
3H-4	52	54	19.02	43.83	78.03	2.74	1.58	0.89	67.59	2.09	15.50
3H-4	55	57	19.05	44.30	79.53	2.71	1.57	0.87	67.79	2.11	15.39
3H-5	51	53	20.51	42.35	73.46	2.75	1.61	0.93	66.31	1.97	15.74
3H-5	51	53	20.51	42.02	72.46	2.75	1.61	0.93	66.00	1.94	15.79
3H-5	54	56	20.54	43.14	75.86	2.73	1.59	0.90	66.90	2.02	15.59
3H-6	48	50	21.98	42.08	72.65	2.69	1.60	0.93	65.60	1.91	15.67
3H-6	48	50	21.98	41.93	72.22	2.69	1.60	0.93	65.46	1.90	15.69
3H-6	51	53	22.01	42.50	73.92	2.72	1.60	0.92	66.26	1.96	15.67
3H-7	45	47	22.95	39.24	64.58	2.76	1.66	1.01	63.46	1.74	16.26
3H-7	45	47	22.95	40.96	69.37	2.76	1.63	0.96	65.11	1.87	15.98
3H-7	48	80	22.98	41.65	71.39	2.70	1.61	0.94	65.27	1.88	15.75
4H-1	84	86	24.34	40.95	69.35	2.76	1.63	0.96	65.08	1.86	15.98
4H-1	84	86	24.34	40.24	67.35	2.75	1.64	0.98	64.41	1.81	16.09
4H-1	87	89	24.37	40.42	67.85	2.72	1.63	0.97	64.29	1.80	15.99
4H-2	72	74	25.72	41.60	71.23	2.72	1.61	0.94	65.36	1.89	15.80
4H-2	72	74	25.72	41.53	71.04	2.72	1.61	0.94	65.30	1.88	15.81
4H-2	75	77	25.75	41.09	69.74	2.73	1.62	0.96	64.99	1.86	15.90
4H-3	70	72	27.20	44.06	78.76	2.75	1.58	0.88	67.89	2.11	15.49
4H-3	70	72	27.20	43.24	76.17	2.75	1.59	0.90	67.15	2.04	15.61
4H-3	73	75	27.23	42.88	75.08	2.70	1.61	0.92	67.30	2.06	15.78
4H-4	50	52	28.50	41.54	71.06	2.74	1.62	0.95	65.83	1.93	15.93
4H-4	50	52	28.50	41.25	70.21	2.74	1.63	0.96	65.56	1.90	15.98

Table 13. Moisture and density (MAD) physical properties for Hole NGHP-01-17A. (To view the complete table, please see the ASCII files.)—Continued

Core, section	Depth, int, from (cm)	Depth, int, to (cm)	Depth (mbsf)	WCt (%)	WCs (%)	Grain density (g/cm³)	Bulk density (g/cm³)	Dry bulk density (g/cm³)	Porosity (%)	Void ratio	Unit weight (kN/m³)
NGHP-01-17A—Continued											
4H-4	53	55	28.53	41.72	71.59	2.75	1.62	0.94	65.77	1.92	15.85
4H-5	39	41	29.89	42.68	74.46	2.73	1.60	0.92	66.50	1.98	15.66
4H-5	39	41	29.89	42.85	74.97	2.73	1.59	0.91	66.65	2.00	15.64
4H-5	42	44	29.92	42.29	73.28	2.72	1.60	0.92	66.03	1.94	15.70
4H-6	33	35	31.33	40.69	68.60	2.77	1.64	0.97	64.93	1.85	16.04
4H-6	33	35	31.33	40.86	69.09	2.77	1.63	0.97	65.09	1.86	16.02
4H-6	36	38	31.36	40.90	69.20	2.74	1.62	0.96	64.82	1.84	15.93
4H-7	28	30	32.28	39.12	64.25	2.77	1.66	1.01	63.42	1.73	16.30
4H-7	28	30	32.28	39.24	64.57	2.77	1.66	1.01	63.54	1.74	16.28
4H-7	31	33	32.31	39.00	63.95	2.76	1.66	1.01	63.23	1.72	16.30
5H-1	91	93	33.91	41.32	70.42	2.72	1.62	0.95	65.15	1.87	15.85
5H-1	91	93	33.91	40.86	69.09	2.72	1.62	0.96	64.71	1.83	15.92
5H-1	94	96	33.94	41.48	70.88	2.70	1.61	0.94	65.12	1.87	15.78
5H-2	41	43	34.91	42.57	74.12	2.73	1.60	0.92	66.33	1.97	15.67
5H-2	41	43	34.91	42.69	74.50	2.73	1.60	0.91	66.45	1.98	15.65
5H-2	44	46	34.94	42.44	73.72	2.72	1.60	0.92	66.18	1.96	15.68
5H-3	68	70	36.68	41.16	69.97	2.71	1.62	0.95	64.90	1.85	15.85
5H-4	73	75	38.23	41.99	72.38	2.71	1.60	0.93	65.70	1.92	15.73
5H-4	73	75	38.23	41.31	70.38	2.71	1.61	0.95	65.07	1.86	15.84
5H-4	77	79	38.27	40.35	67.65	2.70	1.63	0.97	64.07	1.78	15.96
5H-5	61	63	39.61	41.42	70.70	2.75	1.62	0.95	65.49	1.90	15.90
5H-5	61	63	39.61	41.02	69.56	2.75	1.63	0.96	65.12	1.87	15.96
5H-5	64	66	39.64	41.14	69.90	2.72	1.62	0.95	64.99	1.86	15.88
5H-6	65	67	41.15	39.43	65.09	2.72	1.65	1.00	63.34	1.73	16.15
5H-6	65	67	41.15	39.75	65.99	2.72	1.64	0.99	63.66	1.75	16.10
5H-6	68	70	41.18	38.94	63.78	2.73	1.66	1.01	62.93	1.70	16.25
5H-7	12	14	42.12	39.90	66.38	2.74	1.64	0.99	63.95	1.77	16.11
5H-7	12	14	42.12	39.20	64.47	2.74	1.65	1.01	63.27	1.72	16.23
5H-7	15	17	42.15	41.98	72.35	2.73	1.61	0.93	65.80	1.92	15.76
6H-1	23	25	42.73	41.16	69.94	2.72	1.62	0.95	64.98	1.86	15.87
6H-2	32	34	44.26	42.48	73.84	2.73	1.60	0.92	66.32	1.97	15.70
6H-3	31	33	45.75	42.68	74.47	2.76	1.60	0.92	66.75	2.01	15.72
6H-4	31	33	47.25	43.36	76.56	2.71	1.58	0.90	66.90	2.02	15.51
6H-5	31	33	48.75	41.20	70.08	2.74	1.62	0.95	65.18	1.87	15.90
6H-6	31	33	50.25	40.72	68.69	2.72	1.62	0.96	64.54	1.82	15.94
6H-7	33	34	51.77	43.45	76.85	2.70	1.58	0.89	66.91	2.02	15.48
7H-1	23	25	52.23	45.35	82.97	2.77	1.56	0.85	69.17	2.24	15.34
7H-2	33	35	53.83	39.41	65.04	2.75	1.65	1.00	63.54	1.74	16.21
7H-3	33	35	55.33	40.18	67.16	2.70	1.63	0.98	63.91	1.77	15.99
7H-4	15	17	56.65	42.83	74.92	2.73	1.59	0.91	66.60	1.99	15.63
7H-5	33	35	58.33	41.01	69.53	2.72	1.62	0.96	64.84	1.84	15.89
7H-6	33	35	59.83	40.39	67.76	2.72	1.63	0.97	64.28	1.80	16.00
7H-7	19	21	61.19	40.08	66.90	2.71	1.63	0.98	63.87	1.77	16.02
8H-1	17	19	61.67	42.13	72.79	2.73	1.61	0.93	66.00	1.94	15.75
8H-2	36	38	63.36	40.99	69.46	2.72	1.62	0.96	64.80	1.84	15.89
8H-3	32	34	64.82	41.11	69.80	2.74	1.62	0.96	65.09	1.86	15.92
8H-4	23	25	66.23	42.40	73.60	2.72	1.60	0.92	66.10	1.95	15.67
8H-5	31	33	67.81	41.44	70.76	2.72	1.61	0.95	65.26	1.88	15.83
8H-6	31	33	69.31	41.73	71.62	2.75	1.62	0.94	65.77	1.92	15.84
8H-7	31	33	70.31	40.47	67.99	2.74	1.63	0.97	64.54	1.82	16.03
8H-8	15	17	71.02	38.12	61.61	2.70	1.66	1.03	61.83	1.62	16.31
9H-1	71	73	71.71	40.73	68.72	2.69	1.62	0.96	64.29	1.80	15.87
9H-2	29	31	72.39	38.08	61.49	2.71	1.67	1.03	61.94	1.63	16.35
9H-3	29	31	73.89	39.84	66.22	2.74	1.64	0.99	63.87	1.77	16.12
9H-4	29	31	75.39	40.74	68.76	2.75	1.63	0.97	64.89	1.85	16.01
9H-5	29	31	76.89	40.89	69.18	2.71	1.62	0.96	64.65	1.83	15.89
9H-6	29	31	78.39	40.36	67.68	2.71	1.63	0.97	64.13	1.79	15.97
9H-7	10	12	79.70	39.75	65.98	2.67	1.63	0.98	63.22	1.72	15.99

Table 13. Moisture and density (MAD) physical properties for Hole NGHP-01-17A. (To view the complete table, please see the ASCII files.)—Continued

Core, section	Depth, int, from (cm)	Depth, int, to (cm)	Depth (mbsf)	WCt (%)	WCs (%)	Grain density (g/cm³)	Bulk density (g/cm³)	Dry bulk density (g/cm³)	Porosity (%)	Void ratio	Unit weight (kN/m³)
NGHP-01-17A—Continued											
10H-1	21	23	80.71	41.40	70.64	2.71	1.61	0.95	65.14	1.87	15.82
10H-2	20	22	82.20	37.94	61.12	2.71	1.67	1.04	61.78	1.62	16.37
10H-3	20	22	83.70	38.97	63.84	2.67	1.64	1.00	62.46	1.66	16.12
10H-4	20	22	85.20	39.09	64.18	2.70	1.65	1.00	62.85	1.69	16.16
10H-5	20	22	86.70	37.54	60.11	2.66	1.66	1.04	60.94	1.56	16.32
10H-6	20	22	88.20	40.06	66.84	2.68	1.63	0.98	63.62	1.75	15.97
10H-7	20	22	89.64	39.12	64.27	2.67	1.64	1.00	62.62	1.68	16.09
11H-1	80	82	90.80	39.46	65.17	2.71	1.64	1.00	63.29	1.72	16.13
11H-2	58	60	92.08	40.10	66.94	2.68	1.63	0.97	63.61	1.75	15.95
11H-3	80	82	93.80	39.59	65.53	2.69	1.64	0.99	63.25	1.72	16.06
11H-4	88	90	95.38	38.44	62.45	2.70	1.66	1.02	62.15	1.64	16.25
11H-5	42	44	96.42	38.39	62.31	2.68	1.65	1.02	61.97	1.63	16.23
11H-6	60	62	98.10	37.15	59.11	2.69	1.68	1.05	60.82	1.55	16.46
11H-7	26	28	98.76	36.92	58.53	2.70	1.68	1.06	60.67	1.54	16.52
12H-1	72	74	100.22	38.55	62.74	2.76	1.67	1.03	62.78	1.69	16.37
12H-2	92	94	101.92	38.64	62.97	2.68	1.65	1.01	62.23	1.65	16.19
12H-3	96	98	103.46	38.79	63.38	2.66	1.64	1.01	62.22	1.65	16.12
12H-4	86	88	104.86	36.88	58.42	2.66	1.67	1.06	60.22	1.51	16.42
12H-5	58	60	106.08	35.64	55.38	2.69	1.70	1.10	59.26	1.45	16.72
12H-6	60	62	107.60	37.03	58.81	2.72	1.69	1.06	60.92	1.56	16.54
12H-7	80	82	108.80	37.41	59.76	2.71	1.68	1.05	61.24	1.58	16.46
13H-1	91	93	109.91	38.19	61.78	2.72	1.67	1.03	62.07	1.64	16.34
13H-2	56	58	111.06	35.50	55.03	2.71	1.71	1.10	59.29	1.46	16.79
13H-3	82	84	112.82	36.18	56.70	2.69	1.70	1.08	59.84	1.49	16.63
13H-4	78	80	114.28	37.69	60.48	2.66	1.66	1.04	61.10	1.57	16.30
13H-5	50	52	115.50	30.78	44.47	2.74	1.81	1.25	54.34	1.19	17.75
13H-6	46	48	116.96	35.19	54.31	2.71	1.72	1.11	58.95	1.44	16.84
13H-7	64	66	118.07	33.61	50.62	2.71	1.74	1.16	57.20	1.34	17.11
14H-1	30	32	118.80	34.82	53.43	2.68	1.72	1.12	58.26	1.40	16.82
14H-2	64	66	120.64	34.42	52.49	2.70	1.73	1.13	58.07	1.38	16.96
14H-3	51	53	122.01	35.97	56.17	2.72	1.71	1.09	59.82	1.49	16.72
14H-4	56	58	123.56	34.90	53.62	2.65	1.71	1.11	58.09	1.39	16.73
14H-5	97	99	125.47	34.66	53.05	2.69	1.72	1.12	58.17	1.39	16.87
14H-6	50	52	126.50	35.03	53.92	2.70	1.72	1.12	58.69	1.42	16.84
15X-1	10	12	128.20	35.94	56.10	2.74	1.71	1.10	60.03	1.50	16.79
15X-2	10	12	129.20	36.93	58.57	2.74	1.69	1.07	61.03	1.57	16.61
15X-3	10	12	129.82	37.03	58.82	2.75	1.69	1.07	61.18	1.58	16.61
15X-4	10	12	131.32	35.56	55.18	2.66	1.70	1.09	58.91	1.43	16.66
15X-5	10	12	132.82	35.96	56.15	2.74	1.71	1.10	60.01	1.50	16.78
15X-6	10	12	134.32	35.13	54.15	2.74	1.73	1.12	59.15	1.45	16.93
15X-7	10	12	135.82	38.49	62.57	2.70	1.66	1.02	62.28	1.65	16.27
16X-1	16	18	137.86	36.34	57.09	2.73	1.70	1.08	60.30	1.52	16.68
16X-2	16	18	139.36	36.68	57.94	2.76	1.70	1.08	60.93	1.56	16.70
16X-3	16	18	140.86	36.45	57.36	2.66	1.68	1.07	59.84	1.49	16.50
16X-4	16	18	142.36	36.61	57.76	2.67	1.68	1.07	60.07	1.50	16.49
16X-5	16	18	143.70	36.67	57.90	2.74	1.70	1.08	60.75	1.55	16.66
16X-6	16	18	145.05	35.55	55.17	2.72	1.71	1.10	59.35	1.46	16.78
17X-1	19	21	146.79	37.97	61.20	2.72	1.67	1.04	61.93	1.63	16.40
18X-1	21	23	156.51	35.80	55.76	2.72	1.71	1.10	59.70	1.48	16.77
18X-2	21	23	157.77	35.33	54.63	2.70	1.71	1.11	58.99	1.44	16.79
18X-3	21	23	159.27	35.03	53.93	2.66	1.71	1.11	58.30	1.40	16.73
18X-4	21	23	160.77	43.53	77.08	2.69	1.58	0.89	66.94	2.02	15.46
18X-5	21	23	162.27	34.86	53.52	2.71	1.72	1.12	58.63	1.42	16.91
18X-6	21	23	163.52	34.74	53.22	2.72	1.73	1.13	58.55	1.41	16.95
18X-7	21	23	165.02	34.55	52.78	2.74	1.74	1.14	58.48	1.41	17.02
19X-2	32	34	166.65	34.78	53.34	2.71	1.72	1.12	58.47	1.41	16.90
19X-3	32	34	168.15	34.79	53.34	2.72	1.73	1.13	58.62	1.42	16.94
19X-4	32	34	169.65	34.49	52.64	2.65	1.71	1.12	57.67	1.36	16.81

Table 13. Moisture and density (MAD) physical properties for Hole NGHP-01-17A. (To view the complete table, please see the ASCII files.)—Continued

Core, section	Depth, int, from (cm)	Depth, int, to (cm)	Depth (mbsf)	WCt (%)	WCs (%)	Grain density (g/cm³)	Bulk density (g/cm³)	Dry bulk density (g/cm³)	Porosity (%)	Void ratio	Unit weight (kN/m³)
NGHP-01-17A—Continued											
19X-5	32	34	171.15	34.90	53.60	2.65	1.71	1.11	58.10	1.39	16.74
19X-6	32	34	172.65	33.74	50.93	2.71	1.74	1.16	57.42	1.35	17.11
19X-7	32	34	174.15	34.10	51.75	2.71	1.74	1.14	57.78	1.37	17.03
20Y-1	40	42	175.90	36.60	57.74	2.72	1.69	1.07	60.46	1.53	16.61
21X-2	54	56	178.54	35.28	54.51	2.68	1.71	1.10	58.74	1.42	16.74
21X-3	68	70	180.18	33.44	50.24	2.73	1.76	1.17	57.25	1.34	17.21
22X-1	24	26	185.44	31.90	46.85	2.75	1.79	1.22	55.72	1.26	17.56
22X-2	40	42	187.00	30.22	43.31	2.76	1.83	1.27	53.82	1.17	17.90
22X-3	38	40	188.48	31.22	45.40	2.76	1.81	1.24	55.01	1.22	17.71
22X-4	27	29	189.87	32.49	48.13	2.70	1.76	1.19	55.92	1.27	17.30
22X-5	29	31	191.39	29.12	41.09	2.72	1.84	1.30	52.14	1.09	18.00
22X-6	34	36	192.73	28.03	38.95	2.75	1.87	1.35	51.12	1.05	18.33
22X-7	22	24	193.61	28.65	40.15	2.74	1.85	1.32	51.75	1.07	18.16
23X-1	21	23	195.11	33.71	50.85	2.76	1.76	1.17	57.82	1.37	17.25
23X-2	21	23	195.89	32.32	47.74	2.77	1.79	1.21	56.37	1.29	17.54
23X-3	17	19	197.35	27.42	37.78	2.70	1.86	1.35	49.83	0.99	18.27
23X-4	22	24	198.90	27.47	37.88	2.68	1.86	1.35	49.76	0.99	18.21
23X-5	25	27	200.33	25.02	33.37	2.77	1.94	1.46	47.45	0.90	19.07
23X-6	21	23	201.79	31.57	46.14	2.73	1.79	1.22	55.13	1.23	17.55
24X-2	25	27	204.30	32.65	48.48	2.70	1.76	1.19	56.09	1.28	17.27
24X-3	40	42	205.95	34.90	53.61	2.72	1.72	1.12	58.67	1.42	16.90
24X-4	21	23	206.76	35.48	54.98	2.71	1.71	1.11	59.27	1.45	16.80
25X-1	39	41	213.89	39.83	66.19	2.72	1.64	0.99	63.75	1.76	16.09
25X-2	11	13	215.11	38.41	62.37	2.67	1.65	1.02	61.87	1.62	16.19
25X-3	10	12	216.60	38.99	63.90	2.71	1.65	1.01	62.86	1.69	16.21
25X-4	41	43	218.41	37.42	59.79	2.77	1.69	1.06	61.74	1.61	16.59
25X-5	24	26	219.34	42.06	72.60	2.68	1.60	0.93	65.51	1.90	15.66
25X-6	14	16	220.74	35.41	54.83	2.70	1.71	1.10	59.09	1.44	16.78
26X-1	31	33	223.41	43.52	77.06	2.72	1.58	0.89	67.17	2.05	15.52
26X-2	30	32	224.90	36.57	57.66	2.74	1.70	1.08	60.62	1.54	16.66
26X-3	21	23	226.31	37.73	60.60	2.75	1.68	1.05	61.95	1.63	16.51
26X-4	57	59	228.03	42.02	72.47	2.68	1.60	0.93	65.47	1.90	15.66
27X-1	40	42	233.20	40.77	68.82	2.69	1.62	0.96	64.38	1.81	15.88
27X-2	54	56	234.84	38.97	63.85	2.68	1.65	1.00	62.54	1.67	16.14
27X-4	31	33	237.41	41.20	70.07	2.63	1.60	0.94	64.23	1.80	15.67
28X-1	16	18	242.66	45.89	84.81	2.71	1.55	0.84	69.18	2.25	15.16
28X-2	18	20	244.18	42.94	75.25	2.68	1.58	0.90	66.26	1.96	15.52
28X-3	38	40	245.88	40.20	67.21	2.73	1.64	0.98	64.17	1.79	16.05
28X-4	26	28	247.26	39.88	66.32	2.68	1.63	0.98	63.42	1.73	15.99
28X-5	42	44	248.92	37.93	61.11	2.68	1.66	1.03	61.47	1.60	16.29
28X-6	40	42	250.40	39.20	64.47	2.58	1.62	0.98	61.90	1.62	15.88
28X-7	20	22	251.20	39.90	66.39	2.69	1.61	0.97	62.85	1.69	15.84
29X-2	36	38	253.34	42.21	73.05	2.73	1.60	0.93	66.04	1.94	15.73
29X-3	26	28	254.30	39.76	65.99	2.66	1.63	0.98	63.15	1.71	15.97
29X-4	30	32	255.84	43.37	76.58	2.72	1.59	0.90	67.44	2.07	15.63
29X-5	36	38	257.40	45.23	82.57	2.74	1.56	0.85	68.83	2.21	15.30
29X-6	30	32	258.84	43.69	77.58	2.66	1.57	0.88	66.82	2.01	15.38
29X-7	30	32	259.84	39.74	65.96	2.70	1.64	0.99	63.49	1.74	16.06
30X-1	33	35	261.73	47.76	91.43	2.66	1.51	0.79	70.32	2.37	14.80
30X-2	37	39	262.47	42.14	72.83	2.67	1.59	0.92	65.47	1.90	15.62
30X-3	23	25	263.83	44.30	79.55	2.70	1.57	0.87	67.72	2.10	15.37
30X-4	22	24	265.32	43.02	75.49	2.71	1.59	0.91	66.65	2.00	15.58
30X-5	31	33	266.91	42.01	72.45	2.70	1.60	0.93	65.62	1.91	15.70
30X-6	17	19	267.78	43.17	75.98	2.71	1.58	0.90	66.72	2.00	15.54
30x-7	33	35	268.60	42.37	73.53	2.69	1.59	0.92	65.85	1.93	15.62
30X-8	18	20	269.95	40.58	68.31	2.69	1.62	0.96	64.22	1.80	15.91
31X-1	16	18	270.46	45.00	81.81	2.64	1.55	0.85	67.84	2.11	15.16
31X-2	21	23	271.19	43.53	77.07	2.71	1.58	0.89	67.08	2.04	15.49

Table 13. Moisture and density (MAD) physical properties for Hole NGHP-01-17A. (To view the complete table, please see the ASCII files.)—Continued

Core, section	Depth, int, from (cm)	Depth, int, to (cm)	Depth (mbsf)	WCt (%)	WCs (%)	Grain density (g/cm³)	Bulk density (g/cm³)	Dry bulk density (g/cm³)	Porosity (%)	Void ratio	Unit weight (kN/m³)
NGHP-01-17A—Continued											
31X-3	25	27	272.58	41.72	71.58	2.71	1.61	0.94	65.38	1.89	15.76
31X-4	26	29	274.09	40.27	67.41	2.68	1.62	0.97	63.78	1.76	15.92
31X-5	26	28	275.09	39.70	65.85	2.63	1.62	0.98	62.82	1.69	15.91
31X-6	26	28	275.94	39.67	65.76	2.67	1.63	0.98	63.17	1.71	16.01
31X-7	18	20	277.36	40.93	69.30	2.71	1.62	0.96	64.65	1.83	15.88
31X-8	26	28	278.21	38.79	63.36	2.69	1.65	1.01	62.46	1.66	16.19
32X-1	74	76	280.64	40.90	69.20	2.64	1.61	0.95	64.06	1.78	15.75
32X-2	98	100	282.38	41.64	71.34	2.66	1.60	0.93	64.94	1.85	15.68
32X-3	21	23	283.11	41.55	71.08	2.66	1.60	0.93	64.82	1.84	15.69
32X-4	32	34	284.59	37.64	60.37	2.67	1.66	1.04	61.12	1.57	16.32
32X-5	37	39	285.64	41.27	70.26	2.67	1.61	0.94	64.64	1.83	15.75
32X-6	26	28	286.54	42.95	75.27	2.68	1.58	0.90	66.33	1.97	15.53
33X-1	21	23	289.81	44.95	81.67	2.67	1.55	0.85	67.99	2.12	15.21
33X-2	17	19	291.03	41.24	70.17	2.65	1.60	0.94	64.45	1.81	15.71
34X-1	101	103	300.21	42.14	72.83	2.66	1.59	0.92	65.37	1.89	15.60
34X-2	28	30	300.98	39.35	64.87	2.67	1.64	0.99	62.83	1.69	16.06
34X-3	18	20	302.38	40.61	68.38	2.67	1.62	0.96	64.04	1.78	15.85
34X-3	56	58	302.76	41.73	71.63	2.70	1.61	0.94	65.39	1.89	15.75
34X-4	11	13	303.81	40.67	68.54	2.70	1.62	0.96	64.38	1.81	15.92
34X-4	11	13	303.81	41.77	71.72	2.72	1.61	0.94	65.52	1.90	15.77
34X-5	19	21	305.03	36.65	57.85	2.64	1.67	1.06	59.87	1.49	16.42
34X-6	28	30	306.53	41.27	70.28	2.69	1.61	0.95	64.85	1.84	15.80
35X-1	61	63	309.41	40.35	67.66	2.68	1.59	0.95	62.45	1.66	15.56
35X-2	61	63	310.13	40.80	68.93	2.72	1.62	0.96	64.63	1.83	15.92
35X-3	26	28	311.28	40.92	69.25	2.66	1.61	0.95	64.22	1.80	15.78
35X-4	19	21	312.35	40.99	69.47	2.70	1.62	0.95	64.68	1.83	15.86
35X-5	34	36	314.00	40.77	68.84	2.66	1.61	0.95	64.10	1.79	15.81
35X-6	21	23	315.37	39.45	65.15	2.68	1.64	0.99	63.03	1.70	16.06
35X-7	28	30	316.68	39.50	65.28	2.66	1.63	0.99	62.88	1.69	16.01
35X-8	16	18	317.55	40.39	67.77	2.66	1.62	0.96	63.75	1.76	15.87
36X-2	62	64	320.01	42.74	74.63	2.66	1.58	0.91	65.98	1.94	15.52
36X-3	26	28	321.15	47.01	88.73	2.64	1.52	0.80	69.56	2.29	14.88
36X-4	34	36	322.18	40.57	68.28	2.63	1.61	0.96	63.64	1.75	15.77
36X-5	34	36	323.61	39.36	64.92	2.68	1.64	0.99	62.96	1.70	16.08
36X-6	39	41	325.16	40.16	67.10	2.66	1.62	0.97	63.49	1.74	15.90
37P-1	56	58	328.56	38.93	63.73	2.68	1.65	1.01	62.50	1.67	16.14
38Y-1	12	14	329.12	42.65	74.36	2.67	1.58	0.91	65.93	1.93	15.54
38Y-1	32	34	329.32	39.23	64.55	2.65	1.64	0.99	62.57	1.67	16.03
39X-1	113	115	331.13	40.44	67.89	2.70	1.63	0.97	64.15	1.79	15.95
39X-2	30	32	331.80	42.01	72.43	2.69	1.60	0.93	65.56	1.90	15.69
39X-3	58	60	333.58	40.37	67.71	2.68	1.62	0.97	63.93	1.77	15.92
39X-4	26	28	334.76	39.83	66.20	2.64	1.62	0.98	63.03	1.71	15.91
39X-6	4	6	335.82	42.11	72.74	2.66	1.59	0.92	65.38	1.89	15.61
39X-7	22	24	336.33	41.52	71.01	2.68	1.60	0.94	64.95	1.85	15.73
40X-1	10	12	337.70	41.75	71.66	2.64	1.60	0.93	65.02	1.86	15.66
40X-2	10	12	338.03	40.92	69.27	2.66	1.61	0.95	64.24	1.80	15.78
40X-3	11	15	339.54	39.25	64.61	2.67	1.64	1.00	62.73	1.68	16.07
40X-4	11	13	340.95	42.58	74.15	2.67	1.59	0.91	65.92	1.93	15.57
40X-5	12	14	342.40	40.34	67.62	2.69	1.63	0.97	63.98	1.78	15.95
40X-6	12	14	343.80	40.22	67.29	2.72	1.63	0.98	64.08	1.78	16.02
40X-7	11	13	344.79	41.05	69.63	2.67	1.61	0.95	64.44	1.81	15.78
41X-1	14	16	347.44	41.86	72.00	2.68	1.60	0.93	65.33	1.88	15.69
41X-2	14	16	348.94	41.38	70.58	2.65	1.60	0.94	64.61	1.83	15.70
41X-3	17	19	350.47	40.78	68.86	2.67	1.61	0.96	64.23	1.80	15.83
41X-4	16	18	351.96	42.74	74.65	2.63	1.58	0.90	65.73	1.92	15.46
41X-5	13	15	353.04	42.63	74.31	2.61	1.57	0.90	65.40	1.89	15.42
41X-6	8	10	354.15	43.27	76.28	2.62	1.57	0.89	66.09	1.95	15.35

Table 13. Moisture and density (MAD) physical properties for Hole NGHP-01-17A. (To view the complete table, please see the ASCII files.)—Continued

Core, section	Depth, int, from (cm)	Depth, int, to (cm)	Depth (mbsf)	WCt (%)	WCs (%)	Grain density (g/cm³)	Bulk density (g/cm³)	Dry bulk density (g/cm³)	Porosity (%)	Void ratio	Unit weight (kN/m³)
NGHP-01-17A—Continued											
42X-1	15	17	357.15	41.43	70.75	2.64	1.60	0.94	64.60	1.82	15.67
42X-2	18	20	357.97	39.07	64.14	2.67	1.64	1.00	62.52	1.67	16.09
42X-3	4	6	359.33	40.82	68.97	2.63	1.60	0.95	63.90	1.77	15.74
42X-4	4	6	360.83	40.45	67.94	2.67	1.62	0.96	63.92	1.77	15.89
42X-5	10	12	362.39	40.29	67.47	2.69	1.63	0.97	63.90	1.77	15.95
42X-6	8	10	363.37	41.48	70.87	2.68	1.60	0.94	64.91	1.85	15.73
42X-7	4	6	363.99	41.12	69.84	2.69	1.61	0.95	64.66	1.83	15.81
43X-1	18	20	366.98	42.31	73.33	2.68	1.59	0.92	65.73	1.92	15.62
43X-2	3	5	367.83	38.97	63.84	2.67	1.63	0.99	61.92	1.63	15.98
43X-3	18	20	368.88	34.91	53.64	2.66	1.71	1.11	58.19	1.39	16.76
43X-4	16	18	370.36	37.35	59.62	2.65	1.66	1.04	60.62	1.54	16.32
43X-5	15	17	371.35	41.59	71.19	2.59	1.59	0.93	64.30	1.80	15.54
43X-6	4	6	372.07	40.94	69.31	2.66	1.61	0.95	64.29	1.80	15.79
43X-7	10	12	372.98	38.73	63.22	2.60	1.63	1.00	61.63	1.61	16.00
43X-8	6	8	373.93	40.33	67.58	2.61	1.61	0.96	63.28	1.72	15.78
44X-1	14	16	376.24	38.95	63.81	2.64	1.64	1.00	62.19	1.64	16.05
44X-2	8	10	377.68	38.84	63.49	2.62	1.63	1.00	61.87	1.62	16.02
44X-3	4	6	378.64	43.64	77.42	2.61	1.56	0.88	66.35	1.97	15.29
44X-4	5	7	379.31	41.18	70.02	2.58	1.59	0.93	63.79	1.76	15.57
44X-5	7	9	380.83	47.48	90.41	2.56	1.49	0.78	68.96	2.22	14.60
44X-6	12	14	381.88	45.29	82.77	2.57	1.53	0.84	67.49	2.08	14.98
45X-1	17	19	385.87	42.15	72.86	2.65	1.59	0.92	65.32	1.88	15.58
46X-1	9	11	395.49	43.59	77.26	2.63	1.56	0.88	66.43	1.98	15.32
46X-2	9	11	396.73	39.17	64.38	2.63	1.63	0.99	62.25	1.65	15.98
46X-3	6	8	398.20	41.43	70.75	2.59	1.58	0.93	63.99	1.78	15.53
46X-4	6	8	399.70	43.62	77.37	2.58	1.55	0.87	66.03	1.94	15.22
46X-5	9	11	401.23	44.12	78.94	2.56	1.54	0.86	66.38	1.97	15.13
46X-6	3	5	402.14	40.52	68.11	2.62	1.61	0.96	63.48	1.74	15.75
46X-7	10	12	403.21	41.01	69.53	2.61	1.60	0.94	63.87	1.77	15.66
47X-3	24	26	407.84	48.11	92.71	2.54	1.51	0.78	70.76	2.42	14.79
47X-4	21	23	409.01	31.48	45.95	2.62	1.76	1.21	54.03	1.18	17.25
47X-6	17	19	411.50	43.35	76.51	2.68	1.58	0.89	66.65	2.00	15.46
47X-7	18	20	413.01	36.83	58.31	2.62	1.66	1.05	59.80	1.49	16.32
48P-1	34	36	413.04	39.35	64.89	2.56	1.61	0.98	61.84	1.62	15.80
49E-1	30	32	414.00	41.75	71.69	2.59	1.58	0.92	64.45	1.81	15.52
49E-1	61	63	414.31	40.58	68.30	2.57	1.59	0.95	63.10	1.71	15.63
50X-1	54	56	415.24	40.41	67.82	2.63	1.61	0.96	63.50	1.74	15.80
50X-2	21	23	415.91	41.54	71.06	2.61	1.59	0.93	64.41	1.81	15.59
50X-3	50	52	417.20	42.70	74.53	2.58	1.57	0.90	65.21	1.87	15.35
50X-4	34	36	418.54	41.07	69.69	2.58	1.59	0.94	63.70	1.76	15.59
50X-5	30	32	420.00	42.99	75.40	2.59	1.56	0.89	65.58	1.91	15.34
50X-6	24	26	420.73	43.60	77.32	2.56	1.55	0.87	65.84	1.93	15.18
50X-7	22	24	421.58	41.66	71.42	2.59	1.58	0.92	64.36	1.81	15.53
50X-8	22	24	422.63	41.11	69.81	2.57	1.59	0.93	63.61	1.75	15.56
51X-1	58	60	424.88	36.34	57.08	2.61	1.67	1.06	59.21	1.45	16.38
51X-2	49	51	426.22	38.97	63.85	2.64	1.64	1.00	62.20	1.65	16.05
51X-3	50	52	427.73	43.09	75.73	2.58	1.56	0.89	65.57	1.90	15.30
51X-4	28	30	428.70	42.26	73.18	2.57	1.57	0.91	64.76	1.84	15.41
51X-5	50	52	430.42	42.61	74.26	2.56	1.56	0.90	64.94	1.85	15.32
51X-6	41	43	431.83	37.85	60.91	2.63	1.65	1.03	60.99	1.56	16.20
52X-1	31	33	434.31	43.75	77.77	2.60	1.56	0.88	66.40	1.98	15.26
52X-2	54	56	436.04	48.79	95.26	2.56	1.48	0.76	70.41	2.38	14.51
52X-3	54	56	437.54	40.09	66.92	2.61	1.61	0.97	63.01	1.70	15.80
52X-4	45	47	438.95	40.09	66.91	2.60	1.61	0.96	62.89	1.69	15.77
52X-5	9	11	439.59	41.32	70.42	2.69	1.61	0.94	64.89	1.85	15.79
52X-6	5	7	440.12	42.52	73.97	2.66	1.59	0.91	65.74	1.92	15.55
52X-7	47	49	442.04	44.60	80.51	2.63	1.55	0.86	67.39	2.07	15.19

Table 13. Moisture and density (MAD) physical properties for Hole NGHP-01-17A. (To view the complete table, please see the ASCII files.)—Continued

Core, section	Depth, int, from (cm)	Depth, int, to (cm)	Depth (mbsf)	WCt (%)	WCs (%)	Grain density (g/cm³)	Bulk density (g/cm³)	Dry bulk density (g/cm³)	Porosity (%)	Void ratio	Unit weight (kN/m³)
NGHP-01-17A—Continued											
53X-1	29	31	443.99	44.32	79.60	2.65	1.56	0.87	67.28	2.06	15.26
53X-2	47	49	444.73	43.21	76.09	2.60	1.56	0.89	65.85	1.93	15.32
53X-3	29	31	445.64	41.90	72.11	2.63	1.59	0.92	64.89	1.85	15.57
53X-4	36	38	447.21	39.49	65.26	2.63	1.62	0.98	62.57	1.67	15.93
53X-5	34	36	448.52	40.02	66.73	2.64	1.62	0.97	63.23	1.72	15.88
53X-6	14	16	449.32	41.51	70.98	2.61	1.59	0.93	64.38	1.81	15.59
53X-7	33	35	450.13	37.27	59.40	2.64	1.66	1.04	60.50	1.53	16.32
53X-8	10	12	451.40	41.88	72.07	2.70	1.60	0.93	65.53	1.90	15.73
54X-1	34	36	453.74	41.58	71.19	2.60	1.59	0.93	64.38	1.81	15.57
54X-2	57	59	454.56	42.05	72.56	2.60	1.58	0.92	64.79	1.84	15.49
54X-3	44	46	455.72	40.00	66.66	2.62	1.61	0.97	62.99	1.70	15.83
54X-4	83	85	457.57	42.15	72.88	2.62	1.58	0.92	65.06	1.86	15.52
54X-5	55	57	458.79	51.10	104.51	2.63	1.46	0.71	72.82	2.68	14.33
54X-6	17	19	459.91	42.91	75.16	2.64	1.55	0.89	65.06	1.86	15.24
55X-1	17	19	463.17	42.54	74.02	2.65	1.58	0.91	65.69	1.91	15.53
55X-3	23	25	464.80	44.48	80.12	2.62	1.55	0.86	67.23	2.05	15.19
55X-4	23	25	465.12	37.36	59.63	2.67	1.67	1.05	60.85	1.55	16.38
55X-5	22	24	466.61	40.99	69.48	2.71	1.62	0.96	64.78	1.84	15.89
55X-6	14	16	467.60	40.90	69.22	2.66	1.61	0.95	64.20	1.79	15.78
55X-7	19	21	468.65	42.08	72.65	2.64	1.59	0.92	65.18	1.87	15.57
55X-8	11	13	469.23	45.05	81.97	2.62	1.54	0.85	67.68	2.09	15.11
56X-1	32	34	473.02	41.10	69.77	2.67	1.61	0.95	64.49	1.82	15.78
56X-2	29	31	473.99	42.77	74.72	2.65	1.58	0.90	65.91	1.93	15.49
56X-3	20	22	474.89	42.34	73.42	2.70	1.60	0.92	65.92	1.93	15.65
56X-4	31	33	476.50	40.99	69.46	2.68	1.61	0.95	64.50	1.82	15.82
57X-1	18	20	482.58	41.64	71.36	2.60	1.59	0.93	64.41	1.81	15.55
57X-2	49	51	483.28	39.47	65.22	2.64	1.63	0.98	62.66	1.68	15.96
57X-3	33	35	484.51	43.02	75.50	2.62	1.57	0.89	65.85	1.93	15.39
57X-4	33	35	486.01	41.58	71.19	2.65	1.60	0.93	64.81	1.84	15.67
57X-5	44	46	487.12	47.05	88.86	2.62	1.51	0.80	69.42	2.27	14.83
58X-1	33	35	492.33	46.15	85.71	2.59	1.52	0.82	68.37	2.16	14.89
58X-2	35	37	493.63	46.24	86.00	2.66	1.53	0.82	69.03	2.23	15.01
58X-3	26	28	495.04	48.66	94.78	2.64	1.49	0.77	70.96	2.44	14.66
58X-4	28	28	496.06	44.61	80.54	2.62	1.55	0.86	67.30	2.06	15.17
58X-5	26	28	497.49	43.45	76.84	2.68	1.58	0.89	66.75	2.01	15.45
58X-6	28	30	499.01	39.93	66.47	2.62	1.62	0.97	62.91	1.70	15.84
59P-1	47	49	500.07	42.11	72.75	2.56	1.57	0.91	64.49	1.82	15.40
60Y-1	23	24	500.83	48.14	92.83	2.64	1.50	0.78	70.50	2.39	14.72
61X-2	20	22	502.51	39.72	65.88	2.58	1.61	0.97	62.56	1.67	15.83
61X-2	31	32	502.62	38.34	62.18	2.61	1.64	1.01	61.29	1.58	16.07
61X-3	20	22	503.68	36.60	57.74	2.60	1.66	1.05	59.39	1.46	16.31
61X-3	46	48	503.94	37.82	60.82	2.60	1.65	1.02	60.71	1.55	16.14
61X-4	14	16	505.12	39.82	66.17	2.59	1.61	0.97	62.56	1.67	15.79
61X-5	15	17	506.63	41.48	70.88	2.64	1.60	0.93	64.64	1.83	15.67
61X-5	15	17	506.63	40.97	69.39	2.55	1.58	0.94	63.31	1.73	15.54
62X-1	34	36	511.54	43.50	76.98	2.57	1.55	0.88	65.86	1.93	15.22
62X-2	54	56	512.78	41.36	70.53	2.57	1.58	0.93	63.89	1.77	15.53
62X-3	103	105	514.65	46.79	87.94	2.61	1.51	0.81	69.10	2.24	14.85
62X-4	34	36	515.45	41.83	71.90	2.59	1.58	0.92	64.46	1.81	15.49
62X-5	69	71	517.30	40.62	68.40	2.58	1.60	0.95	63.23	1.72	15.65
62X-6	57	59	518.68	42.14	72.84	2.67	1.59	0.92	65.46	1.90	15.62
62X-7	52	54	519.63	41.39	70.62	2.55	1.58	0.93	63.75	1.76	15.48
63X-2	45	47	522.18	41.22	70.12	2.56	1.58	0.93	63.63	1.75	15.52
63X-3	12	14	523.35	41.64	71.35	2.61	1.59	0.93	64.48	1.82	15.57
63X-4	27	29	524.50	44.20	79.21	2.55	1.54	0.86	66.35	1.97	15.09
63X-5	21	23	525.26	44.28	79.48	2.56	1.54	0.86	66.51	1.99	15.10
63X-6	21	23	526.76	40.86	69.10	2.54	1.58	0.94	63.16	1.71	15.54

Table 13. Moisture and density (MAD) physical properties for Hole NGHP-01-17A. (To view the complete table, please see the ASCII files.)—Continued

Core, section	Depth, int, from (cm)	Depth, int, to (cm)	Depth (mbsf)	WCt (%)	WCs (%)	Grain density (g/cm³)	Bulk density (g/cm³)	Dry bulk density (g/cm³)	Porosity (%)	Void ratio	Unit weight (kN/m³)
NGHP-01-17A—Continued											
63X-7	14	16	528.19	44.39	79.82	2.60	1.55	0.86	66.95	2.03	15.16
64X-1	26	28	530.56	40.95	69.34	2.58	1.59	0.94	63.54	1.74	15.60
64X-2	52	53	531.89	42.60	74.21	2.60	1.57	0.90	65.29	1.88	15.41
64X-3	27	29	533.14	38.38	62.29	2.59	1.63	1.01	61.13	1.57	16.01
65X-1	29	31	540.29	44.26	79.42	2.60	1.55	0.86	66.79	2.01	15.17
65X-3	19	21	543.09	40.37	67.69	2.62	1.61	0.96	63.36	1.73	15.78
66X-2	16	18	550.66	39.49	65.27	2.66	1.63	0.99	62.85	1.69	16.00
66X-3	34	36	552.34	41.54	71.07	2.62	1.59	0.93	64.52	1.82	15.61
66X-4	21	23	553.32	39.95	66.52	2.59	1.61	0.97	62.71	1.68	15.78
66X-5	35	37	554.78	39.82	66.18	2.62	1.62	0.97	62.81	1.69	15.86
66X-6	23	25	555.65	37.51	60.02	2.60	1.65	1.03	60.33	1.52	16.17
66X-7	29	31	557.21	38.90	63.66	2.62	1.63	1.00	61.91	1.63	16.00
67X-1	94	96	560.34	20.35	25.55	2.72	2.04	1.62	40.40	0.68	19.96
67X-2	3	5	560.93	28.32	39.51	2.58	1.80	1.29	49.83	0.99	17.69
67X-3	3	5	561.43	27.79	38.49	2.54	1.80	1.30	48.85	0.95	17.67
67X-4	18	20	561.95	24.91	33.18	2.61	1.83	1.37	44.48	0.80	17.95
67X-5	11	13	562.75	26.42	35.91	2.55	1.83	1.35	47.16	0.89	17.95
67X-7	5	7	565.16	26.18	35.47	2.58	1.85	1.36	47.13	0.89	18.10
68X-1	58	60	569.58	38.02	61.35	2.58	1.63	1.01	60.43	1.53	15.98
68X-2	33	35	570.33	40.40	67.79	2.57	1.60	0.95	62.99	1.70	15.67
68X-3	12	14	570.98	36.74	58.09	2.57	1.65	1.05	59.29	1.46	16.22
68X-4	29	31	572.46	40.66	68.51	2.61	1.60	0.95	63.52	1.74	15.71
68X-5	10	12	573.19	40.05	66.79	2.60	1.61	0.97	62.92	1.70	15.80
68X-6	59	61	575.18	41.48	70.88	2.58	1.58	0.93	64.05	1.78	15.52
69X-1	61	63	579.31	38.88	63.63	2.58	1.62	0.99	61.52	1.60	15.91
69X-2	13	15	580.33	41.53	71.02	2.64	1.60	0.93	64.66	1.83	15.65
69X-3	31	33	582.01	42.43	73.72	2.59	1.57	0.90	65.06	1.86	15.41
69X-4	22	24	583.42	46.09	85.48	2.53	1.51	0.81	67.82	2.11	14.80
69X-5	12	14	584.82	44.85	81.33	2.50	1.52	0.84	66.52	1.99	14.91
69X-6	29	31	585.99	44.21	79.25	2.48	1.52	0.85	65.72	1.92	14.94
69X-7	35	37	587.05	42.91	75.15	2.50	1.55	0.88	64.69	1.83	15.16
72X-2	57	59	589.40	41.16	69.95	2.57	1.59	0.93	63.66	1.75	15.55
72X-3	17	19	589.78	42.96	75.32	2.55	1.56	0.89	65.19	1.87	15.26
73X-2	90	92	599.40	43.49	76.96	2.52	1.54	0.87	65.38	1.89	15.11
73X-3	47	49	600.47	42.36	73.50	2.50	1.55	0.89	64.16	1.79	15.23
73X-4	70	72	602.10	39.30	64.75	2.54	1.61	0.97	61.56	1.60	15.75
74X-1	122	124	607.92	44.23	79.31	2.51	1.53	0.85	65.98	1.94	15.00
74X-2	20	22	608.40	43.33	76.47	2.49	1.54	0.87	64.97	1.86	15.07
74X-3	93	97	610.63	38.94	63.78	2.49	1.60	0.98	60.77	1.55	15.69
74X-4	25	27	611.45	40.46	67.95	2.44	1.57	0.93	61.83	1.62	15.36
74X-5	53	55	612.73	24.36	32.20	2.65	1.91	1.44	45.38	0.83	18.73
75X-1	1	3	616.31	47.82	91.64	2.47	1.48	0.77	68.85	2.21	14.47
75X-2	56	58	618.33	45.42	83.22	2.52	1.52	0.83	67.21	2.05	14.88
75X-3	100	102	620.27	42.85	74.97	2.49	1.55	0.88	64.58	1.82	15.15
75X-4	77	79	621.54	41.62	71.30	2.49	1.56	0.91	63.39	1.73	15.31
75X-5	31	33	622.08	44.24	79.35	2.52	1.53	0.85	66.13	1.95	15.03
76X-1	30	32	625.30	41.87	72.03	2.52	1.56	0.91	63.88	1.77	15.34
76X-3	94	96	627.89	42.84	74.95	2.50	1.55	0.88	64.66	1.83	15.17
76X-4	91	93	628.91	42.47	73.81	2.50	1.55	0.89	64.30	1.80	15.22
76X-5	61	63	629.61	44.30	79.55	2.49	1.52	0.85	65.86	1.93	14.94
76X-6	39	41	630.39	44.84	81.28	2.54	1.53	0.84	66.80	2.01	14.98
77X-1	22	24	634.62	40.43	67.88	2.59	1.60	0.95	63.18	1.72	15.71
77X-2	48	50	635.72	41.63	71.31	2.51	1.57	0.91	63.60	1.75	15.36
77X-3	45	47	636.73	39.92	66.44	2.58	1.61	0.97	62.57	1.67	15.76
77X-4	19	21	637.97	39.36	64.90	2.58	1.60	0.97	61.58	1.60	15.73
77X-5	48	52	639.76	42.64	74.33	2.53	1.56	0.89	64.72	1.83	15.26
77X-6	24	26	640.52	41.45	70.80	2.48	1.56	0.91	63.18	1.72	15.32

Table 13. Moisture and density (MAD) physical properties for Hole NGHP-01-17A. (To view the complete table, please see the ASCII files.)—Continued

Core, section	Depth, int, from (cm)	Depth, int, to (cm)	Depth (mbsf)	WCt (%)	WCs (%)	Grain density (g/cm³)	Bulk density (g/cm³)	Dry bulk density (g/cm³)	Porosity (%)	Void ratio	Unit weight (kN/m³)
NGHP-01-17A—Continued											
78X-1	47	49	644.57	43.23	76.14	2.51	1.54	0.88	65.11	1.87	15.14
78X-2	38	40	645.59	37.89	61.01	2.51	1.62	1.01	59.93	1.50	15.90
78X-3	69	71	647.40	41.80	71.83	2.48	1.56	0.91	63.48	1.74	15.27
78X-4	24	26	648.45	40.61	68.39	2.54	1.59	0.94	62.88	1.69	15.57
78X-5	23	25	649.94	40.46	67.95	2.56	1.59	0.95	62.92	1.70	15.63
79X-1	127	129	655.07	42.28	73.26	2.52	1.55	0.89	63.74	1.76	15.16
79X-2	18	20	655.48	39.46	65.19	2.52	1.60	0.97	61.55	1.60	15.68
79X-3	15	17	656.95	40.99	69.47	2.51	1.58	0.93	63.00	1.70	15.45
79X-4	10	12	658.40	41.65	71.39	2.52	1.57	0.92	63.72	1.76	15.38
79X-5	36	38	660.16	35.27	54.48	2.56	1.68	1.09	57.68	1.36	16.44
79X-6	22	24	661.52	39.24	64.58	2.52	1.60	0.97	61.35	1.59	15.72
80X-1	14	16	662.84	41.78	71.76	2.61	1.59	0.92	64.60	1.82	15.55
80X-2	55	57	663.56	38.51	62.64	2.61	1.64	1.01	61.50	1.60	16.05
80X-3	29	31	664.75	34.80	53.37	2.53	1.67	1.09	56.85	1.32	16.42
80X-4	20	22	665.62	37.11	59.01	2.65	1.67	1.05	60.41	1.53	16.37
80X-5	19	21	667.11	38.56	62.75	2.58	1.63	1.00	61.24	1.58	15.97
81E-1	5	7	672.35	36.15	56.61	2.69	1.70	1.08	59.77	1.49	16.62
81E-1	24	44	672.54	1.65	1.67	2.55	2.49	2.45	4.00	0.04	24.39
81E-1	24	44	672.54	36.88	58.42	2.81	1.71	1.08	61.54	1.60	16.78
82X-2	12	14	673.62	43.45	76.83	2.49	1.54	0.87	65.13	1.87	15.07
82X-3	17	19	675.17	41.69	71.50	2.59	1.58	0.92	64.40	1.81	15.53
82X-4	21	23	676.38	45.42	83.22	2.64	1.54	0.84	68.22	2.15	15.10
82X-5	14	16	677.81	44.73	80.94	2.58	1.54	0.85	67.04	2.03	15.07
82X-6	13	15	679.20	45.81	84.54	2.54	1.51	0.82	67.66	2.09	14.85
83X-1	39	41	683.29	42.63	74.29	2.52	1.57	0.90	65.09	1.86	15.35
83X-2	17	19	684.07	43.10	75.75	2.54	1.55	0.88	65.27	1.88	15.23

Table 14. Vane shear strength results for Hole NGHP-01-17A.

Core, section	Sample	Top (cm)	Depth (mbsf)	Sv (kPa)	Sres (kPa)	Srem (kPa)	St
NGHP-01-17A							
1H-1	VS	75	0.75	3.3	1.0	0.7	5.0
1H-2	VS	61	2.11	12.9	6.6	4.9	2.6
1H-3	VS	50	3.50	18.8	9.9	6.7	2.8
2H-1	VS	121	5.71	14.6	10.3	4.9	3.0
2H-2	VS	75	6.75	22.2	16.5	8.2	2.7
2H-3	VS	65	8.15	24.2	16.5	9.1	2.7
2H-4	VS	75	9.75	32.7	28.0	11.5	2.8
2H-5	VS	55	11.05	32.9	22.2	13.2	2.5
2H-6	VS	55	12.55	43.4	27.2	15.5	2.8
2H-7	VS	42	13.92	40.3	23.0	7.7	5.2
3H-1	VS	60	14.60	31.0	No value	11.4	2.7
3H-2	VS	25	15.75	40.2	No value	16.5	2.4
3H-3	VS	68	17.68	39.8	24.7	13.7	2.9

Table 15. Torvane strength results for Hole NGHP-01-17A.

Core, section	Sample	Top (cm)	Depth (mbsf)	Stv (kPa)	Core, section	Sample	Top (cm)	Depth (mbsf)	Stv (kPa)
NGHP-01-17A									
1H-1	TV	76	0.76	5.3	7H-7	TV	28	61.28	64.7
1H-2	TV	69	2.19	18.6	8H-1	TV	22	61.72	63.7
2H-1	TV	128	5.78	24.5	8H-2	TV	32	63.32	52.0
2H-2	TV	67	6.67	29.4	8H-3	TV	31	64.81	41.2
2H-3	TV	72	8.22	33.3	8H-4	TV	27	66.27	41.2
2H-4	TV	68	9.68	23.5	8H-5	TV	26	67.76	72.6
2H-5	TV	49	10.99	39.2	8H-6	TV	26	69.26	61.8
2H-6	TV	48	12.48	48.5	8H-7	TV	22	70.22	63.7
3H-1	TV	62	14.62	34.3	8H-7	TV	27	70.27	62.8
3H-2	TV	53	16.03	49.0	9H-1	TV	11	71.11	53.9
3H-3	TV	60	17.60	55.9	9H-2	TV	57	72.67	23.5
3H-4	TV	45	18.95	51.0	9H-3	TV	7	73.67	51.0
3H-5	TV	48	20.48	76.5	9H-4	TV	23	75.33	66.7
3H-6	TV	46	21.96	62.8	9H-5	TV	23	76.83	73.5
3H-7	TV	27	22.77	53.9	9H-6	TV	23	78.33	25.5
3H-7	TV	39	22.89	31.4	9H-7	TV	26	79.86	22.6
4H-1	TV	63	24.13	67.7	10H-1	TV	6	80.56	41.2
4H-2	TV	63	25.63	60.8	10H-2	TV	16	82.16	40.2
4H-3	TV	69	27.19	48.1	10H-3	TV	7	83.57	28.4
4H-4	TV	67	28.67	61.8	10H-4	TV	7	85.07	24.5
4H-5	TV	60	30.10	63.7	10H-5	TV	7	86.57	57.9
4H-6	TV	49	31.49	62.8	10H-6	TV	7	88.07	53.0
4H-7	TV	26	32.26	84.3	10H-7	TV	23	89.67	67.7
4H-7	TV	41	32.41	38.2	11H-1	TV	60	90.60	68.6
5H-1	TV	76	33.76	63.7	11H-2	TV	30	91.80	57.9
5H-2	TV	67	35.17	64.7	11H-3	TV	72	93.72	48.1
5H-3	TV	75	36.75	61.8	11H-4	TV	72	95.22	66.7
5H-4	TV	68	38.18	58.8	11H-5	TV	30	96.30	73.5
5H-5	TV	46	39.46	53.0	11H-6	TV	27	97.77	68.6
5H-6	TV	62	41.12	53.9	11H-7	TV	7	98.57	62.8
6H-1	TV	18	42.68	29.4	12H-1	TV	25	99.75	73.5
6H-2	TV	28	44.22	49.0	12H-2	TV	19	101.19	49.0
6H-3	TV	23	45.67	49.0	12H-3	TV	38	102.88	58.8
6H-4	TV	23	47.17	49.0	12H-4	TV	19	104.19	68.6
6H-5	TV	22	48.66	49.0	12H-5	TV	23	105.73	54.9
6H-6	TV	28	50.22	65.7	12H-6	TV	35	107.35	63.7
6H-7	TV	16	51.60	56.4	12H-7	TV	36	108.36	64.7
7H-1	TV	33	52.33	83.4	13H-1	TV	19	109.19	15.7
7H-2	TV	24	53.74	78.5	13H-2	TV	30	110.80	54.9
7H-3	TV	28	55.28	72.6	13H-3	TV	29	112.29	49.0
7H-4	TV	43	56.93	59.8	13H-4	TV	30	113.80	69.6
7H-5	TV	22	58.22	64.7	13H-5	TV	39	115.39	57.9
7H-6	TV	22	59.72	78.5	13H-7	TV	46	117.89	48.1

Table 16. Pocket Penetrometer strength results for Hole NGHP-01-17A.

Core, section	Sample	Top (cm)	Depth (mbsf)	Spp (kPa)	Core, section	Sample	Top (cm)	Depth (mbsf)	Spp (kPa)
NGHP-01-17A									
1H-1	PP	18	0.18	0.3	11H-3	PP	70	93.70	49.0
1H-1	PP	72	0.72	1.4	11H-4	PP	70	95.20	93.1
1H-2	PP	75	2.25	6.9	11H-5	PP	39	96.39	58.8
2H-1	PP	31	4.81	10.0	11H-6	PP	54	98.04	58.8
2H-1	PP	69	5.19	3.7	11H-7	PP	60	99.10	76.0
2H-2	PP	82	6.82	11.3	12H-1	PP	69	100.19	85.8
2H-3	PP	75	8.25	9.5	12H-2	PP	60	101.60	56.4
5H-1	PP	31	33.31	4.9	12H-3	PP	94	103.44	58.8
5H-2	PP	51	35.01	24.5	12H-4	PP	94	104.94	100.5
5H-3	PP	71	36.71	46.6	12H-5	PP	57	106.07	105.4
5H-4	PP	65	38.15	36.8	12H-6	PP	66	107.66	83.3
5H-5	PP	54	39.54	24.5	12H-7	PP	18	108.18	49.0
5H-6	PP	50	41.00	14.7	13H-1	PP	90	109.90	49.0
5H-7	PP	22	42.22	36.8	13H-2	PP	86	111.36	39.2
6H-1	PP	15	42.65	49.0	13H-3	PP	78	112.78	49.0
6H-2	PP	15	44.09	36.8	13H-4	PP	90	114.40	85.8
6H-3	PP	18	45.62	24.5	13H-5	PP	60	115.60	85.8
6H-4	PP	18	47.12	24.5	13H-6	PP	23	116.73	85.8
6H-5	PP	18	48.62	49.0	13H-7	PP	6	117.49	78.4
6H-6	PP	24	50.18	73.5	13H-7	PP	12	117.55	76.0
6H-7	PP	24	51.68	29.4	13H-7	PP	72	118.15	78.4
7H-1	PP	16	52.16	4.9	14X-1	PP	72	119.22	49.0
7H-2	PP	16	53.66	29.4	14X-1	PP	86	119.36	49.0
7H-3	PP	16	55.16	36.8	14X-1	PP	100	119.50	49.0
7H-4	PP	13	56.63	24.5	14X-2	PP	60	120.60	39.2
7H-5	PP	16	58.16	58.8	14X-2	PP	81	120.81	53.9
7H-6	PP	16	59.66	36.8	14X-2	PP	90	120.90	53.9
7H-7	PP	8	61.08	49.0	14X-3	PP	43	121.93	63.7
8H-1	PP	15	61.65	24.5	14X-3	PP	47	121.97	61.3
8H-2	PP	16	63.16	24.5	14X-3	PP	50	122.00	68.6
8H-3	PP	25	64.75	9.8	14X-4	PP	33	123.33	68.6
8H-4	PP	16	66.16	24.5	14X-4	PP	38	123.38	49.0
8H-5	PP	23	67.73	49.0	14X-4	PP	52	123.52	61.3
8H-6	PP	23	69.23	49.0	14X-5	PP	50	125.00	58.8
8H-7	PP	23	70.23	29.4	14X-5	PP	63	125.13	49.0
8H-8	PP	9	70.96	24.5	14X-5	PP	133	125.83	44.1
9H-1	PP	45	71.45	34.3	14X-6	PP	18	126.18	76.0
9H-2	PP	16	72.26	24.5	14X-6	PP	35	126.35	73.5
9H-3	PP	16	73.76	39.2	14X-6	PP	60	126.60	76.0
9H-4	PP	16	75.26	39.2	15X-1	PP	26	128.36	49.0
9H-5	PP	16	76.76	73.5	15X-2	PP	26	129.36	85.8
9H-6	PP	16	78.26	73.5	15X-3	PP	26	129.98	53.9
9H-7	PP	16	79.76	53.9	15X-4	PP	26	131.48	36.8
10H-1	PP	16	80.66	39.2	15X-5	PP	26	132.98	83.3
10H-3	PP	16	83.66	49.0	15X-6	PP	29	134.51	53.9
10H-4	PP	16	85.16	58.8	15X-7	PP	29	136.01	78.4
10H-5	PP	16	86.66	68.6	16X-1	PP	25	137.95	61.3
10H-6	PP	16	88.16	36.8	16X-2	PP	25	139.45	61.3
10H-7	PP	16	89.60	39.2	16X-3	PP	25	140.95	78.4
11H-1	PP	77	90.77	49.0	16X-5	PP	25	143.79	53.9
11H-2	PP	56	92.06	49.0	16X-6	PP	25	145.14	78.4

Table 16. Pocket Penetrometer strength results for Hole NGHP-01-17A.—Continued

Core, section	Sample	Top (cm)	Depth (mbsf)	Spp (kPa)	Core, section	Sample	Top (cm)	Depth (mbsf)	Spp (kPa)
NGHP-01-17A—Continued									
17X-1	PP	16	146.76	36.8	24X-2	PP	60	204.65	73.5
18X-2	PP	16	157.72	58.8	24X-3	PP	15	205.70	58.8
18X-3	PP	16	159.22	85.8	24X-3	PP	43	205.98	61.3
18X-4	PP	16	160.72	83.3	24X-4	PP	10	206.65	56.4
18X-5	PP	16	162.22	88.2	24X-4	PP	24	206.79	100.5
18X-6	PP	16	163.47	73.5	25X-1	PP	49	213.99	61.3
18X-7	PP	21	165.02	78.4	25X-1	PP	61	214.11	95.6
19X-2	PP	29	166.62	85.8	25X-2	PP	84	215.84	93.1
19X-3	PP	29	168.12	73.5	25X-3	PP	16	216.66	61.3
19X-4	PP	28	169.61	88.2	25X-3	PP	37	216.87	93.1
19X-5	PP	29	171.12	78.4	25X-4	PP	26	218.26	107.8
19X-7	PP	29	174.12	127.4	25X-4	PP	45	218.45	107.8
20Y-1	PP	30	175.80	134.8	25X-5	PP	110	220.20	88.2
21X-1	PP	12	176.62	31.9	25X-6	PP	12	220.72	122.5
21X-1	PP	60	177.10	34.3	25X-6	PP	50	221.10	122.5
21X-1	PP	116	177.66	46.6	26X-2	PP	35	224.95	93.1
21X-2	PP	16	178.16	107.8	26X-2	PP	65	225.25	93.1
21X-2	PP	70	178.70	71.1	26X-3	PP	19	226.29	53.9
21X-3	PP	16	179.66	83.3	26X-3	PP	40	226.50	46.6
21X-3	PP	90	180.40	73.5	26X-4	PP	95	228.41	46.6
22X-1	PP	42	185.62	51.5	31X-3	PP	68	273.01	132.3
22X-1	PP	70	185.90	61.3	31X-6	PP	49	276.17	137.2
22X-2	PP	44	187.04	88.2	38Y-1	PP	12	329.12	34.3
22X-2	PP	93	187.53	76.0	38Y-1	PP	15	329.15	34.3
22X-2	PP	115	187.75	88.2	38Y-1	PP	29	329.29	205.8
22X-3	PP	53	188.63	122.5	38Y-1	PP	34	329.34	223.0
22X-3	PP	100	189.10	129.9	38Y-1	PP	43	329.43	196.0
22X-3	PP	133	189.43	110.3	38Y-1	PP	78	329.78	223.0
22X-4	PP	31	189.91	73.5	49E-1	PP	67	414.37	225.4
22X-4	PP	100	190.60	102.9	49E-1	PP	74	414.44	210.7
22X-4	PP	130	190.90	161.7	50X-7	PP	20	421.56	225.4
22X-5	PP	26	191.36	156.8	50X-8	PP	39	422.80	225.4
22X-5	PP	53	191.63	144.6	51X-1	PP	36	424.66	225.4
22X-6	PP	30	192.69	159.3	52X-5	PP	11	439.61	225.4
22X-6	PP	72	193.11	132.3	52X-6	PP	6	440.13	225.4
22X-7	PP	28	193.67	151.9	52X-7	PP	49	442.06	225.4
22X-7	PP	56	193.95	174.0	53X-5	PP	34	448.52	225.4
23X-1	PP	30	195.20	102.9	53X-7	PP	34	450.14	225.4
23X-1	PP	65	195.55	110.3	60Y-1	PP	23	500.83	4.9
23X-2	PP	20	195.88	85.8	60Y-1	PP	57	501.17	220.5
23X-2	PP	73	196.41	76.0	60Y-1	PP	64	501.24	225.4
23X-2	PP	120	196.88	122.5	60Y-1	PP	78	501.38	225.4
23X-3	PP	20	197.38	120.1	62X-4	PP	41	515.52	225.4
23X-3	PP	80	197.98	159.3	62X-5	PP	70	517.31	225.4
23X-4	PP	20	198.88	120.1	62X-6	PP	100	519.11	225.4
23X-4	PP	70	199.38	100.5	62X-7	PP	30	519.41	225.4
23X-4	PP	103	199.71	98.0	66X-6	PP	15	555.57	225.4
23X-5	PP	20	200.28	147.0	67X-4	PP	43	562.20	225.4
23X-5	PP	50	200.58	127.4	68X-3	PP	44	571.30	225.4
23X-6	PP	20	201.78	132.3	74X-5	PP	73	612.93	225.4
23X-6	PP	35	201.93	122.5					

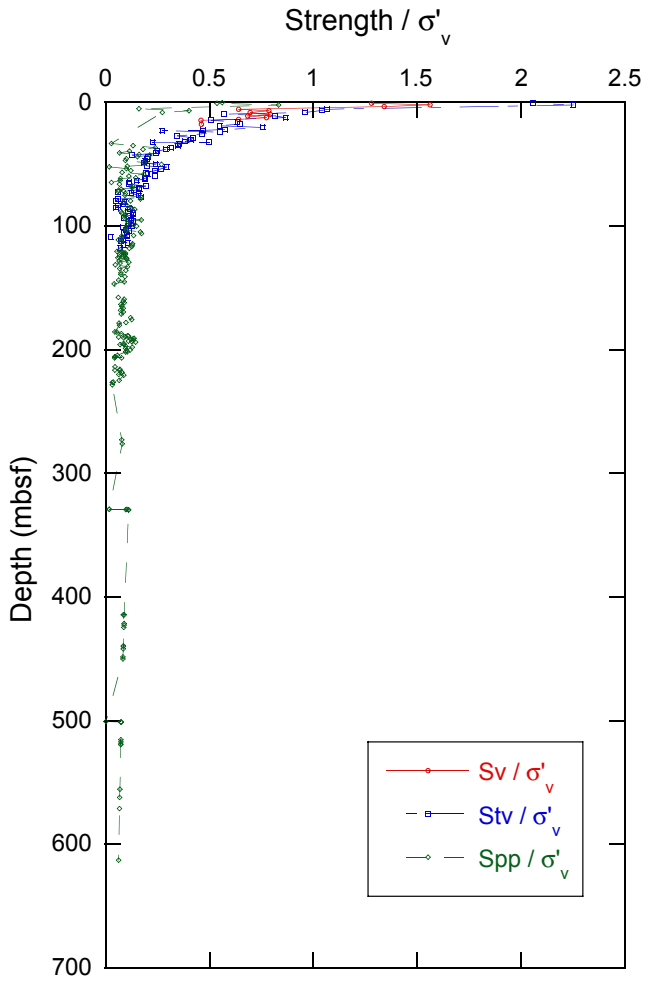


Figure 29. Shear strengths normalized to the effective vertical stress versus sub-bottom depth for Hole NGHP-01-17A.

Core NGHP-01-17A-37P (328.0 mbsf) retrieved a full core (1.00 m) at pressure (table 21). The autoclave was placed in the MSCL-P for X-ray and gamma density measurements, which showed a relatively uniform core in the X-ray of the top half and that sediment existed in the lower half (fig. 35). The core was depressurized, releasing 1.67 L of methane, which was near methane saturation at in situ temperature and pressure (table 22). The core showed no pressure rebounds versus volume or time (figs. 37A and 38A), consistent with little to no methane hydrate. After depressurization, the autoclave was again measured in the MSCL-P, showing gas expansion in both the top (x ray) and bottom half (gamma density) of the core, and a final X-ray image was collected when the outer barrel was removed (fig. 36A). One chlorinity measurement was made on this core (556 mM, 50–60 cm), which was similar to the background chlorinity in surrounding cores (see "Inorganic Geochemistry").

Core NGHP-01-17A-38Y (329.0 mbsf) retrieved a full core (0.86 m) at *in situ* pressure (table 21). Particular care was taken when retracting this core to ensure that the winch speeds were slow and steady. The core sealed immediately after retraction and increased in pressure when it was retrieved to the deck (fig. 33A). Core NGHP-01-17A-38Y was transferred to the MSCL-P and X-ray images, gamma density and *P*-wave velocity measurements were collected (fig. 35A). The core appeared very uniform, with no evidence of gas hydrate. The top 20 cm of core may have been disturbed sediment at the bottom of the hole (cuttings). Core NGHP-01-17A-38Y was depressurized in the MSCL-P, releasing 1.80 L of methane, which was below methane saturation at in situ temperature and pressure (table 22). The core showed no pressure rebounds versus volume or time (figs. 37A and 38A), consistent with little to no methane hydrate. The overestimate of gas in the system at intermediate pressures (fig. 37A) was probably due to trapped air in the pressure system. A final MSCL-P scan was collected at atmospheric pressure which showed an intact core with one large gas expansion void near the bottom (fig. 36B). One chlorinity measurement was made on this core (558 mM, 50–65 cm), which was similar to the background chlorinity in surrounding cores (see "Inorganic Geochemistry").

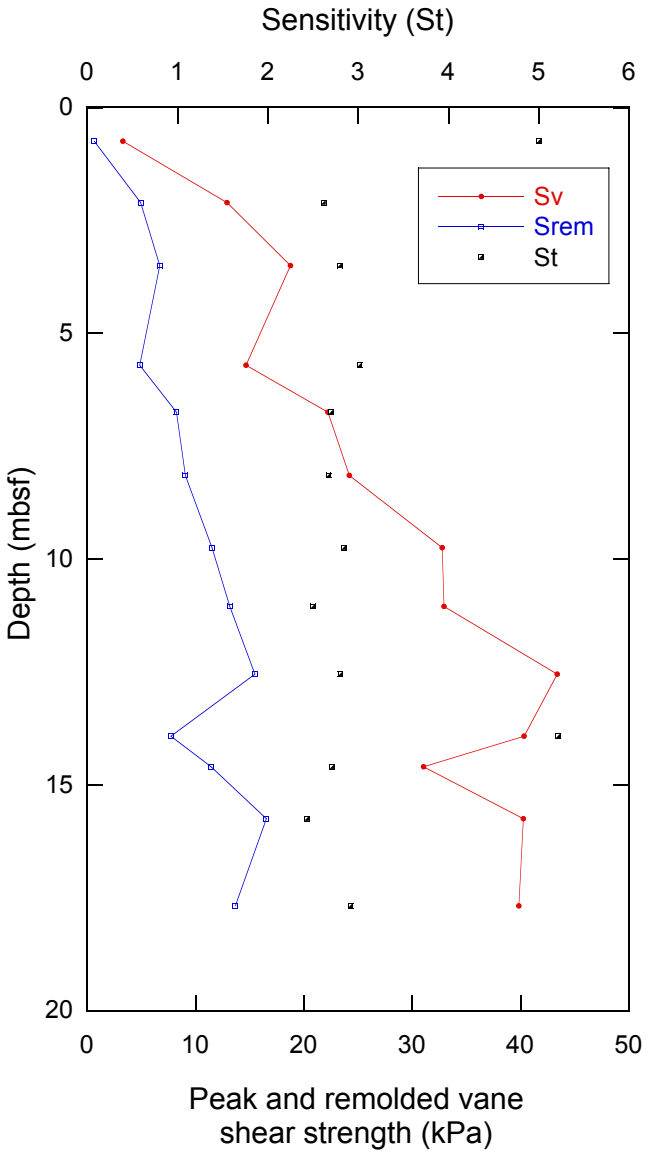


Figure 30. Peak and remolded vane shear strengths and sensitivity for Hole NGHP-01-17A.

Table 17. Wenner array electrical resistivity and formation factor results for Hole NGHP-01-17A. (To view the complete table, please see the ASCII files.)

Core, section	Top (cm)	Depth (mbsf)	Electrical resistivity (W×m)	Apparent formation factor	Core, section	Top (cm)	Depth (mbsf)	Electrical resistivity (W×m)	Apparent formation factor
NGHP-01-17A									
1H-3	10	3.10	0.377	1.885	3H-2	135	16.85	0.434	2.17
1H-3	30	3.30	0.428	2.14	3H-3	15	17.15	0.439	2.195
1H-3	50	3.50	0.376	1.88	3H-3	35	17.35	0.408	2.04
1H-3	70	3.70	0.378	1.89	3H-3	55	17.55	0.446	2.23
1H-3	90	3.90	0.378	1.89	3H-3	75	17.75	0.34	1.7
2H-1	15	4.65	0.343	1.715	3H-3	95	17.95	0.403	2.015
2H-1	41	4.91	0.374	1.87	3H-4	15	18.65	0.452	2.26
2H-1	71	5.21	0.386	1.93	3H-4	35	18.85	0.434	2.17
2H-1	104	5.54	0.366	1.83	3H-4	55	19.05	0.4	2
2H-1	121	5.71	0.395	1.975	3H-4	75	19.25	0.427	2.135
2H-2	15	6.15	0.364	1.82	3H-4	95	19.45	0.406	2.03
2H-2	35	6.35	0.384	1.92	3H-4	115	19.65	0.416	2.08
2H-2	55	6.55	0.372	1.86	3H-4	135	19.85	0.402	2.01
2H-2	75	6.75	0.369	1.845	3H-5	15	20.15	0.463	2.315
2H-2	95	6.95	0.367	1.835	3H-5	35	20.35	0.419	2.095
2H-2	115	7.15	0.373	1.865	3H-5	55	20.55	0.42	2.1
2H-2	135	7.35	0.368	1.84	3H-5	75	20.75	0.399	1.995
2H-3	8	7.58	0.379	1.895	3H-6	15	21.65	0.432	2.16
2H-3	35	7.85	0.378	1.89	3H-6	35	21.85	0.403	2.015
2H-3	65	8.15	0.331	1.655	3H-6	55	22.05	0.441	2.205
2H-3	85	8.35	0.314	1.57	3H-6	75	22.25	0.415	2.075
2H-3	102	8.52	0.347	1.735	3H-6	95	22.45	0.406	2.03
2H-4	15	9.15	0.35	1.75	3H-7	15	22.65	0.442	2.21
2H-4	35	9.35	0.343	1.715	3H-7	35	22.85	0.433	2.165
2H-4	55	9.55	0.337	1.685	3H-7	52	23.02	0.441	2.205
2H-4	75	9.75	0.351	1.755	4H-1	15	23.65	0.415	2.075
2H-4	95	9.95	0.365	1.825	4H-1	35	23.85	0.417	2.085
2H-4	115	10.15	0.363	1.815	4H-1	55	24.05	0.421	2.105
2H-5	15	10.65	0.452	2.26	4H-1	75	24.25	0.436	2.18
2H-5	35	10.85	0.389	1.945	4H-1	95	24.45	0.335	1.675
2H-5	55	11.05	0.362	1.81	4H-1	115	24.65	0.418	2.09
2H-5	75	11.25	0.355	1.775	4H-2	15	25.15	0.441	2.205
2H-5	94	11.44	0.367	1.835	4H-2	35	25.35	0.45	2.25
2H-6	15	12.15	0.373	1.865	4H-2	55	25.55	0.437	2.185
2H-6	35	12.35	0.362	1.81	4H-2	75	25.75	0.453	2.265
2H-6	55	12.55	0.369	1.845	4H-2	95	25.95	0.436	2.18
2H-6	75	12.75	0.377	1.885	4H-2	115	26.15	0.436	2.18
2H-6	95	12.95	0.36	1.8	4H-2	135	26.35	0.455	2.275
2H-6	115	13.15	0.345	1.725	4H-3	15	26.65	0.405	2.025
2H-6	136	13.36	0.356	1.78	4H-3	35	26.85	0.367	1.835
2H-7	15	13.65	0.34	1.7	4H-3	55	27.05	0.398	1.99
2H-7	35	13.85	0.368	1.84	4H-3	75	27.25	0.406	2.03
2H-7	55	14.05	0.352	1.76	4H-3	95	27.45	0.43	2.15
3H-1	30	14.30	0.434	2.17	4H-4	15	28.15	0.467	2.335
3H-1	40	14.40	0.41	2.05	4H-4	35	28.35	0.436	2.18
3H-1	70	14.70	0.417	2.085	4H-4	55	28.55	0.441	2.205
3H-1	90	14.90	0.447	2.235	4H-4	75	28.75	0.496	2.48
3H-1	110	15.10	0.428	2.14	4H-4	95	28.95	0.429	2.145
3H-1	130	15.30	0.703	3.515	4H-4	115	29.15	0.421	2.105
3H-2	15	15.65	0.451	2.255	4H-4	135	29.35	0.487	2.435
3H-2	35	15.85	0.424	2.12	4H-5	15	29.65	0.423	2.115
3H-2	55	16.05	0.43	2.15	4H-5	35	29.85	0.433	2.165
3H-2	75	16.25	0.401	2.005	4H-5	55	30.05	0.436	2.18
3H-2	95	16.45	0.438	2.19	4H-5	75	30.25	0.461	2.305
3H-2	115	16.65	0.458	2.29	4H-6	15	31.15	0.576	2.88

Table 17. Wenner array electrical resistivity and formation factor results for Hole NGHP-01-17A. (To view the complete table, please see the ASCII files.)—Continued

Core, section	Top (cm)	Depth (mbsf)	Electrical resistivity (W×m)	Apparent formation factor	Core, section	Top (cm)	Depth (mbsf)	Electrical resistivity (W×m)	Apparent formation factor
NGHP-01-17A—Continued									
4H-6	35	31.35	0.557	2.785	6H-2	103	44.97	0.46	2.3
4H-6	55	31.55	0.474	2.37	6H-3	20	45.64	1.032	5.16
4H-6	74	31.74	0.466	2.33	6H-3	57	46.01	0.821	4.105
4H-6	95	31.95	0.457	2.285	6H-3	78.5	46.23	0.913	4.565
4H-7	15	32.15	0.506	2.53	6H-3	102	46.46	1.032	5.16
4H-7	34	32.34	0.686	3.43	6H-3	124.5	46.69	0.918	4.59
4H-7	35	32.35	0.617	3.085	6H-4	20	47.14	1.412	7.06
4H-7	52	32.52	0.692	3.46	6H-4	20	47.14	1.433	7.165
5H-1	15	33.15	0.435	2.175	6H-4	30	47.24	1.418	7.09
5H-1	35	33.35	0.437	2.185	6H-4	40	47.34	0.825	4.125
5H-1	55	33.55	0.445	2.225	6H-4	60	47.54	0.637	3.185
5H-1	75	33.75	0.442	2.21	6H-4	80	47.74	0.902	4.51
5H-1	95	33.95	0.451	2.255	6H-4	102	47.96	0.662	3.31
5H-1	115	34.15	0.399	1.995	6H-4	127	48.21	0.696	3.48
5H-1	140	34.40	0.423	2.115	6H-5	10	48.54	0.845	4.225
5H-2	15	34.65	0.417	2.085	6H-5	20	48.64	1.003	5.015
5H-2	35	34.85	0.495	2.475	6H-5	40	48.84	0.837	4.185
5H-2	55	35.05	0.437	2.185	6H-5	62	49.06	0.941	4.705
5H-2	75	35.25	0.42	2.1	6H-5	80	49.24	1.045	5.225
5H-2	95	35.45	0.441	2.205	6H-6	40	50.34	0.925	4.625
5H-2	115	35.65	0.394	1.97	6H-6	62	50.56	1.068	5.34
5H-3	15	36.15	0.431	2.155	6H-6	90	50.84	0.926	4.63
5H-3	35	36.35	0.419	2.095	6H-6	110	51.04	0.9	4.5
5H-3	55	36.55	0.457	2.285	6H-6	130	51.24	0.83	4.15
5H-3	75	36.75	0.428	2.14	6H-7	20	51.64	0.693	3.465
5H-3	95	36.95	0.435	2.175	6H-7	40	51.84	0.883	4.415
5H-3	118	37.18	0.471	2.355	6H-7	60	52.04	0.621	3.105
5H-3	139	37.39	0.466	2.33	6H-7	77.5	52.22	0.609	3.045
5H-4	15	37.65	0.455	2.275	7H-1	14	52.14	0.644	3.22
5H-4	35	37.85	0.453	2.265	7H-1	40	52.40	0.711	3.555
5H-4	55	38.05	0.442	2.21	7H-1	125	53.25	0.856	4.28
5H-4	75	38.25	0.425	2.125	7H-2	20	53.70	0.664	3.32
5H-4	95	38.45	0.453	2.265	7H-2	22	53.72	0.847	4.235
5H-4	115	38.65	0.494	2.47	7H-2	30	53.80	0.687	3.435
5H-5	15	39.15	0.448	2.24	7H-2	40	53.90	0.7	3.5
5H-5	35	39.35	0.475	2.375	7H-2	42	53.92	0.932	4.66
5H-5	58	39.58	0.457	2.285	7H-2	60	54.10	0.742	3.71
5H-5	75	39.75	0.436	2.18	7H-2	62	54.12	1.002	5.01
5H-6	15	40.65	0.452	2.26	7H-2	80	54.30	0.74	3.7
5H-6	35	40.85	0.454	2.27	7H-2	82	54.32	0.809	4.045
5H-6	55	41.05	0.667	3.335	7H-2	100	54.50	0.439	2.195
5H-6	75	41.25	0.43	2.15	7H-2	102	54.52	0.54	2.7
5H-6	95	41.45	0.598	2.99	7H-2	120	54.70	0.729	3.645
5H-6	115	41.65	0.575	2.875	7H-2	140	54.90	0.703	3.515
5H-6	135	41.85	0.561	2.805	7H-4	14	56.64	0.847	4.235
5H-7	15	42.15	0.466	2.33	7H-4	44	56.94	0.676	3.38
6H-1	20	42.70	0.462	2.31	7H-4	64	57.14	0.724	3.62
6H-1	40	42.90	0.448	2.24	7H-4	84	57.34	0.682	3.41
6H-1	60	43.10	0.492	2.46	7H-4	104	57.54	0.672	3.36
6H-1	80	43.30	0.447	2.235	7H-4	124	57.74	0.691	3.455
6H-1	100	43.50	0.443	2.215	7H-4	124	57.74	0.547	2.735
6H-1	120	43.70	0.465	2.325	7H-5	20	58.20	0.663	3.315
6H-2	18	44.12	0.467	2.335	7H-5	40	58.40	0.721	3.605
6H-2	40	44.34	0.443	2.215	7H-5	60	58.60	0.65	3.25
6H-2	68	44.62	0.509	2.545	7H-5	80	58.80	0.46	2.3
6H-2	88	44.82	0.465	2.325	7H-6	20	59.70	0.562	2.81

Table 17. Wenner array electrical resistivity and formation factor results for Hole NGHP-01-17A. (To view the complete table, please see the ASCII files.)—Continued

Core, section	Top (cm)	Depth (mbsf)	Electrical resistivity (W×m)	Apparent formation factor	Core, section	Top (cm)	Depth (mbsf)	Electrical resistivity (W×m)	Apparent formation factor
NGHP-01-17A—Continued									
7H-6	40	59.90	0.776	3.88	9H-3	130	74.90	0.537	2.685
7H-6	60	60.10	0.548	2.74	9H-4	17	75.27	0.446	2.23
7H-6	80	60.30	0.633	3.165	9H-4	40	75.50	0.658	3.29
7H-6	100	60.50	0.717	3.585	9H-4	60	75.70	0.448	2.24
7H-6	120	60.70	0.611	3.055	9H-4	80	75.90	0.638	3.19
7H-7	10	61.10	0.729	3.645	9H-4	100	76.10	0.651	3.255
7H-7	24	61.24	0.515	2.575	9H-4	120	76.30	0.547	2.735
7H-7	46	61.46	0.504	2.52	9H-4	130	76.40	0.658	3.29
8H-1	20	61.70	0.507	2.535	9H-6	20	78.30	0.482	2.41
8H-1	40	61.90	0.924	4.62	9H-6	40	78.50	0.481	2.405
8H-1	60	62.10	0.724	3.62	9H-6	57	78.67	0.609	3.045
8H-1	80	62.30	0.94	4.7	9H-6	80	78.90	0.672	3.36
8H-2	37	63.37	0.588	2.94	9H-6	102	79.12	0.743	3.715
8H-2	57	63.57	0.611	3.055	9H-6	121	79.31	0.679	3.395
8H-2	78	63.78	0.745	3.725	9H-6	138	79.48	0.608	3.04
8H-2	102	64.02	0.506	2.53	9H-7	13.5	79.74	0.553	2.765
8H-2	125	64.25	0.458	2.29	9H-7	30	79.90	0.556	2.78
8H-3	20	64.70	0.837	4.185	9H-7	51	80.11	0.702	3.51
8H-3	25	64.75	0.561	2.805	10H-1	20	80.70	0.454	2.27
8H-3	40	64.90	0.552	2.76	10H-1	40	80.90	0.513	2.565
8H-3	47	64.97	0.604	3.02	10H-1	60	81.10	0.584	2.92
8H-3	66	65.16	0.676	3.38	10H-1	80	81.30	0.573	2.865
8H-3	71	65.21	0.619	3.095	10H-1	98	81.48	0.558	2.79
8H-3	71	65.21	0.662	3.31	10H-1	120	81.70	0.535	2.675
8H-3	90	65.40	0.588	2.94	10H-1	140	81.90	0.521	2.605
8H-3	98	65.48	0.571	2.855	10H-3	20	83.70	0.694	3.47
8H-3	111	65.61	0.598	2.99	10H-3	40	83.90	0.533	2.665
8H-3	118	65.68	0.574	2.87	10H-3	63	84.13	0.614	3.07
8H-3	131	65.81	0.575	2.875	10H-3	83	84.33	0.627	3.135
8H-5	20	67.70	0.555	2.775	10H-3	103	84.53	0.605	3.025
8H-5	40	67.90	0.659	3.295	10H-3	123	84.73	0.694	3.47
8H-5	60	68.10	0.6	3	10H-4	20	85.20	0.67	3.35
8H-5	80	68.30	0.425	2.125	10H-4	40	85.40	0.696	3.48
8H-6	20	69.20	0.433	2.165	10H-4	60	85.60	0.474	2.37
8H-6	40	69.40	0.487	2.435	10H-4	80	85.80	0.492	2.46
8H-6	60	69.60	0.43	2.15	10H-4	100	86.00	0.71	3.55
8H-6	80	69.80	0.559	2.795	10H-4	122	86.22	0.835	4.175
8H-7	20	70.20	0.463	2.315	10H-4	140	86.40	0.673	3.365
8H-7	40	70.40	0.595	2.975	10H-5	20	86.70	0.676	3.38
8H-8	10	70.97	0.853	4.265	10H-5	40	86.90	0.482	2.41
9H-1	20	71.20	0.385	1.925	10H-5	40	86.90	0.532	2.66
9H-1	40	71.40	0.872	4.36	10H-5	60	87.10	0.831	4.155
9H-1	60	71.60	0.579	2.895	10H-5	62	87.12	0.711	3.555
9H-1	80	71.80	0.598	2.99	10H-5	81	87.31	0.746	3.73
9H-1	100	72.00	0.915	4.575	10H-5	83	87.33	0.563	2.815
9H-2	20	72.30	0.585	2.925	10H-5	101	87.51	0.577	2.885
9H-2	45	72.55	0.657	3.285	10H-5	121	87.71	0.58	2.9
9H-2	60	72.70	0.654	3.27	10H-6	20	88.20	0.477	2.385
9H-2	80	72.90	0.689	3.445	10H-7	20	89.64	0.882	4.41
9H-2	100	73.10	0.733	3.665	10H-7	41	89.85	0.615	3.075
9H-3	14	73.74	0.486	2.43	10H-7	61	90.05	0.642	3.21
9H-3	30	73.90	0.558	2.79	11H-1	15	90.15	0.514	2.57
9H-3	50	74.10	0.686	3.43	11H-1	35	90.35	0.631	3.155
9H-3	70	74.30	0.515	2.575	11H-1	55	90.55	0.528	2.64
9H-3	88	74.48	0.547	2.735	11H-1	75	90.75	0.497	2.485
9H-3	110	74.70	0.625	3.125	11H-1	95	90.95	0.635	3.175

Table 17. Wenner array electrical resistivity and formation factor results for Hole NGHP-01-17A. (To view the complete table, please see the ASCII files.)—Continued

Core, section	Top (cm)	Depth (mbsf)	Electrical resistivity (W×m)	Apparent formation factor	Core, section	Top (cm)	Depth (mbsf)	Electrical resistivity (W×m)	Apparent formation factor
NGHP-01-17A—Continued									
11H-1	115	91.15	0.652	3.26	12H-4	55	104.55	0.567	2.835
11H-1	135	91.35	0.573	2.865	12H-4	75	104.75	0.605	3.025
11H-2	15	91.65	0.488	2.44	12H-4	95	104.95	0.711	3.555
11H-2	35	91.85	0.704	3.52	12H-4	115	105.15	0.567	2.835
11H-2	55	92.05	0.649	3.245	12H-4	136	105.36	0.594	2.97
11H-2	75	92.25	0.63	3.15	12H-5	15	105.65	0.634	3.17
11H-2	95	92.45	0.728	3.64	12H-5	35	105.85	0.495	2.475
11H-2	107	92.57	0.665	3.325	12H-5	58	106.08	0.589	2.945
11H-3	50	93.50	0.615	3.075	12H-5	79	106.29	0.581	2.905
11H-3	70	93.70	0.669	3.345	12H-6	12	107.12	0.582	2.91
11H-3	90	93.90	0.484	2.42	12H-6	32	107.32	0.582	2.91
11H-3	110	94.10	0.616	3.08	12H-6	52	107.52	0.559	2.795
11H-4	9	94.59	0.727	3.635	12H-6	77	107.77	0.714	3.57
11H-4	30	94.80	0.668	3.34	12H-6	92	107.92	0.626	3.13
11H-4	50	95.00	0.678	3.39	12H-7	9	108.09	0.572	2.86
11H-4	70	95.20	0.661	3.305	12H-7	91	108.91	0.576	2.88
11H-4	90	95.40	0.58	2.9	13H-1	15	109.15	0.535	2.675
11H-4	110	95.60	0.612	3.06	13H-1	37	109.37	0.499	2.495
11H-4	130	95.80	0.765	3.825	13H-1	57	109.57	0.506	2.53
11H-4	144	95.94	0.637	3.185	13H-1	76	109.76	0.478	2.39
11H-5	15	96.15	0.6	3	13H-1	96	109.96	0.56	2.8
11H-5	35	96.35	0.634	3.17	13H-1	129	110.29	0.734	3.67
11H-5	55	96.55	0.658	3.29	13H-2	23	110.73	0.634	3.17
11H-5	75	96.75	0.582	2.91	13H-2	43	110.93	0.74	3.7
11H-6	7	97.57	0.756	3.78	13H-2	70	111.20	0.66	3.3
11H-6	30	97.80	0.693	3.465	13H-2	90	111.40	0.724	3.62
11H-6	50	98.00	0.663	3.315	13H-2	107	111.57	0.572	2.86
11H-6	74	98.24	0.53	2.65	13H-3	15	112.15	0.705	3.525
11H-6	94	98.44	0.594	2.97	13H-3	35	112.35	0.847	4.235
11H-7	15	98.65	0.787	3.935	13H-3	53	112.53	0.71	3.55
11H-7	35	98.85	0.58	2.9	13H-3	77	112.77	0.751	3.755
11H-7	55	99.05	0.762	3.81	13H-3	97	112.97	0.794	3.97
11H-7	75	99.25	0.678	3.39	13H-3	122	113.22	0.71	3.55
12H-1	15	99.65	0.592	2.96	13H-3	141	113.41	0.698	3.49
12H-1	29	99.79	0.702	3.51	13H-4	15	113.65	0.568	2.84
12H-1	50	100.00	0.637	3.185	13H-4	35	113.85	0.72	3.6
12H-1	71	100.21	0.597	2.985	13H-4	55	114.05	0.702	3.51
12H-1	98	100.48	0.629	3.145	13H-4	75	114.25	0.645	3.225
12H-1	124	100.74	0.58	2.9	13H-4	95	114.45	0.592	2.96
12H-1	138	100.88	0.773	3.865	13H-4	115	114.65	0.592	2.96
12H-2	15	101.15	0.597	2.985	13H-4	135	114.85	0.65	3.25
12H-2	35	101.35	0.581	2.905	13H-5	15	115.15	0.586	2.93
12H-2	55	101.55	0.54	2.7	13H-5	34	115.34	0.644	3.22
12H-2	75	101.75	0.642	3.21	13H-5	55	115.55	0.586	2.93
12H-2	95	101.95	0.593	2.965	13H-5	75	115.75	0.575	2.875
12H-2	112	102.12	0.619	3.095	13H-6	15	116.65	0.616	3.08
12H-3	15	102.65	0.539	2.695	13H-6	35	116.85	0.642	3.21
12H-3	35	102.85	0.575	2.875	13H-6	55	117.05	0.715	3.575
12H-3	55	103.05	0.561	2.805	13H-6	79	117.29	0.567	2.835
12H-3	75	103.25	0.565	2.825	13H-7	15	117.58	0.628	3.14
12H-3	95	103.45	0.6	3	13H-7	68	118.11	0.664	3.32
12H-3	115	103.65	0.541	2.705	14X-1	15	118.65	0.506	2.53
12H-3	139	103.89	0.582	2.91	14X-1	35	118.85	0.537	2.685
12H-4	15	104.15	0.593	2.965	14X-1	55	119.05	0.632	3.16
12H-4	35	104.35	0.682	3.41	14X-1	75	119.25	0.55	2.75

Table 17. Wenner array electrical resistivity and formation factor results for Hole NGHP-01-17A. (To view the complete table, please see the ASCII files.)—Continued

Core, section	Top (cm)	Depth (mbsf)	Electrical resistivity (W×m)	Apparent formation factor	Core, section	Top (cm)	Depth (mbsf)	Electrical resistivity (W×m)	Apparent formation factor
NGHP-01-17A—Continued									
14X-1	95	119.45	0.636	3.18	15X-5	20	132.92	0.536	2.68
14X-1	115	119.65	0.548	2.74	15X-5	40	133.12	0.579	2.895
14X-1	135	119.85	0.673	3.365	15X-5	40	133.12	0.628	3.14
14X-2	15	120.15	0.568	2.84	15X-5	60	133.32	0.544	2.72
14X-2	34	120.34	0.542	2.71	15X-5	75	133.47	0.592	2.96
14X-2	55	120.55	0.579	2.895	15X-6	20	134.42	0.65	3.25
14X-2	75	120.75	0.688	3.44	15X-6	20	134.42	0.555	2.775
14X-2	95	120.95	0.77	3.85	15X-6	20	134.42	0.552	2.76
14X-3	15	121.65	0.576	2.88	15X-6	40	134.62	0.597	2.985
14X-3	35	121.85	0.548	2.74	15X-6	60	134.82	0.651	3.255
14X-3	55	122.05	0.59	2.95	15X-6	80	135.02	0.561	2.805
14X-3	76	122.26	0.487	2.435	15X-6	100	135.22	0.587	2.935
14X-3	96	122.46	0.54	2.7	15X-6	120	135.42	0.582	2.91
14X-3	122	122.72	0.602	3.01	15X-6	140	135.62	0.61	3.05
14X-3	140	122.90	0.562	2.81	15X-7	20	135.92	0.556	2.78
14X-4	20	123.20	0.514	2.57	15X-7	40	136.12	0.612	3.06
14X-4	35	123.35	0.534	2.67	15X-7	60	136.32	0.571	2.855
14X-4	55	123.55	0.582	2.91	16X-1	22	137.92	0.544	2.72
14X-4	75	123.75	0.561	2.805	16X-1	42	138.12	0.529	2.645
14X-5	18	124.68	0.522	2.61	16X-1	62	138.32	0.55	2.75
14X-5	35	124.85	0.566	2.83	16X-1	82	138.52	0.65	3.25
14X-5	55	125.05	0.634	3.17	16X-1	102	138.72	0.571	2.855
14X-5	75	125.25	0.585	2.925	16X-1	122	138.92	0.569	2.845
14X-5	96	125.46	0.567	2.835	16X-1	142	139.12	0.548	2.74
14X-5	115	125.65	0.531	2.655	16X-2	20	139.40	0.54	2.7
14X-5	137	125.87	0.501	2.505	16X-2	40	139.60	0.56	2.8
14X-6	10	126.10	0.704	3.52	16X-2	60	139.80	0.528	2.64
14X-6	15	126.15	0.506	2.53	16X-2	80	140.00	0.622	3.11
14X-6	34	126.34	0.531	2.655	16X-2	100	140.20	0.617	3.085
14X-6	55	126.55	0.608	3.04	16X-3	20	140.90	0.638	3.19
14X-6	75	126.75	0.594	2.97	16X-3	40	141.10	0.626	3.13
15X-1	10	128.20	0.312	1.56	16X-3	60	141.30	0.572	2.86
15X-1	30	128.40	0.576	2.88	16X-3	80	141.50	0.645	3.225
15X-1	50	128.60	0.444	2.22	16X-3	100	141.70	0.625	3.125
15X-1	70	128.80	0.512	2.56	16X-3	120	141.90	0.566	2.83
15X-1	80	128.90	0.511	2.555	16X-3	140	142.10	0.555	2.775
15X-1	90	129.00	0.699	3.495	16X-4	20	142.40	0.506	2.53
15X-2	10	129.20	0.583	2.915	16X-4	40	142.60	0.523	2.615
15X-2	20	129.30	0.572	2.86	16X-4	60	142.80	0.575	2.875
15X-2	30	129.40	0.538	2.69	16X-4	80	143.00	0.603	3.015
15X-3	10	129.82	0.61	3.05	16X-4	100	143.20	0.683	3.415
15X-3	30	130.02	0.596	2.98	16X-4	120	143.40	0.637	3.185
15X-3	40	130.12	0.598	2.99	16X-5	20	143.74	0.536	2.68
15X-3	50	130.22	0.516	2.58	16X-5	40	143.94	0.564	2.82
15X-3	70	130.42	0.577	2.885	16X-5	60	144.14	0.527	2.635
15X-3	90	130.62	0.595	2.975	16X-5	140	144.94	0.539	2.695
15X-3	100	130.72	0.506	2.53	16X-6	20	145.09	0.538	2.69
15X-3	120	130.92	0.586	2.93	16X-6	40	145.29	0.551	2.755
15X-4	20	131.42	0.645	3.225	16X-6	60	145.49	0.578	2.89
15X-4	40	131.62	0.597	2.985	16X-6	70	145.59	0.597	2.985
15X-4	60	131.82	0.603	3.015	17X-1	20	146.80	0.509	2.545
15X-4	80	132.02	0.51	2.55	18X-1	20	156.50	0.592	2.96
15X-4	100	132.22	0.576	2.88	18X-1	40	156.70	0.539	2.695
15X-4	120	132.42	0.641	3.205	18X-1	60	156.90	0.602	3.01
15X-4	140	132.62	0.596	2.98	18X-1	80	157.10	0.579	2.895

Table 17. Wenner array electrical resistivity and formation factor results for Hole NGHP-01-17A. (To view the complete table, please see the ASCII files.)—Continued

Core, section	Top (cm)	Depth (mbsf)	Electrical resistivity (W×m)	Apparent formation factor	Core, section	Top (cm)	Depth (mbsf)	Electrical resistivity (W×m)	Apparent formation factor
NGHP-01-17A—Continued									
18X-1	100	157.30	0.558	2.79	19X-6	80	173.13	0.567	2.835
18X-1	120	157.50	0.668	3.34	19X-6	100	173.33	0.616	3.08
18X-2	20	157.76	0.492	2.46	19X-6	120	173.53	0.591	2.955
18X-2	40	157.96	0.578	2.89	19X-7	15	173.98	0.569	2.845
18X-2	60	158.16	0.561	2.805	19X-7	38	174.21	0.583	2.915
18X-2	80	158.36	0.536	2.68	19X-7	55	174.38	0.599	2.995
18X-2	100	158.56	0.602	3.01	19X-7	75	174.58	0.558	2.79
18X-3	20	159.26	0.676	3.38	19X-7	101	174.84	0.595	2.975
18X-3	40	159.46	0.571	2.855	19X-7	118	175.01	0.6	3
18X-3	57	159.63	0.611	3.055	19X-7	135	175.18	0.583	2.915
18X-3	80	159.86	0.536	2.68	20Y-1	10	175.60	0.823	4.115
18X-3	100	160.06	0.46	2.3	20Y-1	20	175.70	0.918	4.59
18X-4	27	160.83	0.671	3.355	20Y-1	30	175.80	0.849	4.245
18X-4	40	160.96	0.568	2.84	20Y-1	40	175.90	0.745	3.725
18X-4	60	161.16	0.563	2.815	20Y-1	50	176.00	0.728	3.64
18X-4	80	161.36	0.651	3.255	20Y-1	65	176.15	0.762	3.81
18X-4	100	161.56	0.71	3.55	21X-1	15	176.65	0.499	2.495
18X-4	120	161.76	0.667	3.335	21X-1	49	176.99	0.506	2.53
18X-4	140	161.96	0.583	2.915	21X-1	78	177.28	0.437	2.185
18X-5	10	162.16	0.638	3.19	21X-1	115	177.65	0.513	2.565
18X-5	30	162.36	0.572	2.86	21X-2	15	178.15	0.685	3.425
18X-5	50	162.56	0.613	3.065	21X-2	33	178.33	0.609	3.045
18X-6	10	163.41	0.579	2.895	21X-2	47	178.47	0.537	2.685
18X-6	30	163.61	0.587	2.935	21X-2	68	178.68	0.585	2.925
18X-6	50	163.81	0.643	3.215	21X-3	15	179.65	0.615	3.075
18X-6	70	164.01	0.657	3.285	21X-3	36	179.86	0.601	3.005
18X-6	90	164.21	0.668	3.34	21X-3	56	180.06	0.579	2.895
18X-6	110	164.41	0.577	2.885	21X-3	75	180.25	0.66	3.3
18X-6	130	164.61	0.672	3.36	21X-3	96	180.46	0.591	2.955
18X-7	10	164.91	0.524	2.62	21X-3	113	180.63	0.673	3.365
18X-7	32	165.13	0.601	3.005	22X-1	8	185.28	0.793	3.965
19X-2	20	166.53	0.551	2.755	22X-1	32	185.52	0.602	3.01
19X-2	40	166.73	0.556	2.78	22X-1	60	185.80	0.706	3.53
19X-2	60	166.93	0.638	3.19	22X-1	80	186.00	0.678	3.39
19X-2	80	167.13	0.581	2.905	22X-1	89	186.09	0.572	2.86
19X-2	100	167.33	0.735	3.675	22X-2	16	186.76	0.619	3.095
19X-2	120	167.53	0.682	3.41	22X-2	37	186.97	0.598	2.99
19X-3	20	168.03	0.574	2.87	22X-2	55	187.15	0.701	3.505
19X-3	40	168.23	0.609	3.045	22X-2	74	187.34	0.655	3.275
19X-3	60	168.43	0.554	2.77	22X-2	95	187.55	0.7	3.5
19X-3	80	168.63	0.562	2.81	22X-2	115	187.75	0.695	3.475
19X-3	100	168.83	0.633	3.165	22X-2	130	187.90	0.707	3.535
19X-4	20	169.53	0.63	3.15	22X-3	15	188.25	0.707	3.535
19X-4	40	169.73	0.636	3.18	22X-3	35	188.45	0.641	3.205
19X-4	60	169.93	0.561	2.805	22X-3	55	188.65	0.716	3.58
19X-4	80	170.13	0.529	2.645	22X-3	75	188.85	0.768	3.84
19X-4	100	170.33	0.526	2.63	22X-3	95	189.05	0.744	3.72
19X-4	120	170.53	0.591	2.955	22X-3	115	189.25	0.821	4.105
19X-4	140	170.73	0.519	2.595	22X-3	135	189.45	0.715	3.575
19X-5	10	170.93	0.609	3.045	22X-4	15	189.75	0.702	3.51
19X-5	30	171.13	0.615	3.075	22X-4	35	189.95	0.623	3.115
19X-5	50	171.33	0.564	2.82	22X-4	55	190.15	0.694	3.47
19X-5	70	171.53	0.526	2.63	22X-4	75	190.35	0.651	3.255
19X-6	20	172.53	0.542	2.71	22X-4	95	190.55	0.722	3.61
19X-6	40	172.73	0.651	3.255	22X-4	114	190.74	0.636	3.18
19X-6	60	172.93	0.61	3.05	22X-4	134	190.94	0.67	3.35

Table 17. Wenner array electrical resistivity and formation factor results for Hole NGHP-01-17A. (To view the complete table, please see the ASCII files.)—Continued

Core, section	Top (cm)	Depth (mbsf)	Electrical resistivity (W×m)	Apparent formation factor	Core, section	Top (cm)	Depth (mbsf)	Electrical resistivity (W×m)	Apparent formation factor
NGHP-01-17A—Continued									
22X-5	15	191.25	0.63	3.15	25X-2	69	215.69	0.918	4.59
22X-5	33	191.43	0.688	3.44	25X-2	115	216.15	0.886	4.43
22X-5	50	191.60	0.683	3.415	25X-2	132	216.32	1.079	5.395
22X-6	15	192.54	0.719	3.595	25X-3	27	216.77	0.691	3.455
22X-6	39	192.78	0.698	3.49	25X-3	45	216.95	0.679	3.395
22X-6	60	192.99	0.693	3.465	25X-3	82	217.32	0.663	3.315
22X-6	80	193.19	0.719	3.595	25X-3	111	217.61	0.69	3.45
22X-7	15	193.54	0.712	3.56	25X-3	123	217.73	0.682	3.41
22X-7	38	193.77	0.695	3.475	25X-4	16	218.16	1.356	6.78
22X-7	53	193.92	0.762	3.81	25X-4	37	218.37	0.81	4.05
23X-1	7	194.97	0.601	3.005	25X-4	67	218.67	0.605	3.025
23X-1	26	195.16	0.603	3.015	25X-5	30	219.40	0.82	4.1
23X-1	46	195.36	0.555	2.775	25X-5	53	219.63	0.844	4.22
23X-1	66	195.56	0.674	3.37	25X-5	86	219.96	0.727	3.635
23X-2	13	195.81	0.602	3.01	25X-5	120	220.30	0.914	4.57
23X-2	28	195.96	0.658	3.29	25X-5	143	220.53	0.868	4.34
23X-2	55	196.23	0.624	3.12	25X-6	7	220.67	0.71	3.55
23X-2	75	196.43	0.689	3.445	25X-6	28	220.88	0.764	3.82
23X-2	93	196.61	0.627	3.135	25X-6	55	221.15	0.64	3.2
23X-2	122	196.90	0.631	3.155	25X-6	88	221.48	0.789	3.945
23X-2	141	197.09	0.679	3.395	26X-1	6	223.16	0.543	2.715
23X-3	14	197.32	0.624	3.12	26X-1	27	223.37	0.501	2.505
23X-3	35	197.53	0.627	3.135	26X-1	47	223.57	0.515	2.575
23X-3	55	197.73	0.597	2.985	26X-1	78	223.88	0.466	2.33
23X-3	76	197.94	0.651	3.255	26X-1	97	224.07	0.524	2.62
23X-3	94	198.12	0.633	3.165	26X-1	109	224.19	0.519	2.595
23X-4	15	198.83	0.58	2.9	26X-2	13	224.73	0.497	2.485
23X-4	35	199.03	0.678	3.39	26X-2	44	225.04	0.516	2.58
23X-4	55	199.23	0.721	3.605	26X-2	62	225.22	0.566	2.83
23X-4	70	199.38	0.643	3.215	26X-2	79	225.39	0.563	2.815
23X-4	90	199.58	0.671	3.355	26X-2	89	225.49	1.018	5.09
23X-4	110	199.78	0.676	3.38	26X-2	109	225.69	0.556	2.78
23X-4	130	199.98	0.633	3.165	26X-2	129	225.89	0.752	3.76
23X-5	33	200.41	0.634	3.17	26X-3	5	226.15	0.598	2.99
23X-5	51	200.59	0.693	3.465	26X-3	27	226.37	0.62	3.1
23X-5	72	200.80	0.648	3.24	26X-3	48	226.58	0.658	3.29
23X-6	15	201.73	0.623	3.115	26X-4	16	227.62	0.527	2.635
23X-6	38	201.96	0.601	3.005	26X-4	35	227.81	0.532	2.66
24X-2	15	204.20	0.57	2.85	26X-4	51	227.97	0.626	3.13
24X-2	37	204.42	0.512	2.56	26X-4	80	228.26	0.656	3.28
24X-2	57	204.62	0.501	2.505	26X-4	108	228.54	0.54	2.7
24X-3	9	205.64	0.49	2.45	27X-1	10	232.90	0.578	2.89
24X-3	31	205.86	0.566	2.83	27X-1	18	232.98	0.633	3.165
24X-3	57	206.12	0.577	2.885	27X-1	31	233.11	0.535	2.675
24X-3	72	206.27	0.562	2.81	27X-1	48	233.28	0.659	3.295
24X-3	93	206.48	0.563	2.815	27X-1	60	233.40	0.527	2.635
24X-4	5	206.60	0.549	2.745	27X-1	72	233.52	0.629	3.145
24X-4	26	206.81	0.583	2.915	27X-1	85	233.65	0.538	2.69
25X-1	12	213.62	0.465	2.325	27X-1	100	233.80	0.624	3.12
25X-1	27	213.77	0.607	3.035	27X-1	110	233.90	0.622	3.11
25X-1	45	213.95	0.823	4.115	27X-2	20	234.50	0.721	3.605
25X-1	51	214.01	0.613	3.065	27X-2	40	234.70	0.603	3.015
25X-1	58	214.08	0.596	2.98	27X-2	60	234.90	0.584	2.92
25X-2	7	215.07	0.708	3.54	27X-2	80	235.10	0.51	2.55
25X-2	22	215.22	0.839	4.195	27X-2	101	235.31	0.519	2.595
25X-2	52	215.52	0.672	3.36	27X-2	120	235.50	0.532	2.66

Table 17. Wenner array electrical resistivity and formation factor results for Hole NGHP-01-17A. (To view the complete table, please see the ASCII files.)—Continued

Core, section	Top (cm)	Depth (mbsf)	Electrical resistivity (W×m)	Apparent formation factor	Core, section	Top (cm)	Depth (mbsf)	Electrical resistivity (W×m)	Apparent formation factor
NGHP-01-17A—Continued									
27X-2	140	235.70	0.52	2.6	30X-3	10	263.70	0.841	4.205
27X-3	10	235.90	0.487	2.435	30X-3	28	263.88	0.711	3.555
27X-3	20	236.00	0.604	3.02	30X-3	41	264.01	0.566	2.83
27X-3	32	236.12	0.495	2.475	30X-3	56	264.16	0.655	3.275
27X-3	40	236.20	0.499	2.495	30X-4	10	265.20	0.508	2.54
27X-3	50	236.30	0.576	2.88	30X-4	30	265.40	0.697	3.485
27X-4	10	237.20	0.656	3.28	30X-4	50	265.60	0.666	3.33
27X-4	20	237.30	0.693	3.465	30X-4	70	265.80	0.679	3.395
27X-4	30	237.40	0.627	3.135	30X-4	92	266.02	0.767	3.835
27X-4	40	237.50	0.583	2.915	30X-4	110	266.20	0.676	3.38
28X-1	18	242.68	0.519	2.595	30X-4	128	266.38	0.586	2.93
28X-1	36	242.86	0.529	2.645	30X-4	142	266.52	0.763	3.815
28X-1	59	243.09	0.519	2.595	30X-5	10	266.70	0.638	3.19
28X-1	86	243.36	0.508	2.54	30X-5	30	266.90	0.741	3.705
28X-1	116	243.66	0.496	2.48	30X-5	50	267.10	0.677	3.385
29X-2	10	253.08	0.565	2.825	30X-5	70	267.30	0.721	3.605
29X-2	22	253.20	0.575	2.875	30X-5	88	267.48	0.746	3.73
29X-2	37	253.35	0.764	3.82	30X-6	10	267.71	0.631	3.155
29X-2	52	253.50	0.726	3.63	30X-6	25	267.86	0.604	3.02
29X-2	68	253.66	0.673	3.365	30X-7	40	268.67	0.689	3.445
29X-2	78	253.76	0.718	3.59	30X-7	60	268.87	0.619	3.095
29X-3	10	254.14	0.603	3.015	30X-7	79	269.06	0.664	3.32
29X-3	19	254.23	0.547	2.735	30X-7	99	269.26	0.589	2.945
29X-3	40	254.44	0.699	3.495	30X-7	133	269.60	0.718	3.59
29X-3	50	254.54	0.773	3.865	30X-8	10	269.87	0.737	3.685
29X-3	68	254.72	0.657	3.285	30X-8	28	270.05	0.569	2.845
29X-4	19	255.73	0.73	3.65	30X-8	44	270.21	0.574	2.87
29X-4	30	255.84	0.652	3.26	30X-8	70	270.47	1.096	5.48
29X-4	44	255.98	0.688	3.44	30X-8	76	270.53	0.737	3.685
29X-4	58	256.12	0.695	3.475	30X-8	88	270.65	0.522	2.61
29X-4	84	256.38	0.708	3.54	31X-1	23	270.53	0.624	3.12
29X-4	102	256.56	0.697	3.485	31X-1	42	270.72	0.585	2.925
29X-4	127	256.81	0.954	4.77	31X-1	61	270.91	0.547	2.735
29X-4	137	256.91	0.783	3.915	31X-2	34	271.32	1.005	5.025
29X-5	25	257.29	0.817	4.085	31X-2	56	271.54	0.678	3.39
29X-5	37	257.41	0.758	3.79	31X-2	78	271.76	0.825	4.125
29X-5	59	257.63	0.659	3.295	31X-2	104	272.02	0.66	3.3
29X-5	77	257.81	0.842	4.21	31X-3	23	272.56	0.77	3.85
29X-5	87	257.91	0.735	3.675	31X-3	29	272.62	0.761	3.805
29X-5	99	258.03	0.684	3.42	31X-3	47	272.80	0.662	3.31
29X-6	20	258.74	0.704	3.52	31X-3	54	272.87	0.64	3.2
29X-6	31	258.85	0.699	3.495	31X-3	63	272.96	0.721	3.605
29X-6	47	259.01	0.685	3.425	31X-3	79	273.12	0.685	3.425
29X-6	86	259.40	0.76	3.8	31X-5	16	274.99	0.702	3.51
29X-7	17	259.71	0.591	2.955	31X-6	37	276.05	0.581	2.905
29X-7	25	259.79	0.688	3.44	31X-6	55	276.23	1.237	6.185
29X-7	38	259.92	0.518	2.59	31X-6	87	276.55	0.612	3.06
29X-7	60	260.14	0.667	3.335	31X-6	116	276.84	0.941	4.705
30X-1	20	261.60	0.645	3.225	31X-6	135	277.03	1.215	6.075
30X-1	40	261.80	0.607	3.035	31X-7	27	277.45	0.715	3.575
30X-2	20	262.30	0.685	3.425	31X-7	49	277.67	0.872	4.36
30X-2	40	262.50	0.545	2.725	31X-8	33	278.28	1.014	5.07
30X-2	81	262.91	0.661	3.305	31X-8	61	278.56	0.604	3.02
30X-2	101	263.11	0.715	3.575	31X-8	87	278.82	0.964	4.82
30X-2	121	263.31	0.569	2.845	31X-8	105	279.00	0.68	3.4
30X-2	133	263.43	0.625	3.125	32X-1	75	280.65	0.742	3.71

Table 17. Wenner array electrical resistivity and formation factor results for Hole NGHP-01-17A. (To view the complete table, please see the ASCII files.)—Continued

Core, section	Top (cm)	Depth (mbsf)	Electrical resistivity (W×m)	Apparent formation factor	Core, section	Top (cm)	Depth (mbsf)	Electrical resistivity (W×m)	Apparent formation factor
NGHP-01-17A—Continued									
32X-1	128	281.18	0.749	3.745	36X-4	64	322.48	0.683	3.415
32X-2	50	281.90	0.769	3.845	36X-5	16	323.43	0.723	3.615
32X-2	108	282.48	0.755	3.775	36X-5	35	323.62	0.663	3.315
32X-3	57	283.47	0.73	3.65	36X-5	46	323.73	0.542	2.71
32X-4	48	284.75	0.788	3.94	36X-5	53	323.80	0.651	3.255
32X-4	78	285.05	0.704	3.52	36X-5	74	324.01	0.684	3.42
32X-5	30	285.57	0.735	3.675	36X-5	80	324.07	0.783	3.915
33X-1	22	289.82	0.647	3.235	36X-5	101	324.28	0.732	3.66
33X-1	41	290.01	0.734	3.67	36X-5	126	324.53	0.75	3.75
33X-2	18	291.04	0.699	3.495	36X-6	13	324.90	0.598	2.99
33X-2	32	291.18	0.712	3.56	36X-6	24	325.01	0.718	3.59
34X-1	78	299.98	0.714	3.57	36X-6	40	325.17	0.644	3.22
34X-1	102	300.22	0.791	3.955	36X-6	69	325.46	0.615	3.075
34X-2	27	300.97	0.74	3.7	36X-6	87	325.64	0.614	3.07
34X-3	18	302.38	0.776	3.88	36X-6	122	325.99	0.649	3.245
34X-3	27	302.47	0.813	4.065	38Y-1	8	329.08	0.402	2.01
35X-1	11	308.91	0.766	3.83	38Y-1	15	329.15	0.393	1.965
35X-1	26	309.06	0.749	3.745	38Y-1	19	329.19	0.456	2.28
35X-1	46	309.26	0.724	3.62	38Y-1	23	329.23	0.557	2.785
35X-1	61	309.41	0.754	3.77	38Y-1	33	329.33	0.554	2.77
35X-2	15	309.67	0.731	3.655	38Y-1	44	329.44	0.628	3.14
35X-2	35	309.87	0.729	3.645	38Y-1	76	329.76	0.669	3.345
35X-2	61	310.13	0.745	3.725	39X-1	40	330.40	0.51	2.55
35X-2	87	310.39	0.772	3.86	39X-1	64	330.64	0.526	2.63
35X-2	108	310.60	0.78	3.9	39X-1	97	330.97	0.652	3.26
35X-2	133	310.85	0.823	4.115	39X-1	114	331.14	0.697	3.485
35X-3	5	311.07	0.733	3.665	39X-1	130	331.30	0.75	3.75
35X-3	30	311.32	0.747	3.735	39X-2	55	332.05	0.602	3.01
35X-4	15	312.31	0.68	3.4	39X-2	77	332.27	0.637	3.185
35X-4	40	312.56	0.77	3.85	39X-3	20	333.20	0.594	2.97
35X-4	67	312.83	0.68	3.4	39X-3	58	333.58	0.649	3.245
35X-4	92	313.08	0.717	3.585	39X-4	5	334.55	0.598	2.99
35X-4	105	313.21	0.706	3.53	39X-4	23	334.73	0.569	2.845
35X-5	18	313.84	0.634	3.17	39X-4	53	335.03	0.617	3.085
35X-5	35	314.01	0.671	3.355	39X-6	4	335.82	0.534	2.67
35X-5	54	314.20	0.695	3.475	39X-7	11	336.22	0.543	2.715
35X-5	85	314.51	0.675	3.375	39X-7	22	336.33	0.657	3.285
35X-5	106	314.72	0.71	3.55	39X-7	75	336.86	0.602	3.01
35X-5	138	315.04	0.717	3.585	40X-1	11	337.71	0.601	3.005
35X-6	8	315.24	0.641	3.205	40X-1	25	337.85	0.645	3.225
35X-6	22	315.38	0.755	3.775	40X-2	10	338.03	0.636	3.18
35X-6	91	316.07	0.782	3.91	40X-2	30	338.23	0.641	3.205
35X-7	12	316.52	0.702	3.51	40X-2	30	338.23	0.596	2.98
35X-7	29	316.69	0.768	3.84	40X-2	50	338.43	0.562	2.81
35X-8	16	317.55	0.692	3.46	40X-2	70	338.63	0.614	3.07
36X-2	30	319.69	0.647	3.235	40X-2	80	338.73	0.611	3.055
36X-2	64	320.03	0.64	3.2	40X-2	102	338.95	0.634	3.17
36X-2	99	320.38	0.694	3.47	40X-2	122	339.15	0.708	3.54
36X-2	148	320.87	0.684	3.42	40X-2	139	339.32	0.574	2.87
36X-3	22	321.11	0.548	2.74	40X-2	142	339.35	0.58	2.9
36X-3	65	321.54	0.673	3.365	40X-3	10	339.53	0.604	3.02
36X-3	70	321.59	0.622	3.11	40X-3	30	339.73	0.575	2.875
36X-3	75	321.64	0.679	3.395	40X-3	48	339.91	0.558	2.79
36X-3	80	321.69	0.626	3.13	40X-3	70	340.13	0.557	2.785
36X-4	10	321.94	0.605	3.025	40X-3	79	340.22	0.57	2.85
36X-4	36	322.20	0.654	3.27	40X-4	20	341.04	0.727	3.635

Table 17. Wenner array electrical resistivity and formation factor results for Hole NGHP-01-17A. (To view the complete table, please see the ASCII files.)—Continued

Core, section	Top (cm)	Depth (mbsf)	Electrical resistivity (W×m)	Apparent formation factor	Core, section	Top (cm)	Depth (mbsf)	Electrical resistivity (W×m)	Apparent formation factor
NGHP-01-17A—Continued									
40X-4	40	341.24	0.655	3.275	42X-4	122	362.01	0.942	4.71
40X-4	60	341.44	0.57	2.85	42X-5	34	362.63	0.766	3.83
40X-4	100	341.84	0.843	4.215	42X-5	70	362.99	0.968	4.84
40X-4	102	341.86	0.866	4.33	42X-6	16	363.45	0.797	3.985
40X-4	119	342.03	0.691	3.455	42X-6	41	363.70	2.218	11.09
40X-4	134	342.18	0.683	3.415	42X-6	41	363.70	2.145	10.725
40X-5	20	342.48	0.665	3.325	42X-6	54	363.83	1.534	7.67
40X-5	40	342.68	0.653	3.265	42X-7	21	364.16	0.872	4.36
40X-5	60	342.88	0.692	3.46	42X-7	40	364.35	1.544	7.72
40X-6	20	343.88	0.702	3.51	42X-7	79	364.74	1.973	9.865
40X-6	40	344.08	0.641	3.205	43X-1	45	367.25	0.921	4.605
40X-6	60	344.28	0.708	3.54	43X-1	65	367.45	0.711	3.555
40X-6	80	344.48	0.63	3.15	43X-2	20	368.00	1.578	7.89
40X-7	10	344.78	0.588	2.94	43X-2	30	368.10	1.659	8.295
40X-7	28	344.96	0.603	3.015	43X-3	26	368.96	1.103	5.515
40X-8	10	345.68	0.608	3.04	43X-3	44	369.14	1.027	5.135
40X-8	58	346.16	0.65	3.25	43X-3	65	369.35	1.073	5.365
40X-8	81	346.39	0.657	3.285	43X-3	88	369.58	0.888	4.44
40X-8	100	346.58	0.676	3.38	43X-3	110	369.80	1.125	5.625
41X-1	23	347.53	0.647	3.235	43X-3	134	370.04	0.918	4.59
41X-1	42	347.72	0.653	3.265	43X-4	23	370.43	0.847	4.235
41X-1	72	348.02	0.671	3.355	43X-4	43	370.63	0.96	4.8
41X-1	99	348.29	0.642	3.21	43X-4	70	370.90	1.001	5.005
41X-1	126	348.56	0.47	2.35	43X-4	90	371.10	0.943	4.715
41X-2	20	349.00	0.611	3.055	43X-5	20	371.40	1.15	5.75
41X-2	35	349.15	0.643	3.215	43X-5	47	371.67	0.986	4.93
41X-2	60	349.40	0.633	3.165	43X-6	11	372.14	0.711	3.555
41X-3	20	350.50	0.664	3.32	43X-7	20	373.08	0.935	4.675
41X-3	21	350.51	1.44	7.2	43X-7	40	373.28	0.791	3.955
41X-3	41	350.71	0.708	3.54	43X-7	70	373.58	1.962	9.81
41X-3	52	350.82	0.716	3.58	43X-8	33	374.20	0.831	4.155
41X-3	69	350.99	1.602	8.01	43X-8	55	374.42	0.77	3.85
41X-3	82	351.12	0.835	4.175	44X-1	30	376.40	1.057	5.285
41X-5	29	353.20	1.175	5.875	44X-1	50	376.60	0.805	4.025
41X-5	52	353.43	0.777	3.885	44X-1	134	377.44	1.761	8.805
41X-5	72	353.63	1.045	5.225	44X-2	24	377.84	1.043	5.215
41X-5	93	353.84	0.614	3.07	44X-2	40	378.00	1.246	6.23
41X-6	48	354.55	1.984	9.92	44X-2	73	378.33	0.83	4.15
41X-6	48	354.55	1.832	9.16	44X-2	93	378.53	1.546	7.73
41X-6	69	354.76	0.979	4.895	44X-3	13	378.73	0.844	4.22
41X-6	104	355.11	1.007	5.035	44X-4	20	379.46	1.043	5.215
42X-1	17	357.17	0.659	3.295	44X-4	40	379.66	0.794	3.97
42X-1	37	357.37	0.666	3.33	44X-4	66	379.92	0.694	3.47
42X-1	66	357.66	0.526	2.63	44X-5	25	381.01	0.692	3.46
42X-2	20	357.99	0.592	2.96	44X-5	45	381.21	0.725	3.625
42X-2	40	358.19	0.629	3.145	44X-5	65	381.41	0.721	3.605
42X-2	60	358.39	0.626	3.13	44X-5	85	381.61	0.746	3.73
42X-2	80	358.59	0.619	3.095	44X-6	36	382.12	0.722	3.61
42X-2	115	358.94	0.676	3.38	44X-6	54	382.30	0.746	3.73
42X-2	132	359.11	0.731	3.655	46X-1	67	396.07	1.391	6.955
42X-3	20	359.49	0.676	3.38	46X-1	92	396.32	1.224	6.12
42X-3	45	359.74	0.832	4.16	46X-1	117	396.57	1.014	5.07
42X-3	65	359.94	0.68	3.4	46X-2	31	396.95	0.768	3.84
42X-4	41	361.20	0.827	4.135	46X-2	61	397.25	1.127	5.635
42X-4	61	361.40	0.733	3.665	46X-2	83	397.47	0.804	4.02
42X-4	92	361.71	0.752	3.76	46X-2	109	397.73	0.931	4.655

Table 17. Wenner array electrical resistivity and formation factor results for Hole NGHP-01-17A. (To view the complete table, please see the ASCII files.)—Continued

Core, section	Top (cm)	Depth (mbsf)	Electrical resistivity (W×m)	Apparent formation factor	Core, section	Top (cm)	Depth (mbsf)	Electrical resistivity (W×m)	Apparent formation factor
NGHP-01-17A—Continued									
46X-2	129	397.93	0.916	4.58	50X-2	41	416.11	0.654	3.27
46X-3	28	398.42	0.855	4.275	50X-2	64	416.34	0.608	3.04
46X-3	48	398.62	0.805	4.025	50X-2	89	416.59	0.638	3.19
46X-3	68	398.82	0.771	3.855	50X-3	23	416.93	0.584	2.92
46X-3	88	399.02	0.751	3.755	50X-3	52	417.22	0.595	2.975
46X-3	108	399.22	0.825	4.125	50X-3	84	417.54	0.617	3.085
46X-3	128	399.42	0.85	4.25	50X-3	114	417.84	0.616	3.08
46X-4	31	399.95	0.743	3.715	50X-3	136	418.06	0.591	2.955
46X-4	51	400.15	0.887	4.435	50X-4	20	418.40	0.624	3.12
46X-4	71	400.35	0.719	3.595	50X-4	36	418.56	0.671	3.355
46X-5	18	401.32	0.71	3.55	50X-4	57	418.77	0.544	2.72
46X-5	38	401.52	0.729	3.645	50X-5	11	419.81	0.621	3.105
46X-5	52	401.66	0.777	3.885	50X-5	30	420.00	0.61	3.05
46X-6	20	402.31	0.749	3.745	50X-5	50	420.20	0.607	3.035
46X-6	40	402.51	0.927	4.635	50X-6	23	420.72	0.629	3.145
46X-6	60	402.71	0.812	4.06	50X-6	47	420.96	0.607	3.035
46X-6	80	402.91	0.924	4.62	50X-6	76	421.25	0.606	3.03
46X-6	100	403.11	0.854	4.27	50X-7	21	421.57	0.616	3.08
46X-7	26	403.37	0.915	4.575	50X-7	40	421.76	0.585	2.925
46X-7	46	403.57	0.688	3.44	50X-8	8	422.49	0.61	3.05
47X-1	26	405.36	1.043	5.215	50X-8	23	422.64	0.63	3.15
47X-1	46	405.56	1.056	5.28	50X-8	39	422.80	0.662	3.31
47X-1	66	405.76	1.159	5.795	51X-1	38	424.68	0.829	4.145
47X-1	86	405.96	1.286	6.43	51X-1	59	424.89	0.74	3.7
47X-1	106	406.16	0.802	4.01	51X-1	93	425.23	0.699	3.495
47X-1	126	406.36	0.896	4.48	51X-1	116	425.46	0.724	3.62
47X-1	146	406.56	0.923	4.615	51X-2	48	426.21	0.699	3.495
47X-2	20	406.80	0.774	3.87	51X-2	72	426.45	0.707	3.535
47X-2	40	407.00	0.727	3.635	51X-2	107	426.80	0.66	3.3
47X-2	60	407.20	0.721	3.605	51X-2	134	427.07	0.765	3.825
47X-2	80	407.40	0.736	3.68	51X-3	18	427.41	0.751	3.755
47X-2	100	407.60	0.743	3.715	51X-3	49	427.72	0.663	3.315
47X-3	20	407.80	0.796	3.98	51X-3	65	427.88	0.675	3.375
47X-3	40	408.00	0.694	3.47	51X-4	33	428.75	0.861	4.305
47X-3	60	408.20	0.712	3.56	51X-4	56	428.98	0.669	3.345
47X-4	30	409.10	0.786	3.93	51X-4	92	429.34	0.722	3.61
47X-4	50	409.30	0.678	3.39	51X-4	125	429.67	0.718	3.59
47X-5	25	410.08	0.688	3.44	51X-5	34	430.26	0.675	3.375
47X-5	45	410.28	0.776	3.88	51X-5	52	430.44	0.656	3.28
47X-5	65	410.48	0.663	3.315	51X-5	53	430.45	0.655	3.275
47X-6	24	411.57	0.783	3.915	51X-6	22	431.64	0.708	3.54
47X-6	44	411.77	0.645	3.225	51X-6	41	431.83	0.749	3.745
47X-6	64	411.97	0.582	2.91	51X-6	99	432.41	0.671	3.355
47X-6	96	412.29	0.636	3.18	52X-1	32	434.32	0.702	3.51
47X-6	116	412.49	0.594	2.97	52X-1	50	434.50	0.653	3.265
47X-6	139	412.72	0.69	3.45	52X-1	79	434.79	0.576	2.88
47X-7	7	412.90	0.678	3.39	52X-1	103	435.03	0.624	3.12
47X-7	42	413.25	0.614	3.07	52X-2	15	435.65	0.67	3.35
49P-1	28	413.98	0.752	3.76	52X-2	56	436.06	0.67	3.35
49P-1	64	414.34	0.748	3.74	52X-2	102	436.52	0.658	3.29
49P-1	70	414.40	0.744	3.72	52X-2	140	436.90	0.658	3.29
49P-1	78	414.48	0.657	3.285	52X-3	25	437.25	0.647	3.235
50X-1	68	415.38	0.678	3.39	52X-3	56	437.56	0.697	3.485
50X-1	83	415.53	0.65	3.25	52X-3	86	437.86	0.697	3.485
50X-2	9	415.79	0.621	3.105	52X-3	126	438.26	0.656	3.28
50X-2	21	415.91	0.624	3.12	52X-4	10	438.60	0.655	3.275

Table 17. Wenner array electrical resistivity and formation factor results for Hole NGHP-01-17A. (To view the complete table, please see the ASCII files.)—Continued

Core, section	Top (cm)	Depth (mbsf)	Electrical resistivity (W×m)	Apparent formation factor	Core, section	Top (cm)	Depth (mbsf)	Electrical resistivity (W×m)	Apparent formation factor
NGHP-01-17A—Continued									
52X-4	48	438.98	0.722	3.61	54X-5	89	459.13	0.601	3.005
52X-4	70	439.20	0.676	3.38	54X-5	122	459.46	0.617	3.085
52X-4	89	439.39	0.68	3.4	54X-5	136	459.60	0.646	3.23
52X-5	11	439.61	0.745	3.725	54X-6	25	459.99	0.645	3.225
52X-6	58	440.65	0.734	3.67	55X-1	90	463.90	0.714	3.57
52X-7	19	441.76	0.578	2.89	55X-3	29	464.86	0.605	3.025
52X-7	48	442.05	0.651	3.255	55X-4	13	465.02	0.599	2.995
52X-7	97	442.54	0.787	3.935	55X-4	34	465.23	0.723	3.615
53X-1	5	443.75	0.577	2.885	55X-4	54	465.43	0.72	3.6
53X-1	29	443.99	0.602	3.01	55X-4	74	465.63	0.654	3.27
53X-1	50	444.20	0.682	3.41	55X-4	94	465.83	0.74	3.7
53X-2	22	444.48	0.603	3.015	55X-4	124	466.13	0.723	3.615
53X-2	35	444.61	0.629	3.145	55X-5	5	466.44	0.745	3.725
53X-2	45	444.71	0.714	3.57	55X-5	47	466.86	0.761	3.805
53X-2	71	444.97	0.645	3.225	55X-5	66	467.05	0.707	3.535
53X-2	97	445.23	0.632	3.16	55X-5	86	467.25	0.718	3.59
53X-3	10	445.45	0.623	3.115	55X-6	6	467.52	0.702	3.51
53X-3	32	445.67	0.63	3.15	55X-6	28	467.74	0.637	3.185
53X-3	55	445.90	0.623	3.115	55X-7	12	468.58	0.629	3.145
53X-3	73	446.08	0.681	3.405	55X-7	29	468.75	0.667	3.335
53X-3	94	446.29	0.634	3.17	55X-8	35	469.47	0.632	3.16
53X-3	116	446.51	0.771	3.855	56X-1	33	473.03	0.711	3.555
53X-3	135	446.70	0.766	3.83	56X-1	47	473.17	0.696	3.48
53X-4	12	446.97	0.735	3.675	56X-1	62	473.32	0.68	3.4
53X-4	37	447.22	0.684	3.42	56X-1	76	473.46	0.668	3.34
53X-5	16	448.34	0.643	3.215	56X-1	96	473.66	0.665	3.325
53X-5	36	448.54	0.657	3.285	56X-2	9	473.79	0.626	3.13
53X-5	50	448.68	0.671	3.355	56X-2	31	474.01	0.605	3.025
53X-5	76	448.94	0.707	3.535	56X-2	55	474.25	0.606	3.03
53X-5	89	449.07	0.701	3.505	56X-3	11	474.80	0.625	3.125
53X-6	20	449.38	0.723	3.615	56X-3	28	474.97	0.656	3.28
53X-6	30	449.48	0.711	3.555	56X-3	50	475.19	0.643	3.215
53X-7	34	450.14	0.747	3.735	56X-3	65	475.34	0.656	3.28
53X-7	58	450.38	0.672	3.36	56X-4	10	476.29	0.559	2.795
53X-7	83	450.63	0.68	3.4	56X-4	23	476.42	0.616	3.08
53X-7	120	451.00	0.645	3.225	56X-4	32	476.51	0.656	3.28
53X-7	139	451.19	0.651	3.255	57X-1	20	482.60	0.644	3.22
53X-8	11	451.41	0.639	3.195	57X-2	31	483.10	0.715	3.575
54X-1	35	453.75	0.613	3.065	57X-2	51	483.30	0.699	3.495
54X-1	46	453.86	0.659	3.295	57X-2	75	483.54	0.689	3.445
54X-2	28	454.27	0.583	2.915	57X-2	95	483.74	0.63	3.15
54X-2	46	454.45	0.591	2.955	57X-2	115	483.94	0.631	3.155
54X-2	58	454.57	0.629	3.145	57X-2	135	484.14	0.642	3.21
54X-2	76	454.75	0.575	2.875	57X-3	23	484.41	0.722	3.61
54X-3	27	455.55	0.619	3.095	57X-3	48	484.66	0.616	3.08
54X-3	45	455.73	0.639	3.195	57X-3	68	484.86	0.693	3.465
54X-3	67	455.95	0.664	3.32	57X-4	21	485.89	0.71	3.55
54X-4	9	456.83	0.613	3.065	57X-4	45	486.13	0.658	3.29
54X-4	38	457.12	0.626	3.13	57X-4	65	486.33	0.562	2.81
54X-4	56	457.30	0.629	3.145	57X-4	85	486.53	0.618	3.09
54X-4	83	457.57	0.693	3.465	57X-5	20	486.88	0.593	2.965
54X-4	108	457.82	0.638	3.19	57X-5	40	487.08	0.698	3.49
54X-4	125	457.99	0.626	3.13	58X-1	27	492.27	0.614	3.07
54X-5	14	458.38	0.656	3.28	58X-1	51	492.51	0.589	2.945
54X-5	36	458.60	0.592	2.96	58X-1	81	492.81	0.713	3.565
54X-5	56	458.80	0.613	3.065	58X-1	105	493.05	0.595	2.975

Table 17. Wenner array electrical resistivity and formation factor results for Hole NGHP-01-17A. (To view the complete table, please see the ASCII files.)—Continued

Core, section	Top (cm)	Depth (mbsf)	Electrical resistivity (W×m)	Apparent formation factor	Core, section	Top (cm)	Depth (mbsf)	Electrical resistivity (W×m)	Apparent formation factor
NGHP-01-17A—Continued									
58X-2	44	493.72	0.633	3.165	62X-3	46	514.08	0.627	3.135
58X-2	69	493.97	0.68	3.4	62X-3	69	514.31	0.625	3.125
58X-2	99	494.27	0.593	2.965	62X-3	97	514.59	0.629	3.145
58X-2	124	494.52	0.682	3.41	62X-3	129	514.91	0.596	2.98
58X-2	142	494.70	0.53	2.65	62X-4	14	515.25	0.589	2.945
58X-3	16	494.94	0.658	3.29	62X-4	34	515.45	0.641	3.205
58X-3	36	495.14	0.594	2.97	62X-5	18	516.79	0.668	3.34
58X-3	60	495.38	0.634	3.17	62X-5	36	516.97	0.675	3.375
58X-3	80	495.58	0.647	3.235	62X-5	52	517.13	0.697	3.485
58X-4	20	495.98	0.571	2.855	62X-5	74	517.35	0.701	3.505
58X-4	40	496.18	0.625	3.125	62X-6	40	518.51	0.702	3.51
58X-4	60	496.38	0.567	2.835	62X-6	59	518.70	0.626	3.13
58X-4	77	496.55	0.607	3.035	63X-2	26	521.99	0.702	3.51
58X-5	18	497.41	0.638	3.19	63X-2	54	522.27	0.704	3.52
58X-5	38	497.61	0.633	3.165	63X-2	76	522.49	0.686	3.43
58X-5	62	497.85	0.608	3.04	63X-2	96	522.69	0.668	3.34
58X-6	24	498.97	0.615	3.075	63X-2	116	522.89	0.685	3.425
58X-6	44	499.17	0.614	3.07	63X-2	136	523.09	0.695	3.475
58X-6	66	499.39	0.656	3.28	63X-3	20	523.43	0.717	3.585
58X-6	86	499.59	0.635	3.175	63X-4	65	524.88	0.644	3.22
58X-6	103	499.76	0.685	3.425	63X-5	10	525.15	0.849	4.245
60P-1	59	501.19	0.66	3.3	63X-5	38	525.43	0.67	3.35
60P-1	69	501.29	0.669	3.345	63X-5	58	525.63	0.659	3.295
61X-2	10	502.41	0.648	3.24	63X-5	78	525.83	0.702	3.51
61X-2	30	502.61	0.696	3.48	63X-5	104	526.09	0.678	3.39
61X-2	46	502.77	0.573	2.865	63X-5	137	526.42	0.676	3.38
61X-2	62	502.93	0.678	3.39	63X-6	10	526.65	0.628	3.14
61X-2	80	503.11	0.517	2.585	63X-6	45	527.00	0.723	3.615
61X-2	100	503.31	0.711	3.555	63X-6	73	527.28	0.667	3.335
61X-3	28	503.76	0.715	3.575	63X-6	101	527.56	0.677	3.385
61X-3	50	503.98	0.694	3.47	63X-6	137	527.92	0.683	3.415
61X-3	70	504.18	0.551	2.755	63X-7	45	528.50	0.701	3.505
61X-3	90	504.38	0.603	3.015	63X-7	65	528.70	0.758	3.79
61X-3	110	504.58	0.551	2.755	64X-2	52	531.89	1.442	7.21
61X-3	127	504.75	0.631	3.155	64X-2	53	531.90	0.979	4.895
61X-4	26	505.24	0.651	3.255	64X-2	73	532.10	1.472	7.36
61X-4	26	505.24	0.639	3.195	64X-2	75	532.12	1.124	5.62
61X-4	46	505.44	0.65	3.25	64X-2	97	532.34	0.754	3.77
61X-4	47	505.45	0.636	3.18	64X-2	127	532.64	0.774	3.87
61X-4	68	505.66	0.644	3.22	64X-3	18	533.05	0.695	3.475
61X-5	31	506.79	0.59	2.95	64X-3	47	533.34	0.807	4.035
61X-5	51	506.99	0.675	3.375	64X-3	69	533.56	0.546	2.73
61X-5	78	507.26	0.57	2.85	65X-1	20	540.20	0.646	3.23
61X-5	96	507.44	0.623	3.115	65X-1	46	540.46	0.697	3.485
62X-1	10	511.30	0.657	3.285	65X-1	61	540.61	0.76	3.8
62X-1	30	511.50	0.641	3.205	65X-1	80	540.80	0.595	2.975
62X-1	42	511.62	0.66	3.3	65X-1	101	541.01	0.706	3.53
62X-1	72	511.92	0.672	3.36	65X-1	122	541.22	0.734	3.67
62X-1	92	512.12	0.706	3.53	65X-1	122	541.22	0.734	3.67
62X-2	10	512.34	0.722	3.61	65X-1	132	541.32	0.734	3.67
62X-2	32	512.56	0.658	3.29	65X-1	132	541.32	0.717	3.585
62X-2	61	512.85	0.703	3.515	65X-1	139	541.39	0.722	3.61
62X-2	80	513.04	0.703	3.515	65X-2	8	541.58	0.735	3.675
62X-2	105	513.29	0.692	3.46	65X-2	30	541.80	0.736	3.68
62X-2	122	513.46	0.712	3.56	65X-2	50	542.00	0.955	4.775
62X-3	10	513.72	0.698	3.49	65X-3	11	543.01	0.766	3.83

Table 17. Wenner array electrical resistivity and formation factor results for Hole NGHP-01-17A. (To view the complete table, please see the ASCII files.)—Continued

Core, section	Top (cm)	Depth (mbsf)	Electrical resistivity (W×m)	Apparent formation factor	Core, section	Top (cm)	Depth (mbsf)	Electrical resistivity (W×m)	Apparent formation factor
NGHP-01-17A—Continued									
65X-3	33	543.23	0.701	3.505	69X-1	86	579.56	0.889	4.445
65X-3	51	543.41	0.793	3.965	69X-1	116	579.86	0.821	4.105
66X-1	27	549.97	0.682	3.41	69X-1	135	580.05	0.779	3.895
66X-1	49	550.19	0.763	3.815	69X-2	14	580.34	0.77	3.85
66X-1	69	550.39	1.46	7.3	69X-2	65	580.85	0.759	3.795
66X-1	89	550.59	0.791	3.955	69X-2	92	581.12	0.772	3.86
66X-1	110	550.80	0.955	4.775	69X-2	115	581.35	0.752	3.76
66X-1	129	550.99	0.802	4.01	69X-2	137	581.57	0.732	3.66
66X-3	10	552.10	0.803	4.015	69X-2	147	581.67	0.677	3.385
66X-3	19	552.19	0.903	4.515	69X-3	8	581.78	0.651	3.255
66X-3	32	552.32	0.823	4.115	69X-3	32	582.02	0.749	3.745
66X-3	43	552.43	0.746	3.73	69X-3	70	582.40	0.733	3.665
66X-3	66	552.66	0.85	4.25	69X-3	85	582.55	0.746	3.73
66X-3	82	552.82	0.82	4.1	69X-3	139	583.09	0.762	3.81
66X-3	102	553.02	0.768	3.84	69X-4	24	583.44	0.662	3.31
66X-5	55	554.98	0.809	4.045	69X-4	35	583.55	0.793	3.965
66X-7	22	557.14	0.889	4.445	69X-4	49	583.69	0.652	3.26
66X-7	57	557.49	0.916	4.58	69X-5	13	584.83	0.694	3.47
66X-7	75	557.67	0.875	4.375	69X-5	30	585.00	0.703	3.515
66X-7	92	557.84	0.713	3.565	69X-5	60	585.30	0.687	3.435
66X-7	102	557.94	0.704	3.52	69X-5	75	585.45	0.68	3.4
67X-4	45	562.22	0.73	3.65	69X-6	30	586.00	0.74	3.7
67X-5	57	563.21	0.689	3.445	69X-6	30	586.00	0.731	3.655
67X-5	71	563.35	0.672	3.36	69X-6	43	586.13	0.752	3.76
67X-5	91	563.55	0.667	3.335	69X-7	36	587.06	0.827	4.135
67X-5	119	563.83	0.636	3.18	72X-2	46	589.29	0.946	4.73
67X-5	139	564.03	0.596	2.98	72X-2	58	589.41	0.903	4.515
67X-7	30	565.41	0.693	3.465	72X-2	75	589.58	0.77	3.85
68X-1	54	569.54	0.731	3.655	72X-3	19	589.80	0.849	4.245
68X-1	90	569.90	0.755	3.775	73X-2	44	598.94	0.824	4.12
68X-2	5	570.05	0.756	3.78	73X-2	74	599.24	0.896	4.48
68X-2	42	570.42	0.721	3.605	73X-2	91	599.41	0.862	4.31
68X-2	74	570.74	0.751	3.755	73X-2	139	599.89	0.811	4.055
68X-3	24	571.10	0.799	3.995	73X-3	49	600.49	0.889	4.445
68X-3	52	571.38	0.773	3.865	73X-4	106	602.46	0.9	4.5
68X-3	84	571.70	0.758	3.79	74X-2	59	608.79	0.823	4.115
68X-3	115	572.01	0.771	3.855	74X-2	71	608.91	0.79	3.95
68X-4	5	572.22	0.751	3.755	74X-3	20	609.90	0.914	4.57
68X-4	42	572.59	0.731	3.655	74X-3	97	610.67	1.018	5.09
68X-4	61	572.78	0.697	3.485	74X-4	27	611.47	0.925	4.625
68X-4	88	573.05	0.792	3.96	74X-4	59	611.79	0.908	4.54
68X-5	27	573.36	0.728	3.64	74X-4	93	612.13	1.04	5.2
68X-5	35	573.44	0.671	3.355	75X-2	31	618.08	0.767	3.835
68X-5	35	573.44	0.674	3.37	75X-2	57	618.34	0.773	3.865
68X-5	35	573.44	0.683	3.415	75X-3	19	619.46	0.762	3.81
68X-5	42	573.51	0.79	3.95	75X-3	37	619.64	0.78	3.9
68X-5	56	573.65	0.723	3.615	75X-3	56	619.83	0.789	3.945
68X-5	69	573.78	0.701	3.505	75X-3	73	620.00	0.826	4.13
68X-5	69	573.78	0.712	3.56	75X-3	102	620.29	0.793	3.965
69X-1	10	578.80	0.734	3.67	75X-3	126	620.53	0.817	4.085
69X-1	40	579.10	0.781	3.905	75X-4	25	621.02	0.831	4.155
69X-1	63	579.33	0.803	4.015	75X-4	39	621.16	0.839	4.195

Table 17. Wenner array electrical resistivity and formation factor results for Hole NGHP-01-17A. (To view the complete table, please see the ASCII files.)—Continued

Core, section	Top (cm)	Depth (mbsf)	Electrical resistivity (W×m)	Apparent formation factor	Core, section	Top (cm)	Depth (mbsf)	Electrical resistivity (W×m)	Apparent formation factor
NGHP-01-17A—Continued									
75X-4	78	621.55	0.833	4.165	78X-4	121	649.42	1.224	6.12
75X-5	5	621.82	0.847	4.235	78X-4	141	649.62	1.07	5.35
75X-5	32	622.09	0.89	4.45	78X-5	48	650.19	1.27	6.35
75X-5	53	622.30	0.884	4.42	78X-5	81	650.52	1.348	6.74
76X-1	31	625.31	0.826	4.13	78X-5	101	650.72	1.189	5.945
76X-1	49	625.49	0.871	4.355	79X-1	130	655.10	1.057	5.285
76X-3	24	627.19	0.865	4.325	79X-1	148	655.28	1.179	5.895
76X-3	36	627.31	0.934	4.67	79X-2	20	655.50	1.033	5.165
76X-3	94	627.89	0.906	4.53	79X-2	40	655.70	1.178	5.89
76X-4	6	628.06	0.877	4.385	79X-2	60	655.90	1.122	5.61
76X-4	92	628.92	0.922	4.61	79X-2	80	656.10	1.08	5.4
76X-5	4	629.04	0.879	4.395	79X-2	100	656.30	0.941	4.705
76X-6	21	630.21	0.916	4.58	79X-2	120	656.50	1.175	5.875
76X-6	40	630.40	0.874	4.37	79X-2	140	656.70	1.684	8.42
77X-1	14	634.54	1.048	5.24	79X-3	18	656.98	1.064	5.32
77X-1	16	634.56	0.829	4.145	79X-3	38	657.18	0.979	4.895
77X-1	24	634.64	1.12	5.6	79X-3	54	657.34	1.05	5.25
77X-1	29	634.69	0.635	3.175	79X-3	74	657.54	1.164	5.82
77X-1	46	634.86	1.081	5.405	79X-3	100	657.80	1.035	5.175
77X-1	63	635.03	0.922	4.61	79X-3	120	658.00	2.28	11.4
77X-1	65	635.05	1.148	5.74	79X-3	120	658.00	0.808	4.04
77X-1	68	635.08	0.887	4.435	79X-3	140	658.20	0.785	3.925
77X-1	77	635.17	1.178	5.89	79X-4	20	658.50	0.816	4.08
77X-1	80	635.20	0.931	4.655	79X-4	40	658.70	0.869	4.345
77X-2	11	635.35	1.12	5.6	79X-4	60	658.90	0.838	4.19
77X-2	28	635.52	1.168	5.84	79X-5	20	660.00	0.902	4.51
77X-2	49	635.73	1	5	79X-5	40	660.20	0.993	4.965
77X-2	65	635.89	1.052	5.26	79X-5	60	660.40	0.899	4.495
77X-2	82	636.06	1.123	5.615	79X-5	80	660.60	0.92	4.6
77X-3	19	636.47	0.993	4.965	79X-5	100	660.80	0.987	4.935
77X-3	46	636.74	1.037	5.185	79X-5	120	661.00	0.952	4.76
77X-3	72	637.00	1.145	5.725	79X-5	140	661.20	0.964	4.82
77X-4	20	637.98	1.078	5.39	79X-6	20	661.50	0.952	4.76
77X-4	60	638.38	1.071	5.355	79X-6	44	661.74	1.141	5.705
77X-4	81	638.59	1.131	5.655	79X-6	64	661.94	0.948	4.74
77X-4	119	638.97	1.131	5.655	79X-6	84	662.14	0.951	4.755
77X-4	145	639.23	1.038	5.19	79X-6	104	662.34	1.036	5.18
77X-5	12	639.40	1.037	5.185	80X-1	16	662.86	1.083	5.415
77X-5	51	639.79	1.091	5.455	80X-2	12	663.13	1.026	5.13
77X-5	73	640.01	1.066	5.33	80X-2	32	663.33	0.987	4.935
77X-5	92	640.20	1.123	5.615	80X-2	58	663.59	1.05	5.25
77X-6	6	640.34	1.138	5.69	80X-3	61	665.07	1.087	5.435
77X-6	25	640.53	1.156	5.78	80X-3	88	665.34	0.979	4.895
77X-6	39	640.67	1.153	5.765	80X-4	20	665.62	1.073	5.365
78X-1	48	644.58	0.975	4.875	80X-4	35	665.77	1.124	5.62
78X-2	40	645.61	1.199	5.995	80X-4	55	665.97	0.975	4.875
78X-2	119	646.40	1.146	5.73	80X-4	107	666.49	1.039	5.195
78X-2	141	646.62	1.083	5.415	80X-4	127	666.69	1.028	5.14
78X-3	6	646.77	1.266	6.33	80X-5	38	667.30	1.174	5.87
78X-3	38	647.09	1.8	9	83X-1	19	683.09	0.962	4.81
78X-4	93	649.14	1.419	7.095					

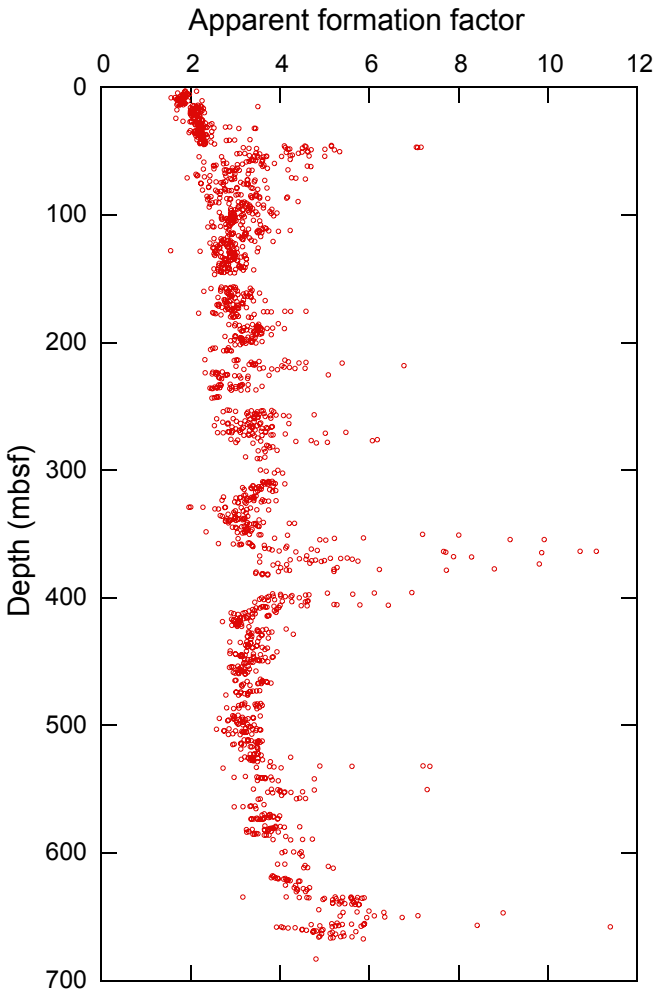


Figure 31. Apparent formation factor versus sub-bottom depth for Hole NGHP-01-17A.

Table 18. Contact *P*-wave velocity results determined on split cores sections from Hole NGHP-01-17A.

Core, section	Sample	Top (cm)	Depth (mbsf)	VP (km/s)
NGHP-01-17A				
1H-1	VP	45	0.45	1.480
1H-2	VP	61	2.11	1.480
1H-3	VP	50	3.50	1.494
2H-1	VP	121	5.71	1.494
2H-2	VP	75	6.75	1.494
2H-3	VP	65	8.15	1.497
2H-4	VP	75	9.75	1.514
2H-5	VP	56	11.06	1.512
2H-6	VP	55	12.55	1.515
2H-7	VP	35	13.85	1.522
3H-1	VP	70	14.70	1.514
3H-2	VP	35	15.85	1.514
3H-3	VP	75	17.75	1.524
3H-4	VP	35	18.85	1.517
3H-5	VP	35	20.35	1.539
3H-6	VP	35	21.85	1.548
3H-7	VP	35	22.85	1.551
4H-1	VP	55	24.05	1.519

Core NGHP-01-17A-48P (412.7 mbsf) retrieved a full core (1.00 m) at pressure (table 21). The autoclave was placed in the MSCL-P for X-ray and gamma density measurements, which showed a uniform core in the X-ray image of the top half and that sediment existed in the lower half (fig. 36C). The core was depressurized, releasing 2.44 L of methane, corresponding to 4.4 mL of gas hydrate or 0.6 percent methane hydrate as a percent of pore volume (table 22). The core showed small pressure rebounds with time, indicating small amounts of distributed gas hydrate or a very tightly sealed core (fig. 38A). After depressurization, the autoclave was again measured in the MSCL-P, showing a core with regular gas voids, and a final X-ray image was collected when the outer barrel was removed (fig. 36C). One chlorinity measurement was made on this core (556 mM, 18–30 cm), which was similar to the background chlorinity in surrounding cores (see "Inorganic Geochemistry").

Core NGHP-01-17A-49E (413.7 mbsf) retrieved a core (0.79 m) at *in situ* pressure (table 21). The core was transferred to the MSCL-P and X-ray images, gamma density and *P*-wave velocity measurements were collected (fig. 35B). Core NGHP-01-17A-49E showed a uniform density with some subtle structure in the velocity, but there was no evidence of gas-hydrate structures. A plastic portion of the piston separated during coring and can be seen at the top of the sediment (high *P*-wave velocity). Core NGHP-01-17A-49E was depressurized in the MSCL-P, releasing 1.84 L of methane, which was near methane saturation at *in situ* temperature and pressure (table 22). The core measurements showed no pressure plateaus or rebounds (fig. 37B), consistent with little to no methane hydrate. A final MSCL-P scan was collected at atmospheric pressure which showed an intact core (fig. 36D). One chlorinity measurement was made on this core (543 mM, 45–60 cm), which was similar to the background chlorinity in nearby cores (543–549 mM; see "Inorganic Geochemistry").

Core NGHP-01-17A-70P (586.3 mbsf) retrieved a very short core (0.12 m) at low pressure (32 bar; table 21). The corer was having a difficult time penetrating the formation, and only advanced 0.5 m instead of the usual 1.0 m. The corer likely sealed near 300–400 m below sea level (fig. 33B) and could have lost methane or other constituents. The autoclave was placed in the MSCL-P for X-ray and gamma density measurements but no core could be seen detected. Despite this the core was depressurized, releasing 1.53 L of methane, corresponding to 7.3 mL of gas hydrate or 7.6 percent methane hydrate as a percent of pore volume, though the sediment volume was not well-constrained (table 22). This core also released 0.4 L of nitrogen, which is a very large volume of nitrogen considering the small amount of sediment, and the ethane concentration was 490 ppm. After depressurization, the inner barrel was removed from the autoclave, and a small amount of fractured sediment fell out of the inner barrel in small pieces. No chlorinity measurements were made on this core.

Table 19. Thermal conductivity results for Hole NGHP-01-17A.

Core, section	Sample	Top (cm)	Depth (mbsf)	Thermal conductivity (W/[m×K])	Core, section	Sample	Top (cm)	Depth (mbsf)	Thermal conductivity (W/[m×K])
NGHP-01-17A									
1H-2	TC	52	2.02	0.914	36X-3	TC	20	321.09	0.815
2H-3	TC	55	8.05	0.947	39X-1	TC	75	330.75	0.765
3H-1	TC	65	14.65	1.033	40X-3	TC	61	340.04	0.887
3H-7	TC	32	22.82	1.059	41X-3	TC	69	350.99	0.988
4H-1	TC	65	24.15	1.059	42X-7	TC	48	364.43	0.817
4H-6	TC	55	31.55	1.053	43X-3	TC	70	369.40	1.059
5H-1	TC	75	33.75	0.972	44X-4	TC	40	379.66	0.804
5H-6	TC	75	41.25	0.996	45X-1	TC	27	385.97	0.927
6H-1	TC	83	43.33	0.950	46X-3	TC	75	398.89	0.870
6H-7	TC	44	51.88	0.800	47X-3	TC	35	407.95	0.754
7H-1	TC	35	52.35	0.838	50X-3	TC	70	417.40	0.834
7H-6	TC	75	60.25	0.928	51X-3	TC	44	427.67	0.639
8H-1	TC	70	62.20	0.863	52X-3	TC	90	437.90	0.923
9H-3	TC	62	74.22	0.890	53X-3	TC	91	446.26	0.930
10H-3	TC	65	84.15	0.870	54X-3	TC	64	455.92	0.871
11H-3	TC	65	93.65	0.914	55X-3	TC	18	464.75	0.814
12H-3	TC	65	103.15	0.939	56X-3	TC	59	475.28	0.860
13H-3	TC	65	112.65	0.847	57X-3	TC	43	484.61	0.758
14X-3	TC	65	122.15	1.017	58X-3	TC	62	495.40	0.829
15X-3	TC	65	130.37	1.031	61X-3	TC	75	504.23	0.899
16X-3	TC	65	141.35	1.002	62X-3	TC	75	514.37	0.842
17X-1	TC	17	146.77	0.999	63X-4	TC	31	524.54	0.841
18X-3	TC	10	159.16	1.027	64X-2	TC	74	532.11	0.892
19X-3	TC	70	168.53	1.005	65X-2	TC	35	541.85	0.886
21X-3	TC	70	180.20	1.019	66X-3	TC	29	552.29	0.844
22X-3	TC	75	188.85	1.000	67X-3	TC	12	561.52	0.912
23X-3	TC	55	197.73	1.011	68X-3	TC	75	571.61	0.966
24X-2	TC	40	204.45	0.942	69X-3	TC	66	582.36	0.875
25X-3	TC	75	217.25	0.942	72X-2	TC	40	589.23	0.809
26X-3	TC	33	226.43	0.959	73X-3	TC	30	600.30	0.737
27X-3	TC	75	236.55	0.910	74X-3	TC	60	610.30	0.747
28X-3	TC	75	246.25	0.811	75X-3	TC	75	620.02	0.760
29X-3	TC	75	254.79	0.977	76X-3	TC	50	627.45	0.633
30X-3	TC	45	264.05	0.890	77X-3	TC	48	636.76	0.754
31X-2	TC	72	271.70	0.925	78X-3	TC	45	647.16	0.602
32X-3	TC	35	283.25	0.904	79X-3	TC	79	657.59	0.709
33X-2	TC	72	291.58	0.908	80X-3	TC	88	665.34	0.767
34X-3	TC	45	302.65	0.920	82X-3	TC	67	675.67	0.726
35X-3	TC	26	311.28	0.949					

Core NGHP-01-17A-81E (672.3 mbsf) retrieved a partial core (0.40 m) at pressure (table 21). Core NGHP-01-17A-81E was transferred to the MSCL-P and X-ray images, gamma density and *P*-wave velocity measurements were collected (fig. 35C). The X-ray image showed that the core was studded with centimeter-size denser material. Core NGHP-01-17A-81E was depressurized in the MSCL-P, releasing 3.87 L of methane and surprisingly releasing 1.7 L of nitrogen. The methane released would correspond to 12.8 mL of methane gas or 2.9 percent free methane as a percent of pore volume, assuming the core was taken below the base of gas-hydrate stability (table 22). (If the core had been above the base of gas-hydrate stability, the methane volume would correspond to 14.7 mL of methane hydrate or 3.3 percent methane hydrate as a percent of pore volume.) The core showed no pressure plateaus or rebounds (figs. 37B and 38B), consistent with the presence of a free gas phase rather than a methane hydrate phase. The hydrocarbon gas released was up to 1,200 ppm ethane and 60 ppm propane, similar to the composition of void gases at these depths (see "Organic Geochemistry"). A final MSCL-P scan was collected at atmospheric pressure which showed that the top of the core had expanded slightly but that the lower portion of the core was homogenized (fig. 36E). The core was too disturbed for any porewater samples, so no chlorinity measurements were made on this core. Some of the hard dense pebbles were retrieved from the core and their density measured. The densities were around 2.5 g/cc compared with a matrix density of around 1.8 g/cc (see "Physical Properties").

Table 20. *In situ* temperature measurements for Hole NGHP-01-17A.

Depth (mbsf)	Core	Assumed thermal conductivity (W/m•K)	Tool	Temperature (°C)	Ad-hoc calibration correction	Corrected temperature (°C)	Estimated uncertainty (°C)	Data quality
23.5	A03H	0.95	APCT-3	6.4	0	6.4	0.4	poor-fair
42.5	A05H	0.95	APCT-3	6.45	0	6.45	0.15	good
61.5	A07H	0.95	APCT-3	6.78	0	6.78	0.06	good
205.3	A23X	0.95	DVTP	8.75	0.39	9.14	0.1	good
330	A38Y	0.95	DVTP	11.2	0.39	11.59	0.3	fair
368.2	A42X	0.95	DVTP	11.79	0.39	12.18	0.1	good
416.1	A49E	0.95	DVTP	12.69	0.39	13.08	0.3	fair
503	A60Y	0.95	DVTP	NA	0.39	NA	NA	poor
587.8	A71E	0.95	DVTP	14.5	0.39	NA	NA	poor
627	A75X	0.95	DVTP	17.7	0.39	18.09	0.2	good
664.1	A79X	0.95	DVTP	17.64	0.39	18.03	0.01	good

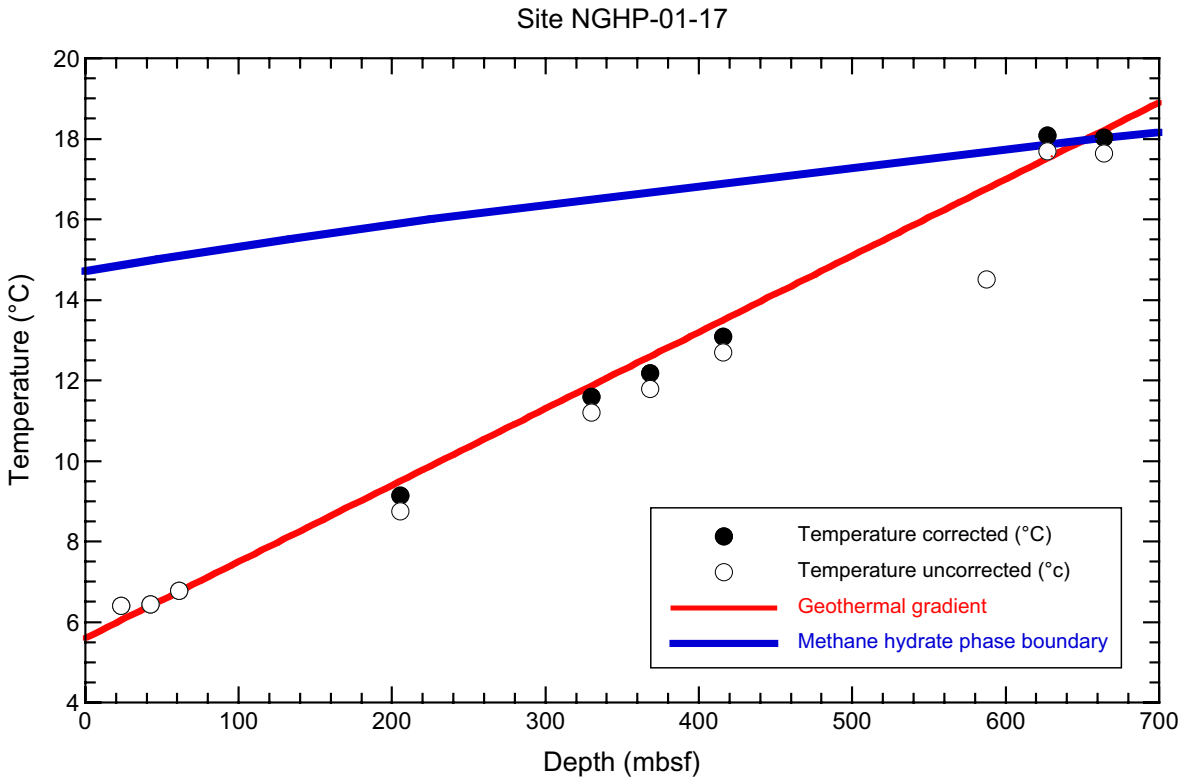


Figure 32. Geothermal gradient and estimated depth to the BSR from *in situ* temperature measurements for Hole NGHP-01-17A. [BSR, bottom-simulating reflector]

Gas-Hydrate Concentration, Nature, and Distribution from Pressure Coring

Six of the ten pressure cores at Site NGHP-01-17 were recovered at sufficient pressures to accurately assess the total concentration of methane and hence the predicted amount of gas hydrate. The calculated methane concentration for these cores is shown in figure 39 in relation to the phase boundaries for Structure I methane hydrate. Gas-hydrate concentrations in pressure cores were near zero in three cores in the middle of the gas-hydrate stability zone, with one core (Core NGHP-01-17A-48P) at 0.6 percent methane hydrate as a percent of pore space. One core near the BSR (Core NGHP-01-17A-70P) may have contained gas hydrate. A core taken below the BSR and below the base of methane hydrate stability (Core NGHP-01-17A-81E) contained free gas, confirming that the BSR was a gas-hydrate-related feature.

At Site NGHP-01-17, gas hydrate was found in discrete zones (see "Infrared Imaging" in "Physical Properties"), in association with ash layers or distributed ashes (see "Inorganic Geochemistry"). No such layers were recovered in pressure cores, which was unfortunate but statistically likely, and four pressure cores taken above the base of gas-hydrate stability recovered only very small amounts of gas hydrate. The

Table 21. Summary of pressure-coring operations at Site NGHP-01-17.

Core ID	Top of core (mbsf)	Length recovered (cm)*	Length curated (cm)*	Pressure at core depth (bar)	Pressure recovered (bar)		Comments
					logged**	gauge***	
NGHP-01-17A							
20Y	175.5	--	81	154	0	--	overretracted
37P	328.0	100	93	169	52.0	54	normal operation
38Y	329	86	87	169	152.0	167	lifted extremely slowly on sandline during core retraction
48P	412.7	100	89	177	104.0	105	normal operation
49E	413.7	79	87	178	126.0	125	used auger bit
59P	499.6	--	60	186	0	--	no pressure
60Y	500.6	--	87	186	0	--	valve o-ring displaced
70P	586.3	12	13	195	34.0	32	drilled for 30 min
71E	586.8	0	0	195	137.0	148	used auger bit
81E	672.3	40	42	204	148.0 @5 °C	160	used diamond bit

Notes:

Water depth at Site NGHP-01-17 is 1356 m. P=PCS, Y=FPC, E=HRC.

*Length measured from X-ray and gamma density analysis, which may not match curated core length.

**Last pressure recorded before data logger disconnected from corer autoclave. Temperature 2–4 °C unless otherwise noted.

***Pressure measured when autoclave pressure transducer connected to external gauge. Pressure measured at 7 °C unless otherwise noted.

chlorinity measured on pressure cores that contained no gas hydrate agreed well with the baseline chlorinity, showing that there was little to no gas hydrate disseminated throughout the formation.

Core NGHP-01-17A-81E was taken below the base of gas-hydrate stability, so the excess methane found in the core corresponded to a free gas phase. This core represented the first example where a pressure core taken below the base of gas-hydrate stability retrieved methane quantities significantly above saturation. While there was some uncertainty in the exact depth of the base of gas-hydrate stability at Site NGHP-01-17, as the thermal gradient was so shallow (see "Downhole Temperature Measurements" in "Physical Properties"), Core NGHP-01-17A-81E, at 672.3 mbsf, was definitely below the base of gas-hydrate stability. The downhole sonic logs also indicated the presence of free gas at depths of 580 mbsf to the bottom of the hole at nearby Hole NGHP-01-17B (see "Downhole Logging"), possibly calling the interpretation of Core NGHP-01-17A-70P as containing gas hydrate into question.

The presence of nitrogen in large quantities in both Cores NGHP-01-17A-81E and -70P was unexpected. Core NGHP-01-17A-81E released 1.7 L of nitrogen, 26 percent of the total gas released from this core. All of the nitrogen was released in the first 2 L of gas, and, based on the estimation of gas remaining in the pressure system, this nitrogen was released from the core in the pressure drop from 160 bar to 100 bar. Core NGHP-01-17A-70P also released large amounts of nitrogen (400 mL) compared to the volume of core (~12 cm) or volume of methane (1.53 L). Similar to Core NGHP-01-17A-81E, the nitrogen was 28 percent of total gas released from the core. One of these cores was captured above the base of gas-hydrate stability and the BSR, and the other core was below these features. The nitrogen in these cores did not come from air contamination when sampling, as air contamination was removed from all gas samples before reporting their composition (see "Pressure Coring" in the "Methods" chapter). We currently have no explanation for this observation.

Downhole Logging

Operations

The last core in Hole NGHP-01-17A was recovered from 2047.6 mbrf (691.6 mbsf) at 2205 hr on July 25, 2006. The initial plan was to log this hole with the triple combo, the FMS/Sonic and a VSP, but after failing to lower the triple combo tool string below 1,500 mbrf (144 mbsf) during a first attempt, and below 1,550 mbrf (191 mbsf) after lowering the pipe below the first obstruction, it was decided to drill a new hole to achieve the logging objectives in Site NGHP-01-17.

Hole NGHP-01-17B was drilled to the total depth (TD) of 2074 mbrf (718 mbsf) at 0400 hr on July 28, 2006. The hole was then conditioned for logging: it was swept with 50 bbl sepiolite mud; a go-devil was pumped to open the lockable flapper at the bottom of the drill string; it was displaced with 260 bbls of barite; and, based on the drilling record and on the experience in the previous hole, the pipe was pulled to logging depth of 1,483.6 mbrf (127.6 mbsf). At 0820, the wire line was spooled and the logging sheaves brought to prepare the rig floor for logging.

Assembly of the triple combo started at 0945 hr. The tool string was complete at 1010 hr, run-in-hole (RIH) at 1020 hr, and reached the bit at 1120 hr. After exiting the pipe without problems and encountering some dragging from the formation immediately below the pipe, the bottom of the tool could not pass below 1.594 mbrf (~238 mbsf) at 1125 hr. After 0.5 hr of fruitless efforts, we decided to log up from here, and to lower the pipe past this point to a depth where recovery and drilling records suggested that the hole would be more stable. The log up showed a very large hole, except immediately below the pipe. The caliper was closed at 1212 hr, and after failing to reenter the pipe on the first attempt, the drill string had to be rotated by 180° to bring the triple combo fully inside the pipe at 1230 hr. The pass was complete when the gamma ray log

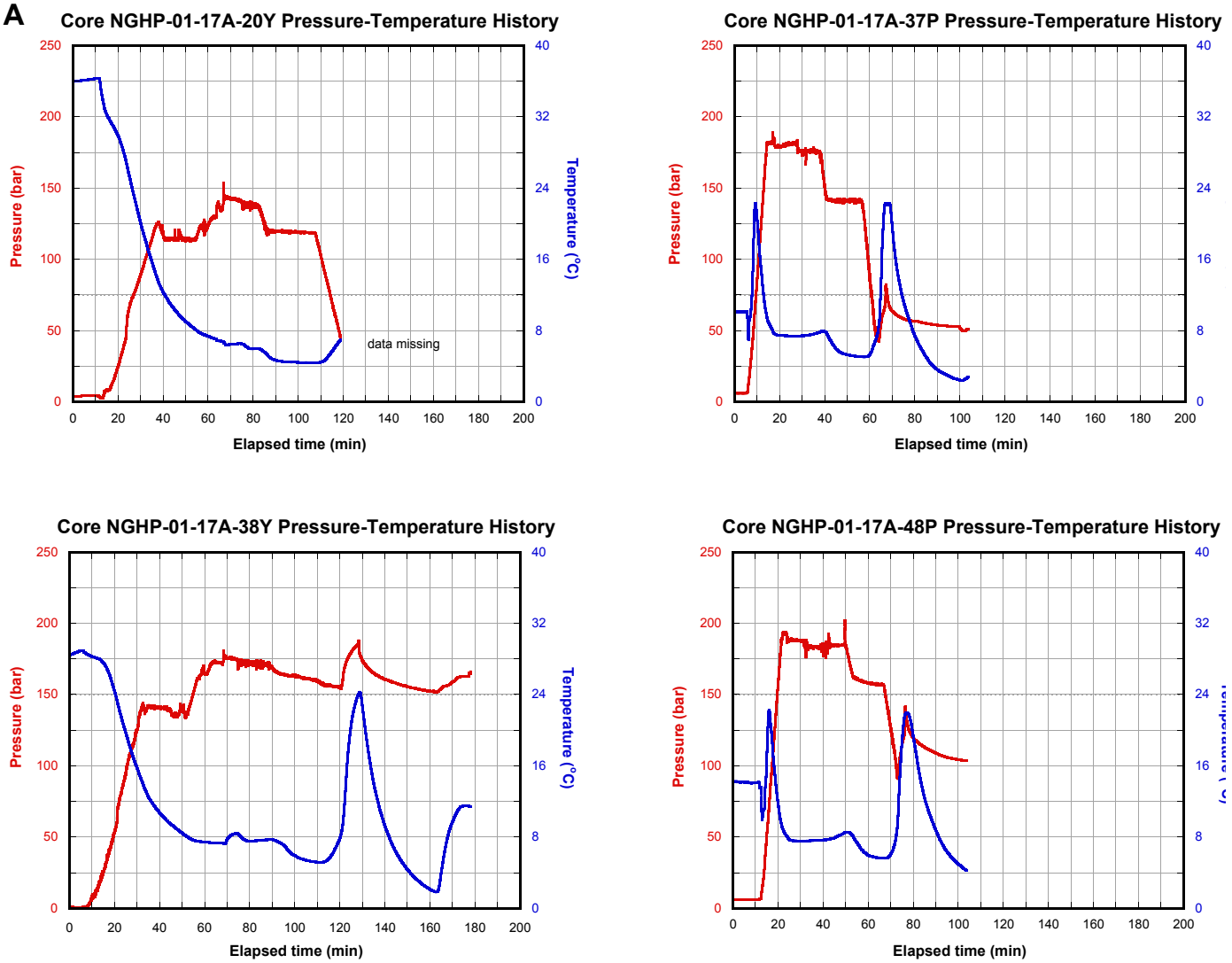


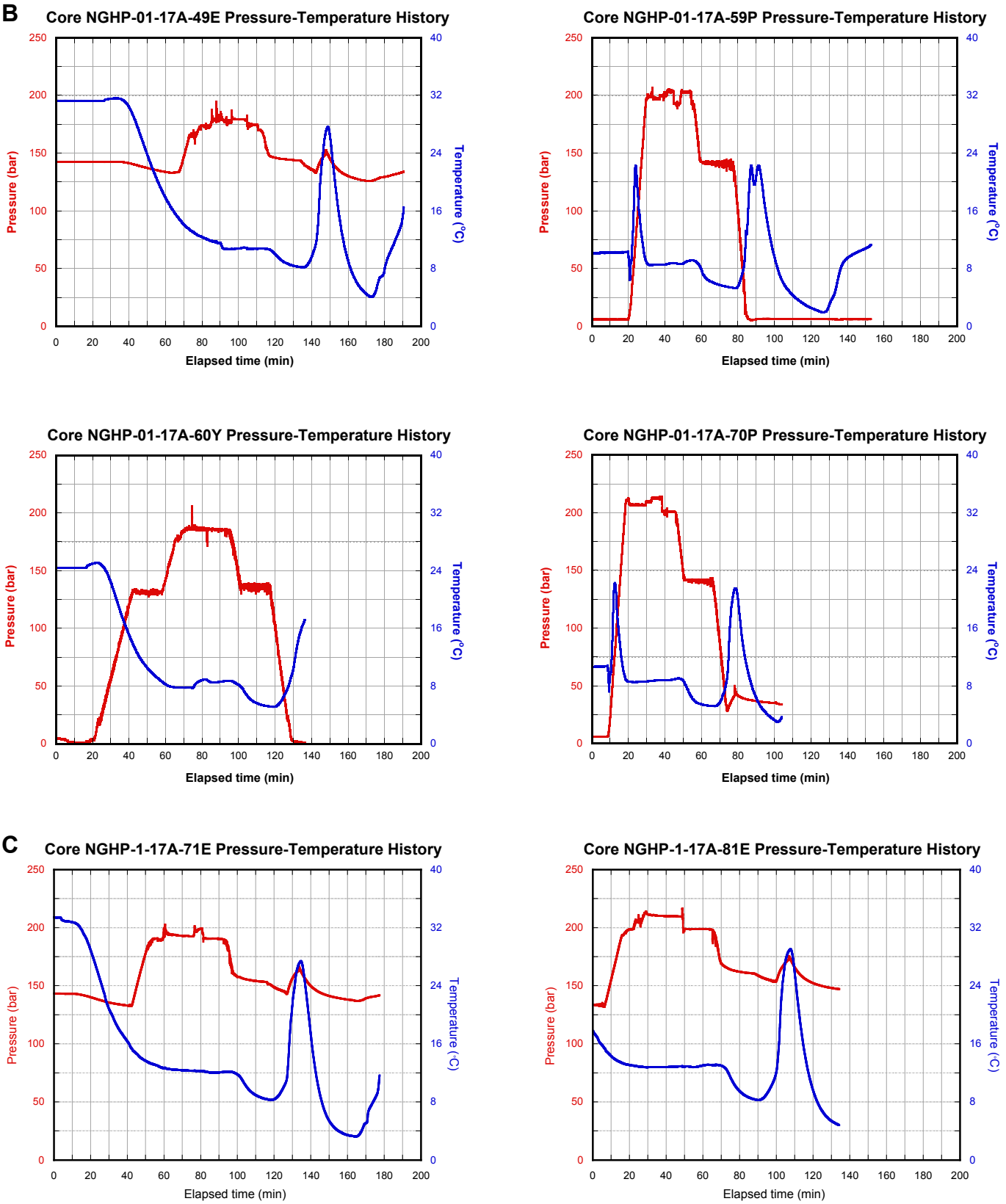
Figure 33. Temperature and pressure versus elapsed time for each pressure-corer deployment as recorded by the corer's internal data logger.

identified the seafloor at 1356 mbrf at 1250 hr. The tool was then brought to the surface at 5,000 ft/hr. It was back on deck at 1330 hr and partially rigged down at 1405 hr.

After lowering the bit to 1,626 mbrf (270 mbsf), the triple combo was RIH at 1530 hr, and with the assistance of mud circulation to facilitate the exit from the pipe, the tool was in open hole at 1635 hr. The log up started at 1655 hr after reaching the bottom of the hole (2.075 mbrf) and the HLDS caliper was closed and the wire-line heave compensator (WHC) turned off at 1825 hr before reentering the pipe. There was no problem at the bit and the pass was complete when the tool was fully inside pipe at 1835 hr. The triple combo was at the surface at 1930 hr and rigged down at 2000 hr.

Rig up of the FMS/Sonic string followed immediately. The string was complete at 2025 hr, RIH at 2055 hr, and at the bit at 2155 hr. It exited the pipe without problems and the first pass started from the bottom of the hole (2.076 mbrf) at 2227 hr after encountering only a few tight intervals on the way down, in particular at 1,990 mbrf. The DSI was configured for the following acquisition modes: low-frequency monopole, low-frequency upper dipole, standard frequency lower dipole and stoneley. Except for an interval at ~1830 mbrf where the caliper had to be closed because of high tension in the wire-line, the pass proceeded without trouble. Instead of having to work one more time through the sticky formation immediately below the bit and the bit itself, it was decided to go down for the second pass immediately after closing the FMS calipers at 1,668 mbrf at 2357 hr. On the way down a tight spot at 1805 mbrf was the only place requiring some efforts, and the second pass started from TD (2,076 mbrf) at 0045 hr on July 29, 2006, with the DSI configured for Medium frequency monopole and cross-dipole modes. At 0215 hr, with the bottom of the tool at 1,669 mbrf, the FMS calipers were closed and the WHC was turned off before entering the pipe. The pass was concluded when the tool was fully inside the pipe at 0225 hr. The FMS/Sonic was back at the surface at 0330 hr, and it was cleaned, checked and disassembled at 0415 hr.

B



C

Figure 33. Temperature and pressure versus elapsed time for each pressure-corer deployment as recorded by the corer's internal data logger.—Continued

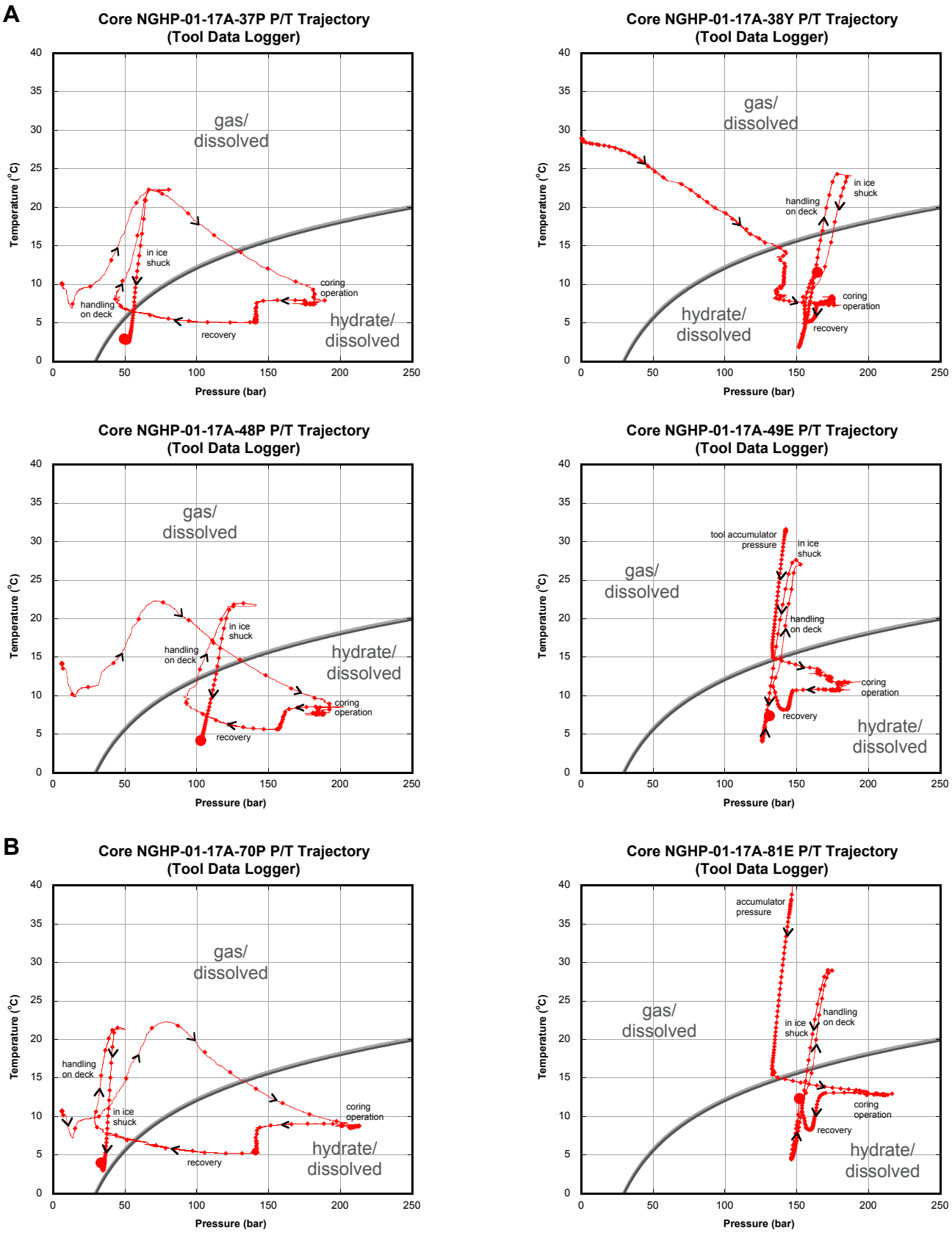


Figure 34. Temperature versus pressure for each successful pressure corer deployment, showing trajectories relative to gas-hydrate stability at 30 ppt and 35 ppt salinity, calculated from Xu (2002, 2004). Small dots are approximately every minute. Large dot is final temperature and pressure of autoclave prior to data logger removal.

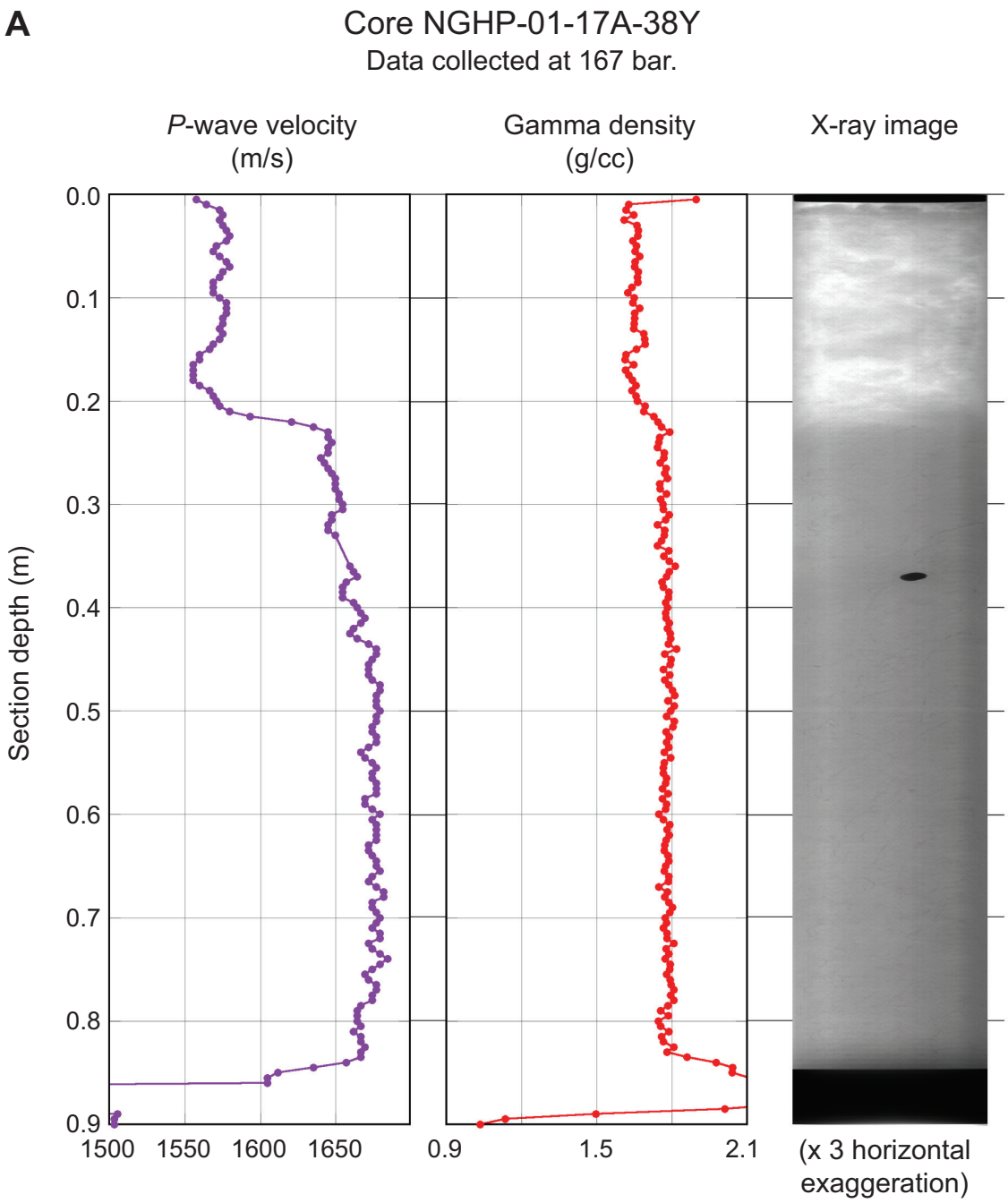


Figure 35. Data collected at near in situ pressure and 7 °C for Cores NGHP-1-17A-38Y, -49E, and -81E, including X-ray images, gamma density, and *P*-wave velocity. X-ray images have been stretched 300 percent in the cross-core direction to show detail.

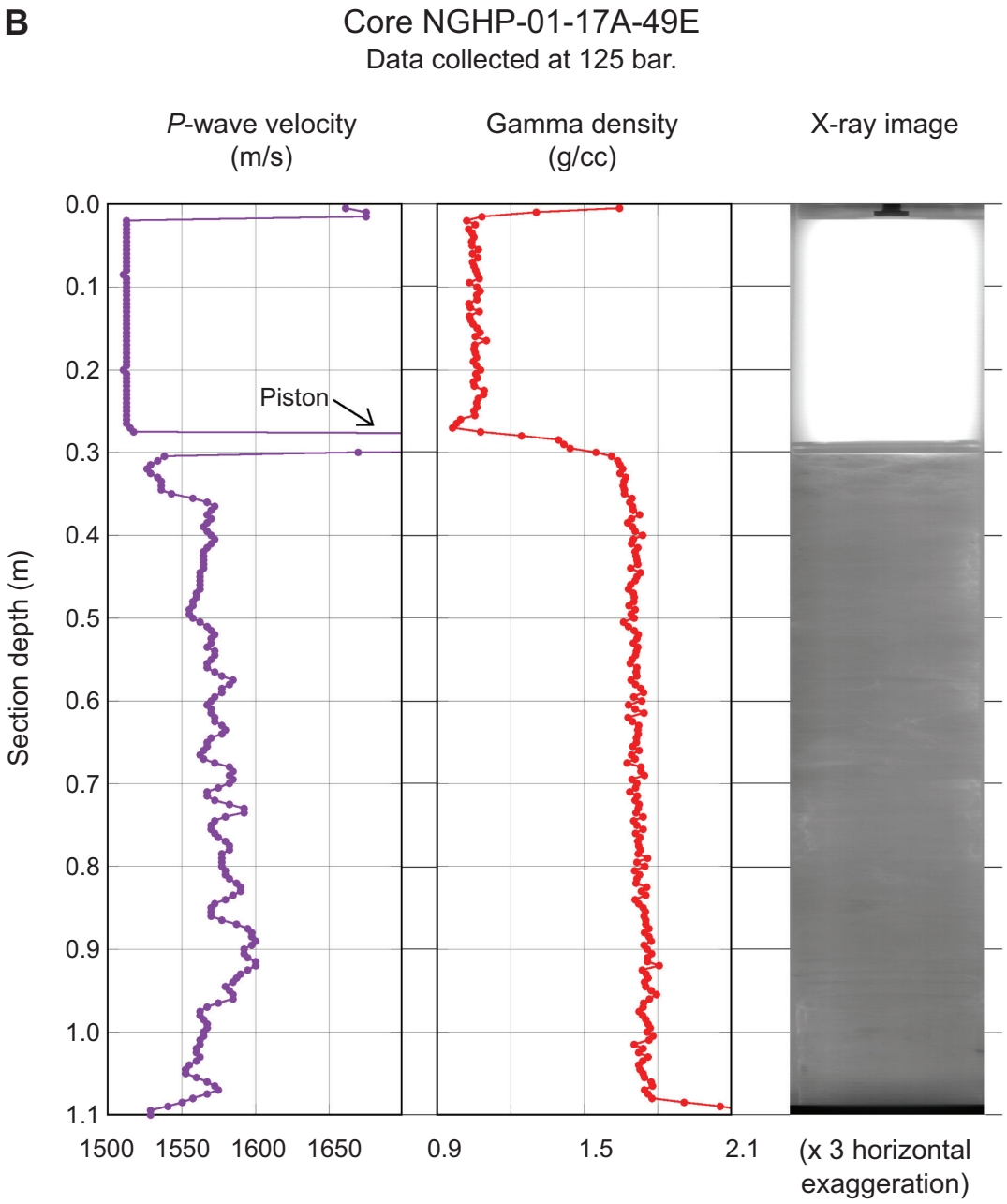


Figure 35. Data collected at near in situ pressure and 7 °C for Cores NGHP-1-17A-38Y, -49E, and -81E, including X-ray images, gamma density, and *P*-wave velocity. X-ray images have been stretched 300 percent in the cross-core direction to show detail.—Continued

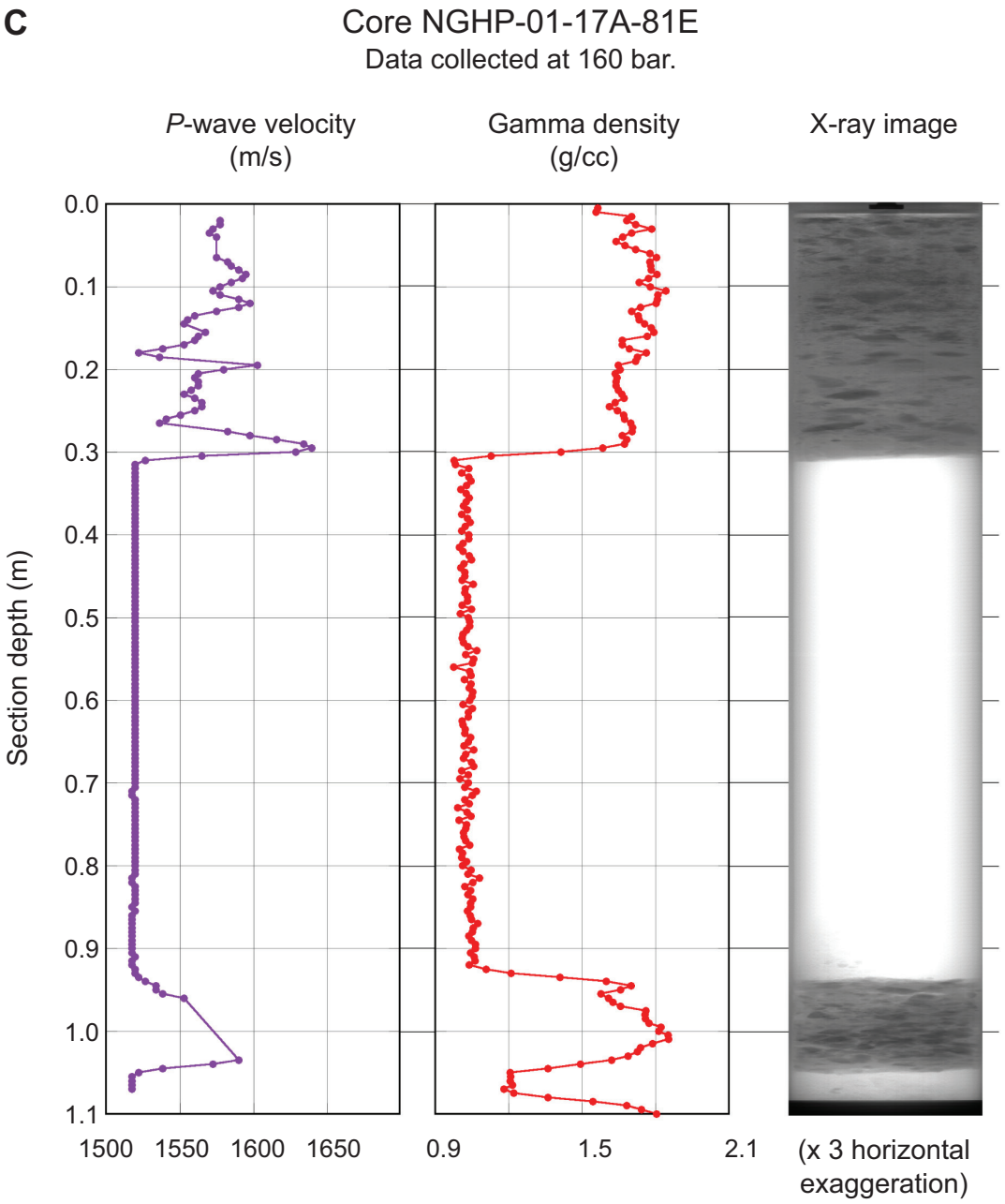


Figure 35. Data collected at near in situ pressure and 7 °C for Cores NGHP-1-17A-38Y, -49E, and -81E, including X-ray images, gamma density, and *P*-wave velocity. X-ray images have been stretched 300 percent in the cross-core direction to show detail.—Continued

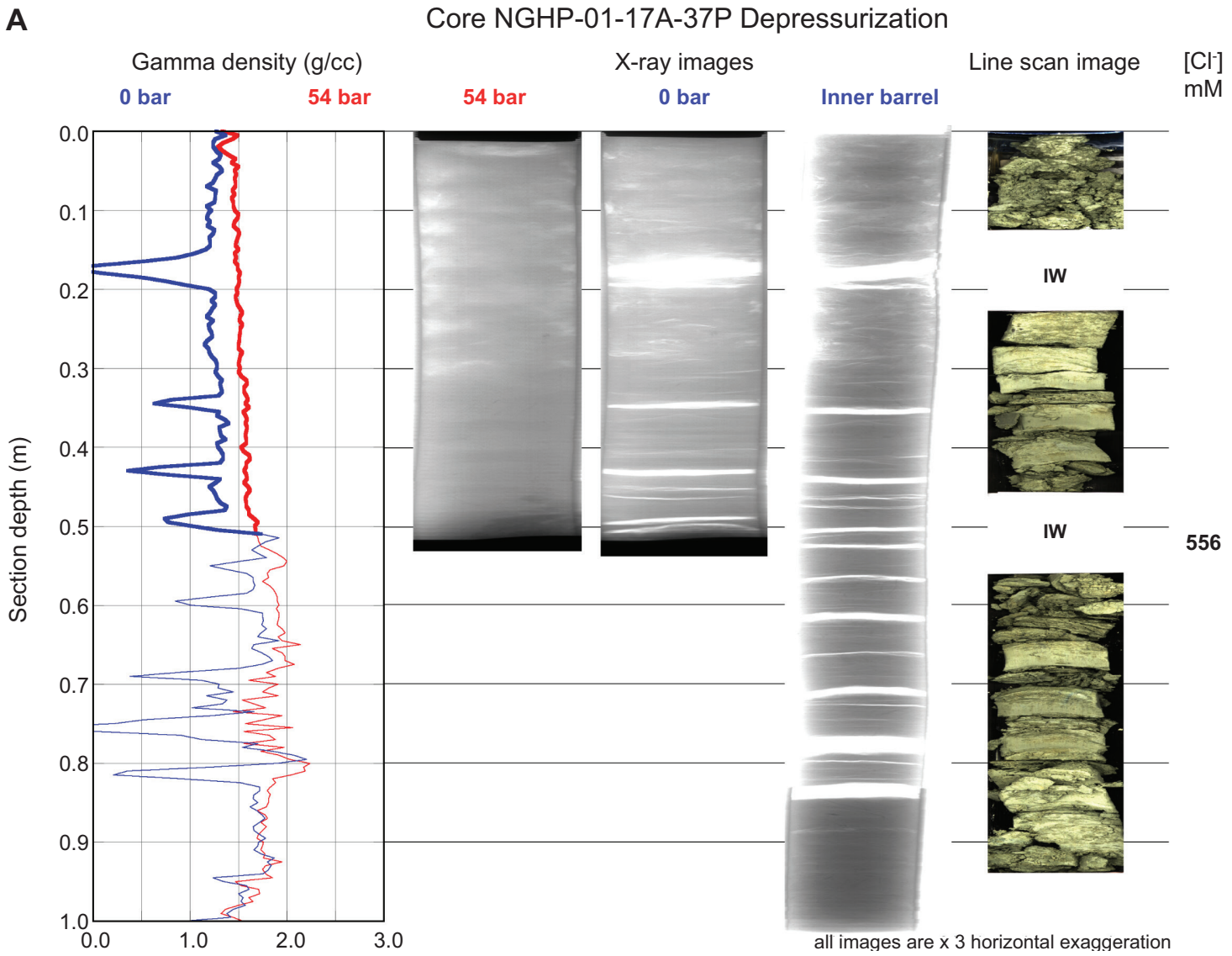


Figure 36. Summary of data taken from successful pressure cores before, during, and after depressurization, including gamma-density profiles collected before and after depressurization, X-ray images collected before and after depressurization, and line-scan images collected after depressurization.

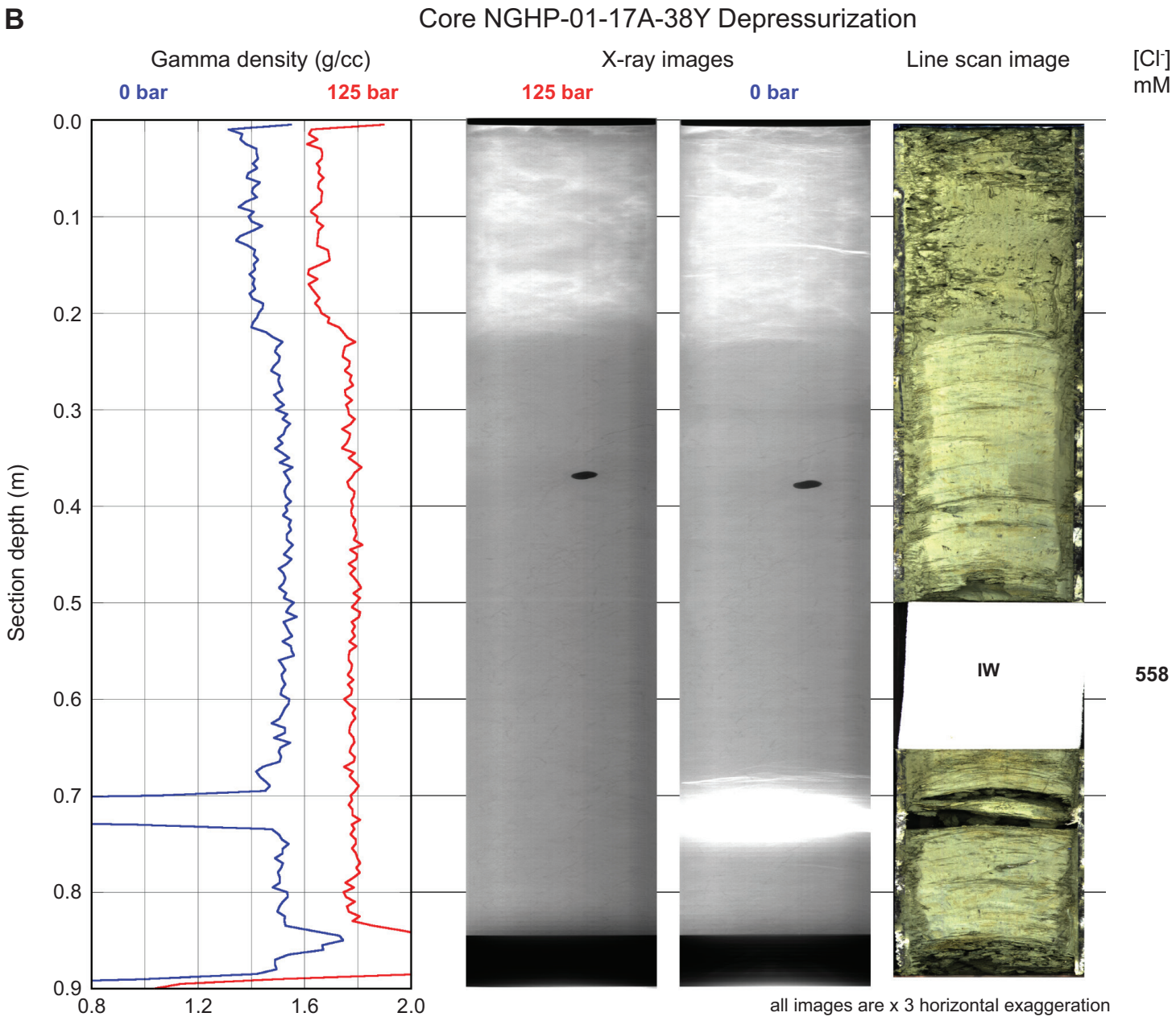


Figure 36. Summary of data taken from successful pressure cores before, during, and after depressurization, including gamma-density profiles collected before and after depressurization, X-ray images collected before and after depressurization, and line-scan images collected after depressurization.—Continued

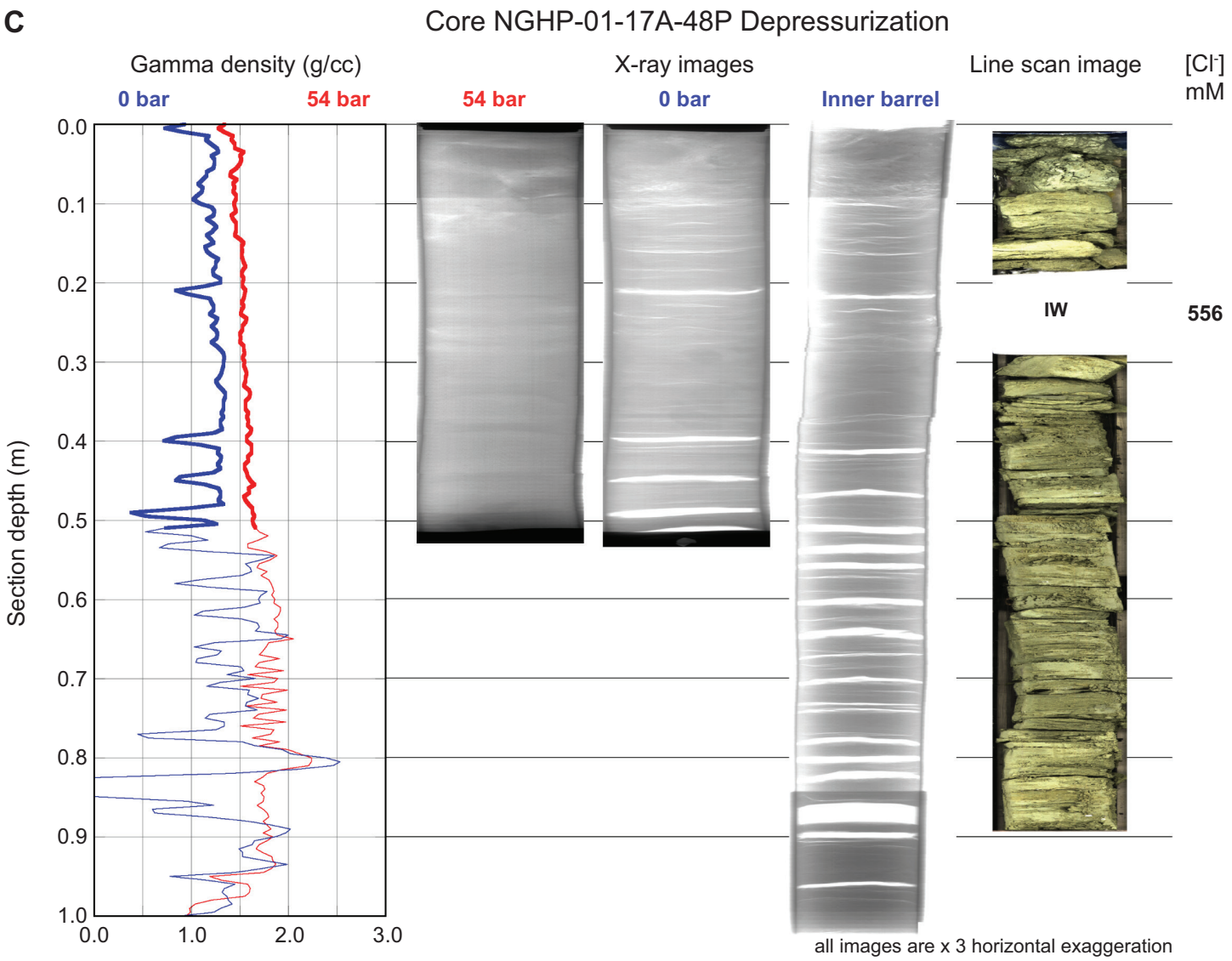


Figure 36. Summary of data taken from successful pressure cores before, during, and after depressurization, including gamma-density profiles collected before and after depressurization, X-ray images collected before and after depressurization, and line-scan images collected after depressurization.—Continued

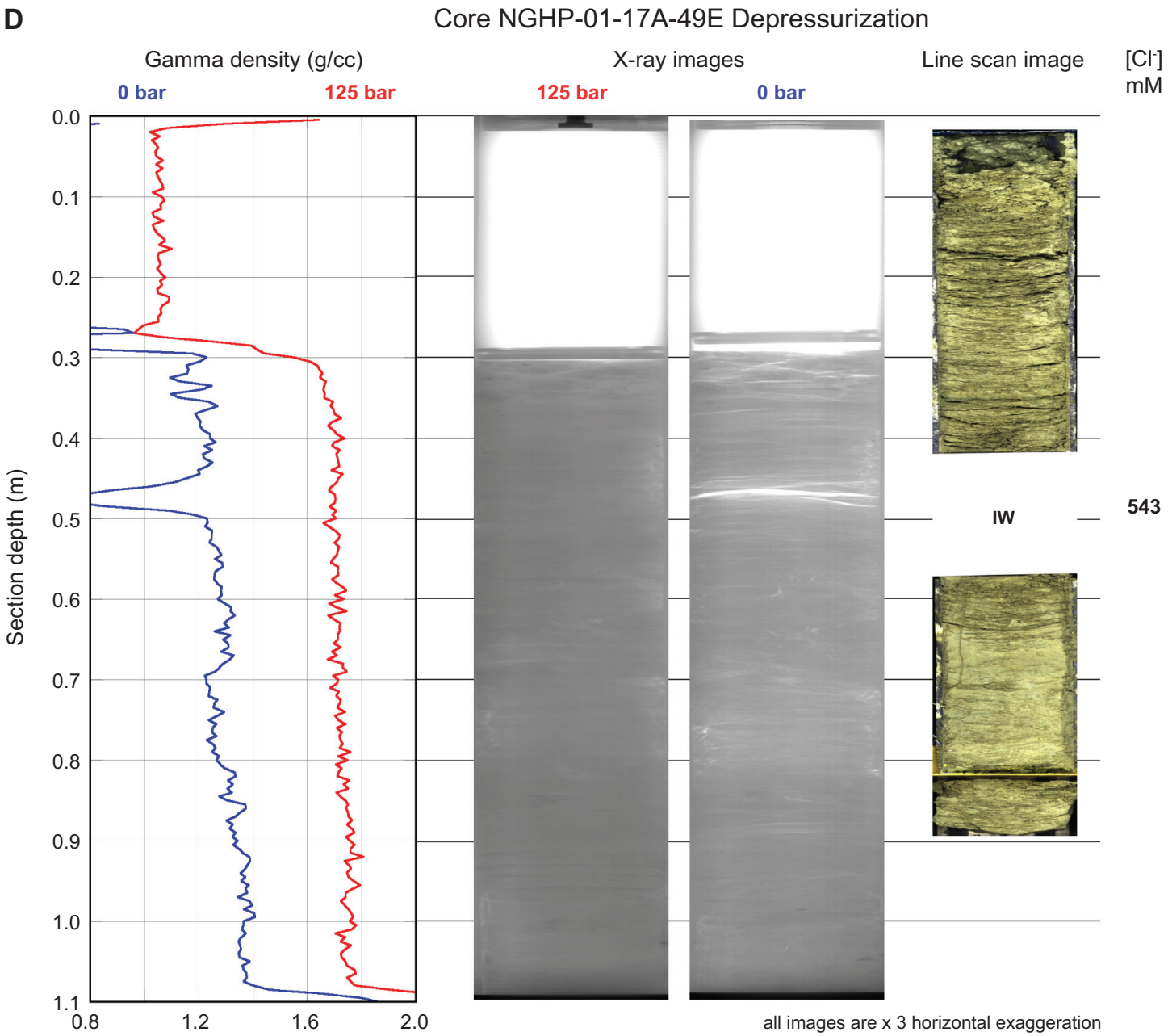


Figure 36. Summary of data taken from successful pressure cores before, during, and after depressurization, including gamma-density profiles collected before and after depressurization, X-ray images collected before and after depressurization, and line-scan images collected after depressurization.—Continued

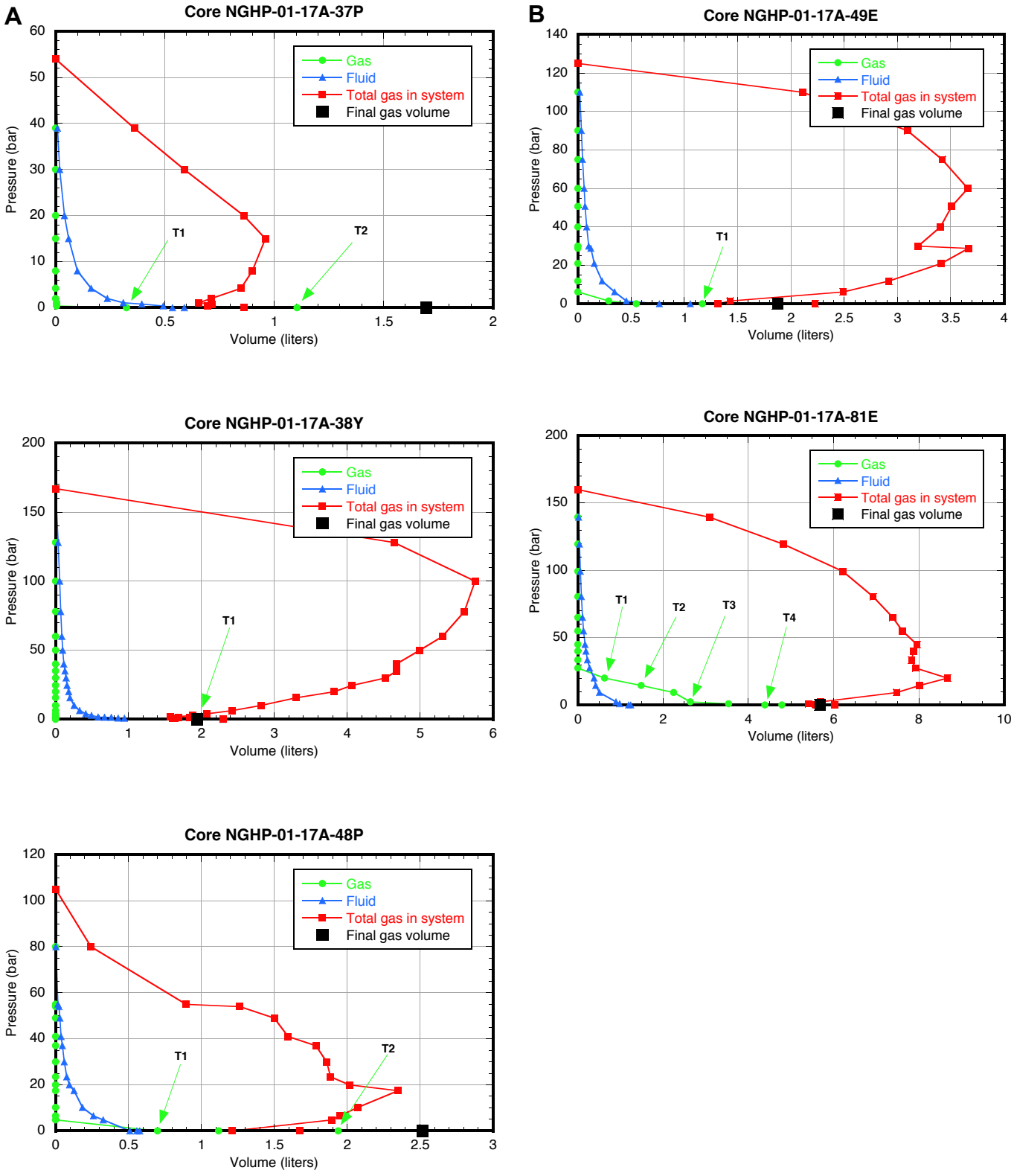


Figure 37. Pressure versus volume for successful pressure cores, also showing placement of gas samples (see "Organic Geochemistry"). [Green circles, gas volume; blue triangles, fluid volume; red squares, total gas volume in system (calculated as described in the "Methods" chapter); large black square, final calculated gas from cores; T (number), gas samples]

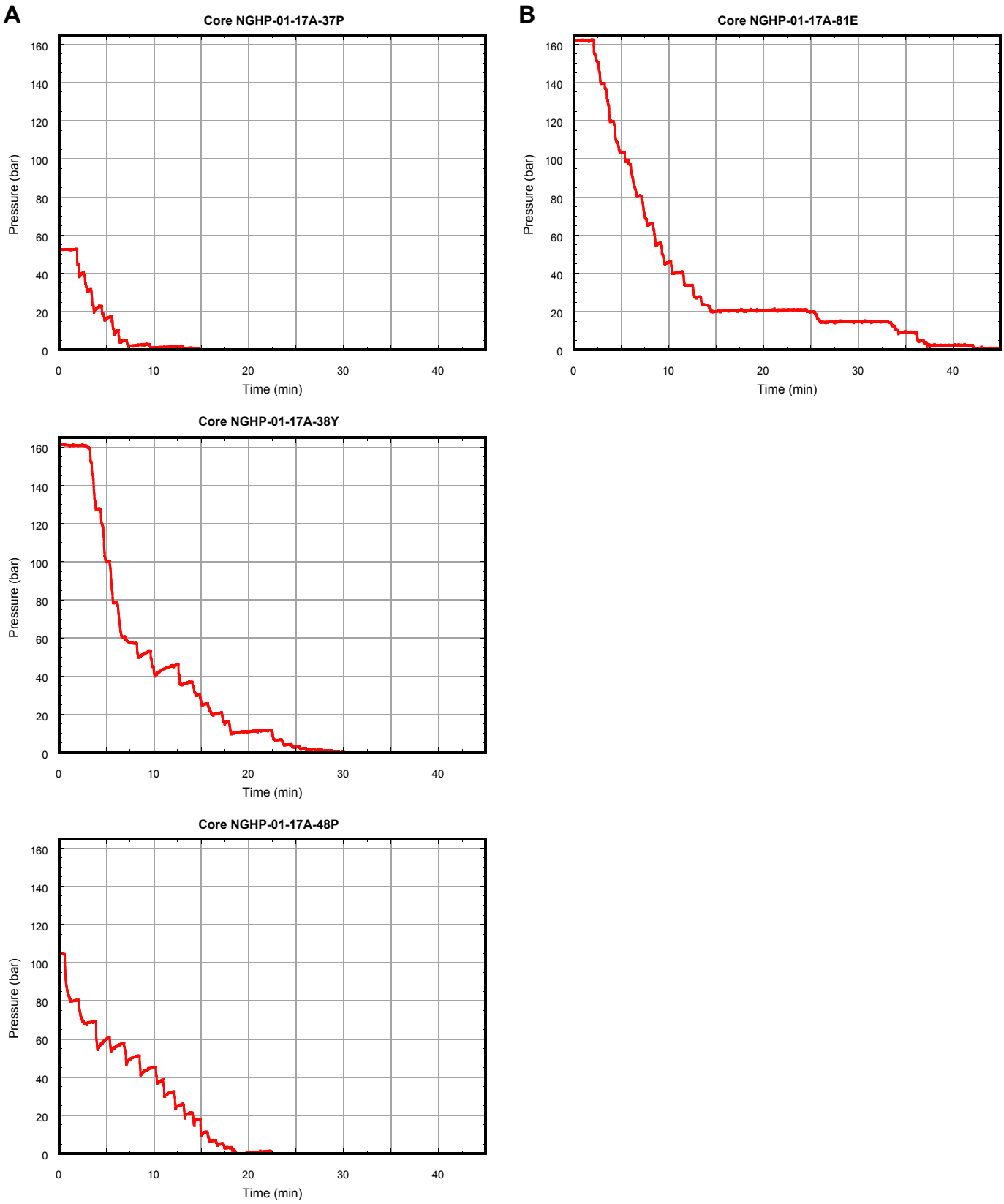


Figure 38. Pressure versus time for the depressurization of successful pressure cores. Note the small rebounds indicating tight core.

Table 22. Methane-hydrate volume and concentration in pore space for successful pressure cores at Site NGHP-01-17. Values required for calculation of methane-hydrate concentration are also included.

Parameter	units	NGHP-01-17A-37P	NGHP-01-17A-38Y	NGHP-01-17A-48P	NGHP-01-17A-49E	NGHP-01-17A-70P	NGHP-01-17A-81E (free gas)
Core diameter	mm	43.2	57	43.2	51	43.2	51
Sediment length	cm	100	86	100	79	12	40
Sediment porosity	%	55	55	55	55	55	55
Pore volume	*liters*	*0.805*	*1.205*	*0.805*	*0.886*	*0.097*	*0.449*
Volume methane collected	liters	1.67	1.80	2.44	1.84	1.53	4.16
Methane concentration in pore fluids	mM	2	0.6	3.5	1.9	0*	0*
Total methane in core	*mmol*	*74.0*	*79.0*	*109.0*	*81.8*	*66.3*	*180.1*
In situ salinity	ppt	33.0	33.0	33.0	33.0	33.0	33.0
Methane saturation**	mM	83.9	84	95	95.2	132.7	162.7
Methane in pore fluids, assuming saturation	*mmol*	*67.5*	*101.2*	*76.4*	*84.3*	*12.8*	*73.0*
Excess methane	*mmol*	*6.5*	*-22.2*	*32.5*	*-2.5*	*53.5*	*107.8*
Volume of methane hydrate or free gas	*ml*	*0.9*	*0.0*	*4.4*	*0.0*	*7.3*	*12.8*
*Methane hydrate or free gas, % of pore volume****	*%*	*0.1*	*0.0*	*0.6*	*0.0*	*7.6*	*2.9*

Notes:

Rows in *italics* are calculated parameters.

*Methane concentration (via headspace) was not measured on these cores. Zero concentration generates a conservative (minimum) estimate of gas hydate volume.

**Methane saturation calculated from Xu (2002, 2004) using a water depth of 1356 mbsl, the above salinities, and either a thermal gradient of 17.9 °C/km and a seafloor intercept of 5.6 °C (Cores NGHP-01-17A-37P and -38Y), or a thermal gradient of 21.1 °C/km and a seafloor intercept of 4.35 °C (Cores NGHP-01-17A-48P, -49E, -70P, & -81E).

***Assuming all gas hydrate evenly distributed throughout the pore space.

Assembly of the VSI string followed. The tool was complete at 0425, RIH at 0440 hr, and left in standby inside the pipe while waiting for day break to start the watch for marine mammal activity. After a one-hour watch had established that no marine mammals were in sight, the first GI air gun shots were fired at 0555 hr, ramping up to the desired operational intensity over 30 min.

The VSI was in open hole at ~0730 hr, but could not pass below 1,986 mbrf (~630 mbsf) at 0755 hr, and we decided to start from this depth, which was just below the predicted depth of the BSR (~600 mbsf, see "Background and Objectives"). Considering the length of open hole available, we attempted stations every 5 m in the vicinity of the BSR, increased the spacing to 10 m above 1,950 mbrf, and finally to 20 m when the bad hole conditions and time constraints required it. The first shot was fired at 0805 hr with the tool anchored at 1,986 mbrf, and the last one was fired at 1305 hr, with the tool at 1,686 mbrf. A total of 654 shots were fired. Out of 32 attempts, 28 stations allowed to stack 5 or more shots and get reliable first arrivals. None of the shallower stations, where the hole was more rugose, produced good data. After deanchoring from the last station, the WHC was turned off before trying to enter the pipe at 1312 hr. This proved once more difficult, and it was necessary to raise, lower and rotate the drill string and to circulate heavily to finally bring the VSI inside the pipe at 1430 hr. When the tool got back to the surface at 1515 hr, some minor external damage was observed on the cable head. The tool was cleaned and rigged down at 1530 hr, and the rig floor was ready to pull out of the hole at 1615 hr.

Logging Data Quality

Figure 40 shows the main logs recorded during the two runs with the triple combo in Hole NGHP-01-17B. The hole size calculated from the HLDS caliper (see "Downhole Logging" in the "Methods" chapter) shows that during the first attempt that failed to go deeper than 238 mbsf, the hole was extremely irregular, with a size exceeding in some places the maximum reach of the caliper arm. The hole size measured in the second run shows that the hole remains irregular above ~365 mbsf, in particular between 300 and 320 mbsf where a series of small washouts might have degraded the quality of the data. Below 365 mbsf, except for a few ledges, the hole was in very good conditions and mostly in gauge with the 11 7/16 in (29 cm) drill bit, indicating that the data should be of good quality.

The data quality in the lower part of the hole is confirmed by the good agreement below 320 mbsf between the density log and the density measurements made on core samples recovered from Hole NGHP-01-17A. Above 320 mbsf, and particularly in the shallower section logged during the first attempt, the bad hole conditions produced erroneously low density values.

The density porosity was calculated from the density log and from the grain density measured on core samples, by using at each depth the grain density from the closest sample. Hence the good agreement between the density-porosity log and the porosity measurements from core samples is a direct consequence of the good agreement in the density data. The

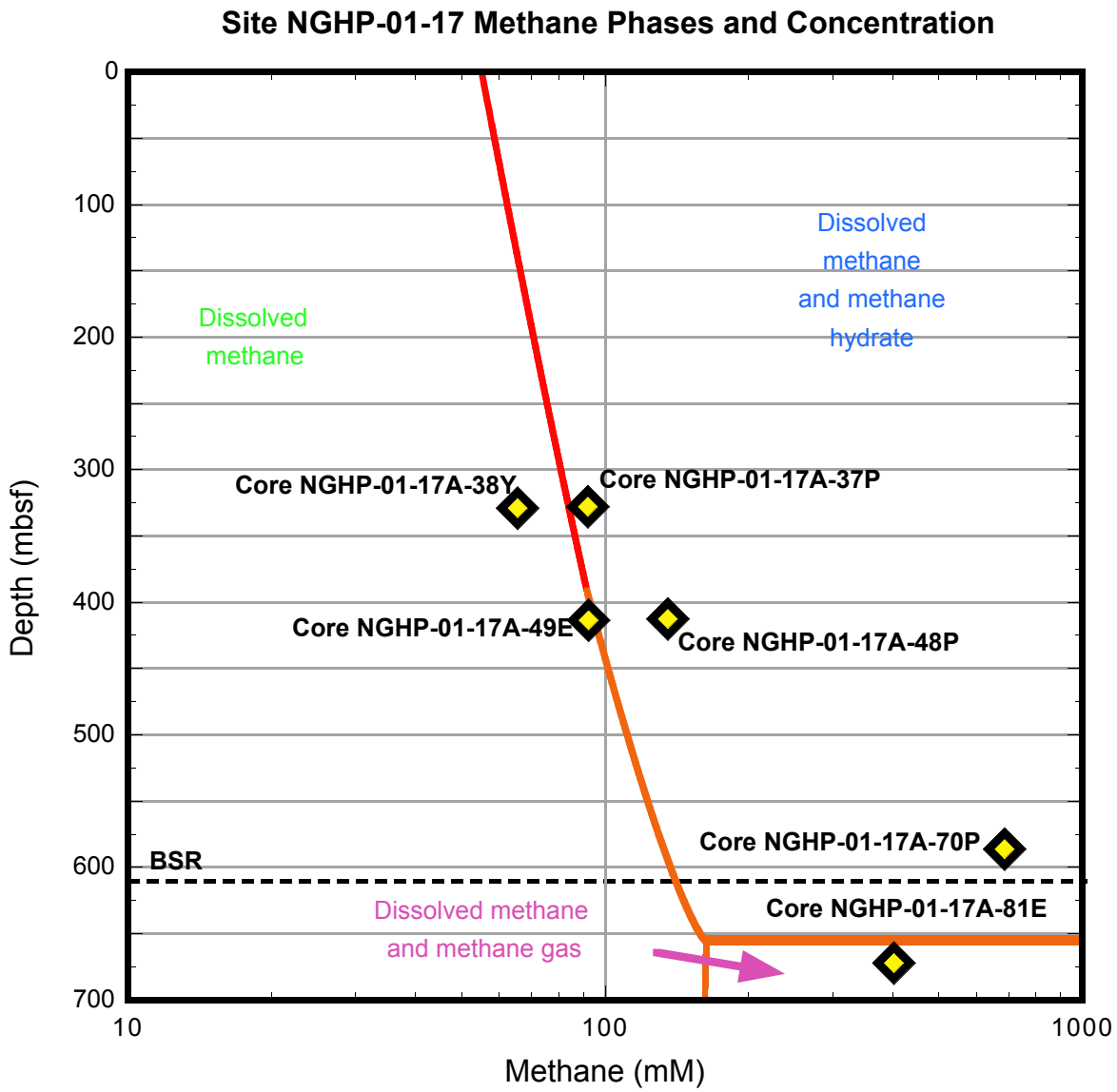


Figure 39. Methane phase diagram for Site NGHP-01-17, with total methane concentration measured from the three successful pressure cores at Site NGHP-01-17. The shipboard-calculated seafloor temperature (4.35 °C) and thermal gradient (21.1 °C/km) were taken from "Downhole Temperature Measurements" in "Physical Properties," the salinity was the average background salinity around the depths of the pressure cores (33 ppt; from table 4), and methane saturation was calculated according to Xu (2002, 2004). [ppt, parts per thousand]

neutron porosity is consistently higher than the other porosity estimates because of the influence of mineral-bound water in these clay-dominated sediments.

The FMS calipers in figure 41 show that the hole conditions had remained stable to the time of the FMS/Sonic run, except for two new ledges at ~450 and ~475 mbsf and for the slight expansion of one of the deepest ledges, none of which posed any problems for the tool. The strong amplitude and coherence of the sonic waveforms show that the compressional and shear velocity logs (V_p and V_s, respectively) provide reliable measurements of the velocity of the formation, and only minimal additional reprocessing was necessary. Throughout the interval logged, a series of fine layers associated with high resistivity have very distinct signatures in the waveform amplitudes that will need particular attention.

While the triple combo and the FMS/Sonic tool strings were heavy enough to pass the ledge at 630 mbsf which was indicated by the caliper in these runs (figs. 40 and 41), the light weight of the VSI prevented it from going below this depth. Figure 42 shows all the preliminary stacks that were derived from the most reliable shots recorded in Hole NGHP-01-17B, and the travel times picked from these stacks. Based on these data, the BSR, which at this site is at a two-way travel time of 2,500 ms, is at 600 mbsf. This is in good agreement

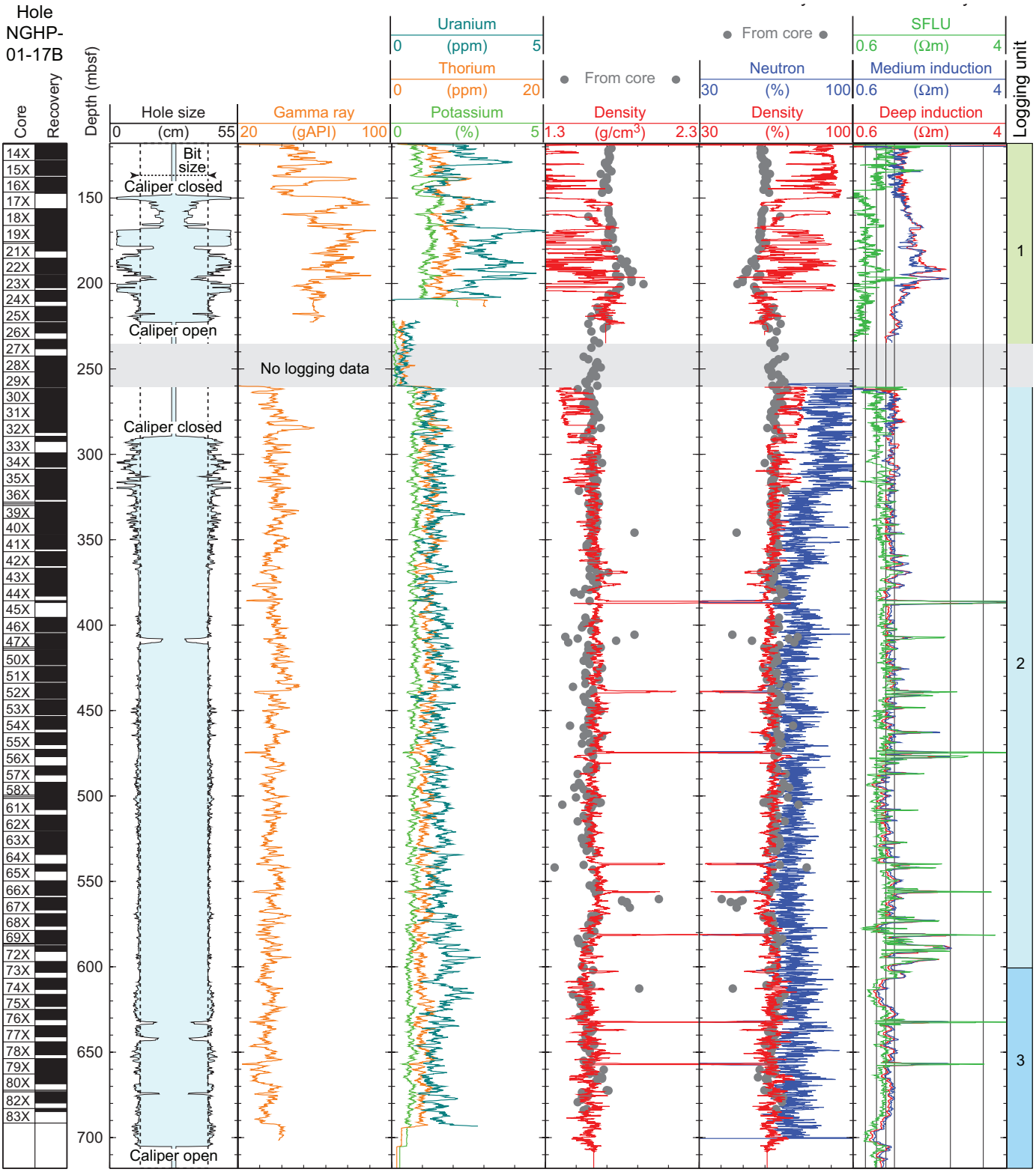


Figure 40. Summary of the wireline logs recorded during the two triple-combo runs in Hole NGHP-01-17B. The hole size is calculated from the Hostile Litho Density Sonde (HLDS) caliper. The density and porosity measurements made on core samples from Hole NGHP-01-17A are shown for comparison. [SFLU, spherically focused unaveraged resistivity]

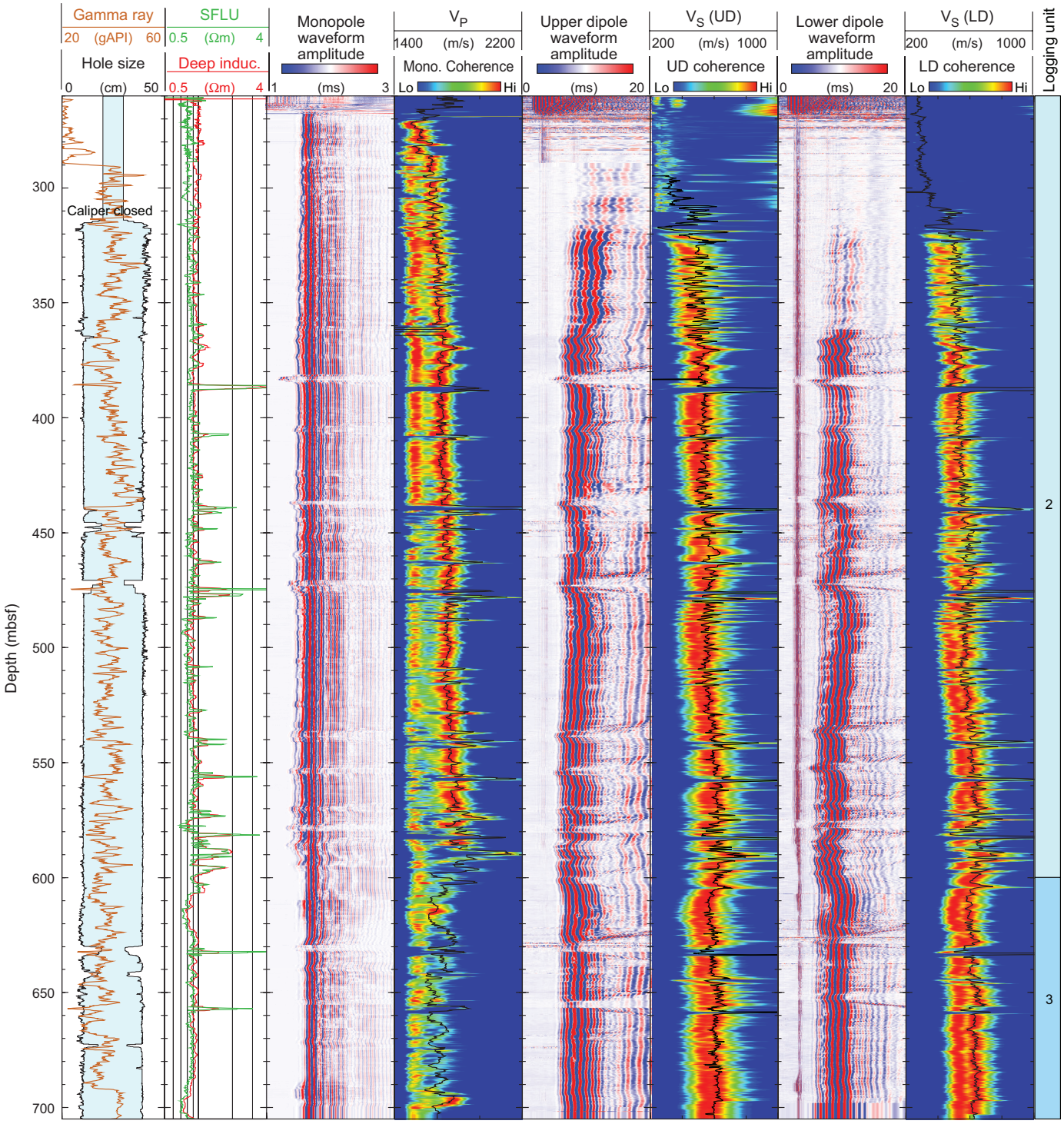


Figure 41. Sonic waveform amplitude and coherence data and velocity logs measured by the DSI in Hole NGHP-01-17B. The hole size, calculated from the FMS calipers, and the gamma ray and resistivity logs are shown for quality control and correlation. [V_p, *P*-wave velocity; V_s, S-wave velocity; LD, Lower dipole; UD, Upper dipole; DSI, dipole sonic log; FMS, formation micro scanner]

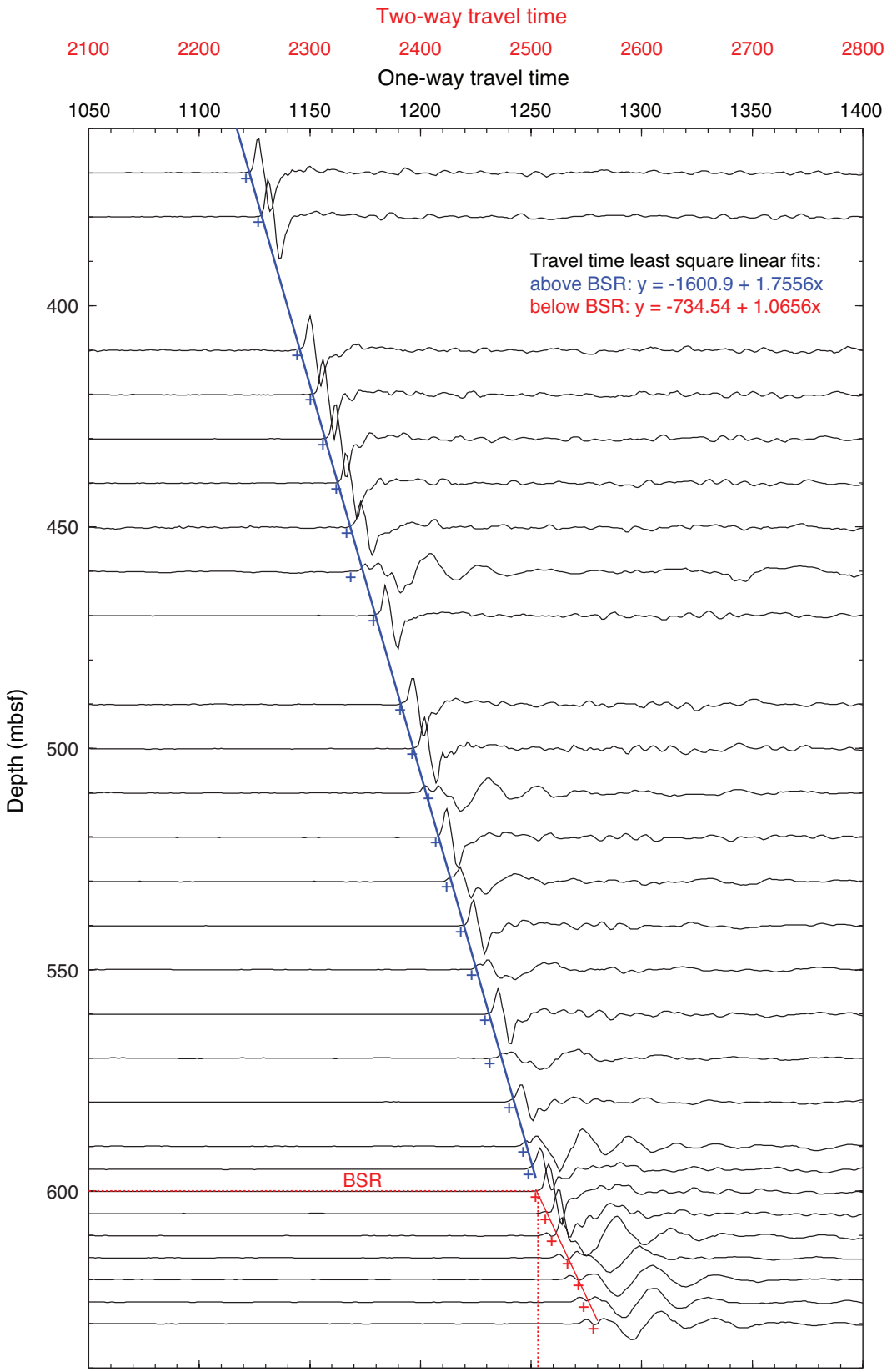


Figure 42. Preliminary stacks derived from the waveforms recorded during the VSP survey in Hole NGHP-01-17B. The travel times picked automatically at the time of the acquisition are shown (crosses), as well as least square linear fits for these travel times as a function of depth above and below the BSR. [VSP, vertical seismic profile; BSR, bottom-simulating reflector]

with the predicted depth (see "Background and Objectives"), and coincides also with decreases in the velocity logs in figure 41. While only six stations were recorded below this depth, and most of the travel times will need to be carefully picked because of the weakness of the arrival, figure 42 shows that there is a clear change in the slope of the least square linear fit for the travel times at this depth indicating a decrease in velocity from ~1,760 m/s above to ~1,070 m/s below. This extremely low value below the BSR will likely be reevaluated after reprocessing.

Logging Units

The trends in the main logs displayed in figures 40 and 41 (particularly in the resistivity and velocity logs) allow the definition of three logging units in Hole NGHP-01-17B:

Logging unit 1 (118–238 mbsf) was logged only during the first attempt, and the irregular hole size makes the interpretation of the data questionable. However the resistivity and gamma ray logs both display higher values than the deeper part of the hole, indicating a very distinct formation in this interval. The higher gamma ray counts are produced by a higher uranium content, which may correspond to the occurrence of finely dispersed authigenic carbonates observed in this interval (see "Lithostratigraphy"). The increase in resistivity with depth above 200 mbsf coincides with an increase in density measured on core samples, suggesting that the high resistivity values are not related to gas hydrate.

Logging unit 2 (260–600 mbsf) is defined most clearly by a steady increase with depth in V_p and V_s. The density and resistivity logs are mostly uniform over the entire unit, except for a series of spikes corresponding to fine (a few cm to ~1 m) layers of high resistivity, some of them associated with high density. While the strongest resistivity spikes correspond to similar peaks in density and are generated by thin indurated layers, likely carbonate layers similar to the one that was recovered at 386 mbsf, the smaller resistivity excursions are not related to density changes and indicate the occurrence of gas hydrate in fine layers, most notably in ash-bearing intervals (see below and "Lithostratigraphy").

The top of Logging unit 3 (600–718 mbsf) is defined by the drop in sonic velocity that produces the BSR at 600 mbsf. It also coincides with a decrease in resistivity. Velocity and resistivity then remain mostly constant over the unit. The decrease in both V_p and V_s indicates that the velocity change is more likely due to the absence of hydrate than to the presence of free gas below the BSR. The absence of amplitude or coherence loss in the sonic waveforms shows that only limited amounts of free gas should occur in this unit.

Gas-Hydrate and Free Gas Occurrence

As previously discussed (see "Downhole Logging" in the "Methods" chapter), the presence of gas hydrate is generally identified by increases in electrical resistivities and acoustic velocities that are not accompanied by a corresponding density increase. While the largest resistivity spikes observed between 260 and 600 mbsf are associated with density peaks due to thin indurated sediment layers, most of the smaller resistivity peaks have no counterpart in the density log and are due to the occurrence of gas hydrate in ash bearing layers (see "Lithostratigraphy"). No visible gas-hydrate samples were actually recovered, but many of the ash layers were associated with cold temperature anomalies measured by the infrared (IR) camera.

To make a quantitative estimate of the amount of gas hydrate present, we followed the procedure described in "Downhole Logging" in the "Methods" chapter, to apply the Archie relationship to the resistivity and porosity logs recorded in Hole NGHP-01-17B. Because no LWD logs were recorded in this site, we used the wire-line resistivity logs to make this estimate. The procedure and the results are illustrated in figure 43. The pore fluid resistivity (R_w) was estimated from Fofonoff (1985) using a temperature profile derived from a linear fit of the in situ temperature measurements at Site NGHP-01-17 (5.5 °C at the seafloor; gradient of 20 °C/km, see "Physical Properties") and the water salinity values measured on interstitial water samples in this hole. All anomalous salinity values lower than 30 ppt that could be due to the dissociation of gas hydrate were removed. The estimated m curve was derived from R_w, the porosity (φ) and resistivity (R_t) logs ($m_{est} = -\log F/\log\varphi$, where $F = R_t / R_w$). As this relationship is defined for water-saturated sediments, the chosen value of $m = 2.5$ is given by the baseline of this curve in the low-resistivity intervals where there is likely no gas hydrate. Using the porosity log and Archie's equation ($R_0 = (a\, R_w) / f^m$), we derive the predicted resistivity of the water-saturated formation R_o. A qualitative influence of gas hydrate on the resistivity log is indicated by the difference between the R_0 and the measured resistivity R_t. The estimated water saturation, assumed to be the numerical complement of the hydrate saturation, is $S_w = (R_0/R_t)^{1/n}$, where n = 2 (Pearson and others, 1983). We used the density porosity and two resistivity measurements to derive the results shown in figure 43. The Spherically Focused unaveraged resistivity (SFLU) has the highest resolution, but the shallowest penetration, of the resistivity measurements made by the DIT tool and is more sensitive to drilling disturbances; the Deep Induction log (ILD) has the deepest penetration, but a lower vertical resolution. The combination of these two estimates provides a possible range of gas-hydrate distribution around Hole NGHP-01-17B.

The results indicate that gas hydrate could occupy as much as ~20 percent of the pore space in fine layers occurring in the entire section logged above the BSR. Most of the highest saturation values coincide with IR anomalies shown in the same figure. In addition, gas-hydrate saturation in the ~20 m immediately above the BSR are consistently above 10 percent. The significant saturation values below the BSR could be associated to the presence of free gas, but are suspiciously high when compared to the modest V_p drop below the BSR.

Because of the irregular hole above 320 mbsf and of the closed caliper above 290 mbsf, the anomalously low density readings in some intervals generate unreliably high porosity values, and the saturation values are likely overestimated. These intervals are underlined in grey in figure 43.

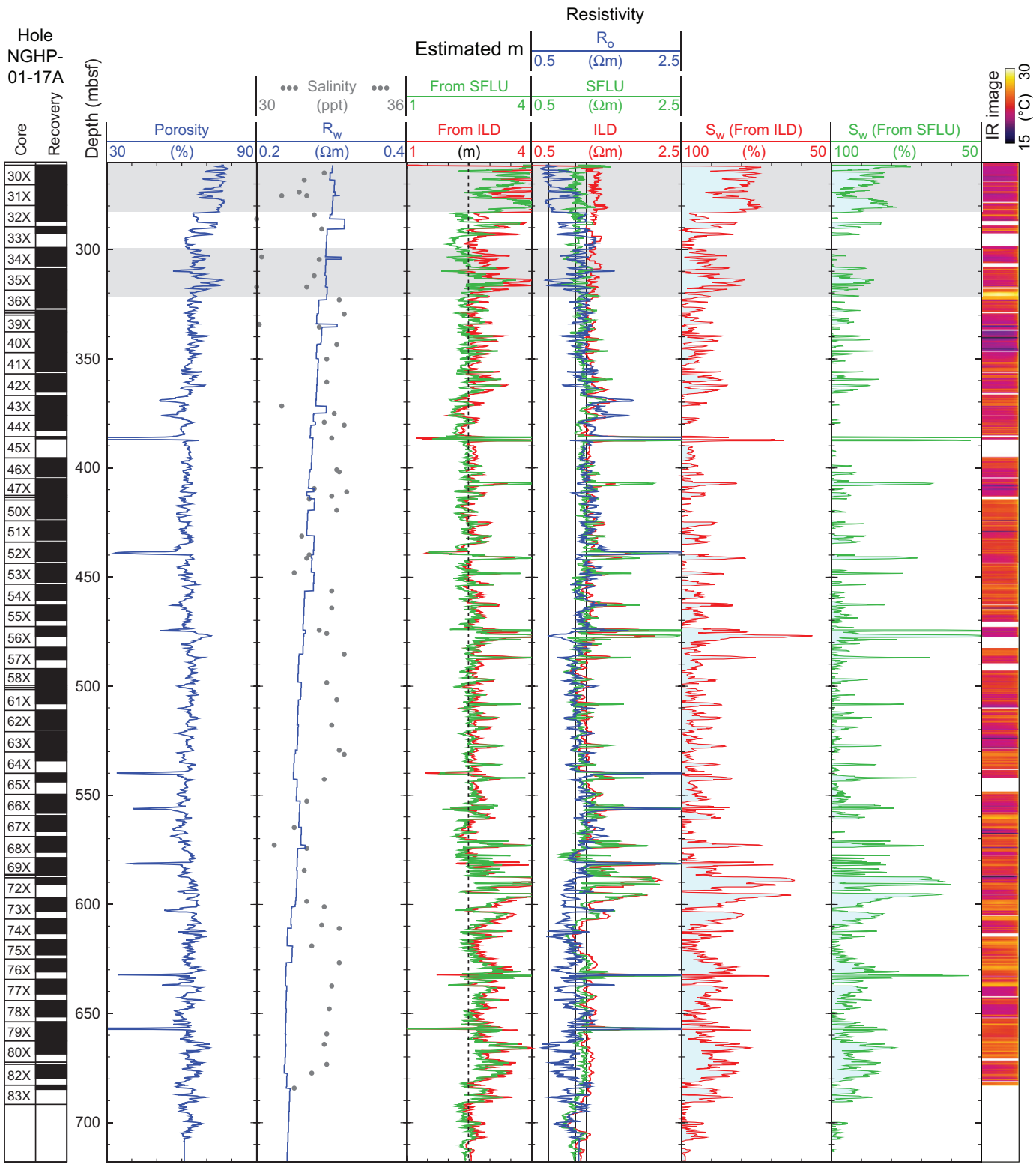


Figure 43. Water saturations from Archie's equation and wireline porosity and resistivity logs in Hole NGHP–01–17B. The gray area indicates degraded data quality. On the right track, a summary of the infrared (IR) images recorded on the cores recovered from Hole NGHP–01–17A shows the intervals where cold anomalies identify the presence of gas hydrate. [R_w, formation water resistivity, R_0, computed formation resistivity for 100 percent water saturation; R_t, measured resistivity; S_w, water saturation; SFLU, spherically focused unaveraged resistivity; ILD, deep induction resistivity log]

References Cited

Bjerrum, L., 1972, Embankments on soft ground: Proceedings of the ASCE Specialty Conference on Performance of Earth and Earth-Supported Structures, Purdue University, v. 22, p. 1–54.

Clift, P.D., 2006, Controls on the erosion of Cenozoic Asia and the flux of clastic sediment to the ocean: Earth and Planetary Science Letters, v. 241, p. 571–580.

Davis, E.E., Hyndman, R.D., and Villinger, H., 1990, Rates of fluid expulsion across the northern Cascadia accretionary prism—Constraints from new heat flow and multichannel seismic reflection data: Journal of Geophysical Research, v. 95, p. 8869–8889.

Dickens, G.R., and Owen, R.M., 1999, The latest Miocene-early Pliocene biogenic bloom—A revised Indian Ocean perspective: Marine Geology, v. 161, p. 75–91.

Duan, Z., Møller, N., Greenberg, J., and Weare, J.H., 1992, The prediction of methane solubility in natural waters to high ionic strengths from 0° to 250 °C and from 0 to 1600 bar: Geochimica et Cosmochimica Acta, v. 56, p. 1451–1460.

Farrell, J.W., Raffi, I., Janecek, T.R., Murray, D.W., Levitan, M., Dadey, K.A., Emeis, K.-C., Lyle, M., Flores, J.-A., and Hovan, S., 1995, Late Neogene sedimentation patterns in the eastern equatorial Pacific, *in* Pisias, N.G., Mayer, L.A., Janecek, T.R., Palmer-Julson, A., and van Andel, T.H., eds., Proceedings of the Ocean Drilling Program, scientific results, v. 138, p. 717–756.

Fofonoff, N.P., 1985, Physical properties of seawater: Journal of Geophysical Research, v. 90, no. C2, p. 3332–3342.

Hermoyian, C.S., and Owen, R.M., 2001, Late Miocene-early Pliocene biogenic bloom—Evidence from low-productivity regions of the Indian and Atlantic Oceans: Paleoceanography, v. 16, p. 95–100.

Holtz, R.D., and Kovacs, W.D., 1981, An introduction to geotechnical engineering: Englewood Cliffs, N.J., Prentice-Hall, Inc., 733 p.

Hunt, R.E., 1984, Geotechnical engineering investigation manual: New York, McGraw-Hill Book Company, 983 p.

Kvenvolden, K.A., and Lorenson, T.D., 2000, Methane and other hydrocarbon gases in sediment from the southeastern North American continental margin, *in* Paull, C.K., Matsumoto, R., Wallace, P.J., Black, N.R., Borowski,W.S.,Collett, T.S., Damuth, J.E., Dickens, G.R., Egeberg, P.K., Goodman,K., Hesse, R.F., Hiroki, Y., Holbrook, W.S., Hoskins, H., Ladd, J. ,Lodolo, E., Lorenson, T.D.,Musgrave, R.J., Naehr, T.H., Okada, H., Pierre, C., Ruppel, C.D., Satoh, M., Thiery, R., Watanabe, Y., Wehner, H., Winters, W.J.,and Wood, W.T., Gas hydrate sampling on the Blake ridge and Carolina rise; covering leg 164 of the cruises of the drilling vessel JOIDES Resolution, Halifax, Nova Scotia, to Miami, Florida, sites 991–997, 31 October–19 December 1995: Proceedings of the Ocean Drilling Program, Scientific Results, v. 164, p. 29–36.

Ladd, C.C., Foote, R., Ishihara, K., Schlosser, F., and Poulos, H.G., 1977, Stress-deformation and strength characteristics—State-of-the-art report: Proceedings of the Ninth International Conference on Soil Mechanics and Foundation Engineering, Tokyo, v. 2, p. 421–494.

Lambe, T. W. and Whitman, R.V., 1969, Soil mechanics: New York, John Wiley and Sons, 553 p.

Mix, A.C., Tiedemann, R., Blum, P., and others, 2003, Proceedings of the Ocean Drilling Program, initial Reports, v. 202, available at *http://www-odp.tamu.edu/publications/202_IR/202ir.htm*.

Novosel, I., Winters, W.J., Boldina, O.M., Labails, C., and Geli, L., 2007, Thermal conductivity of sediment recovered from the IMAGES VIII/PAGE 127 Gas Hydrate and Paleoclimate Cruise on the R/V Marion Dufresne in the Gulf of Mexico, 2–18 July 2002, *in* Winters, W.J., Lorenson, T.D., and Paull, C.K., eds., Initial report of the IMAGES VIII/PAGE 127 gas hydrate and paleoclimate cruise on the *RV Marion Dufresne* in the Gulf of Mexico, 2–18 July 2002: U.S. Geological Survey Open-File Report 2004–1358.

Pearson, C.F., Halleck, P.M., McGuire, P.L., Hermes, R., and Mathews, M., 1983, Natural gas hydrate deposits—A review of in situ properties: Journal of Physical Chemistry, v. 87 p. 4180–4185.

Pimmel, A., and Claypool, G., 2001, Introduction to shipboard organic geochemistry on the *JOIDES Resolution*. Ocean Drilling Program Technical Note, *v.* 30. Accessed September 30, 2005 at *http://www-odp.tamu.edu/publications/tnotes/tn30/INDEX.HTM*.

Riedel, M., Collett, T. S., Malone, M. J., and the Expedition 311 Scientists, 2006, Proceedings of the Integrated Ocean Drilling Program, Volume 311. doi:10.2204/iodp.proc.311.101.206

Sloan, E.D., 1998, Clathrate Hydrates of Natural Gases (2nd ed.): New York (Marcel Dekker), 705 p.

Thompson, P.R., Bé, A.W.H., Duplessy, J-C., and Shackleton, N.J., 1979, Disappearance of pink-pigmented *Globigerinoides ruber* at 120,000 yr BP in the Indian and Pacific oceans: Nature, v. 280, p. 554–558.

Winters, W.J., 2000, Stress history and geotechnical properties of sediment from the Cape Fear diapir, Blake Ridge diapir, and Blake Ridge, *in* Paull, C.K., Matsumoto, R., Wallace, P.J., and Dillon, W.P., eds., Proceedings of the Ocean Drilling Program Scientific Results, v. 164.

Xu, W., 2002, Phase balance and dynamic equilibrium during formation and dissociation of methane gas hydrate: Proceedings of the 4th International Conference on Gas Hydrates, Yokohama, Japan, p. 195–200.

Xu, W., 2004, Modeling dynamic marine gas hydrate systems: American Mineralogist, v. 89 p. 1271–1279.